Copyright ©

The polar and subpolar North Atlantic during the last five glacial-interglacial cycles

Dissertation
zur Erlangung des Doktorgrades
der Mathematisch-Naturwissenschaftlichen Fakultät
der Christian-Albrechts-Universität
zu Kiel

vorgelegt von
Jan P. Helmke

Kiel, 2001

Abstract

The main goal of this study was to determine Late Quaternary climatic variations of the high northern latitudes on glacial-interglacial as well as on millennial time-scales using a range of paleoceanographic proxy records, i.e., sediment color, carbonate content, ice-rafted debris (IRD), stable oxygen isotopes, and carbonate preservation, from deep-sea sediments from the Northeast Atlantic Ocean and the Nordic Seas.

Carbonate preservation analysis of deep-sea sediments from the Nordic Seas revealed a distinct glacial-interglacial carbonate preservation pattern during the last five climate cycles: Foraminiferal tests showed good glacial preservation and increasing corrosion during interglaciations. This pattern is similar to Pleistocene records from the deep Pacific Ocean, but seems to be out of phase with the rest of the Atlantic Ocean. The generally good carbonate preservation suggests well-ventilated deep water at the study areas in the Norwegian and Iceland Seas throughout most of the last 12 marine isotope stages (MIS), regardless of the climatic mode. There are two mechanisms that could have caused this distinctive Nordic Seas carbonate preservation pattern: (1) The enhanced calcite corrosion during interglacial periods may be due to high regional planktic productivity with an increased downward flux rate of organic material to the sea floor and, thus, to more corrosive bottom water due to carbondioxide enrichment. (2) It may be linked to global scale variations in the marine carbonate system, which caused a change in ocean alkalinity, i.e., altered the depth of the calcite saturation horizon.

In order to use color data for further paleoclimatic investigations the factors that control sediment lightness and red-green color in the North Atlantic were specified. Analysis of a Northeast Atlantic deep-sea sediment core proved that during the last five climate cycles changes in sediment lightness were controlled mainly by fluctuations of the fine (<20 μm) carbonate fraction. Additionally, changes in carbonate corrosion also have a strong influence on total sediment lightness, as stronger corrosion of the carbonate fraction will lead to increased sediment lightness values. This lightness increase of the entire sediment is caused by corrosional effects on the surface structure of foraminifera and, probably, coccoliths. Changes in the red-green color of the sediment are caused by variations in the iceberg-rafted input of terrigenous, reddish iron-containing minerals. Spectral analysis of the red-green color record revealed persistent millennial-scale climate variability during the last 500,000 years. It seems that maxima of climate variability were tied to times of changes in ice mass and coincided to times when sea level was 40% below present-day global sea level indicating threshold behaviour. This threshold controlled the amplitude of climatic variations on millennial time-scales during the Late Quaternary. Intervals of relatively stable ice volume, i.e., peak interglacial and also peak glacial periods, showed reduced short-term variability of the climate system.

Abstract

Proxy records from the Northeast Atlantic and the Nordic Seas unveiled that, in contrast to the more frequent occurrence of warm interglacial conditions in the subpolar North Atlantic, full interglacial conditions in the polar North Atlantic occurred during MIS 1, 5e, and 11 only. A comparison of planktic $\delta^{18}O$ from the North Atlantic suggests colder sea-surface temperatures during MIS 11 than during other peak warm periods, i.e., MIS 1, 5e, and 9. IRD data indicate a major temperature gradient in the polar North Atlantic and less advection of warm Atlantic surface water into the Nordic Seas during interglacial MIS 11 than at present. IRD input in the Northeast Atlantic and the Nordic Seas increased almost coherently during glaciations and terminations. A general lack of synchroneity in the recurrence periods of IRD maxima points at differences in the timing of iceberg discharges between Northern Hemisphere ice sheets. However, the subpolar and polar North Atlantic were synchronously affected by the mechanisms that caused variability of the glacial climate system on millennial time-scales.

These new results from Northeast Atlantic and Nordic Seas deep-sea sediments point at distinct climatic variability in the Northern Hemisphere on longer, glacial-interglacial as well as on shorter, millennial time-scales. The investigations revealed partly synchronous forcing of the glacial climate system in the polar and subpolar North Atlantic. In contrast, peak interglacial conditions in the polar North Atlantic were less frequent than in the subpolar North Atlantic region indicating pronounced differences in the paleoclimatic and paleoceanographic conditions between the two areas during these intervals.

Zusammenfassung

Das Hauptanliegen dieser Arbeit war es, Schwankungen im Klimasystem der hohen nördlichen Breiten während des späten Pleistozäns sowohl auf glazial-interglazialen als auch auf kürzeren, tausendjährigen Zeitskalen zu erfassen. Zu diesem Zweck wurde an Tiefseesedimenten des Nordost-Atlantiks und des Europäischen Nordmeeres ein breites Spektrum paläo-ozeanographischer Untersuchungsparameter (im einzelnen: Sedimentfarbe, Karbonatgehalt, Anteil eistransportierten, terrigenen Materials, stabile Sauerstoffisotope, Grad der Karbonaterhaltung) bestimmt und ausgewertet.

Die Analysen zur Karbonaterhaltung an Sedimenten des Europäischen Nordmeeres ergaben für den Zeitraum der letzten fünf Klimazyklen ein spezifisches glazial-interglaziales Muster in der Erhaltung des karbonatischen Materials: Die untersuchten Foraminiferenproben zeigten eine gute Erhaltung in glazialen Phasen und zunehmende Anlösungserscheinungen während der Interglaziale. Diese Ergebnisse entsprechen dem Muster pleistozäner Karbonaterhaltung im Pazifischen Ozean, stehen aber im Gegensatz zum Karbonaterhaltungsmuster wie es aus anderen Gebieten des Atlantischen Ozean bekannt ist. Die generell gute Karbonaterhaltung der Proben deutet darauf hin, daß es unabhängig von der Ausprägung des Klimas während der letzten 12 marinen Isotopenstadien mit Ausnahme kurzer Phasen eine ausreichende Durchlüftung des Tiefenwassers in den Untersuchungsgebieten in der Norwegen- und Island-See gegeben hat. Zwei Mechanismen könnten das Muster der Karbonaterhaltung im Europäischen Nordmeer verursacht haben: (1) Eine erhöhte Anlösung des Karbonates während interglazialer Phasen könnte auf eine hohe regionale planktische Produktivität zurückzuführen sein, die ein verstärktes Absinken organischen Materials zum Meeresboden und damit korrosiveres Bodenwasser durch eine erhöhte Freisetzung von Kohlendioxid zur Folge hat. (2) Die Karbonaterhaltung im Europäischen Nordmeer wird möglicherweise durch Veränderungen im globalen marinen Karbonatsystem gesteuert, wobei diese eine veränderte Alkalinität der Ozeane und damit Schwankungen in der Tiefe des Sättigungshorizontes von Kalzit im Ozean bewirkt.

Um eine paläo-ozeanographische Interpretation von Sedimentfarbdaten aus dem Nord-Atlantik durchführen zu können, wurden die Faktoren, die in diesem Gebiet die Helligkeit des Sedimentes sowie dessen rot-grüne Farbe kontrollieren, bestimmt. Untersuchungen an einem Sedimentkern aus dem Nordost-Atlantik belegten dabei, daß die Sedimenthelligkeit während der letzten fünf Klimazyklen im wesentlichen durch Fluktuationen in der feinen (<20 µm) Karbonatfraktion gesteuert wird. Darüber hinaus haben Veränderungen in der Karbonaterhaltung einen starken Einfluß auf die Helligkeit des Sedimentes, da eine erhöhte Anlösung der Karbonatfraktion mit einem Ansteigen der Sedimenthelligkeitswerte einhergeht. Dieser Anstieg in der Helligkeit des gesamten Sedimentes ist auf Anlösungseffekte an der

kalzitischen Oberfläche von Foraminiferen und - wahrscheinlich - auch von Coccolithen zurückzuführen. Veränderungen in der rot-grünen Farbe des Sedimentes sind durch Schwankungen im eisbergtransportierten Eintrag von roten, eisenhaltigen Mineralien in das Sediment verursacht. Eine Spektralanalyse des rot-grünen Farbkanals indiziert für den Zeitraum der letzten 500.000 Jahre eine permanente klimatische Variabilität auf Zeitskalen von 1.000 bis 10.000 Jahren. Dabei sind die Maxima klimatischer Variabilität an Phasen gekoppelt, in denen sich das Volumen der kontinentalen Eismassen verändert hat. Die Maxima fallen dabei mit Zeiten zusammen, in denen der Meeresspiegel 40% unter dem heutigen globalen Wert gelegen hat. Das Auftreten der verstärkten klimatischen Variabilität ist an das Überschreiten dieses Schwellenwertes gekoppelt, der somit die Amplitude von klimatischen Veränderungen auf kurzen Zeitskalen kontrolliert. Intervalle mit einem vergleichsweise stabilen Eisvolumen, d.h. die ausgeprägten warmen und kalten Phasen der Interglaziale und Glaziale, zeigten dagegen für die kurzfristigen Zeitskalen eine reduzierte Variabilität innerhalb des Klimasystems.

Ein Vergleich geochemischer und sedimentologischer Daten aus dem Nordost-Atlantik und dem Europäischen Nordmeer, die den Zeitraum der letzten 500.000 Jahre abdecken, konnte zeigen, daß es voll ausgeprägte interglaziale Bedingungen im polaren Nord-Atlantik nur in drei Phasen der marinen Isotopenstadien 1, 5e und 11 gegeben hat, wohingegen solche Bedingungen im subpolaren Nord-Atlantik regelmäßiger vorgeherrscht haben. Die planktischen $\delta^{18}O$-Werte aus dem Nordost-Atlantik lassen vermuten, daß die Meeresoberflächen-Temperaturen im Isotopenstadium 11 geringer waren als während anderer ausgeprägter Warmphasen der jüngeren Isotopenstadien 1, 5e und 9. Die Untersuchungen an terrigenem, eisverfrachteten Material indizieren für das Stadium 11 einen deutlichen Temperaturgradienten im polaren Nord-Atlantik, wobei es vermutlich einen geringeren Einstrom warmen Oberflächenwassers aus dem Atlantik in das Europäische Nordmeer gegeben hat als rezent. Der Eintrag eisverfrachteten Materials in den Nordost-Atlantik und das Europäische Nordmeer erfolgte weitestgehend zeitgleich während der Glaziale und in den anschließenden Terminationen, den Übergangsphasen von Glazialen zu Interglazialen. Die in den untersuchten Regionen zeitlich asynchronen Perioden der Eintragsmaxima in den Zeiten erhöhter Anlieferung von eisverfrachtetem Material sind ein Hinweis dafür, daß die Hauptkalbungsphasen der Eisberge an den einzelnen Eisschilden der nördlichen Hemisphere zu unterschiedlichen Zeitpunkten erfolgten. Generell wurden der subpolare und der polare Nord-Atlantik jedoch scheinbar synchron durch Mechanismen beeinflußt, die zu einer rapiden Variabilität im glazialen Klimasystem geführt haben.

Die hier präsentierten neuen Erkenntnisse aus Untersuchungen an Sedimenten des Nordost-Atlantiks und des Europäischen Nordmeeres zeigen deutlich, daß die nördliche Hemisphere in den letzten 500.000 Jahren durch charakteristische klimatische Variabilität sowohl auf glazial-

interglazialer Ebene als auch auf kürzeren Zeitskalen geprägt war. Die Untersuchungen belegten dabei vergleichbare Auswirkungen des glazialen Klimasystems auf die Verhältnisse im polaren und im subpolaren Nord-Atlantik. Im Gegensatz dazu zeigten die interglazialen Warmphasen, die im polaren Nord-Atlantik weit weniger häufig auftraten als im subpolaren Sektor, daß es in diesen Abschnitten deutliche Unterschiede in den paläoklimatischen und paläo-ozeanographischen Bedingungen beider Untersuchungsgebiete gegeben haben muß.

Chapter I - Introduction

I.1. Main objectives

The major task of this study was to determine distinct climatic variability in the Northem Hemisphere during the past 500,000 years by applying several sedimentological, micropaleontological, and geochemical analyses to deep-sea sediments from the Northeast Atlantic and the Nordic Seas. Today, the high northem latitudes are the world ocean's major place of deep-water formation, i.e., North Atlantic Deep Water (NADW) is an integrated a part of the global conveyor belt. During Late Quatemary intervals of repeated Northern Hemisphere ice-sheet waxing and waning this modern-type thermohaline circulation pattern declined or evolved. The strong differences in the climatic conditions of glacial and interglacial intervals in the high northern latitudes have been imprinted on deep-sea sediments from this region. Accordingly, much paleoceanographic research of the last decades has concentrated on the North Atlantic and the Nordic Seas. However, few data of long, continuous high-resolution sediment records exist that document both long-scale glacial-interglacial climate change, and rapid climatic variations on millennial time scales. In this study several records from deep-sea sediments with varying temporal resolution were used in order to obtain detailed knowledge about orbitally induced mechanisms that effect the climate on Milankovitch time-scales as well as into climatic variability on shorter, millennial time-scales. This approach was to unveil new insights into the forcing and the feedback mechanisms of climate fluctuations in the Northern Hemisphere during glacial and interglacial times.

Changes in the marine carbonate system are documented in deep-sea carbonate preservation records, because they are closely linked to paleoceanographic conditions, i.e., surface productivity, ice cover, ventilation of the bottom water, and alkalinity of the oceans (Berger, 1992; Archer and Maier-Reimer, 1994; Henrich, 1998). Glacial-interglacial carbonate dissolution cycles from the Atlantic and Pacific Oceans have been studied in great detail (e.g., Crowley, 1983; Farrell and Prell, 1989; Karlin et al., 1992). However, investigations on carbonate dissolution in the northemmost Atlantic region have so far been limited to qualitative descriptions of coarse carbonate preservation (Henrich, 1986; Henrich et al., 1989; Huber et al., 2000). A new method to analyse carbonate preservation will be presented in order to estimate the total carbonate loss in the Nordic Seas caused by dissolution during the last five climate cycles. This will give new insights into one of the current problems of climate research: The large amplitude glacial-interglacial change in the atmospheric CO_2 concentration documented by air bubbles trapped in Greenland and Antarctic ice cores (Sowers et al., 1991; Jouzel et al., 1993, Petit et al., 1997). The terrestrial biosphere and soil carbon reservoirs are too small to trigger the preanthropogenic atmospheric carbondioxide increase of about 80 ppm known since the last glacial period. Hence, changes in the marine carbonate system are believed to

be responsible for these fluctuations (Sarmiento and Toggweiler, 1984; Broecker and Peng, 1993; Broecker et al., 1999; Archer et al., 2000).

Color is one of the fundamental sediment properties. The relationship between sediment color, i.e., lightness L* and the carbonate component of a Northeast Atlantic core site will be investigated in detail. In general, color of glacial-interglacial deep-sea sediments from the North Atlantic is characterized by an alternating light-dark-pattern of carbonate-rich sediments and sediments rich in detrital particles. Previous studies of North Atlantic sediments have shown a good correlation between sediment lightness (or comparable measurements like gray scale or brightness) and carbonate content (Nagao and Nakashima, 1992; Cortijo et al., 1995). Therefore, lightness has been used to estimate sediment carbonate content (e.g., Ortiz et al., 1999). However, it will be shown that the relationship between sediment color and carbonate content is not that straightforward. It is crucial to determine the effects of the main sediment components on total sediment color to avoid misleading results when interpreting color records of late Quaternary sediments for paleoceanographic purposes.

High-resolution North Atlantic sediment records and Greenland ice core data covering the last climate cycle both document climate instability on millennial time scales during the last glaciation, i.e., the periodic occurrence of so called Heinrich and Dansgaard-Oeschger events (Broecker et al., 1992; Bond et al., 1992; Dansgaard et al., 1993; Grootes and Stuiver, 1997). Sediment color records can provide a much higher resolution than conventinal proxy methods (Andrews and Freeman, 1996), consequently they are suitable to investigate rapid climate fluctuations (e.g., Cortijo et al., 1995). However, sediment color has so far not been used to document the evolution of millennial-scale climatic variability during the late Pleistocene. Thus, a Northeast Atlantic sediment color record will be studied by means of time series analysis to investigate millennial-scale climate change during the past five glacial-interglacial cycles. The color record will help to reveal distinct pattems of short-term climate instability and be used to identify mechanisms that can force the climate system to undergo fluctuations on short time scales

Since first detailed studies from the polar and subpolar North Atlantic showed that severe glacial-interglacial climatic variability was imprinted on deep-sea sediments (Ruddiman and McIntyre, 1976; Kellogg, 1977; 1980) much paleoceanographic research in the high northern latitudes concentrated on the conditions of specific glacial and interglacial intervals during the late Pleistocene (e.g., Boyle and Keigwin, 1987; McManus et al., 1994; Oppo et al., 1997; Vidal et al., 1999). In general, it could be documented that complex climatic interactions appeared during each glacial and interglacial period. However, so far glacial and interglacial sediment records from the polar and subpolar North Atlantic region have not been compared in detail. In this study several

sedimentological and geochemical parameters from Northeast Atlantic and Nordic Seas sediment records will be used to compare the climate characteristics of interglacial and glacial times and to reveal possible, distinct synchronous or asynchronous trends between the areas under study. This can help to decipher the complex forcing and feedback mechanisms that drove the Quaternary climate system at high northern latitudes.

I.2. Regional hydrography of the study area

Three sites from the Northeast Atlantic (M23414) and the Nordic Seas (M23352 and PS 1243) were selected for this study (Fig. I-1, Fig. I-2).

At present, warm and salty surface water, i.e., the North Atlantic Current (NAC), advects from the North Atlantic into the eastern Norwegian-Greenland Sea (NGS). As Norwegian Current (NC) it forms the water of the Atlantic Domain (AND) that flows along the Norwegian and Svalbard shelf margins into the eastern Arctic Ocean (Swift, 1986; Fig. I-1). The Polar Front separates these Atlantic inflow from cold and less salty Arctic surface water of the East Greenland Current (EGC) that makes up the Polar Domain (POD) and conveys south along Greenland and through Denmark Strait into the North Atlantic (Swift, 1986). Polar and Atlantic domains are separated by mixed waters of the Arctic Domain (ARD), which is the main location of deep water formation in the Nordic Seas (Fig. I-1).

The formation of deep water in the Nordic Seas is generated by cooling and evaporation of warm surface waters leading to a vertical overturn of these waters to form dense and cold waters in the Greenland and Iceland Seas (Broecker and Denton, 1990). The outflow of these waters into the North Atlantic across the Greenland-Scotland Ridge (Aagaard and Carmarck, 1994) contributes to the formation of cold and well ventilated NADW that flows south through the Atlantic and Indian Oceans into the Pacific (Broecker, 1991). A major part of the cold deep water upwells in the northern Pacific and returns as a warm and less saline surficial flow into the North Atlantic, increases temperature and salinity in the Carribean and conveys as Gulf Stream heat and moisture into the high northern latitudes. Any disturbance of these flow pattern in the past may have led to a shallower and weaker deep circulation and to a southward migration of Atlantic deep water production with strong influence on the climatic conditions of the high northern latitudes, because of less heat transfer to the north (Rahmstorf, 1994).

At present, Site M23352 from the Iceland Plateau is located in the ARD near the recent Polar Front (Fig. I-1, Fig. I-2), whereas Site PS1243 from the western part of the southern Norwegian Sea is located at the western edge of the warm NC near the Arctic Front in the AND (Fig. I-1, Fig. I-2). During the last five climate cycles the severe differences between glacial and interglacial climate

modes in the high northern latitudes, as documented by repeated south- and northward movement of the Polar and Arctic Fronts, caused highly variable surface and bottom water mass conditions in the entire Nordic Seas and at the study sites in the Norwegian and Iceland Seas (e.g., Labeyrie et al., 1987; Dokken and Hald, 1996; Hebbeln and Wefer, 1997; Henrich, 1998; Bauch et al., 2000a).

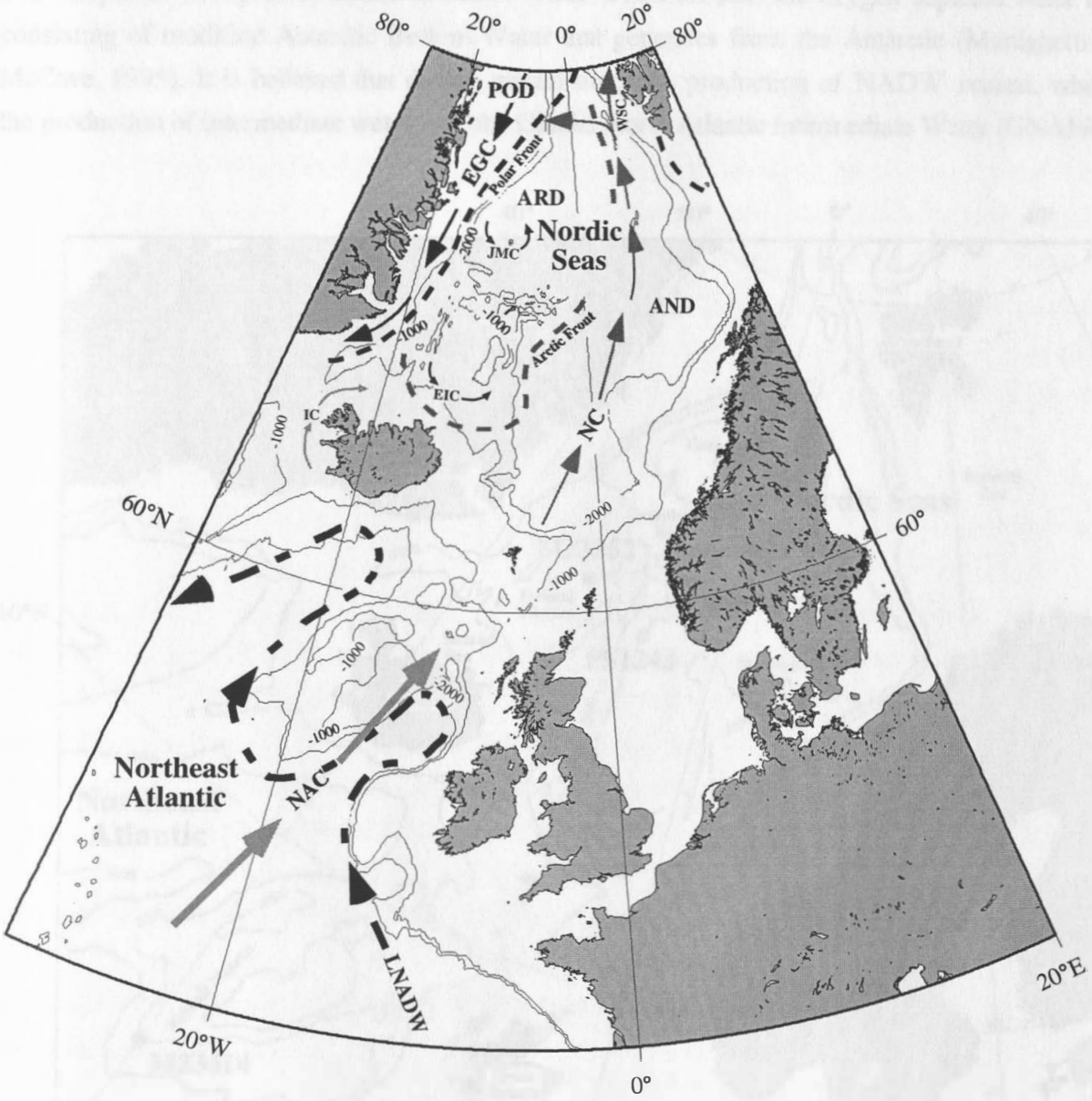

Fig. I-1: Simplified modern surface water circulation of the Northeast Atlantic and the Nordic Seas and the major oceanographic regimes of the later (Swift, 1986); POD (Polar Domain); ARD (Arctic Domain), AND (Atlantic Domain); Dotted lines indicate Polar (black line) and Arctic (gray line) Fronts. Gray and black arrows denote warmer and cooler surface currents, respectively; NAC (North Atlantic Current), NC (Norwegian Current), EGC (East Greenland Current), WSC (West Spitsbergen Current), JMC (Jan Mayen Current), EIC (East Iceland Current), IC (Irminger Current). Water circulation of the Lower North Atlantic Deep Water (LNADW) is denoted also (thick, dashed black line). Water depth is in m.

Today, study Site M23414 on the southern Rockall Plateau in the Northeast Atlantic at about 2200 m water depth is under influence of the Lower North Atlantic Deep Water (LNADW; Fig. I-1, I-2). LNADW is a mixture of dense overflows from the Nordic Seas and Labrador Sea Water (McCave and Tucholke, 1986), which in the Northeast Atlantic is located between 2000 and 3500 m water depth (Venz et al., 1999). The deepest parts of the Rockall area at the Plateau slope below 3500 m water depth are occupied by Southern Ocean Water, a nutrient-rich and oxygen-depleted water mass consisting of modified Antarctic Bottom Water that generates from the Antarctic (Manighetti and McCave, 1995). It is believed that during glacial times the production of NADW ceased, whereas the production of intermediate water, i.e., the Glacial North Atlantic Intermediate Water (GNAIW)

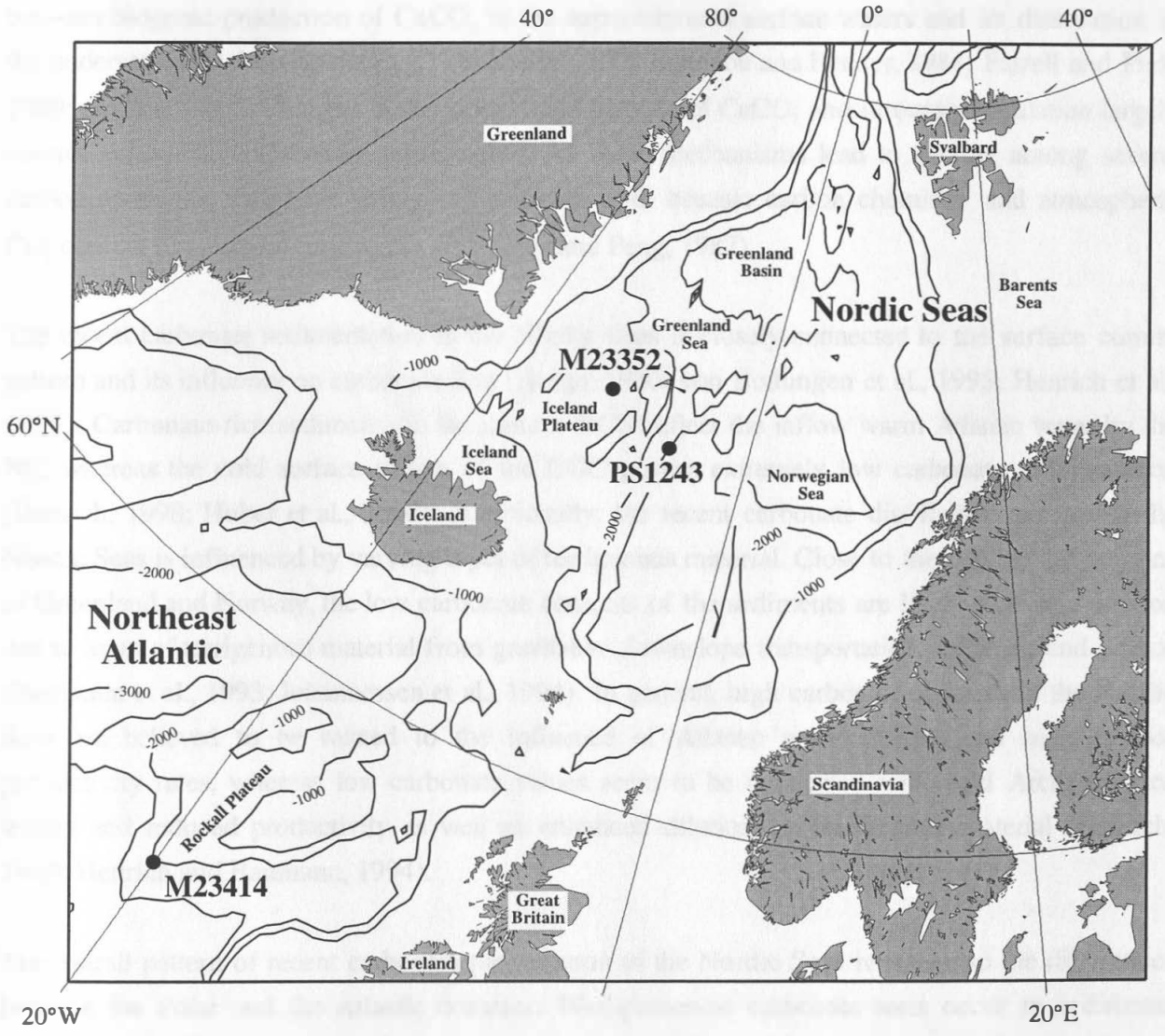

Fig. I-2: Geographical position of investitgated core sites in the Northeast Atlantic and the Nordic Seas. Water depth is in m.

was enhanced (Boyle and Keigwin, 1987; Oppo and Fairbanks, 1987; Venz et al., 1999). During the late Pleistocene Site M23414 was bathed by the well ventilated water masses of either LNADW during interglacial or GNAIW during glacial times (Venz et al., 1999). At present, the Rockall Plateau area is directly underlying the NAC (Fig. I-1).

I.3. The marine carbonate system

Calcium carbonate is a major component of deep-sea sediments and a large and reactive carbon reservoir. Accordingly, its accumulation and dissolution on the seafloor plays an important role in the global carbon cycle. The distribution of calcite in deep-sea sediments is determined by the kinetics of carbonate dissolution competing with the rate of carbonate burial, i.e., by the balance between biogenic production of $CaCO_3$ in the supersaturated surface waters and its dissolution in the undersaturated deep waters (e.g., Takahashi, 1975; Emerson and Bender, 1981; Farrell and Prell, 1989; Archer, 1991). Changes in the global mass balance of $CaCO_3$ and in ocean circulation largely control variations in carbonate preservation. As these mechanisms lead to cycling among several carbon reservoirs, they have strong influence on both oceanic carbon chemistry and atmospheric CO_2 content over orbital time scales (Broecker and Peng, 1987).

The recent carbonate sedimentation in the Nordic Seas is closely connected to the surface current pattern and its influence on carbonate flux (Honjo, 1990; von Bodungen et al., 1995; Henrich et al., 1995). Carbonate-rich sediments in the eastern NGS reflect the inflow warm Atlantic water by the NC, whereas the cold surface waters of the EGC govern extremely low carbonate sedimentation (Henrich, 1998; Huber et al., 2000). Additionally, the recent carbonate distribution pattern of the Nordic Seas is influenced by varying input of terrigenous material. Close to the continental margins of Greenland and Norway, the low carbonate contents of the sediments are likely to reflect dilution due to input of terrigenous material from gravitative downslope transportation, icebergs, and sea-ice (Baumann et al., 1993; Johannessen et al., 1994). In general, high carbonate contents in the Nordic Seas are believed to be related to the influence of Atlantic water masses and high surface productivity rates, whereas low carbonate values seem to be connected with cold Arctic surface waters and reduced productivity as well as enhanced dilution by terrigenous material (Henrich, 1989; Henrich and Baumann, 1994).

The overall pattern of recent carbonate preservation in the Nordic Seas reveals also the differences between the Polar and the Atlantic domains: Well-preserved carbonate tests occur in sediments underlying ventilated Atlantic surface waters (Henrich, 1998), as the pore waters of these carbonate-rich sediments will be supersaturated with respect to calcite (Huber et al., 2000). In contrast, modern carbonate tests that are influenced by the EGC show increased dissolution (Helmke, 1996). Here, ice cover in the Polar Domain throughout most of the year causes low surface water production and

low carbonate rain to the seafloor (Honjo, 1990), consequently the pore waters are undersaturated with respect to calcite. Enhanced recent carbonate dissolution is also reported from sites near the continental margins (Huber et al., 2000) and in the deep Greenland Basin. An enhanced dissolution close to continental margins can be explained by increased supply of organic matter and thus high release of respirative CO_2, whereas carbonate tests from the deep Greenland Basin were deposited close to the calcite saturation horizon in the Nordic Seas (Huber et al., 2000). In general, carbonate dissolution of deep-sea sediments in the Nordic Seas can be triggered by significant changes in the chemistry of deep-waters, i.e., by a reduction of deep-water renewal. A disturbance of deep-water renewal would decrease the formation and transport of oxygen-rich water masses in the NGS and imply reduced ventilation and aging of bottom water masses in the Nordic Seas (Henrich, 1986). Both study sites from the Nordic Seas (water depth about 1800 and 2700 m) were positioned above the calcite saturation horizon, i.e., the calcite lysocline, during the last five glacial-interglacial cycles. Thus, the late Pleistocene carbonate preservation mode of M23352 and PS1243 will also be influenced by supralysoclinal processes, e.g., by glacial-interglacial changes in regional surface bioproductivity and differences in the rain ratio between organic carbon and carbonate particles that reach the seafloor.

I.4. Color of marine sediments

Much information about oceanographic and sedimentological conditions at the time of sediment deposition is recorded directly in the color of fresh marine sediments. As optical scanning of sediment cores provides a fast and non-invasive paleoceanographic method, much effort has been taken into the development of technical systems to determine sediment color variations (Mix et al., 1992, 1995; Schaaf and Thurow, 1994; Merrill and Beck, 1995; Ortiz and Rack, 1999).

Color measurements have the potential to monitor a wide variety of sedimentological environments: For example, the ratio between goethite and goethite + hematite, which serves as a proxy for continental climate, as it increases with increasing precipitation, was recorded with sediment color measurements from Ocean Drilling Program (ODP) Leg 154 and used to characterize late-Pleistocene wet periods in the Amazon lowlands (Harris and Mix, 1999). Diffuse reflectance spectra analysis of Quaternary sediments from the Atlantic and Pacific Oceans suggest that sediment color can be used as a proxy for estimating organic carbon and opal contents (Balsam et al., 1996). However, as color records are strongly dependent on the sedimentary system of the area under study, interpretation of sediment color is not a stand-alone method, but has to be used together with further sedimentological proxy data.

The hand-held, Minolta CM-2002 spectrophotometer (Minolta Corporation, 1994)used in this study is a rather inexpensive, easily maintained instrument that provides extreme mobility. ODP, the

French research vessel Marion Dufresne, as part of the IMAGES program, and several German research vessels operate with the Minolta CM-2002. When used carefully to avoid measurement error during hand-held operation color data from the Minolta CM-2002 can resolve information at the 1-cm scale indicating that century-scale and even decadal-scale fluctuations are likely to be investigated (Chapman and Shackleton, 1998).

I.5. Individual studies

This thesis comprises four manuscripts (Chapter III-VI) which have been submitted to peer-reviewed scientific journals. Together with the references from Chapters I and II the references from each of this manuscripts have been combined into one reference list:

Chapter III:

Glacial-interglacial carbonate preservation records in the Nordic Seas

Jan P. Helmke and Henning A. Bauch; *Global and Planetary Change*, in press.

A new method to investigate carbonate dissolution was used to determine the glacial-interglacial carbonate preservation pattern of deep-sea sediments from the Nordic Seas during the last 500,000 years. This new methodical approach is a combination of weight and color measurements as well as Scanning Electron Microscope analyses on planktic foraminiferal tests. The results were discussed with carbonate preservation records from the Atlantic and Indo-Pacific Oceans.

Chapter IV:

Glacial-interglacial relationship between carbonate components and sediment reflectance in the North Atlantic

Jan P. Helmke and Henning A. Bauch; submitted to *Geo-Marine Letters*

The purpose of this manuscript was to qualify the factors that govern the relation between carbonate content and sediment lightness in the North Atlantic during glacial-interglacial times. Therefore, a detailed analysis of the coarse (>20 μm) and the fine (<20 μm) carbonate fraction from a Northeast Atlantic sediment core was carried out. Moreover, the influence of changing carbonate preservation on sediment lightness was discussed.

Chapter V:

Sediment-color record from the Northeast Atlantic reveals patterns of millennial-scale climate variability during the last 500,000 years

Jan P. Helmke, Michael Schulz and Henning A. Bauch; to be submitted to *Quaternary Research*

For the first time, a marine sediment color record was used to give insight into the evolution of climate change on millennial time scales throughout the last five climate cycles. Spectral analysis was applied to a red-green color record from Northeast Atlantic sediments to reveal variations in the

amplitude of millennial-scale variability during the last 500,000 years. The patterns of variability were then linked to changes in continental ice mass.

Chapter VI:

Comparison of glacial and interglacial conditions between the polar and subpolar North Atlantic Region over the last five climatic cycles

Jan P. Helmke and Henning A. Bauch; to be submitted to *Paleoceanography*

Sedimentological and geochemical proxy records of sediment cores from the Northeast Atlantic and the Nordic Seas were compared to evaluate the glacial and interglacial conditions between the areas under study during the last five climate cycles. The records were used to reveal synchroneity or asynchroneity in climatic behaviour between the subpolar and polar North Atlantic.

Chapter II - Material and strategy

II.1. Sample material

Seven sediment cores (Tab. II-1, Fig. I-2) from the Northeast Atlantic Site M23414 (cruise Meteor 17; Suess & Altenbach, 1992) and the Nordic Seas Sites PS1243 (cruise Arktis 2; Augstein et al., 1984) and M23352 (cruise Meteor 7; Hirschleber et al., 1988) were investigated:

Tab. II-1:

Core	Corer	Latitude	Longitude	Water Depth (m)	Recovery (cm)
PS1243-2	Trigger box core	69°22,5´N	06°31,3´W	2710	49
PS1243-1	Gravity core	69°22,3´N	06°32,4´W	2712	767
M23352-2	Trigger box core	70°00,5´N	12°25,5´W	1819	35
M23352-3	Kasten core	70°00,4´N	12°25,8´W	1822	826
M23414-6	Trigger box core	53°32,2´N	20°17,4´W	2201	36
M23414-8	Gravity core	53°32,3´N	20°17,5´W	2199	1339
M23414-9	Kasten core	53°32,2´N	20°17,3´W	2196	908

In the course of previous investigations sediment samples of the trigger box core M23414-6 and the upper 650 cm of the kasten core M23414-9 were taken at sampling intervals of 1 and 2.5 cm, respectively (Nees, 1997; Didié and Bauch, 2000). The lower about 2.5 m of the kasten core (from 651 cm core depth down to the core base) and the lower about 6 m of the gravity core M23414-8 (from 720 cm core depth down to the core base) were sampled at 2.5 cm intervals. Sediment lightness and carbonate records were taken to produce a composite record of Site M23414 (Fig. II-1; M23414-8 is corrected by +75 cm with respect to M23414-9). All sediment samples were freeze-dried and washed over a 63 µm sieve. After drying of the >63 µm residues they were sieved into the subfractions 63-125, 125-250, 250-500, and >500 µm for further sedimentological, micropaleontological, and geochemical investigation.

Both cores from the Nordic Seas have previously been sampled at intervals between 1 and 10 cm (Birgisdottir, 1991; Henrich, 1992, 1998; Bauch et al., 2000a, 2000b).

II.2. Stratigraphy

Stratigraphy of the Northeast Atlantic site is based on the planktic $\delta^{18}O$ record of *Globigerina bulloides* (data partly from Jung, 1996). In Chapter III benthic oxygen isotopes of *Cibicidoides wuellerstorfi* were used for stratigraphy of core M23414 (data from Jung, 1996). Due to the good agreement between planktic isotopes and sediment lightness at the Rockall Plateau site the

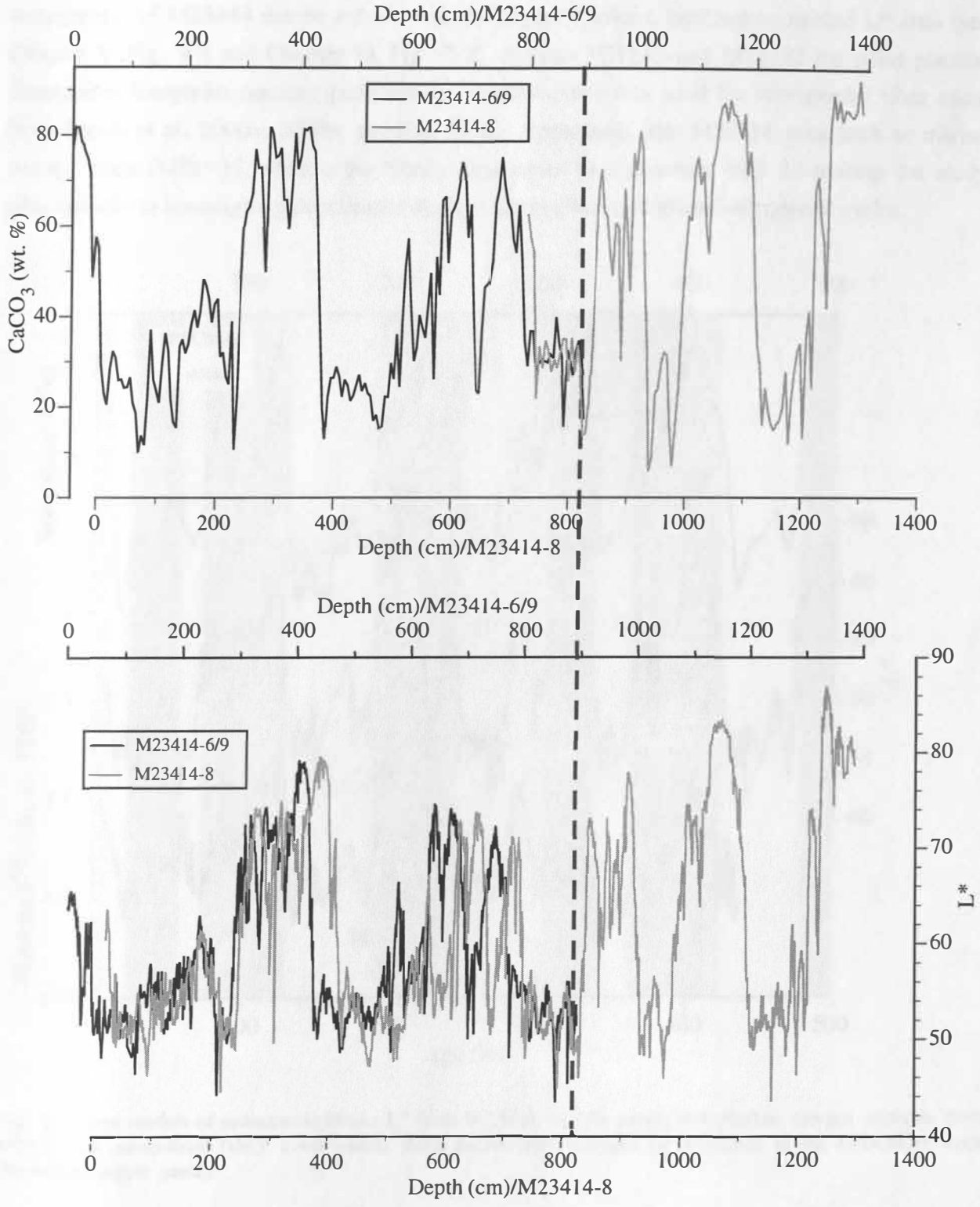

Fig. II-1: Correlation between the carbonate (weight% of bulk samples, upper panel) and the L* (lower panel) records of composite core M23414–6/9 (black line; original depth of M23414-9 is corrected by + 6 cm with respect to trigger box core M23414-6) and M23414-8 (gray line). Dotted dark gray line denotes point of correlation between the two cores. In composite core M23414 the original depth of M23414-8 (from 820 cm to the core base) is corrected by + 75 cm with respect to M23414-6/9.

stratigraphy of M23414 can be refined with the higher resolved, centimeter-sampled L* data (see Chapter V, Fig. V-1 and Chapter VI, Fig VI-2). At Sites PS1243 and M23352 the polar planktic foraminifer *Neogloboquadrina pachyderma* sinistral (sin.) was used for stratigraphy (data taken from Bauch et al., 2000a; 2000b; see Fig. IV-5). Apparently, Site M23414 goes back to marine isotope stage (MIS) 13, whereas the Nordic Seas cores both penetrate MIS 12 making the study sites suitable to investigate paleoclimatic changes during the last 5 glacial-interglacial cycles.

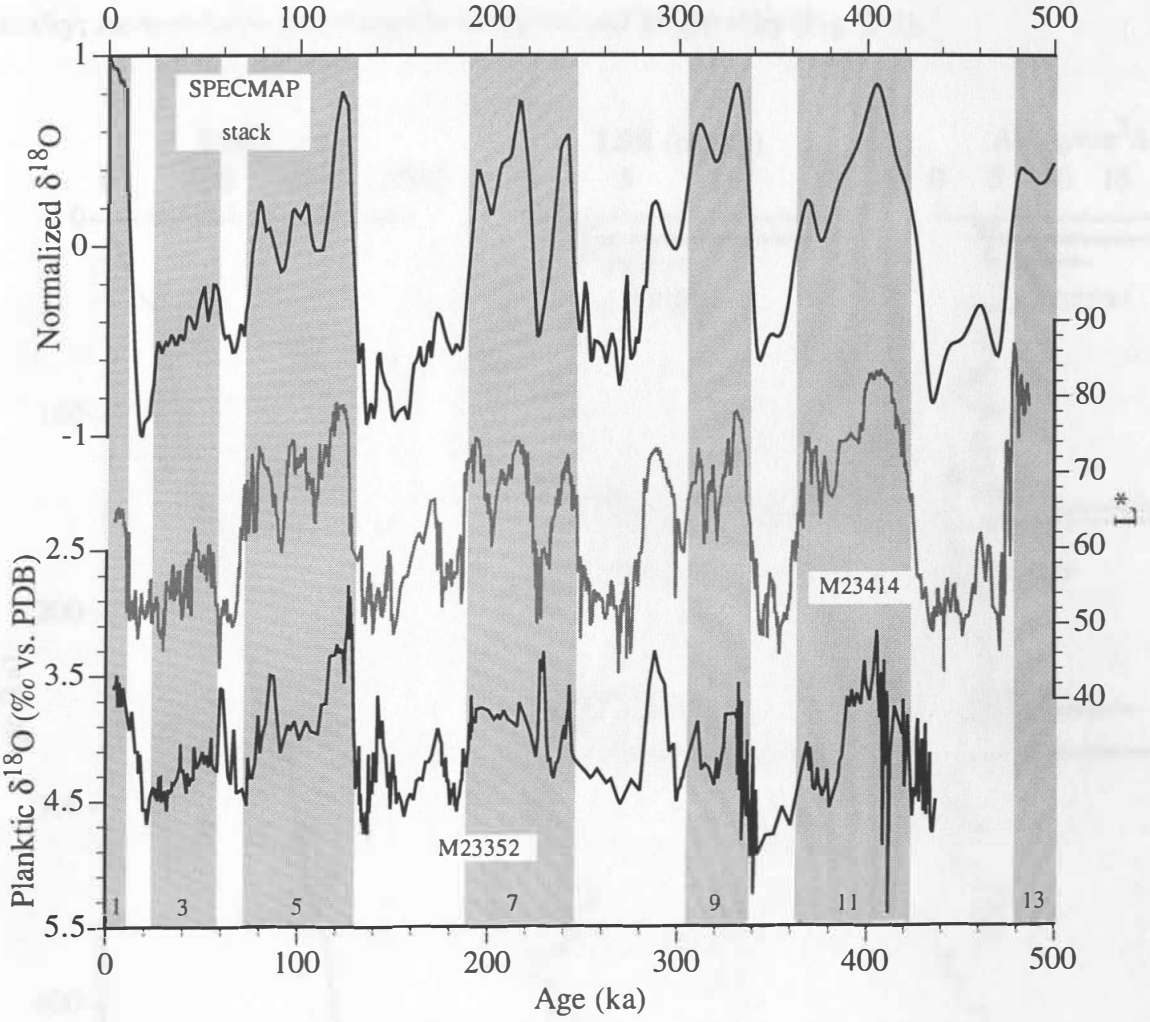

Fig. II-2: Age models of sediment lightness L* from M23414 (middle panel) and planktic oxygen isotopes from M23352 (*N. pachyderma* (sin.), lower panel). Both records were produced by alignment to the SPECMAP-stack chronology (upper panel).

Ages were assigned to the composite core M23414 by correlation of the centimeter-sampled lightness record to the stacked SPECMAP oxygen isotope chronology (Imbrie et al., 1984; Martinson et al., 1987) using the software AnalySeries (Fig. II-2). Between the stratigraphic correlation levels, the sedimentation rate was assumed to be constant and linear interpolation was applied to produce the depth-age relations of the M23414-proxy data lightness L*, red-green color

a*, $CaCO_3$, and ice-rafted debris (IRD) (see Chapters V and VI). In the upper part of the record, 4 AMS ^{14}C ages (C. Didié, unpubl.), which were converted into calendar ages using CALIB 4.1.2. (Stuiver et al., 1998) and the calibration model of Voelker et al. (1998), were included. Ages of Heinrich events H 1-6 (according to Sarnthein et al., in press) were also used to refine the uppermost part of the record. The positions of H 1-6 at Site M23414 have been previously identified by determining the concentration of lithic grains in the dry residues of size fraction >250 µm (Didié and Bauch, 2000). Average sedimentation rates of M23414 range between 0.25 and 14.5 cm/ky; Accumulation rates range between 0.4 and 24 g/cm²/ky (Fig. II-3).

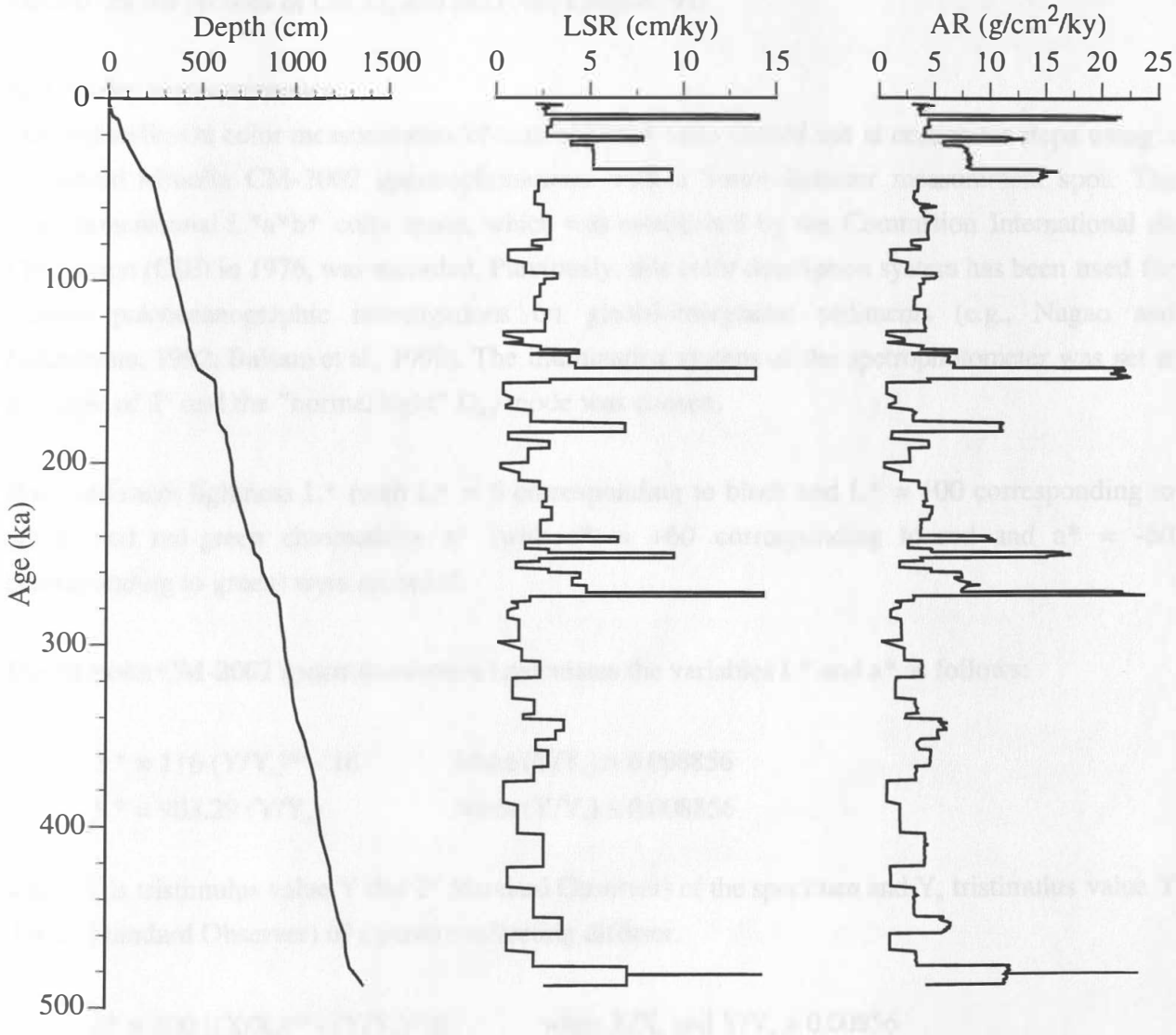

Fig. II-3. Age/depth control, linear sedimentation rates (LSR), and accumulation rates (AR) of Site M23414.

The age model for the oxygen isotope record of M23352 (sample resolution 1-4 cm) was produced likewise by synchronization to the SPECMAP stack (Fig. II-2). The age model of the younger part was refined by 7 AMS ^{14}C ages (C. Didié, unpubl.; converted using CALIB 4.1.2.) and by including the age of H 6 (according to Sarnthein et al., in press; identification of H 6 as described for core M23414) as well as the age of the Vedde ash layer (following Voelker, 1999; position of the ash layer according to Bauch, unpubl.). Prior to the alignment, the data were smoothed with a 14-point least square smooth. This was necessary to avoid misinterpretations of the lowermost part of the M23352 record, which is characterized by massive IRD-input and reveals atypical large scale fluctuations in isotope values. As for M23414, linear interpolation was used to establish the age models for the records of $CaCO_3$ and IRD (see Chapter VI).

II.3. Color measurements

Distinct sediment color measurements of core M23414 were carried out at centimeter steps using a hand-held Minolta CM-2002 spectrophotometer with a 8-mm-diameter measurement spot. The three-dimensional L*a*b* color space, which was established by the Commision International de l'Eclairage (CIE) in 1976, was recorded. Previously, this color description system has been used for various paleoceanographic investigations on glacial-interglacial sediments (e.g., Nagao and Nakashima, 1992; Balsam et al., 1999). The illumination system of the spetrophotometer was set at an angle of 2° and the "normal light" D_{65}-mode was chosen.

Both sediment lightness L* (with L* = 0 corresponding to black and L* = 100 corresponding to white) and red-green chromaticity a* (with a* = +60 corresponding to red and a* = -60 corresponding to green) were recorded.

The Minolta CM-2002 spectrophotometer calculates the variables L* and a* as follows:

$$L^* = 116\,(Y/Y_n)^{1/3} - 16 \qquad \text{when } (Y/Y_n) > 0.008856$$
$$L^* = 903.29\,(Y/Y_n) \qquad \text{when } (Y/Y_n) \leq 0.008856$$

where Y is tristimulus value Y (for 2° Standard Observer) of the specimen and Y_n tristimulus value Y (for 2° Standard Observer) of a perfect reflecting diffuser.

$$a^* = 500\,[(X/X_n)^{1/3} - (Y/Y_n)^{1/3})] \qquad \text{when } X/X_n \text{ and } Y/Y_n > 0.00856$$
$$a^* = 500\,[7.787\,(X/X_n) + 16/116 - 7.787\,(Y/Y_n) + 16/116] \qquad \text{when } X/X_n \text{ and } Y/Y_n < 0.00856$$

where X and Y are tristimulus values X and Y (for 2° Standard Observer) of the specimen and X_n and Y_n tristimulus value Y (for 2° Standard Observer) of a perfect reflecting diffuser.

Repeated measurements of the white calibration standard of CM-2002 demonstrates that the spectrophotometer provides a precise tool for measuring lightness and red-green chromaticity. Mean and standard deviation σ of 50 measurements were L* 96.63 ±0.01 and a* -0.11 ±0.01. The variations in the measured color of the sediments obtained L* values between 43.52 and 86.98 and a* values between -0.52 and 4.19, thus, the signal/noise ratio of the instrument is large. To avoid long-term instrumental drift (Chapman and Shackleton, 1998) the spectrophotometer was recalibrated every 200 measurements.

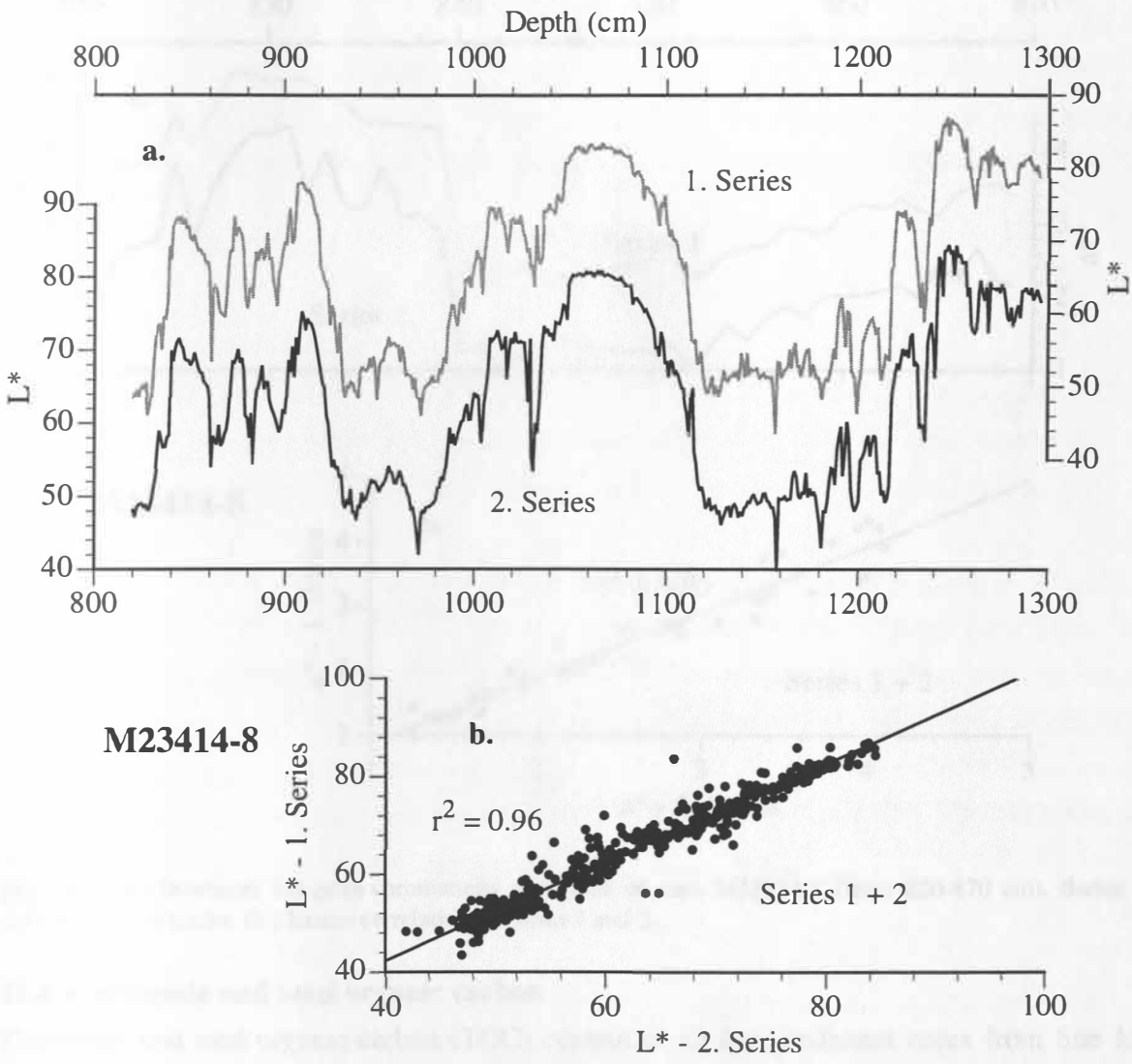

Fig. II-4: (a.) Downcore lightness variations of core M23414-8 (from 820 cm to the core base). Series 1 and 2 follow separate tracks. (b.) Linear correlation of Series 1 and 2.

Additionally, the precision of the sediment color measurements was tested using a set of 10 repeated measurements at 5 single positions in the core. The mean standard deviation of these sample sets is 0.06 for L* and 0.01 for a*. Two separate tracks of downcore lightness measurements on the lower 5 m of core M23414-8 show negligible differences between the records and reveal a correlation coefficient of 0.96 (Fig. II-4). Two shorter tracks of red-green chromaticity (Series 1 and 2 followed separate tracks) also obtain a high correlation coefficient of 0.95 (Fig. II-5). These comparisons suggest that lateral downcore color changes, e.g., caused by bioturbation, have a rather small effect on the measurements and that the centimeter-sampled color data reflect real features of the sediment record rather than analytical noise.

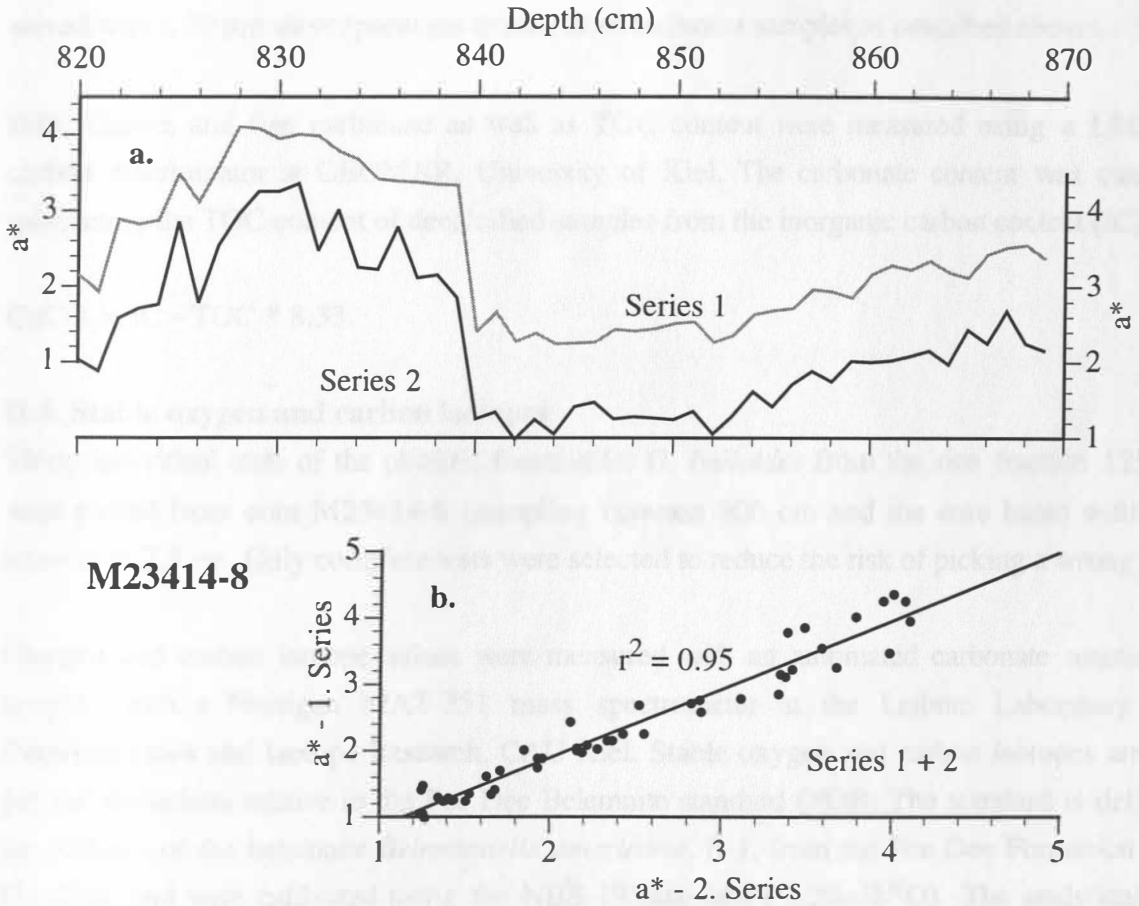

Fig. II-5: (a.) Downcore red-green chromaticity variations of core M23414-8 (from 820-870 cm). Series 1 and 2 follow separate tracks. (b.) Linear correlation of Series 1 and 2.

II.4. Carbonate and total organic carbon

Carbonate and total organic carbon (TOC) content of all three sediment cores from Site M23414 were analyzed at a sampling interval of 5 cm. All dry sediment residues were grinded using a hand-held pestle and mortar to provide a well homogenized sample for the quantitative elemental determination. For the TOC analyses the samples had to be decalcified prior to measurement. For

this purpose a few drops of hydrochlorid acid were added several times to the samples until the whole calcium carbonate was removed an no further reaction took place. To accelerate the reaction the samples were placed on a warm plate. Each sample was measured twice to reduce measurement errors by minimizing deviations, as the results were rejected if two measurements of the same sample differed by more than 0.2%.

As the biogenic component of the >20 µm fraction consists mainly of foraminifers while the <20 µm fraction is composed mostly of coccoliths, these fractions will be refered to as coarse and fine, respectively. It is recognized that the <20 µm fraction consists partly of detrital carbonate. In order to measure the coarse and fine carbonate content parts of the sampled sediments had to be wet-sieved with a 20 µm sieve (previous treatment of sediment samples as described above).

Bulk, coarse, and fine carbonate as well as TOC content were measured using a LECO C-200 carbon determinator at GEOMAR, University of Kiel. The carbonate content was calculated by subtracting the TOC content of decalcified samples from the inorganic carbon content (IC):

$CaCO_3 = IC - TOC * 8.33.$

II.5. Stable oxygen and carbon isotopes

Thirty individual tests of the planktic foraminifer *G. bulloides* from the size fraction 125-250 µm were picked from core M23414-8 (sampling between 800 cm and the core base) with a sample interval of 2.5 cm. Only complete tests were selected to reduce the risk of picking a wrong species.

Oxygen and carbon isotope values were measured with an automated carbonate reaction device, coupled with a Finnigan MAT-251 mass spectrometer at the Leibniz Laboratory for Age Determinations and Isotope Research, CAU Kiel. Stable oxygen and carbon isotopes are given as per mil deviations relative to the Pee Dee Belemnite standard (PDB; The standard is defined from the rostrum of the belemnite *Beleminitella americana*, B-1, from the Pee Dee Formation of South Carolina) and were calibrated using the NBS-19 standard (-2.2‰ $\delta^{18}O$). The analytical standard deviation is ±0.06‰ and ±0.03‰ for $\delta^{18}O$ and $\delta^{13}C$, respectively.

II.6. Ice-rafted debris (IRD)

To determine the amount of IRD at Site M23414-8 lithic grains in the size fraction >250 µm were counted with a spacing of 2.5 cm from 820 cm core depth down to the core base and are expressed as lithic grains per gram dry sediment. Investigations on the amount of IRD in the entire trigger box

and kasten cores have previously been carried out using the identical sampling scheme (Didié and Bauch, 2000).

II.7. Scanning Electron Microscope (SEM)

Surface structures of planktic foraminiferal tests using *N. pachyderma* (sin.) were investigated with the SEM at GEOMAR, University of Kiel to characterize glacial-interglacial carbonate preservation changes in cores PS1243 and M23352. In the Nordic Seas the left-coiled variety of *N. pachyderma* is the only species that occurs in both glacial and interglacial periods and therefore available for carbonate preservation analyses. Two principal surface textures of *N. pachyderma* (sin.) have to be distinguished: The reticulate form with a microcrystalline ultrastructure representing an earlier stage of calcification and the crystaline form with a secondary calcified crust that leads to a coarse crystalline ultrastructure. Most foraminiferal test are transition forms between these two types with the youngest chamber being still reticulate while the older chambers are crystalline. To avoid ambigous results only the oldest chambers on the umbilical side of the tests, which were always completely calcified, were analyzed. Previous SEM investigations on the ultrastructure of planktic foraminiferal tests from the Nordic Seas (e.g., Henrich, 1986, 1998) indicated good to excellent carbonate preservation during glacial and interglacial times, with increased corrosion being limited to short episodes, which were linked to diamiction horizons in the sediment. These results are partly in contrast to the SEM records presented in this study (see Chapter III). This may be due to the differences in the preselection of the examined tests: In contrast to this study, the results of Henrich (e.g., 1986) are a compilation of investigations on foraminiferal tests using both the reticulate and the crystalline form. Moreover, these previous studies have a lower average sample resolution of only 10 cm.

Based on the planktic oxygen isotope stratigraphy of PS1243 and M23352 (Bauch et al., 2000a; Bauch et al., 2000b) all samples were selected from depth intervals that respresent full glacial or interglacial periods, i.e., MIS 1, 2, 5.5, 6, 10, and 11. About 30 tests were randomly picked from various dry residues of the size fraction 125-250 µm and investigated with the SEM. The SEM analyses of corrosionial features on the ultrastructure of foraminiferal tests were used in combination with weight and color measurements to record downcore changes in carbonate preservation. The following successive steps in corrosion of the calcite crystals could be distinguished (see Appendix, Plate 1, Fig. III-4):

Step 1: Tests with sharp-edged, well preserved calcite crystals.
Step 2: First signs of corrosion of the coarse skalenoedra fabric with slight rounding of the crystal edges.

Step 3: Strong corrosion of the skalenoedra with loosening of the densley packed fabric of prisms and rounding of the crystal edges. Tests are still complete but can be easily disintegrated at this stage.

In general, carbonate corrosion at Sites PS1243 and M23352 is to low to produce ghost structures of the tests skalenoedra or even test fragmentation.

II.8. Weight and color measurements of foraminiferal tests

Weight and lightness of planktic foraminiferal tests of *N. pachyderma* (sin.) from cores PS1243 and M23352 were measured at sampling intervals between 1 and 10 cm. Weight measurements on varying amounts of foraminiferal specimens from size fractions 125-250 and 224-250 µm were determined using a microbalance (standard deviation is ±0.03 mg). The surface of all selected tests had no visible contamination of the surface with silt material. The tests were picked regardless of their surface texture, i.e., reticulate or crystalline morphotype.

Color of the previously weighed foraminiferal tests was measured using a Minolta CM-2002 spectrophotometer and was recorded as lightness L* in the L*a*b* color system. A cone-shaped depression (0.3 cm diameter) in a black metallic standard (mean and standard deviation of 50 measurements were L* 19.87 ±0.05) attached to the illumination system of the spectrophotometer was used to carry out the color measurements of foraminiferal tests. Lightness of the foraminiferal tests (500 foraminifers, 224-250 µm) and the black standard varies between 35.63 and 47.31, hence, as described above for the sediment measurements, the signal/noise ratio is large. Precision of the foraminiferal test measurements was calculated using 10 repeated measurements of 5 randomly selected tests (500 foraminifers, 224-250 µm). Mean standard deviation of the lightness from these set of tests is 0.11.

II.9. X-ray-fluorescence-spectrometry

This method can be used to give insight into the elemental composition of sediment samples. In this study it was used exclusively to investigate changes in the iron content of the sediments from Site M23414.

All analyses were carried out on about 1 gram of fine (<20 µm) and coarse (>20 µm) fraction sediment samples using the PW 1480 X-ray-flourescence-spectrometer at GEOMAR, University of Kiel. Prior to the measurements the samples were homogenized by grinding with a hand-held pestle and mortar and than oven dried at 110°. In a next step, the samples were vitrifed at a maximum temperature of 1150° C, additionally about 3.6 gram of flux component had to be added to the sediment samples to lower the melting points of some of the elements the samples contained. After

cooling of a melted sample flourescence of particular elements was stimulated with the X-ray source of the PW 1480. Whether the sample consisted a certain element could be identified by seting an internal crystal at the diffracted angel of the deflection peak of specific elements. The intensity of the diffracted angel of a X-ray peak was used to quantify the total amount of a specific element in the bulk sample. The analytical standard deviation for the Fe-analyses is ±0.4%.

II.10. Spectral analysis

In this study spectral analysis was applied to the sediment color record of Site M23414. Spectral analysis was performed using the software REDFIT (Schulz and Mudelsee, subm.), which allows direct processing of unevenly spaced time series. This program is based on the Lomb-Scargle Fourier transform (Lomb, 1976) for unevenly spaced time series in combination with a Welch-Overlapped-Segment-Averaging procedure (Welch, 1967). With this method a shortcoming of spectral analysis programs for evenly spaced time series, e.g., the Blackman-Tukey method (e.g., Jenkins and Watts, 1968), can be avoided: Interpolation of the unevenly time series may lead to an underestimation of the high frequency components in a spectrum, i.e., a 'reddening' of the spectrum (Horowitz, 1974, Schulz and Stattegger, 1997).

Time-dependent changes in the variance of the red-green-chromaticity color time series from Site M23414 was quantified using a sliding rectangular window, after high-pass filtering the unevenly spaced time-series (Rybicki and Press, 1995). The data were filtered with a cut-off frequency of 1/12 ky^{-1}. This is close to the accuracy of the age model from Site M23414, which is at least half the period of the precessional cycle. The width of the sliding rectangular window was 8 ky, thus offering a good compromise between statistical and systematic errors.

Chapter III: Glacial-interglacial carbonate preservation records in the Nordic Seas

Jan P. Helmke and Henning A. Bauch

III.1. Abstract

A combination of weight and lightness measurements as well as Scanning Electron Microscope (SEM) analyses on planktic foraminiferal tests from two sites in the Nordic Seas were used to investigate the pelagic carbonate preservation during the last 5 glacial-interglacial cycles. In general, a pattern showing good preservation during glacial times and enhanced corrosion during interglacial times can be observed. Marine Isotope Stage 11 (MIS 11) reveals the strongest corrosional features with estimated 45% total loss of foraminiferal carbonate before shell fragmentation. One reason for the enhanced interglacial corrosion may be a high regional surface productivity during these intervals, which led to increased dissolution rates in the deep sea driven by metabolic carbon dioxide. Yet, the carbonate preservation changes may also be linked to global changes in the marine carbonate system. Although the reason for the observed dissolution pattern in the Nordic Seas remains speculative, it is in phase with the rhythm of glacial-interglacial carbonate preservation in the Pacific Ocean but out of phase with the rest of the Atlantic. The data further support the hypothesis that much of the glacial decrease in atmospheric CO_2 may be attributed to changes in the alkalinity of the oceans.

III.2. Introduction

One key problem in interpreting past variations in the global carbon cycle is the massive decrease in atmospheric carbon dioxide during the last glacial period (Neftel et al., 1982; Barnola et al., 1987; Stauffer et al., 1998). The ocean is a large and sensitive carbon reservoir and, therefore, many studies on the origin of the glacial-interglacial atmospheric CO_2 changes have been focused on the marine carbonate system (e.g., Volk and Hoffert, 1985; Broecker and Peng, 1989, 1993; Archer and Maier-Reimer, 1994; Sanyal and Bijma, 1999; Broecker et al., 1999).

The pelagic $CaCO_3$ distribution in sediments is controlled by the balance between biogenic production in surface waters and dissolution in the deep sea (Catubig et al., 1998). Productivity processes determine the input of calcium carbonate but changes in the dissolution rate are mainly responsible for variations in calcium carbonate preservation. The dissolution rate of marine carbonate is dictated by the ratio of the in situ CO_3^{2-} ion concentration to the calcite saturation CO_3^{2-} ion concentration of sea water. Carbonate dissolution increases with increasing water depth because of the effects of hydrostatic pressure on the solubility of CO_2 (Hawley and Pytkowicz, 1969). Shallower water depths are supersaturated with respect to $CaCO_3$ and show only minor dissolution, whereas water masses of greater depth are undersaturated with respect to $CaCO_3$ and show complete dissolution. The crossover between these depth sections is called transition zone (e.g., Broecker and Peng, 1993). The top of the transition zone is defined by the lysocline, the shallowest depth where effects of carbonate dissolution are clearly visible, and the bottom by the Calcite Compensation Depth (CCD), the shallowest depth where the $CaCO_3$ is being completely dissolved.

The carbonate component of deep-sea sediments reveals a characteristic Pleistocene glacial-interglacial dissolution pattern. The Pacific and Indian Oceans show good glacial and poor interglacial carbonate preservation, with an estimated fluctuation in the water depth of the Pacific lysocline in the order of 400-800 m (Peterson and Prell, 1985; Farrell and Prell, 1991; Bassinot et al., 1994). Several investigations of carbonate preservation in the Atlantic (e.g., Crowley, 1983) showed evidence for stronger dissolution during glacial times. Estimates about the shallowing of the Atlantic lysocline during these dissolution pulses are still uncertain and vary between 300-500 m (Crowley, 1983; Howard and Prell, 1994) and more than 1000 m (Balsam, 1983). However, the interpretation of the data points to an out-of-phase preservation pattern between the Atlantic and Indo-Pacific ocean basins. Among the proposed explanations for a mechanism that can dramatically alter the alkalinity profile of the ocean and change the depth of the calcite saturation horizon by several hundred meters is the so called "coral reef hypothesis" (Berger, 1982; Opdyke and Walker, 1992). According to this scenario weathering and deposition of shallow water reef carbonate vary as a function of sea level, and trigger the glacial-interglacial input of alkalinity to the deep ocean.

Previous carbonate preservation analyses from the Nordic Seas (Henrich, 1998), the northermost part of the Atlantic Ocean, described good preservation within the past 300 kyr with peak interglacial carbonate preservation and dissolution pulses that were limited to short events during glacial times. Here we present new carbonate preservation records from the Nordic Seas using a new methodological approach in order to analyse the general Late Quaternary dissolution pattern. These records will then be discussed with carbonate preservation data from the Atlantic and Indo-Pacific Oceans.

III.3. Methods

Previously developed methods to describe carbonate dissolution involve establishing of a fragmentation index of planktic foraminifers or calculating the ratio between benthic and planktic foraminifers (Thunell, 1976; Diester-Haass, 1985; Le and Shackleton, 1992). Such methods work well for analyzing sediments with a strongly dissolved carbonate component but to estimate carbonate corrosion prior to foraminiferal test fragmentation other methods are needed.

We investigated two sediment cores from the Nordic Seas (Fig. III-1), PS1243 (69°22´N, 6°32´W, 2715 m water depth) and M23352 (70°0´N, 12°25´W, 1819 m water depth), each going back to MIS 12 (representing the past 5 glacial-interglacial cycles). Previous investigations on carbonate preservation in the Nordic Seas are based on corrosion indices of planktic foraminiferal tests using Scanning Electronic Microscope (SEM) analyses (Henrich, 1986, 1989; Baumann et al., 1996). We present here a new method to investigate carbonate corrosion of relatively well preserved foraminiferal specimens. This method is a combination of weight and lightness measurements as well as SEM analyses of planktic foraminiferal tests of the polar species *Neogloboquadrina pachyderma* (sin.). We used *N. pachyderma* (sin.) because this is by far the most common foraminiferal species in the Nordic Seas during the investigated time period.

The lightness of foraminiferal tests was measured using the Minolta CM-2002 spectrophotometer. Measurements were carried out on the level L* (%) in the L*a*b*-color space. All lightness measurements of foraminiferal tests were carried out using a small (0.3 cm diameter) cone-shaped depression in a black metallic standard that was attached to the illumination system of the spectrophotometer. For all lightness measurements the mean of five measurements was taken.

For 5 peak glacial and interglacial depth intervals 5000 specimens from a small size range (224-250 µm) were picked and weighed. In addition, 500 foraminifers from each sample were measured for lightness. For both study sites complete downcore records of foraminiferal test weight and

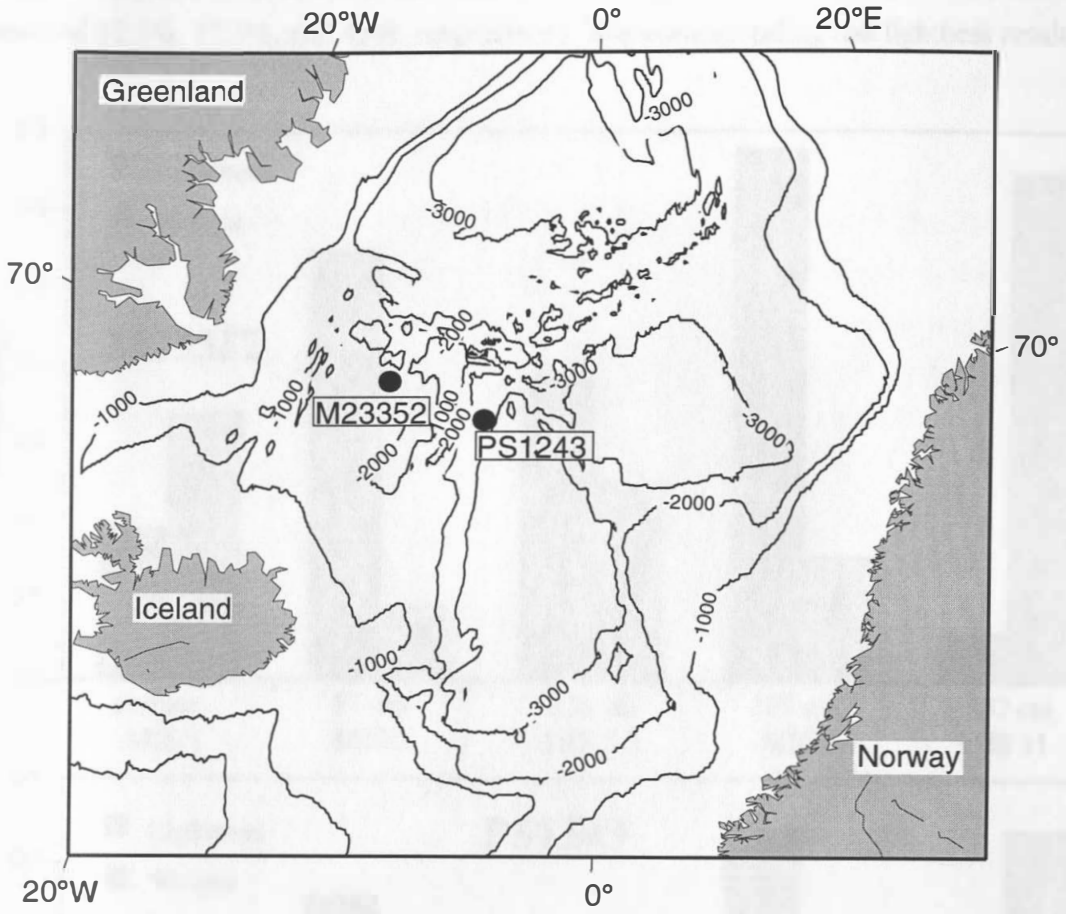

Fig. III-1: Overview of work area and position of studied sites (PS1243: 69°22´N, 6°32´W, 2715 m water depth and M23352: 70°0´N, 12°25´W, 1819 m water depth). Water depth is in m.

lightness were produced using 500 foraminifers from the size fraction 125-250 µm. These measurements have a sample interval of 1-5 cm in M23352 (with gaps between 526-586 and 672-737 cm, where the samples are barren or almost barren of *N. pachyderma* sinistral) and 5-10 cm in PS1243. Because variations in carbonate corrosion cause changes in the crystalline ultrastructure of foraminiferal tests, tests from different glacial and interglacial depth sections were also analysed with the SEM.

III.4. Results

III.4.1. Records of foraminiferal carbonate preservation

Carbonate corrosion essentially removes calcite from foraminiferal shells. Therefore, the loss in calcite should show up during weight measurements. In general, both weight records shown in Figure III-2 reveal a remarkably good agreement, if one considers the distance between the two sites and the difference in water depth of about 1000 m. The heaviest tests occur within glacial MIS 2 and

6. By comparison with MIS 2/6, the tests within interglacial MIS 1, 5.5, and 11 show mean weight losses of 32.5%, 17.5%, and 45%, respectively. The corresponding test lightness results reveal

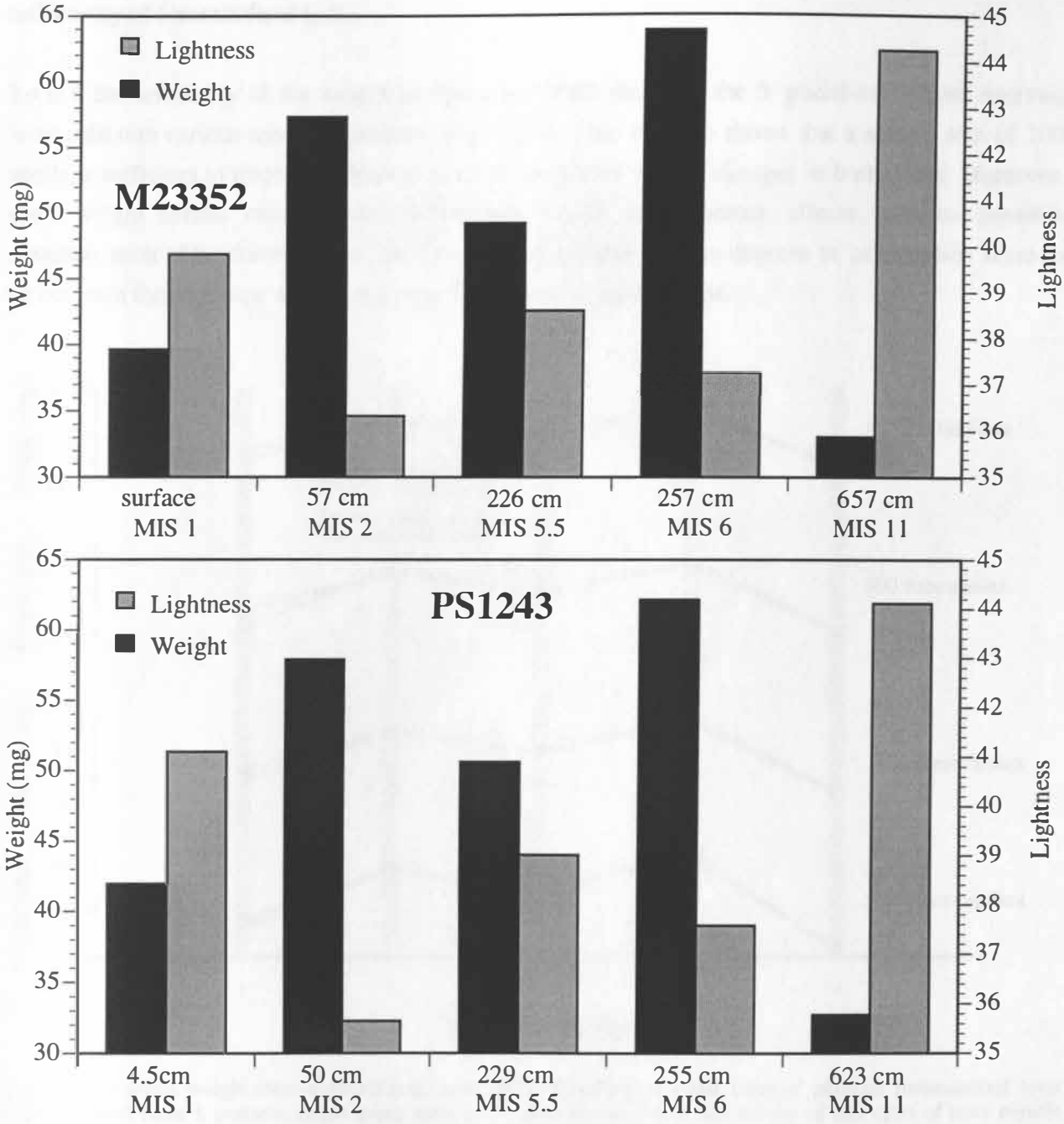

Fig. III-2: Comparison of weight and lightness data of tests of *N. pachyderma* sinistral (224-250 µm) from 5 glacial and interglacial stages. The black columns show the weight results (mg) of 5000 specimens, the columns the lightness results (L*%) of 500 specimens. The well preserved glacial tests (MIS 2 and 6) are characterized by highest weight and lowest lightness values. In contrast, the enhanced carbonate corrosion of MIS 11 is documented by lowest weight and highest lightness. Slightly corroded tests of the interglacials MIS 1 and 5.5 are somewhere between glacial tests and MIS 11. Estimates about the foraminiferal carbonate loss indicate a maximum value of 45% in comparison of MIS2/6 and MIS 11.

inverse trends. In other words, the glacial tests show lowest lightness values, whereas MIS 11 is characterized by highest test lightness values. This implicates that carbonate corrosion leads to changes in the surface structure of the calcite crystals and has a profound influence on the reflectivity of foraminiferal tests.

To test the sensitivity of the weight analyses, the 5000 shells of the 5 glacial-interglacial intervals were split into various smaller fractions (Fig. III-3). This exercise shows that a sample size of 100 shells is sufficient to trace the absolute glacial-interglacial weight changes in both cores. Moreover, shell weight results can be used to estimate calcite loss because effects such as possible contamination of the foraminiferal shell with silt material or varying degrees of calcification seem to be constant through time and have a minor influence on shell weight.

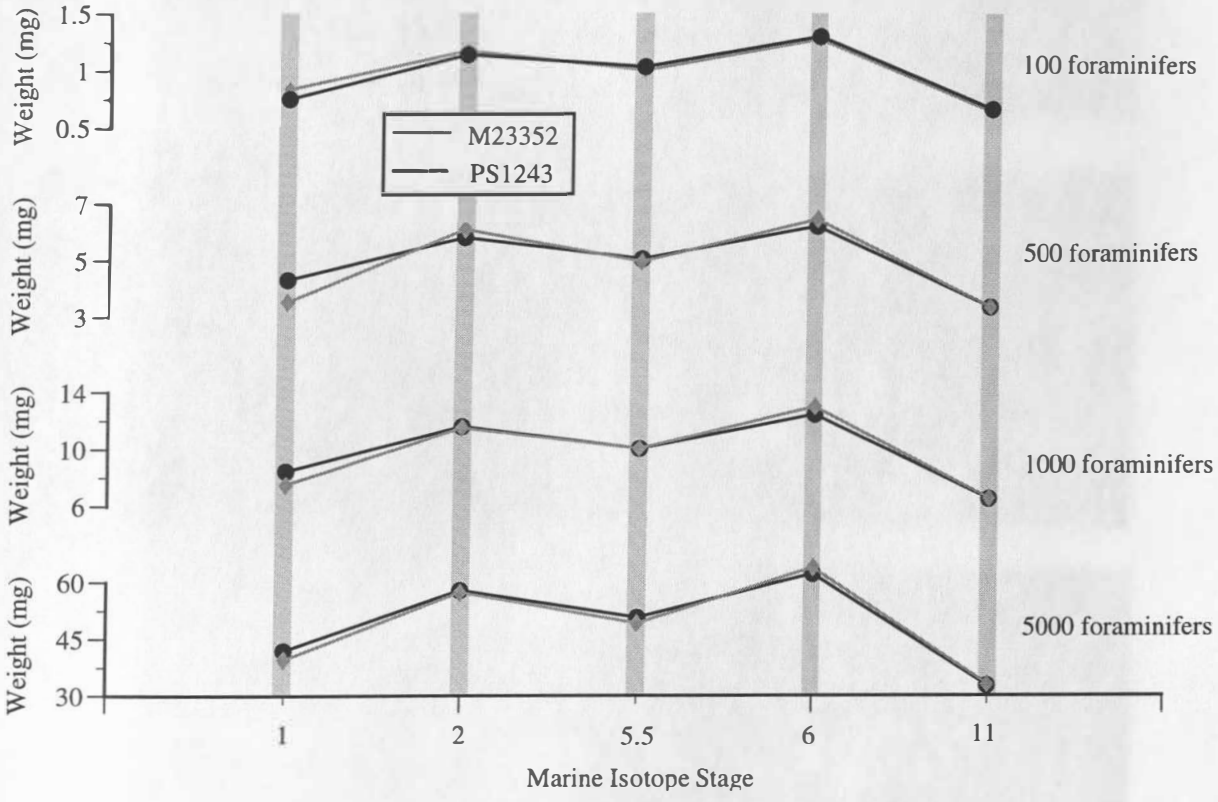

Fig. III-3: Various weight measurements (mg; note different scaling of value axis) of planktic foraminiferal tests (224-250 µm) from 5 isotopic stages using tests of *N. pachyderma* (sin.). The results of this split of tests reveals that the absolute foraminiferal test weight changes between different climatic intervals can be documented with a sample size of 100 foraminiferal specimens.

Tests of *N. pachyderma* (sin.) from glacial MIS 2/6 as well as from the interglacial MIS 1, 5.5, and 11 were examined with a SEM. In both cores the SEM analyses reveal a pattern of better glacial than interglacial preservation (Fig. III-4). The glacial foraminiferal tests seem to be unaffected by corrosion and show perfect calcite rhombohedra, whereas the interglacial tests (from MIS 1 and 5.5)

are characterized by early signs of carbonate corrosion, i.e., dissolution along the rims of the crystal edges with rounding of the crystal edges. Strongest corrosional features can be observed in MIS 11, where all calcite crystals are rounded and preferential dissolution around the chamber pores is visible. In MIS 11, the foraminiferal shells are very fragile and can be easily broken by any slight mechanical attack but the chamber structure is still complete. This weak chamber structure of specimens from MIS 11 verifies the observed strong weight loss in calcite during this period.

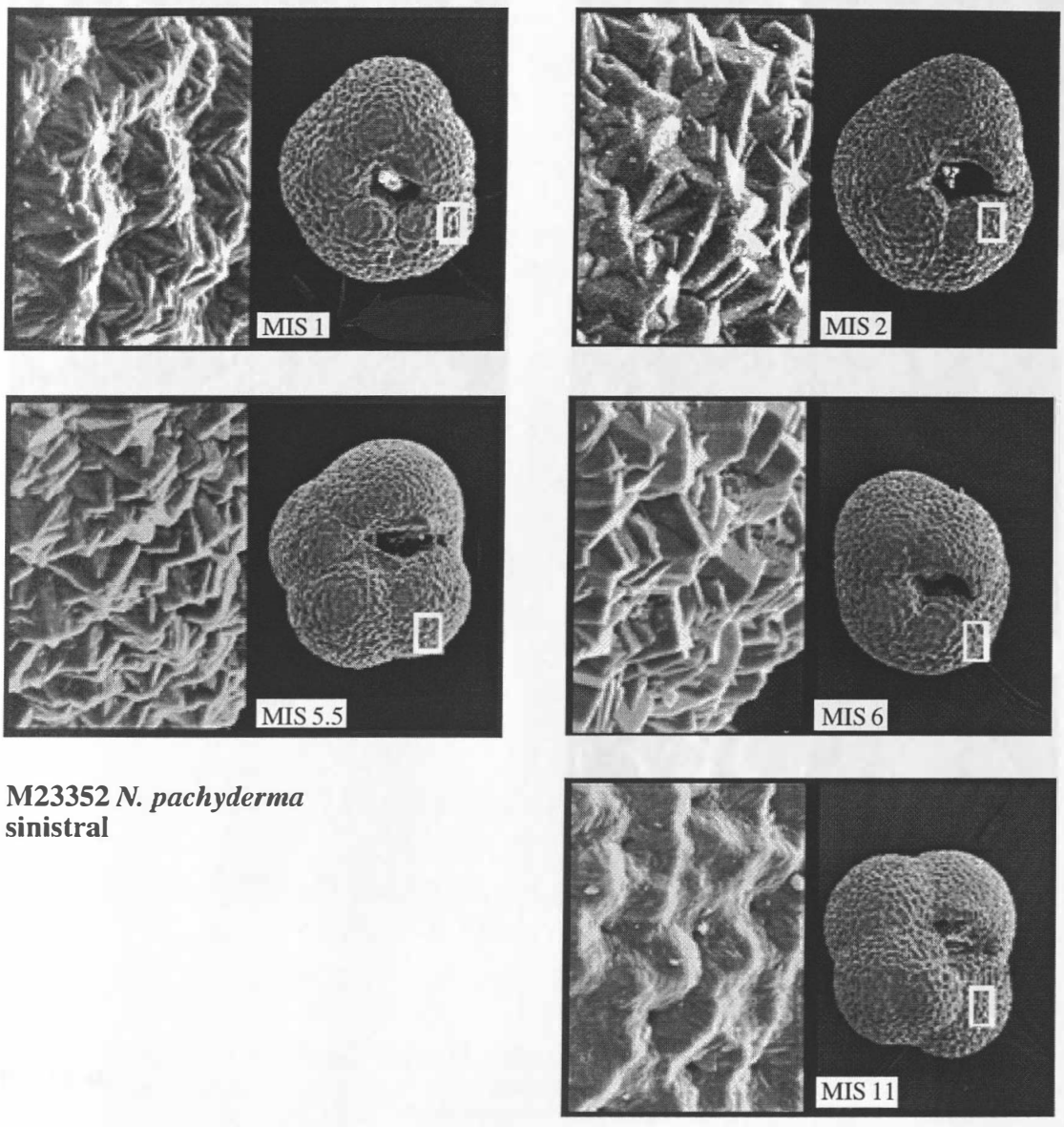

M23352 *N. pachyderma* sinistral

Fig. III-4: Comparison of various surface structures of *N. pachyderma* (sin.) tests from different depth sections taken from cores (a) M23352 and (b) PS1243. White rectangle indicates the part of the foraminiferal chamber that is magnified. Sharp-edged, well preserved calcite crystals are found on tests from glacial periods, whereas rounded crystals are observed on tests from MIS 11, indicating enhanced calcite corrosion. Tests from MIS 1 and 5.5 are characterized by first slight corrosional features.

III.4.2. Weight and lightness of foraminiferal tests

Figure III-5 shows the downcore records of foraminiferal test weight, reflectance and oxygen isotopic composition of *N. pachyderma* (sin.). Both weight records are marked by a decrease intest weight from MIS 6 to 1 with MIS 6 showing the highest weight results of the entire records. Two

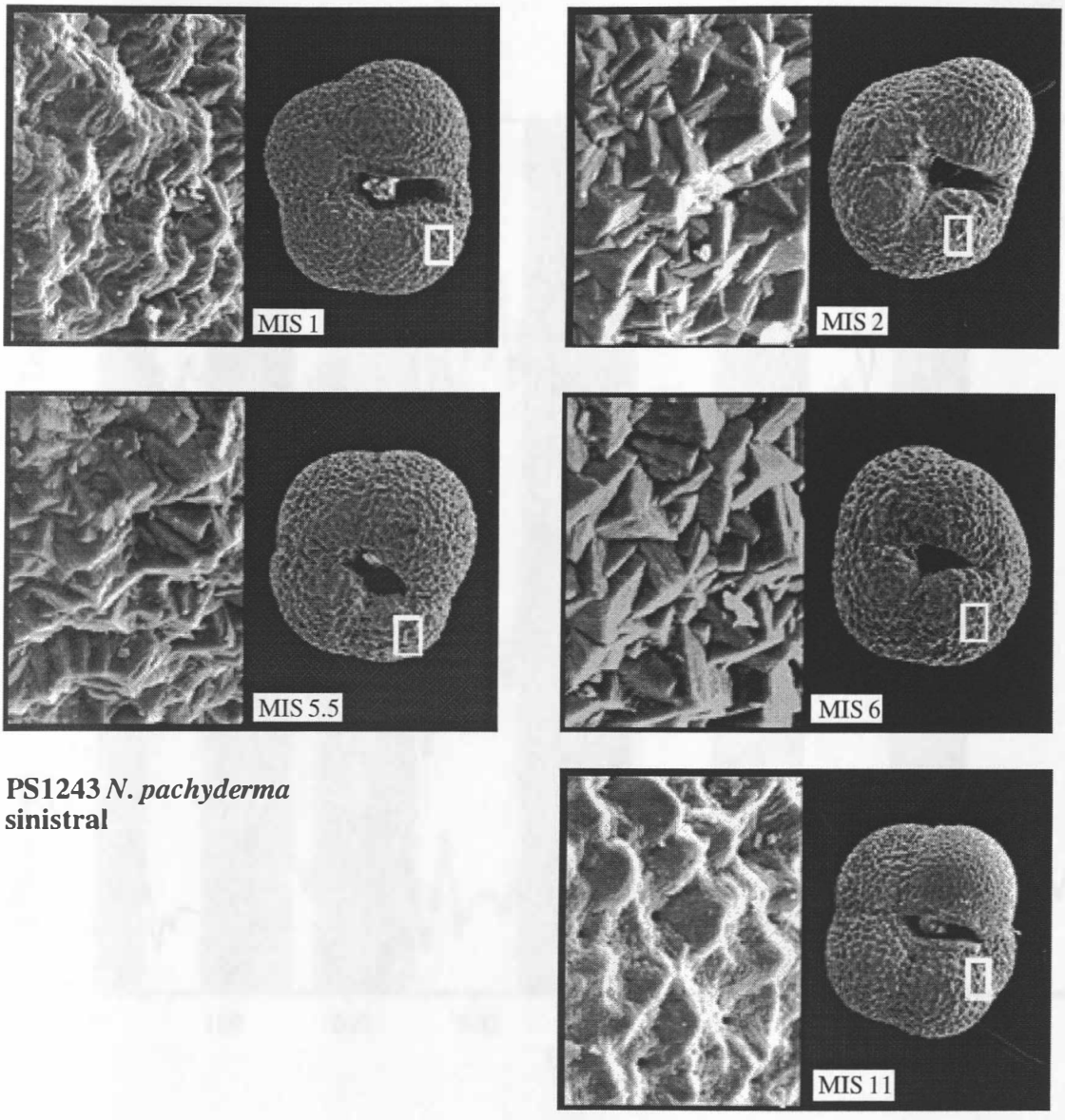

PS1243 *N. pachyderma* sinistral

Fig. III-4b.

low-weight intervals, one in MIS 1 and the other in MIS 5.5, also occur. From MIS 11 to 6 the records reveal a general trend of increasing weight, with MIS 11 being characterized by the lowest total foraminiferal test weights. Inverse to the minimum test weight values, MIS 11 shows the maximum test lightness values. In addition, there are high lightness values in MIS 1 and 5.5 and low values in MIS 2 and 10 that are inverse to the weight data of these periods. Besides the low-weight

intervals of MIS 1, 5.5, and 11, several other interglacial low-weight intervals occur in MIS 7 and 9 but they do not always correlate between cores. High foraminiferal test weights occur throughout MIS 2-4, 6, and 10, although some tests of these glacial periods show low test weight comparable to the interglacial range. In general, however, the test weight data indicate a pattern of pronounced carbonate preservation during glacial periods and enhanced carbonate corrosion during interglacial periods.

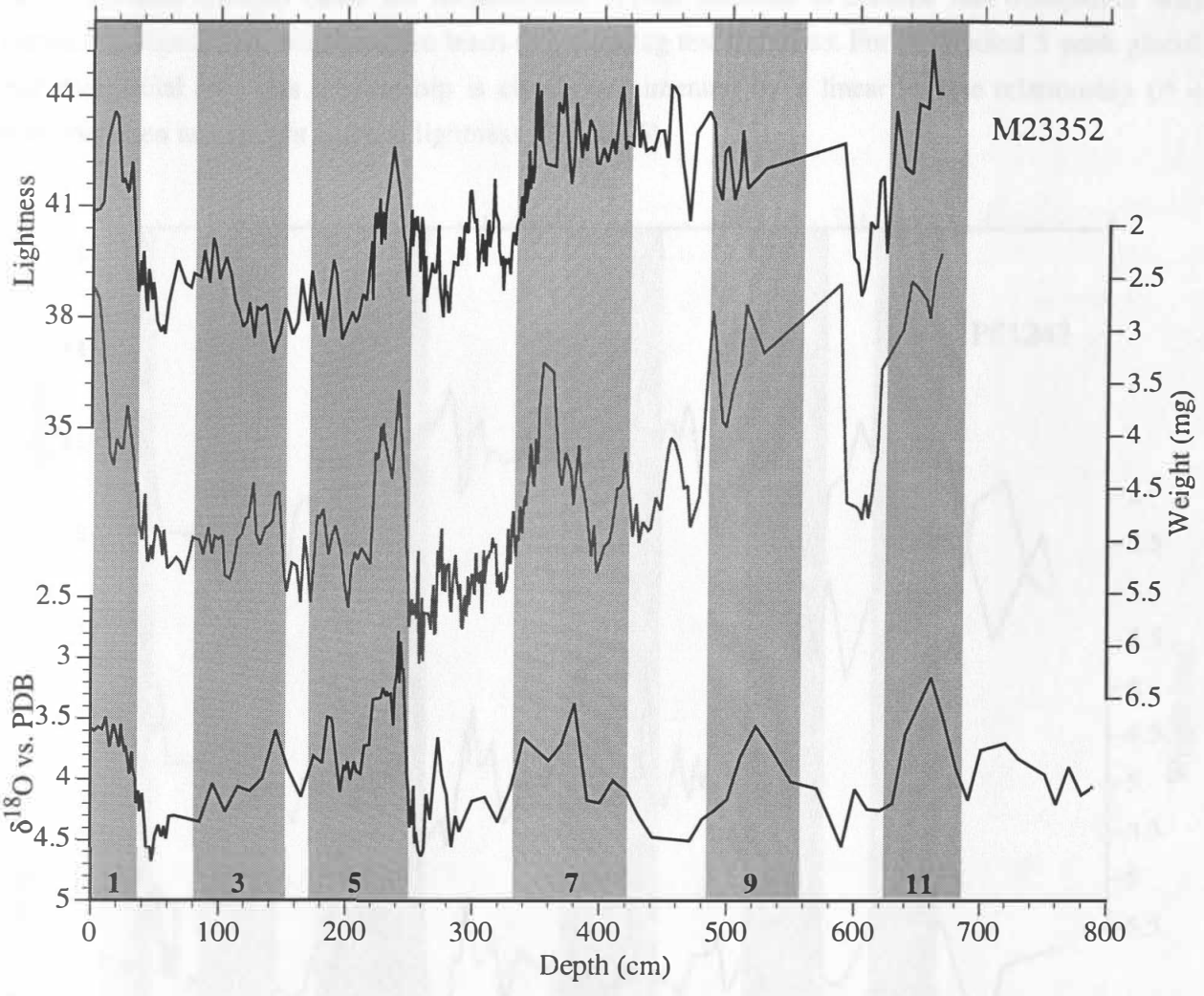

Fig. III-5: Records of test lightness, weight and $\delta^{18}O$ of *N. pachyderma* sinistral for (a) M23352 and (b) PS1243 (the data of the planktic oxygen isotopic curves are taken from Bauch et al., 2000a and Bauch et al., 2000b; Odd numbers indicate marine isotope stages (MIS) for reference and are shaded in gray). High test weight and low test lightness indicates good test preservation, whereas low test weight and high test lightness characterizes periods of enhanced corrosion. Despite some deviations between the weight and lightness data the records reveal glacials (MIS 2-4, intervals of MIS 6 and 8) as times of good carbonate preservation and peak interglacials (MIS 1, 5.5, intervals of MIS 7 and 9, and especially, MIS 11) as times when increasing carbonate corrosion prevailed.

When comparing the test lightness and weight records, it is notable that the inverse relationship between these variables, as observed for the peak glacial and interglacial periods (Fig. III-2), does

not extend over the entire downcore records (Fig. III-5). For example, the maximum weight values of MIS 6 do not correspond with minimum test lightness. Also, the high lightness results of the entire MIS 7 in core M23352 are not in accordance with the weight record in this interval.

III.5. Discussion

Recent investigations from the Nordic Seas identified a relationship between carbonate preservation and foraminiferal test lightness (Bauch and Helmke, 1999). Their study indicated that microstructural changes cause the foraminiferal crystal surfaces to become less transparent with increasing dissolution, which in turn leads to increasing test lightness. For the studied 5 peak glacial and interglacial tests this relationship is clearly documented by a linear inverse relationship (r^2 = 0.84) between test weight and test lightness (Fig. III-6).

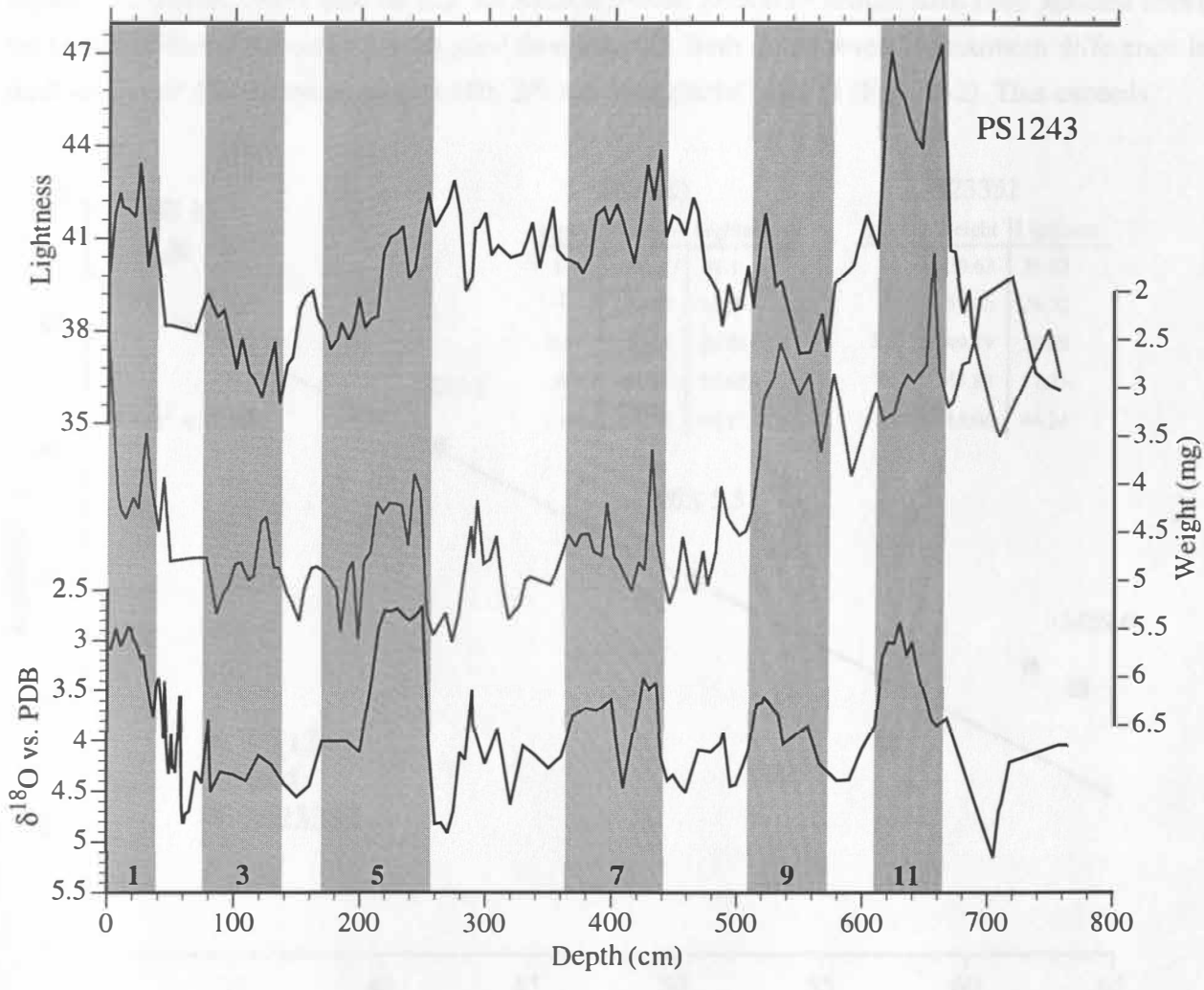

Fig. III-5b.

Previous studies of carbonate preservation in the Nordic Seas established qualitative foraminiferal dissolution indices (e.g., Henrich, 1986). Our analyses represent a direct approach to estimating the total carbonate loss caused by Late Quaternary dissolution in this region. At our two study sites, the coarse carbonate fraction commonly dominates the bulk carbonate content throughout the past 12 marine isotope stages, and within most core intervals the coarse carbonate is composed mainly of *N. pachyderma* (sin.). For these reasons we used foraminiferal test weight of *N. pachyderma* (sin.) to estimate carbonate loss. This method is limited to regions and time intervals where carbonate preservation is generally good. In this respect, the investigated sites are suitable because throughout both cores the shells of *N. pachyderma* (sin.) show no fragmentation.

Estimates about glacial-interglacial fluctuations of the water depth of the lysocline in the North Atlantic (Crowley, 1983) indicate that the studied Nordic Seas sites should have been situated above the lysocline during the entire investigated time interval. Both cores reveal a maximum difference in shell weight of 45% between glacial MIS 2/6 and interglacial MIS 11 (Fig. III-2). This exceeds

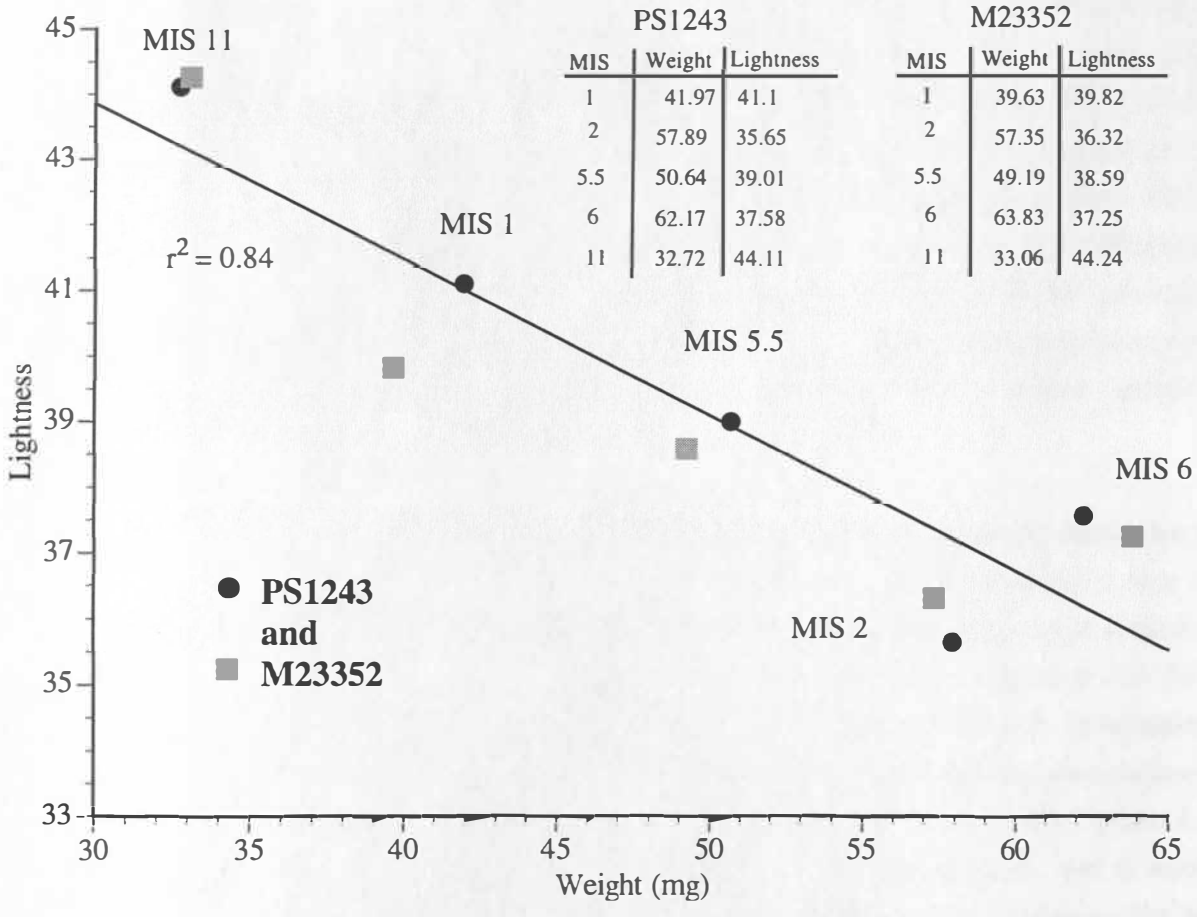

Fig. III-6: Foraminiferal test weight versus test lightness of the previously described 5 glacial-interglacial samples (see Fig. III-2). The comparison of the two parameters reveals an inverse linear relationship ($r^2 = 0.84$) between test weight and lightness.

previous estimates of carbonate loss above the lysocline as reported by Peterson and Prell (1985), who observed maximum values of 30% in the Pacific. In the North Atlantic, shell density analyses of *N. pachyderma* (sin.) were used to calculate total foraminiferal carbonate loss (McManus and Lohmann, 1998). For the last glacial-interglacial cycle these authors observed the highest carbonate loss (more than 30%) in MIS 4, and found this dissolution pulse associated with foraminiferal shell fragmentation. In contrast, our analyses reveal that in the Nordic Seas the carbonate loss of *N. pachyderma* (sin.) can be much higher without any shell fragmentation occurring. In this respect it has to be considered that the left coiled variety of *N. pachyderma* is most resistant to carbonate dissolution among planktic foraminifers (Berger, 1968; Malmgren, 1983).

Many studies have focused on carbonate preservation in marine sediments, most of them emphasizing the out-of-phase dissolution pattern of the Indo-Pacific and Atlantic Oceans. It is believed that during glacial times carbonate dissolution was lesser in the Pacific (Farrell and Prell, 1989) and greater in the Atlantic (Berger et al., 1983; Crowley, 1983). However, certain preservation and dissolution events of the Indo-Pacific and Atlantic Oceans seem to be in phase (Crowley, 1983). Today the formation of well-ventilated North Atlantic Deep Water (NADW) makes the Atlantic Ocean less corrosive to calcite than the rest of the world´s ocean (Archer, 1991). A weakening in the strength of NADW formation during glacials (Mix and Fairbanks, 1985) is thought to be one major reason for decreasing carbonate preservation in the Atlantic (Crowley, 1983; Diester-Haass, 1985). It is still an open discussion as to whether the good glacial Pacific carbonate preservation can be attributed to a source of well-ventilated deep water in the Pacific (Moore et al., 1978; Keigwin, 1987; Curry et al., 1988). Our study confirms previous investigations that indicated generally good carbonate preservation in the Nordic Seas (Henrich, 1998). The preservation records point to well-ventilated deep water in the Nordic Seas throughout most of the last 12 marine isotope stages, regardless of the climatic mode.

One mechanism that might have caused the enhanced interglacial carbonate corrosion is high surface productivity. In the Nordic Seas, the interglacial MIS 11 was probably a time of high productivity (Bauch et al., 2000a). Increased plankton productivity leads to a high vertical flux of organic carbon to the sea floor, and consequently more carbon dioxide is released into the bottom water by decay of organic matter, lowering the pH and increasing carbonate dissolution. High carbonate accumulation in shallow water depth and enhanced deep sea carbonate dissolution in MIS 11 is also reported from other parts of the world ocean (Droxler et al., 1996; Howard, 1997). However, in all probability core M23352 is way above the saturation horizon, and it would need massive interglacial organic rain to trigger carbonate corrosion. This is not verified by the generally low TOC concentration (the mean less than 0.5%) of the bulk sediment (Henrich, 1992), yet certain benthic foraminifers indicate enhanced vertical flux of TOC in MIS 11 (Struck, 1997). Though

increased surface productivity seems to be an appropriate explanation for a generally stronger pelagic interglacial carbonate corrosion and the observed dissolution event during MIS 11 in the Nordic Seas, it has to be considered that high surface productivity has been invoked to explain both higher carbonate preservation and dissolution (Berger, 1970; Thunell, 1976; Arrhenius, 1988; Archer, 1991).

With the present data set we are not able to quantify which part of the foraminiferal test corrosion may be caused by porewater undersaturation with respect to calcite. In a scenario with effects of porewater chemistry on carbonate preservation, a higher relative rate of organic carbon rain decreases the porewater saturation with respect to calcite and would lead to a proportionally greater dissolution in the sediment driven by respiratory carbon dioxide (Berelson et al., 1990; Archer, 1991; Jahnke et al., 1997). A recent study on carbonate preservation in sediments from the Norwegian-Greenland Sea (Huber et al., 2000) also observes supralysoclinal calcite dissolution in the Nordic Seas. In this context the authors emphasize the importance of the molar ratio between organic carbon and carbonate particles that reach the sea floor for triggering dissolution above the calcium saturation horizon. An increase in the organic carbon/calcite ratio of material reaching the sediments was postulated for the last glacial (Archer and Maier-Reimer, 1994). This would lead to an increase of the carbonate ion in the bottom water and, through the mechanism of $CaCO_3$ compensation, would decrease the atmospheric carbon dioxide content. However, the sites investigated in this study were probably situated above the North Atlantic lysocline throughout the Late Quaternary, and in situ measurements of porewater by several authors are in contrast to each other: While Jahnke et al. (1994) found no evidence for dissolution driven by metabolic carbon dioxide above the saturation horizon, Hales et al. (1994) observed dissolution.

Another proposed explanation for a higher carbonate ion concentration in the ocean, and hence, lower atmospheric CO_2 content during glacials, is the "coral reef hypothesis" (Berger, 1982; Opdyke and Walker, 1992). According to this hypothesis the coral growth rates were lower during glacials when the sea level had dropped and the continental shelves were exposed. This would imply a shift of $CaCO_3$ deposition to the deep sea and therefore would have led to a deepening of the oceans saturation horizon and better carbonate preservation. However, this hypothesis calls for a global ocean increase in the saturation state (Opdyke and Walker, 1992; Archer and Maier-Reimer, 1994), and cannot be invoked to explain the observed preservation difference between the Nordic Seas and the rest of the Atlantic or between the Atlantic and the Indo-Pacific, respectively.

The observed Late Quaternary preservation cycles are consistent with estimated glacial-interglacial pH changes in the Atlantic and Pacific (Sanyal et al., 1995) wherein the deep water of both oceans had a higher pH during the last glacial period. Accordingly, both the Atlantic and Pacific Oceans

had a higher glacial deep-sea carbonate ion concentration. However, it is very likely that the boron isotope-based carbonate ion change will not be equivalent to the amount of change in preservation, as the boron based paleo-pH estimates need to be coupled with dissolution driven by metabolic CO_2 so as not to have an unrealistic change in lysocline depth of several kilometers.

At present, the glacial-interglacial changes in the bottom water saturation state of the Nordic Seas cannot be exactly quantified. The two cores have a depth difference of about 1000 m which would translate to a difference in the saturated CO_3^{2-} ion concentration in the bottom water of about 15 µmol/kg. However, no significant differences show up in the lightness data of the two cores. Therefore, future work on the exact relationship between the carbonate ion concentration and test lightness is needed in order to further quantify the changes in the depth of the Nordic Seas lysocline during the Pleistocene.

Given that the Nordic Seas data are out of phase with the rest of the Atlantic Ocean, changes in $CaCO_3$ production seem to be a more likely explanation for the observed preservation pattern than mechanism with effects on a global scale. Regardless of the mechanism that drives the changes in glacial-interglacial carbonate preservation, our results indicate that the Late Quaternary carbonate dissolution and preservation episodes occurred synchronously throughout the Nordic Seas and Indo-Pacific ocean basins, with better preservation during glacial periods. A better deep-sea carbonate preservation implies a high deep-sea carbonate-ion concentration, which in turn would lead to a lowered glacial atmospheric carbon dioxide content. Therefore, our data support previous investigations (Archer and Maier-Reimer, 1994; Sanyal, et al., 1995) that attributed much of the glacial drop in atmospheric carbon dioxide content to global changes in the marine carbonate system between the climatic modes.

III.6. Conclusions

The carbonate preservation of two intermediate water depth sites from the Nordic Seas were investigated using weight measurements as well as lightness and SEM analyses on planktic foraminiferal tests.

Within the last 12 marine isotope stages a generally good carbonate preservation with better glacial than interglacial preservation is indicated for this region. Although the foraminiferal tests are not fragmented, estimates about the foraminiferal carbonate loss reveal maximal values of 45% in comparison between peak glacial stages and interglacial MIS 11.

As a glacial-interglacial pattern with stronger interglacial dissolution is also known from the Indo-Pacific Ocean, our data point at an in-phase carbonate preservation pattern of the Nordic Seas and the Indo-Pacific Ocean. However, it has to be considered that the main phases of dissolution in the Nordic Seas seem to be out of phase compared to the rest of the Atlantic.

Whether regional processes like stronger surface productivity during interglacials or global changes in the marine carbonate system are responsible for the observed preservation record from the Nordic Seas is still uncertain. However, a late-Pleistocene carbonate dissolution pattern with better glacial preservation supports scenarios that attribute much of the drop in atmospheric carbon dioxide during the last glacial to changes in the alkalinity of the oceans.

Chapter IV: Glacial-interglacial relationship between carbonate components and sediment reflectance in the North Atlantic

Jan P. Helmke and Henning A. Bauch

IV.1. Abstract

A high resolution composite sediment record from intermediate water depth in the North Atlantic that dates back to marine isotope stage (MIS) 13 was investigated in order to determine the relationship between sediment reflectance (lightness L*) and carbonate content (weight %). For this purpose, a detailed analysis of the coarse (>20 µm) and fine (<20 µm) carbonate content was carried out to define which of the two carbonate components drives glacial-interglacial changes in sediment lightness. The bulk carbonate content is dominated by the fine carbonate fraction regardless of glacial or interglacial climatic mode, suggesting that the sediment lightness is normally controlled by fluctuations of the fine carbonate content. However, a comparison of MIS 1 and 5.5 indicates that, besides this difference in the content of the two carbonate size fractions, changing modes in carbonate preservation, i.e., the preservational state of planktic foraminifers, may also have a profound influence on total sediment reflectance.

IV.2. Introduction

In recent years, the North Atlantic region has been the focus to study rapid climatic oscillations during the Late Quaternary (e.g. Heinrich, 1988; Bond et al., 1992, 1993; Oppo et al., 1998). To be able to investigate centennial to millenial-scale climatic fluctuations using marine sediment records, it is crucial to produce data series with densely sampled resolution. Sediment color analyses can be a usefull tool, both to investigate such rapid fluctuations and to make estimates of varying sediment components. For example, Mix et al. (1995) measured reflectance spectra of Pacific Ocean sediments to estimate biogenic calcite and opal contents, whereas Grousset et al. (1993) used sediment gray level as a proxy for identifying time intervals with increased iceberg rafting in the North Atlantic, so-called "Heinrich events".

However, to use sediment color variations for paleoceanographic reconstructions requires information on the main sediment components of the general area under study. In the North Atlantic, sediments are mainly composed of biogenic carbonate which is predominantly deposited during warmer periods and detrital, terrigenous components such as iceberg-rafted debris (IRD) which is deposited during colder periods (Ruddiman and McIntyre, 1976; Smythe et al., 1985). Previous studies have shown a good correlation between bulk carbonate content and sediment reflectance as the result of changes in biogenic carbonate productivity and IRD input (Nagao and Nakashima, 1992; Cortijo et al., 1995; Ortiz et al., 1999). Increased carbonate deposition marks warmer climatic periods and contributes to higher gray-level values, whereas low carbonate content and increased input of terrigenous material during colder periods yields lower gray-level values. However, this simple correlation may not always be that straightforward. For instance, the data from the North Atlantic (Cortijo et al., 1995) clearly reveal a significant mismatch between bulk carbonate content and corresponding gray-level values when comparing the present and previous interglacial periods, MIS 1 and 5.5. Despite similarly high bulk carbonate content in both of these warm intervals, the sediment gray-level values in MIS 1 are significantly lower. In fact, they are even lower than in the colder substages MIS 5.1 and 5.3 when total carbonate content is less than in MIS 1.

Recent investigations on sediments from the Nordic Seas using lightness data (Bauch and Helmke, 1999) demonstrated that the particular preservational mode of foraminiferal tests can have a significant influence on total sediment lightness reflectance. Consequently, to determine the effects of carbonate on sediment lightness, measurements of bulk, fine, and coarse carbonate as well as analyses of foraminiferal preservation changes may be necessary. The purpose of this paper is, therefore, to qualify the factors that govern the relation between carbonate content and sediment lightness in the North Atlantic during the Late Quaternary.

III.3. Methods

Sediment lightness and carbonate content were investigated using core M23414 (53°32´N, 20°17´W, 2196 m water depth; Fig. IV-1).

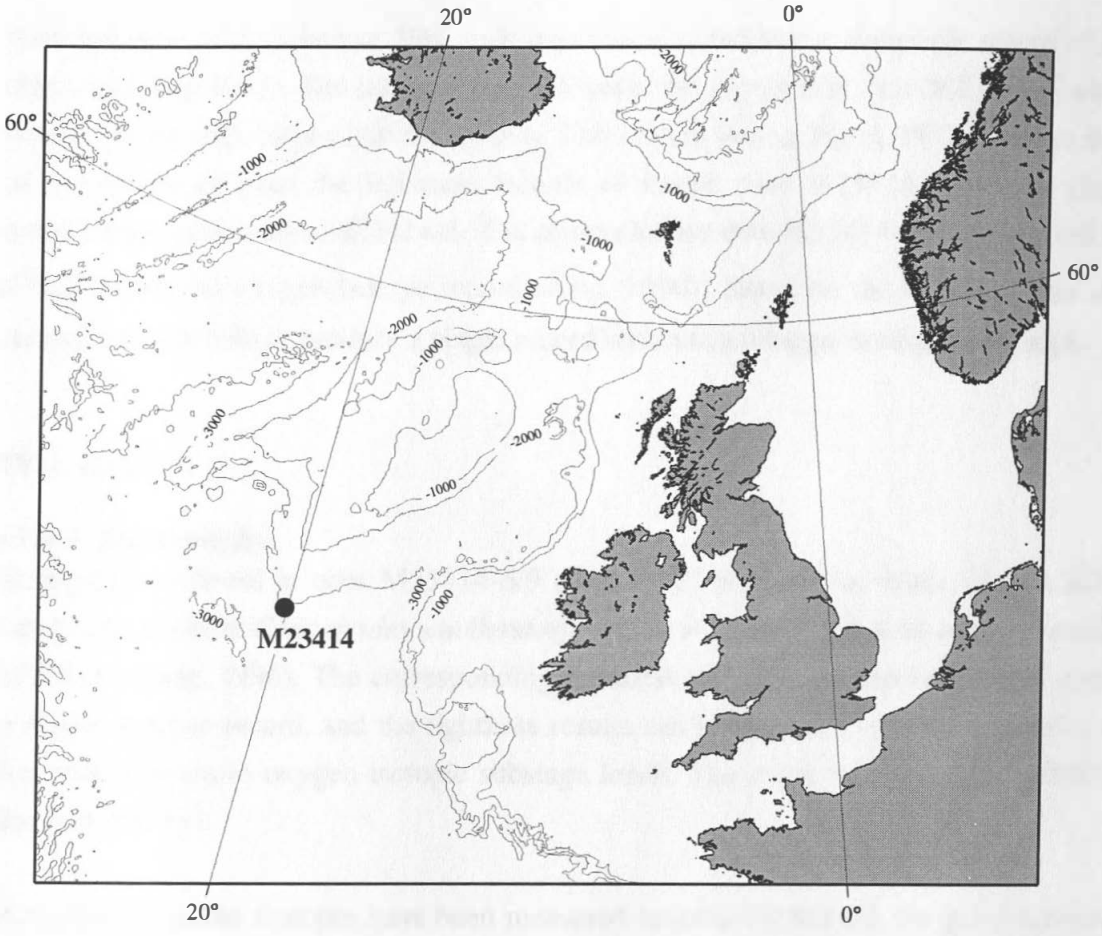

Fig. IV-1: Overview of work area and position of studied site where sediment cores were obtained (53°32´N, 20°17´W, 2196 m water depth). Water depth is in m.

Color measurements were obtained with a hand-held Minolta CM 2002 spectrophotometer. For all measurements the illumination system of the spectrophotometer was set at an angle of 2° and the "normal light" D65-mode was chosen. All measurements were carried out at centimeter steps and the lightness value L* in the spherical L*a*b* color space was recorded. In this color space L* is defined as the brightness-axis with L*=0% corresponding to black and L*=100% corresponding to white. All lightness measurements in this work were smoothed using a five-point moving average.

With the exception of trigger box core M23414-6, which was measured every 1.5-5 cm, the carbonate content was measured every 5 cm using a LECO-200. To better distinguish between the principle carbonate components and their influence on sediment color the samples were wet-sieved over a 20 μm mesh. It is assumed in this study that the fine (<20 μm) and coarse (>20 μm)

carbonate is mainly composed of coccoliths and foraminifers, respectively. The terms coarse and fine carbonate are used to refer to the two size fractions. However, we recognize that the size fraction <20 μm) may also partly consist of detrital carbonate

Both lightness and carbonate data were then taken to produce a composite record of Site M23414 (Fig. IV-2, Fig. IV-3). The upper 31 cm are based on trigger box core M23414-6 which was used because of its undisturbed surface section. The dashed line in Figure IV-2 indicates the main point of correlation between the lightness records of kasten core M23414-9 and the stratigraphically much longer piston core M23414-8. The shorter kasten core M23414-9 was also used here because it had already an oxygen isotope record (Jung, 1996). Based on the lightness data and the $\delta^{18}O$ record we were able to produce a single record with a much longer stratigraphic range.

IV.4. Results

IV.4.1. Stratigraphy

Stratigraphic control in core M23414-6/9 (Fig. IV-2) is based on stable oxygen isotopes of the benthic foraminifer *Cibicidoides wuellerstorfi*, which were measured at an average sample resolution of 2.5 cm (Jung, 1996). The corresponding lightness and carbonate records are in good agreement with the isotopic record, and the lightness results can be used to construct a detailed stratigraphic framework down to oxygen isotopic substage levels. The entire record penetrates MIS 8 (approx. the past 250 ky).

Although no stable isotopes have been measured on core M23414-8, the good agreement between lightness and stable isotopes in M23414-6/9 allowed to construct an oxygen isotope stratigraphy also for this core which dates back to MIS 13 (approx. the past 500 ky).

IV.4.2. Lightness and carbonate data

The bulk carbonate record is characterized by strong glacial-interglacial variations (Fig. IV-3). Peak interglacial values fluctuate between 70 and 90%, whereas glacial values can decrease down to less than 10%, although, mostly remain between 20 and 30% during colder intervals. A comparison of the fine and coarse carbonate fractions reveals that for most core intervals the bulk carbonate content is dominated by the fine component. Especially during the warm interglacial periods between MIS 5 and 13 up to 80% of the total carbonate is composed of fine carbonate with maximal values occurring in MIS 13. Through most of the glacial periods the fine carbonate also slightly dominates the bulk content. At least for the interval stages 13 to 7 there seems to be a decreasing trend in peak

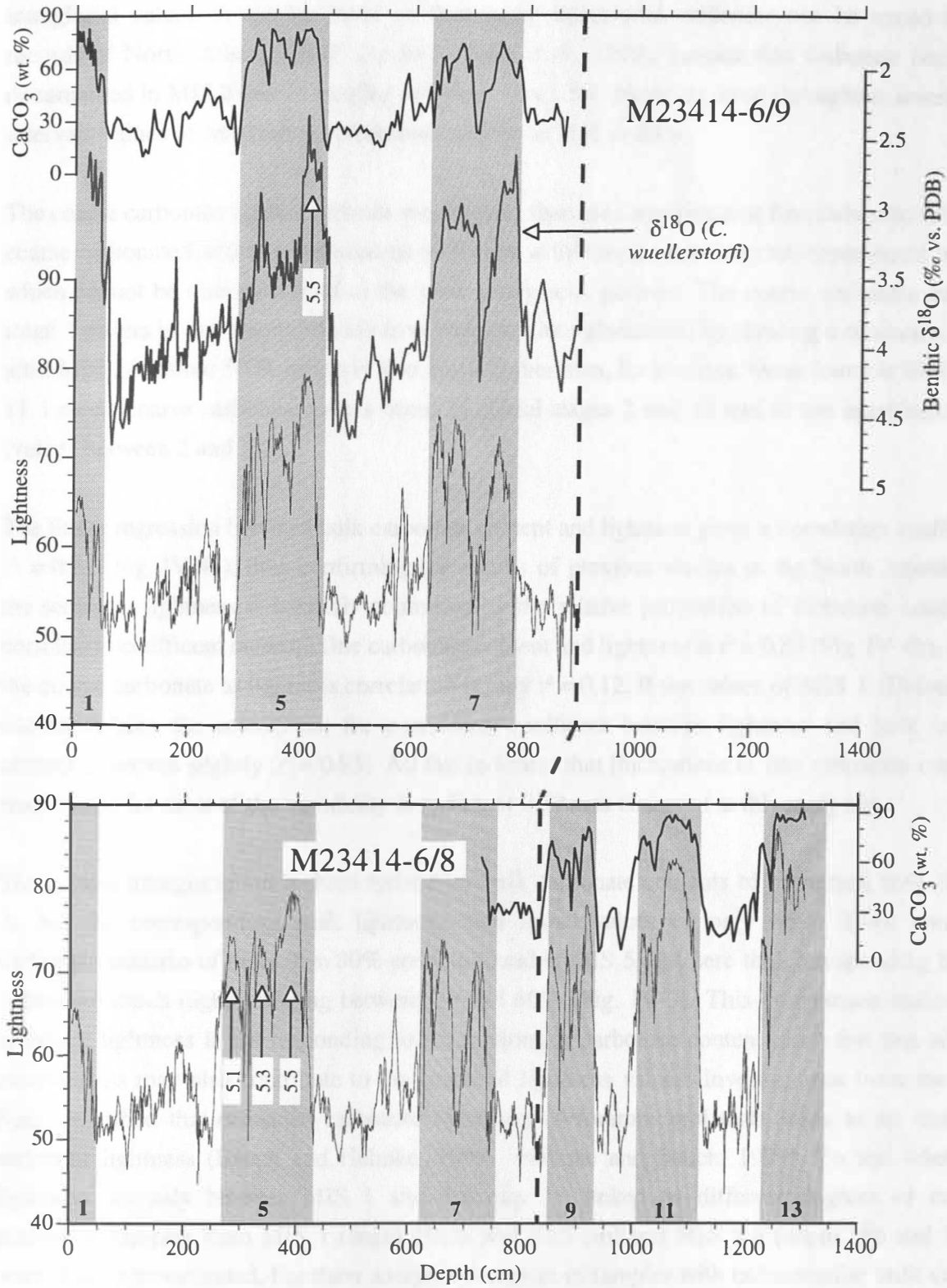

Fig. IV-2: Results of the sediment lightness measurements as well as $CaCO_3$ content (weight % of bulk sediment samples) results for the composite cores M23414-6/9 and 23414-6/8 (some carbonate data of M23414-6 from Andruleit, 1995). The benthic oxygen isotopes of *C. wuellerstorfi* from M 23414-9 are shown. Dashed line indicates depth of splicing.

interglacial values. A similar trend of decreasing interglacial carbonate can be traced from the records of North Atlantic ODP site 982 (Venz et al., 1999). Lowest fine carbonate contents are documented in MIS 2 and 12 ranging between 1 and 3%. However, even throughout several glacial intervals values of fine carbonate contents may be as high as 20%.

The coarse carbonate content remains much lower than the corresponding fine carbonate values. The coarse carbonate fraction often exceeds 40% only within some short intervals represented by spikes which cannot be directly related to the peak interglacial periods. The coarse carbonate content of stage 1 differs in this respect clearly from the other interglaciations by showing a consistent increase after MIS 2 to about 50 % which is also much higher than, for instance, those found in MIS 5.5 and 11. Lowest coarse carbonate values occur in glacial stages 2 and 12 and in late interglacial stage 7 (values between 2 and 3%).

The linear regression between bulk carbonate content and lightness gives a correlation coefficient of $r^2 = 0.81$ (Fig. IV-4a), thus confirming the results of previous studies in the North Atlantic, where the sediment lightness is basically controlled by the relative proportion of carbonate content. The correlation coefficent between fine carbonate content and lightness is $r^2 = 0.83$ (Fig. IV-4b), whereas the coarse carbonate to lightness correlation is only $r^2 = 0.12$. If the values of MIS 1 (Holocene) are excluded from the calculation, the correlation coefficent between lightness and bulk carbonate content improves slightly ($r^2 = 0.83$). All this indicates that fluctuations in fine carbonate content are responsible for most of the variability in sediment lightness observed at this study site.

The present interglaciation is characterized by bulk carbonate contents of more than 80% (Fig. IV-3), but the corresponding peak lightness data reveal values of only 66%. Three comparable carbonate maxima of more than 80% are also found in MIS 5, but here the corresponding lightness values are much higher ranging between 70 and 80% (Fig. IV-3). This comparison indicates that sediment lightness is not responding to fluctuations in carbonate content alone but that additional mechanisms may also contribute to the observed lightness values. Investigations from the Nordic Seas described that enhanced carbonate corrosion of foraminiferal tests leads to an increase in sediment lightness (Bauch and Helmke, 1999; Helmke and Bauch, 1999). To test whether the lightness anomaly between MIS 1 and 5.5 may be linked to different degrees of carbonate corrosion, samples from MIS 1 (depth 10.25 and 17.5 cm) and MIS 5.5 (depth 386 and 391 cm) were closely investigated. For these analyses two pairs of samples with rather similar bulk carbonate contents and likewise similar fine to coarse carbonate ratios were selected which demonstrates the general lightness discrepancy between MIS 1 and 5 (Fig. IV-5a). In order to investigate if carbonate corrosion is responsible for the lightness discrepancy, the dry sediment residues from the size

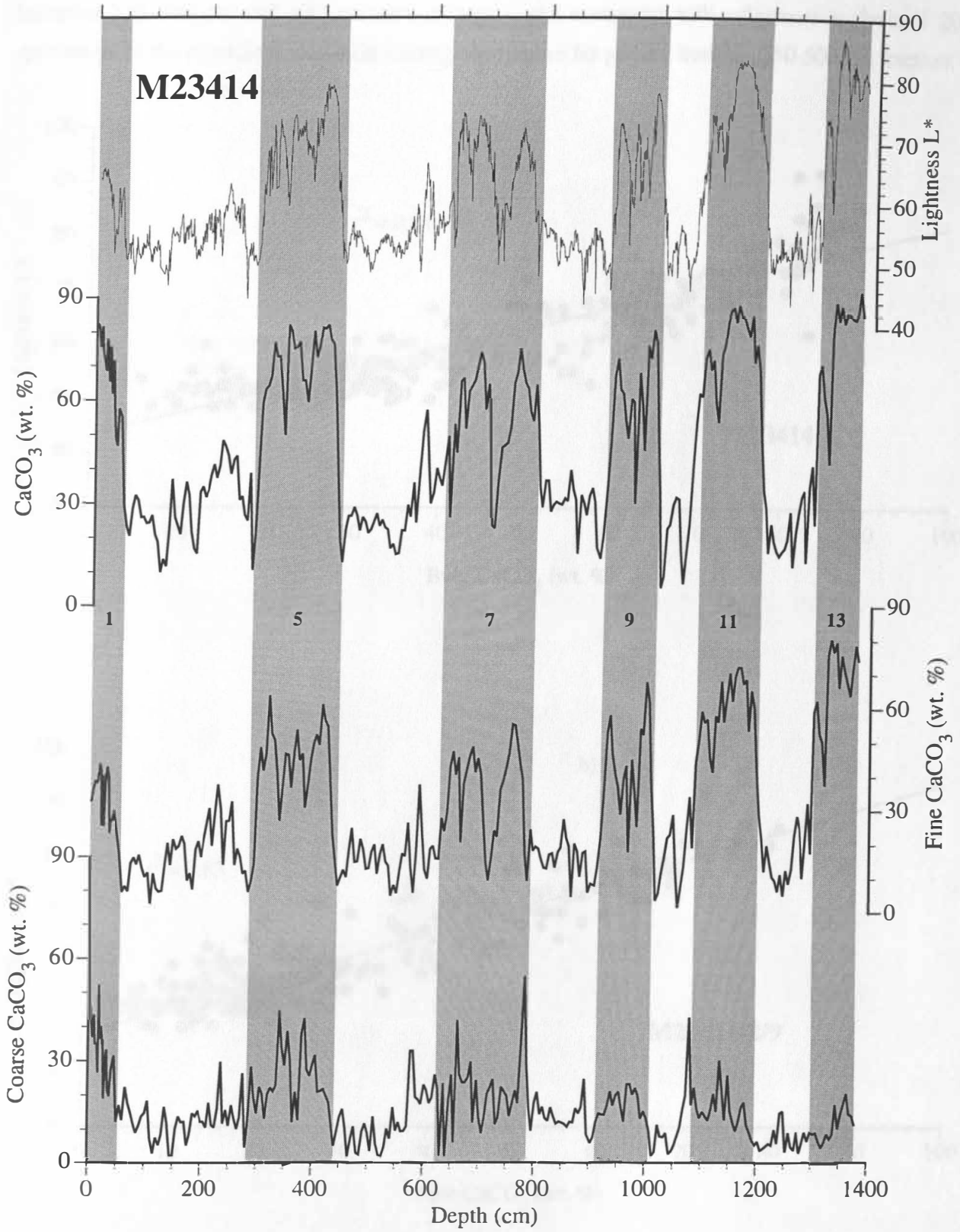

Fig. IV-3: Records of lightness, $CaCO_3$ content (weight % of bulk sediment samples) as well as fine and coarse $CaCO_3$ content (weight % of bulk $CaCO_3$) in composite core M23414.

fractions 250-500 µm and <20 µm were measured and compared with reflectance analysis of 200 specimens of the planktic foraminifer *Globigerina bulloides* picked from the 250-500 µm fraction.

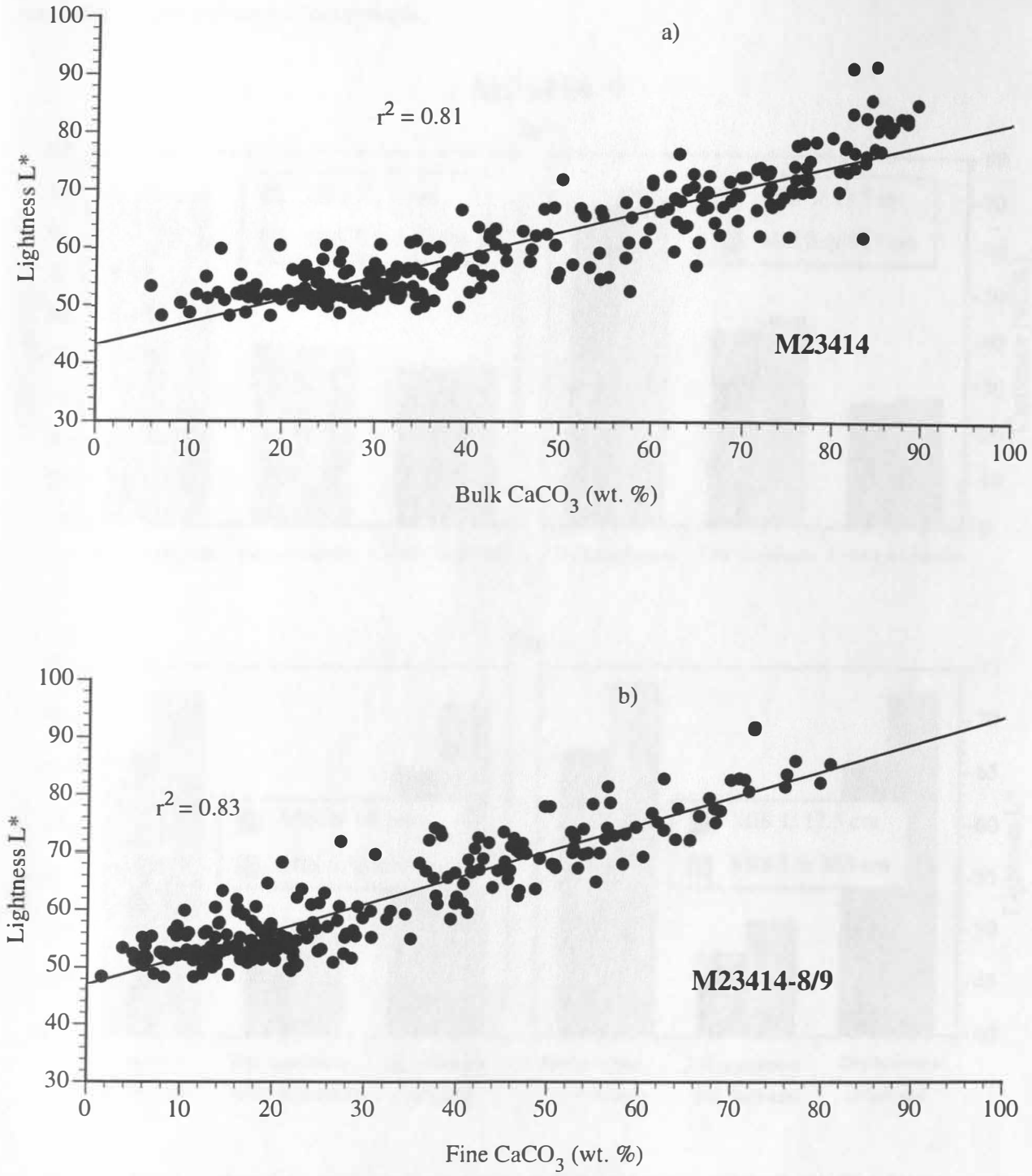

Fig. IV-4: (a) Correlation of sediment lightness to bulk carbonate content (weight % of bulk samples) for core M23414. (b) Correlation of sediment lightness to fine carbonate content (weight % of bulk carbonate) for core M23414-8/9.

All of the resulting lightness values clearly show a lower reflectance for MIS 1 than for MIS 5.5 (Fig. IV-5b) regardless of the fine to coarse ratio of the carbonate component. This indicates that the higher sediment lightness values found in the latter interval were probably caused by enhanced corrosion of the carbonate component.

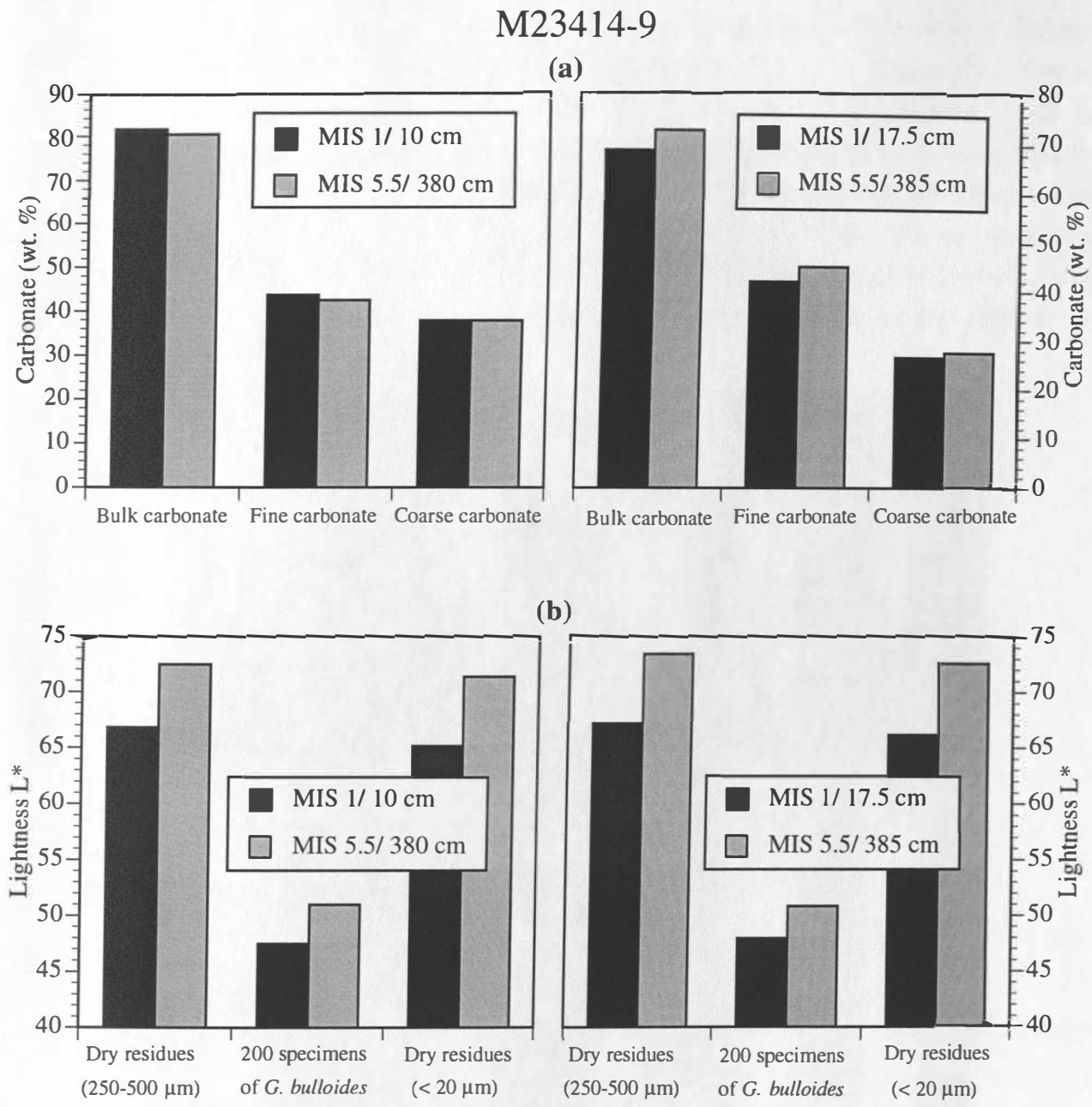

Fig. IV-5: Comparison of (a) bulk, fine, and coarse carbonate (bulk carbonate is weight % of bulk sediment samples; fine and coarse carbonate content are weight % of bulk carbonate) and (b) lightness values of dry sediment residues from size fractions < 20µm and 250-500 µm as well as of 200 picked specimens of *G.bulloides* (250-500 µm) for two samples from MIS 1 (depth 10 and 17.5 cm) and 5.5 (depth 380 and 385 cm).

IV-5. Discussion and conclusions

It is well known that coccolith accumulation rates in the North Atlantic are strongly coupled to glacial-interglacial climate oscillations (Ruddiman and McIntyre, 1976). Typically, in the North Atlantic peak interglacial periods correspond to high fine carbonate values, whereas glacial and cold interglacial/interstadial periods correspond to intervals of low fine carbonate (also van Krefeld et al., 1996; Lotoskaya et al., 1998). However, in core M23414 on average the fine carbonate dominates the bulk carbonate content in interglacial and glacial intervals (Fig. IV-6). Except for a few core sections, variations in the bulk carbonate are therefore controlled by fluctuations in the fine carbonate content. This is corroborated by other studies from further south in the northeastern North Atlantic also showing that fine carbonate contents generally dominate the bulk carbonate content during glacial as well as interglacial periods (Lotoskaya et al., 1998). As it can be assumed that the fine carbonate component is mainly composed of coccoliths, temporal changes in North Atlantic sediment lightness records are thus strongly coupled to variations in coccolith content.

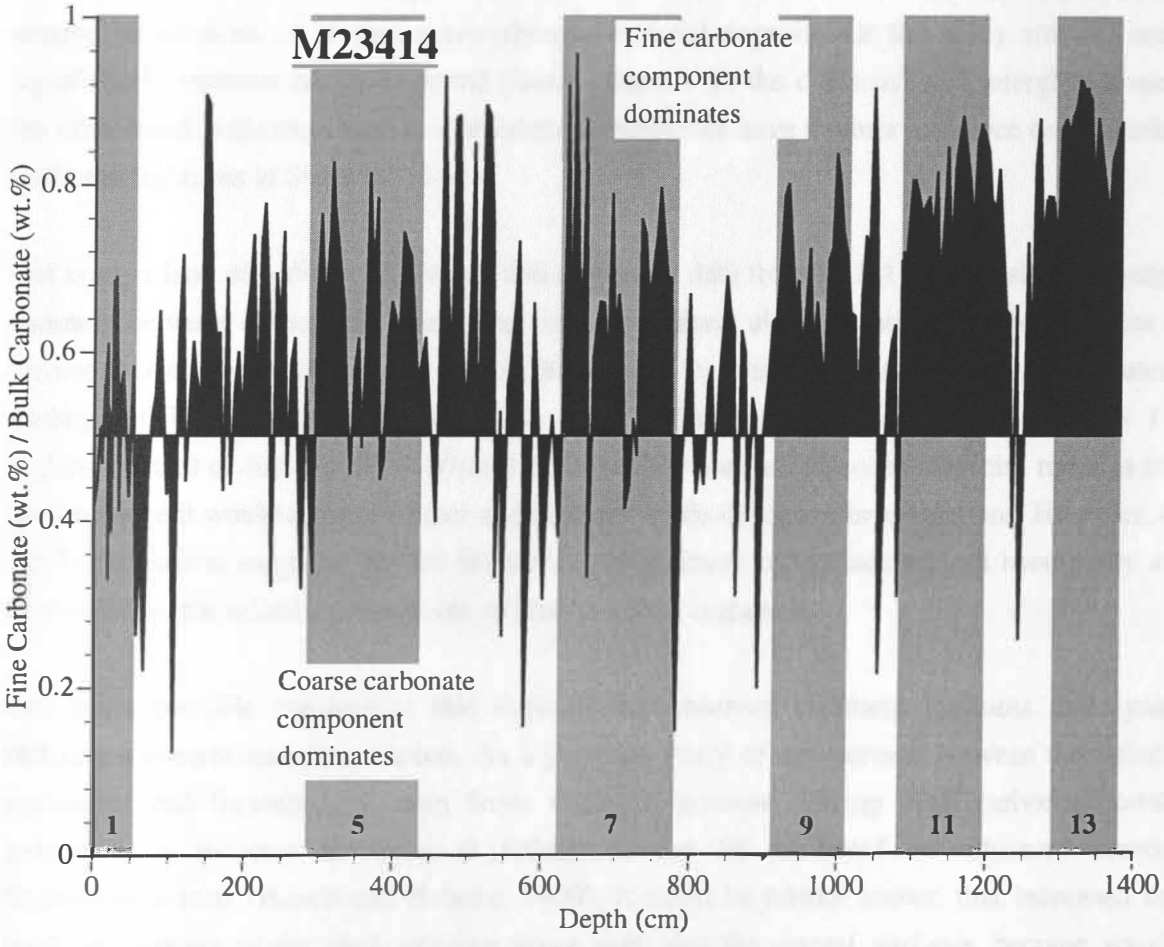

Fig. IV-6: Record of fine carbonate content divided through bulk carbonate content indicating the depth sections where the bulk carbonate content is dominated by the <20 µm fraction (values > 0.5) and the >20 µm fraction (values < 0.5), respectively.

Fluctuations of biogenic carbonate that are driven by glacial-interglacial climate change, i.e., the south- and northward movement of polar water masses (Ruddiman and McIntyre, 1976), are clearly imprinted on North Atlantic sediments. Due to varying input of clastic sediments via iceberg-rafting during cold periods alternating with times showing high carbonate bioproductivity and no IRD deposition, the North Atlantic sediments have an excellent potential for high resolution color analyses. Since in this region sediment color is basically controlled by productivity changes of carbonate-bearing microfossils, several authors have used reflectance values to estimate carbonate content (Harris et al., 1997; Ortiz et al., 1999) and to interpret climatic changes (Cortijo et al., 1995). There is also input of some ice-rafted carbonate during glacial intervals (see e.g., Bond and Lotti, 1995), however, this input is too low to have a strong influence on sediment color..

Recent investigations (Balsam et al., 1999) have shown that changes in the non-carbonate sediment fraction may significantly alter the reflectance of sediment sequences with constant carbonate content. The content of total organic matter in core M23414 does not exceed 0.5%. Moreover, the relative proportions of further non-carbonate material deposited at the study site did not change significantly between the investigated glacial intervals on the one hand and interglacial intervals on the other hand, indicating that such sediment components have a minor influence on the variations of sediment lightness at Site M23414.

Our comparison of sediment lightness and carbonate data from MIS 1 and 5.5 shows a stage 1/5.5-anomaly between carbonate content and lightness values, also indicating that the lightness changes are not necessarily controlled directly by fluctuations in total carbonate content alone. Based on the analysis of fine and coarse carbonate it is obvious that of all peak interglaciations MIS 1 has the highest content of foraminifers. What this means in terms of paleoceanography remains unclear at present since it would require further and different methodological investigations. However, the MIS 1/5.5 comparison suggests that the differences in sediment reflectance are not necessarily attributed to changes in the relative proportions of fine to coarse carbonate.

One other possible mechanism that explains the observed sediment lightness discrepancy is a difference in carbonate preservation. As a previous study of comparison between the reflectance of sediments and foraminiferal tests from sediment sections having high carbonate content has indicated, an increase in sediment reflectance can be attributed to enhanced corrosion of foraminiferal tests (Bauch and Helmke, 1999). It could be further shown that increased corrosion leads to changes in the shell microstructure such that the crystal surfaces become rougher and opaque, essentially not only making the tests appear whiter but also the entire sediment.

During the late Pleistocene the North Atlantic switched from a deep convection mode (production of NADW-North Atlantic Deep Water) during interglacial periods to an intermediate one (production of GNAIW-Glacial North Atlantic Intermediate Water) during glacial times (Oppo and Fairbanks, 1987; Venz et al., 1999). Throughout glacial times the boundary between GNAIW and SOW (Southern Ocean Water) is suggested to have been near 2200 m (Zahn et al., 1987; Oppo et al., 1997) indicating that at these periods the study site was located at a boundary of two water masses. Consequently, during interglacial times the core location is characterized by well ventilated water masses. This suggests that the observed variations in interglacial carbonate corrosion are more likely caused by some regionally limited changes in carbonate preservation due to variations in pore and bottom water chemistry (e.g. remineralization of organic matter).

Although most investigations of corrosional effects on calcite shell microstructure were on foraminifers (e.g., Henrich, 1986, 1989), the means by which foraminifers and coccoliths are being transported downward to the sea floor is rather different (Honjo, 1982; Pilskaln and Honjo, 1987). Because coccoliths are encapsulated into coproliths and thus buried, corrosional effects on the sea floor may differ from those of foraminifers. However, the lightness measurements on the coarse and fine fraction as well as on the foraminifers show a similar trend between MIS 1 and 5.5 (Fig. IV-5b), suggesting that corrosion affects both coarse and fine carbonate components. It therefore may well be that the decreasing trend observed in the fine carbonate during interglacial intervals since MIS 13 - the values in MIS 5 being the exception - may be caused by some unknown chemical changes rather than the result of variations in carbonate productivity. Recognizing this effect of carbonate corrosion on total sediment lightness may be important when it comes to interpret glacial-interglacial records for paleoceanographic purposes.

Chapter V - Sediment-color record from the Northeast Atlantic reveals patterns of millennial-scale climate variability during the last 500,000 years

Jan P. Helmke, Michael Schulz, and Henning A. Bauch

V.1. Abstract

A 500,000-year long deep-sea sediment color record from the Northeast Atlantic was investigated to reconstruct the evolution of late-Pleistocene climate variability on millennial time scales. Variations of the red-green color intensity are probably caused by climatically induced changes in the ice-rafted input of red-colored, iron-bearing terrigenous material to the core site. The resolution of the age model impedes the detection of distinct spectral features at sub-Milankovitch periods. Hence, millennial-scale climate variability is quantified as time-dependent variance of the high-pass filtered color time series. The course of the estimated variance shows distinct patterns, which can be linked to continental ice mass. During the past 500,000 years, large-amplitude millennial-scale climate variability occurs only if continental ice mass exceeds a threshold level, equivalent to sea level at approximately -40% and is tied to times of change in ice mass. For sea level below the threshold, reduced climate variability is associated with short time intervals of relatively stable phases of sea level.

V.2. Introduction

Climate proxy data from various archives document large-amplitude climate fluctuations during the last glacial period on millennial time scales: On longer time scales these include "Heinrich events" (e.g. Bond et al., 1992) with an average recurrence time of approximately 7 thousand years (ky) (Sarnthein et al., in press) and on shorter scales "Dansgaard-Oeschger events" (Dansgaard et al., 1993; Grootes and Stuiver, 1997) with an average spacing of about 1.5 ky (Bond et al., 1997, 1999). Heinrich events are thought to be linked to internal oscillations of the Laurentide ice sheet (MacAyeal, 1993), whereas the origin of the Dansgaard-Oeschger events remains controversial, ranging from internal oscillations of the ocean-atmosphere system (Broecker et al., 1990; Winton, 1993; Sakai and Peltier, 1997) to periodic calving of the Greenland ice sheet (van Kreveld et al., in press), and to external forcing mechanisms (van Geel et al., 1999; Keeling and Whorf, 2000). Furthermore, it was suggested that millennial-scale climate variability, although with smaller amplitude, is not restricted to the last glacial period but is a pervasive feature of the recent interglacial, the Holocene (Bond et al., 1997; deMenocal et al., 2000).

The possible interference of anthropogenic climate perturbations with natural climate fluctuations on millennial time scales poses a challenging task for predicting future climate change. Previous studies demonstrated the suitability of color records from marine sediments to quantify millennial-scale climate change with high temporal resolution (Cortijo et al., 1995; Ortiz et al., 1999). However, marine sediment color records have so far not been used to document the evolution of millennial-scale climate fluctuations throughout the Late Quaternary. To gain better insight into these natural variations we analyse high-resolution color records from Northeast Atlantic deep-sea sediments, which document climate variability down to millennial time-scales over the last five glacial-interglacial cycles.

V.3. Data and stratigraphy

Sediment color measurements of composite core M23414 from the Rockall Plateau in the Northeast Atlantic (53°32´N, 20°17´W, 2200 m water depth; details of core splicing in Helmke and Bauch, subm.) were carried out at centimeter steps, using a hand-held Minolta CM 2002 spectrophotometer. We use lightness L* and red-green chromaticity a* of the spherical L*a*b* color space (b* denotes blue-yellow chromaticity). Precision of the downcore color measurements was investigated using a set of 10 repeated measurements at 3 spots of the core. The mean standard deviation for these measurements is 0.06 for L* and 0.01 for a*. Additionally, the lightness and red-green color variations of 2 separate tracks down the core were measured. The differences are negligible with correlation coefficients of 0.96 (L*) and 0.95 (a*). The signal-to-noise-ratio is very large. These results clearly prove that the spectrophotometer color data can faithfully be used to determine the downcore color fluctuations at the study site. Sediment lightness is affected by several

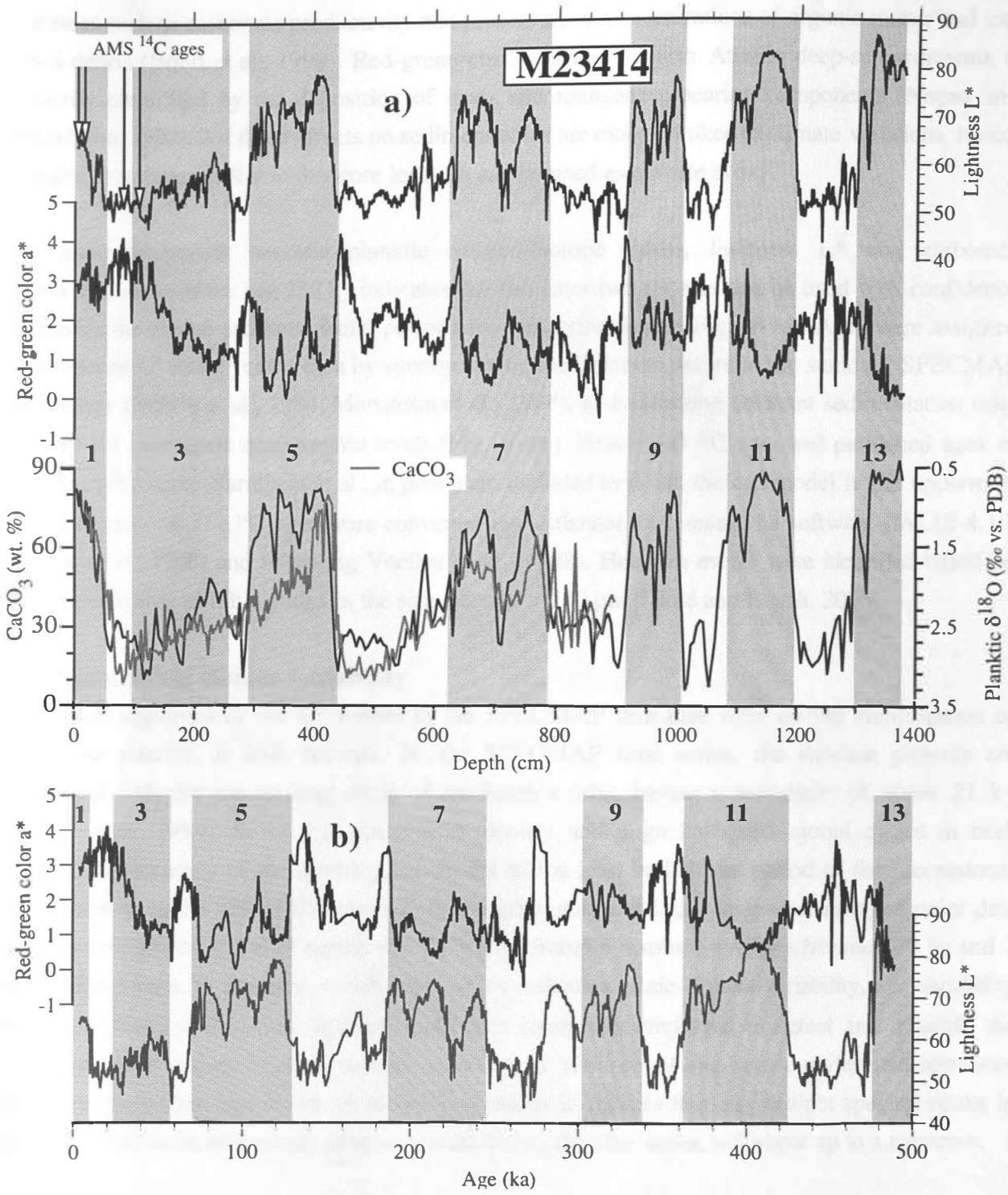

Fig. V-1: (a) Downcore records of lightness L*, red-green chromaticity a*, and $CaCO_3$ content (weight % of bulk sediment) from composite core M23414. Oxygen isotopes values of planktic foraminifer *Globigerina bulloides* from M23414-9 (gray line) cover only the upper 900 cm. $CaCO_3$ content and oxygen isotopes were measured at average sample resolutions of 5 cm (Helmke and Bauch, subm.) and 2.5 cm (Jung, 1996), respectively. Arrows mark depth sections with AMS ^{14}C ages. Odd numbers indicate marine isotope stages for reference and are shaded in gray. (b) Red-green chromaticity a* (top) and lightness L* (bottom, gray line) *vs.* age. The age model is based on the spliced SPECMAP time scale (Imbrie et al., 1984; Martinson et al., 1987).

processes such as carbonate productivity and preservation, concentrations of organic matter and ice-rafted debris (Bond et al., 1999). Red-green chromaticity in North Atlantic deep-sea sediments is primarily controlled by the deposition of iron- and manganese-bearing components (Nagao and Nakashima, 1992). All these effects on sediment color are closely linked to climate variations, hence, changes in sediment color at this core location can be used as climate proxy.

The good agreement between planktic oxygen-isotope values, lightness L* and carbonate concentrations over the last 250 ky indicates that the latter two proxies can be used with confidence to identify the glacial and interglacial periods for the entire record (Fig. V-1a). Ages were assigned to downcore L* and a* color data by synchronizing the lightness record to the standard SPECMAP chronology (Imbrie et al., 1984; Martinson et al., 1987), and assuming constant sedimentation rates between the correlated stratigraphic levels (Fig. V-1b). Four AMS ^{14}C ages and published ages of six Heinrich events (Sarnthein et al., in press) are included to refine the age model in the uppermost part of the record. The ^{14}C ages were converted into calendar ages using the software CALIB 4.1.2 (Stuiver et al., 1998) and following Voelker et al. (1998). Heinrich events were identified based on the concentration of lithic grains in the size fraction > 250 μm (Didié and Bauch, 2000).

V.4. Quantifying climate variability

The visual alignment of the L* record to the SPECMAP timescale rests on the identification of congruent patterns in both records. In the SPECMAP time series, the shortest patterns are associated with the precessional cycle of the Earth's orbit, having a periodicity of about 21 ky (Imbrie et al., 1984). Since it is possible to identify and align half-precessional cycles in both records, the accuracy of the resulting age model will at least be half the period of the precessional cycle (relative to the SPECMAP chronology). On the other hand, the centimeter-sampled color data have an average resolution of approximately 360 yr (sample resolution ranges between 70 yr and 2 ky), making them, in principle, suitable to resolve millennial-scale climate variability, i.e., variability between 10^3 and $< 10^4$ years. Spectral analysis is commonly employed to detect and quantify the contribution of millennial-scale variance to the total variance of the series under consideration. However, the uncertainty of the age model used makes it unlikely that any distinct spectral peaks in the millennial band, which may have been recorded by the time series, will show up in a spectrum.

To nevertheless quantify climate variability in the millennial band, we first filtered the red-green color time series with a high-pass filter (Rybicki and Press, 1995) using a cut-off frequency of 1/12 ky^{-1}, which is about half of the precessional period, i.e., the shortest pattern of the SPECMAP time series (Fig. V-2). The filtered time series thus reflects climate variability from millennial down to multi-centennial time scales (limited by the average temporal resolution of the color record). In a

second step, the time-dependent variance of the filtered time series was estimated by means of a 8-ky wide sliding rectangular window. This width offers a good compromise between statistical and

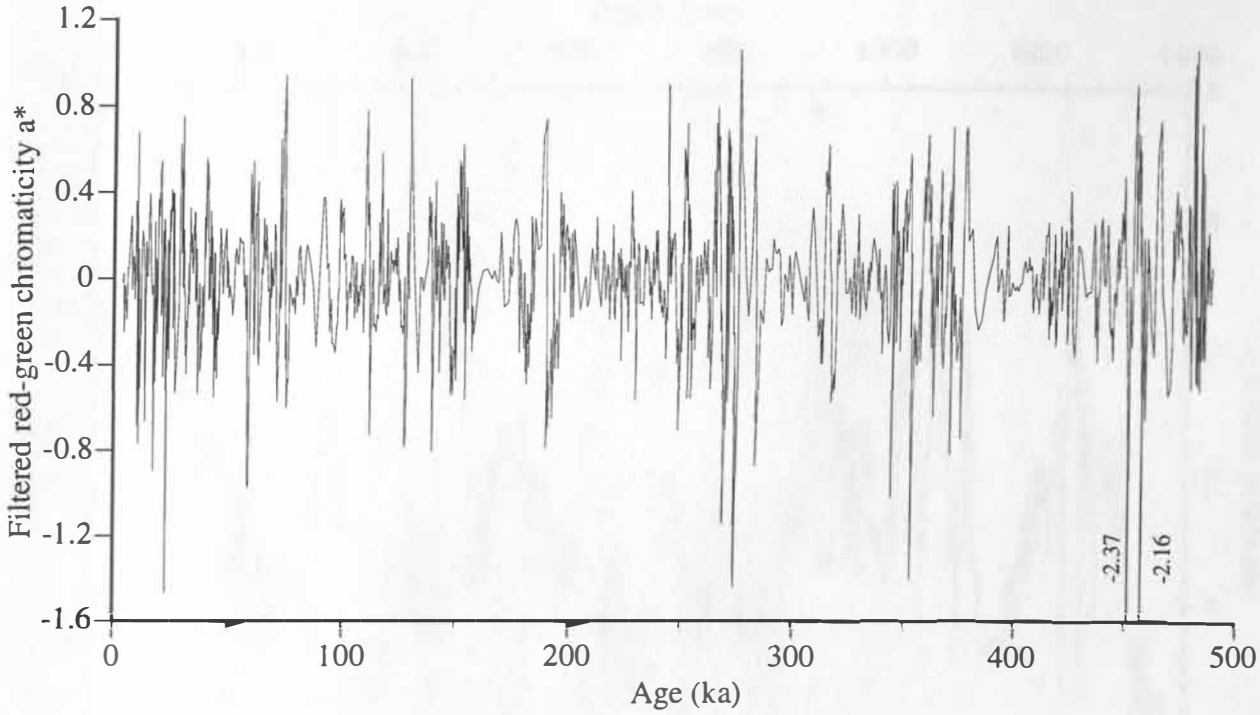

Fig. V-2: High-pass filtered red-green color time series (see Fig. V-1b). Cutoff frequency is 1/12 ky^{-1}.

systematic errors. Since variance and the area under a spectrum measure the same quantity (Parseval's theorem; Bendat and Piersol, 1986), this approach indirectly estimates spectral power in the entire millennial-to-multi-centennial band as function of time. Both computational steps were performed on the unevenly spaced time series to prevent any bias in spectral character caused by interpolation to an even sampling interval (Horowitz, 1974; Schulz and Stattegger, 1997).

V.5. Patterns of climate variability

Time-dependent variance of the red-green color shows that millennial-scale fluctuations with different amplitudes persisted during the past half a million years. It is most likely that variations in the concentration of red-colored, iron-bearing minerals are responsible for the observed changes in the red-green chromaticity of the sediment. Several studies at sites in the vicinity of M23414 have indicated that the deposition of a red-colored mineral, i.e., hematite, in the Northeast Atlantic during the last 40 ky is linked to millennial-scale climate variations (Bond and Lotti, 1995; Bond et al., 1997, 1999). These authors proposed that hematite-stained lithic grains stemming from continental red beds were transported via ice-rafting to the core sites. X-ray-flourescence analysis of samples

from M23414 prove that changes in iron content correlate to changes in the a* color record, i.e., a higher iron content goes along with higher a* values and vice versa (Fig. V-3a).

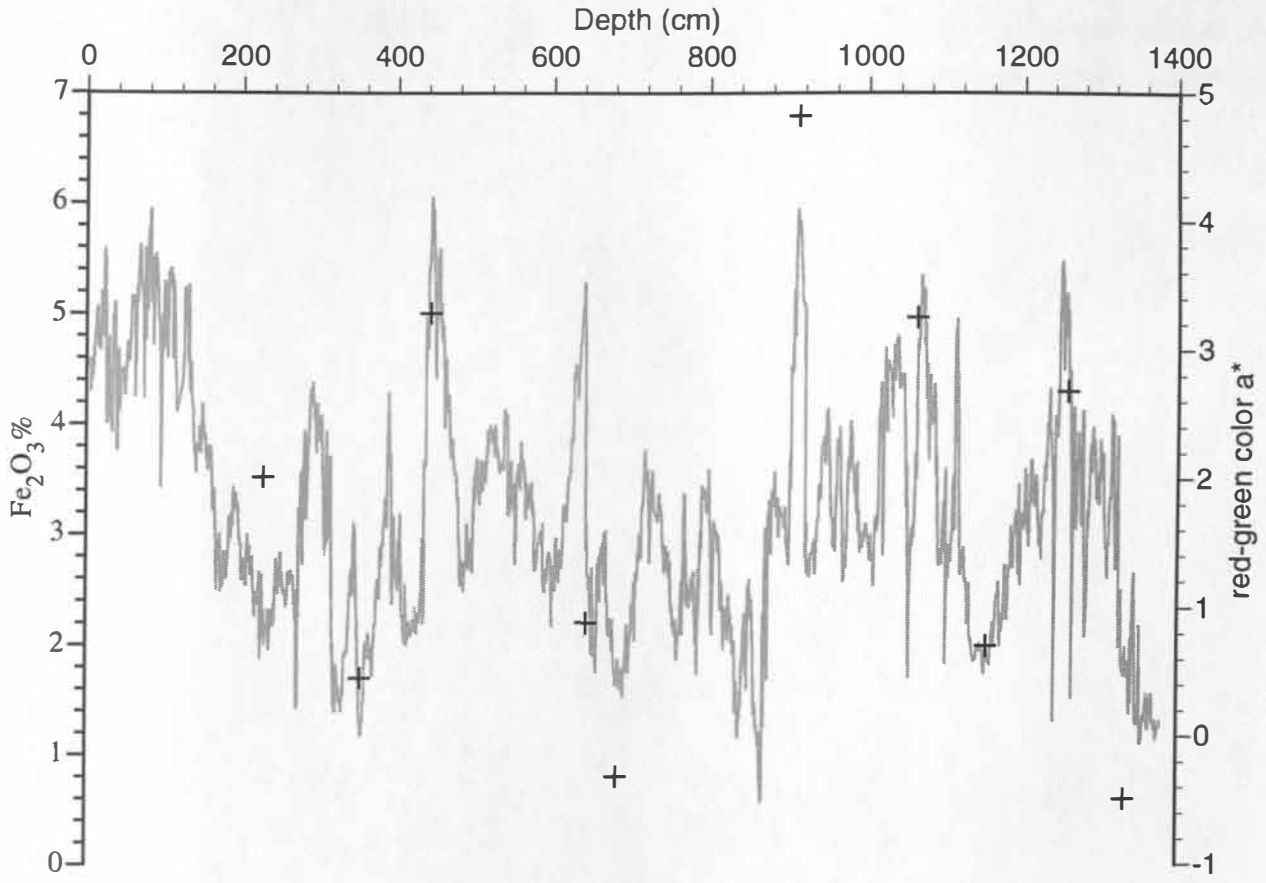

Fig. V-3b: Red-green color (gray line) and corresponding Fe_2O_3 content (weight % of bulk sediment) for a series of 10 sediment samples (data points denoted as +) from M23414.

The correlation is significant on the basis of Spearman´s rank-order correlation coefficient (rho =0.89, $p < 0.001$, n = 10; Fig. V-3b). However, iron concentrations are too low to identify iron-bearing minerals using the X-ray-diffraction method.

A comparison of red-green color and ice-rafted debris (IRD) reveals a generally good agreement between the patterns of variability (Fig. V-4). Especially the younger part of the record (Fig. V-4b) strongly suggests that changes in a* are linked to changes in the input of IRD. However, a dependance of red-green color from the input rate of IRD cannot be verified for the entire record (Fig. V-4a). This may be due to various sources of IRD input on the Rockall Plateau during the last 500 ky. A correlation of red-green chromaticity and total organic matter (TOC) shows a very weak correlation coefficient (rho = 0.23, <0.001, n = 268), thus it is unlikely that organic matter should have a strong influence on the red-green color record. Without knowledge about the pore water

chemistry at the study site an influence of sediment geochemistry on the red-green color record cannot be ruled out completely. However, an oxidation of sediment components containing Fe^{3+} into red-colored components containing Fe^{2+} during intervals of low sediment accumulation seems to be unlikely: A comparison of accumulation rates and a* during the last 60 ky indicates that a* is not triggered by changes in accumulation rate (correlation is not significant: rho = -0.05, p = 0.911, n = 8).

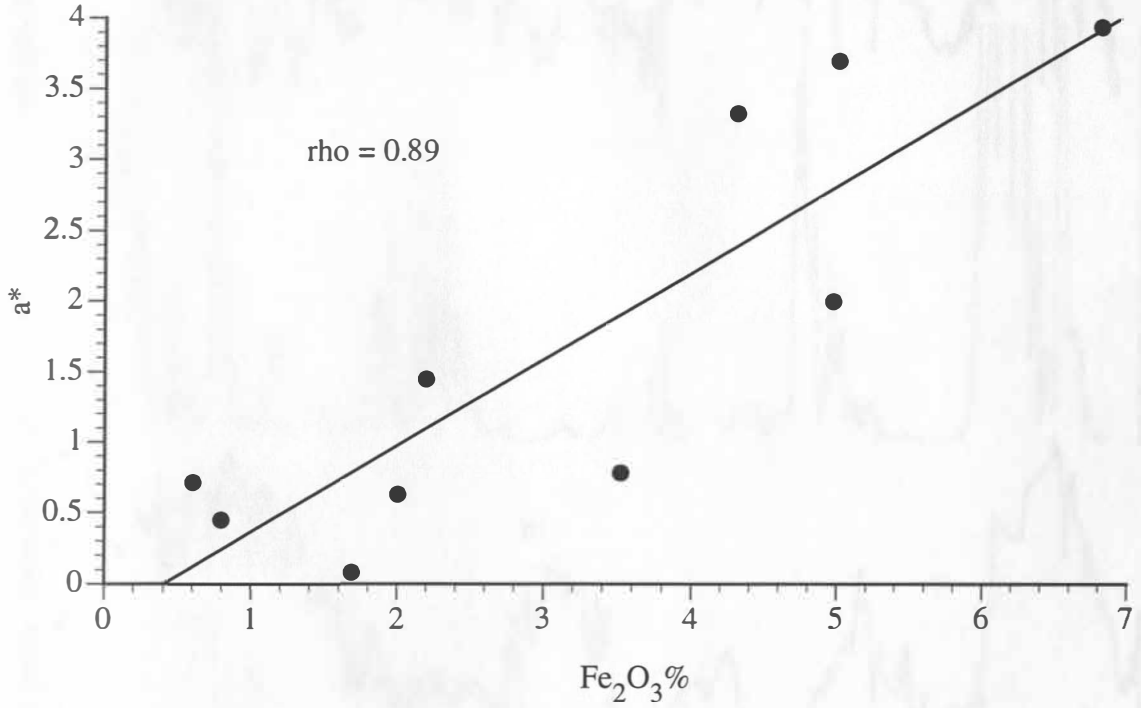

Fig. V-3b: Correlation of Fe_2O_3 (weight % of bulk sediment) and red-green chromaticity a* for a series of 10 sediment samples from M23414.

Hence, we surmise that variations in red-green chromaticity over the last 500 ky are mainly controlled by fluctuations in the input rate of reddish iron-bearing minerals into the sediment, which in turn is linked to climate variations. In contrast, the interpretation of the lightness record is hampered by the fact that sediment lightness is affected by several mechanisms that may even counterbalance each other during the course of a climatic perturbation (Bond et al., 1999). To avoid ambiguous interpretations, we restrict our analysis to the red-green time series.

The comparison of the time-dependent variance of the red-green color record with the SPECMAP oxygen-isotope record, which is a proxy for continental ice mass and, therefore, global sea level (Imbrie et al., 1984), reveals that nine variance maxima occurred during time intervals of ice-sheet

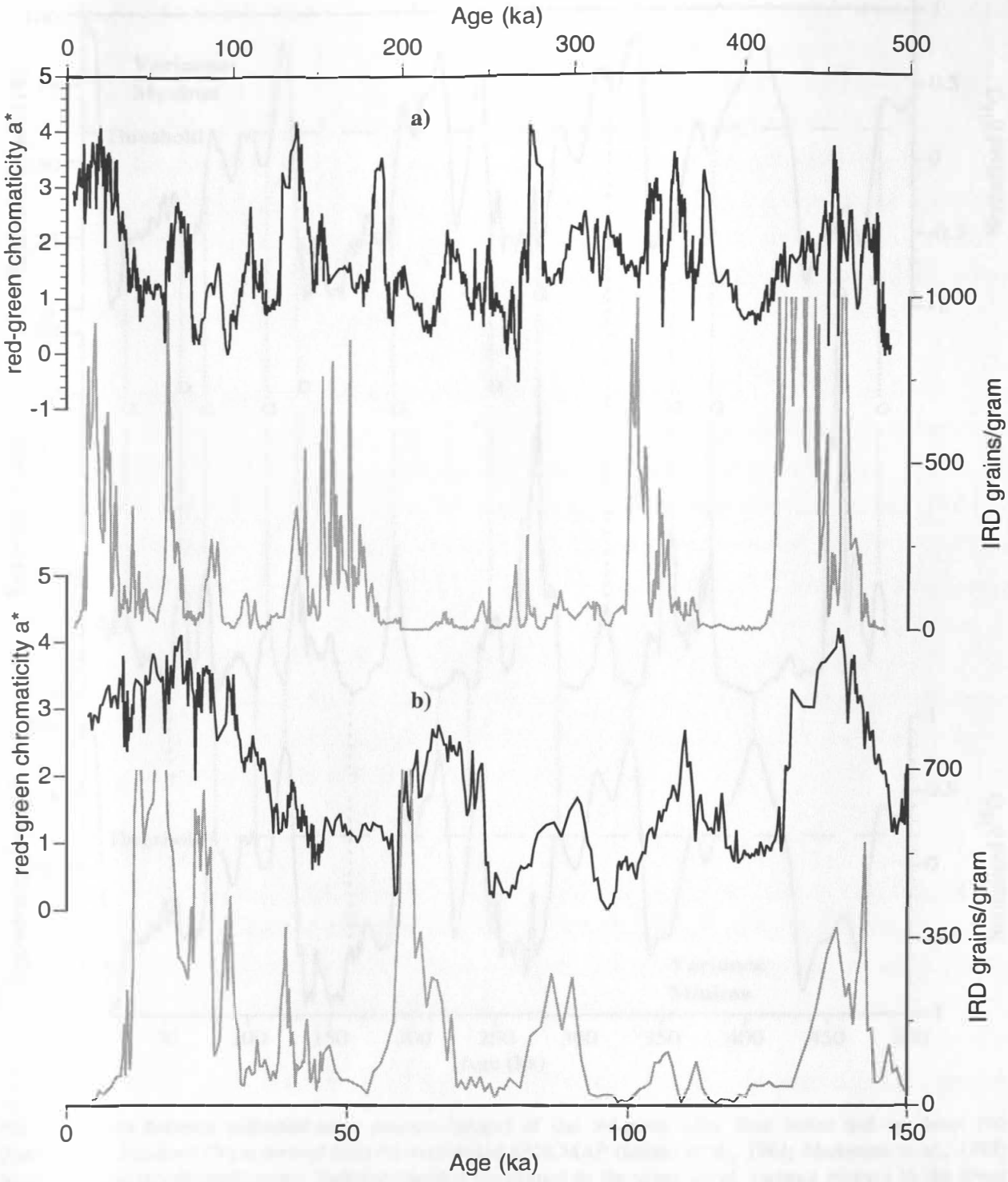

Fig. V-4: (a) Records of red-green chromaticity a* and IRD (lithic grains per gram) from M23414 *vs.* age. (b) Same records than in (a) for the upper 150 ky. Note that IRD is cut off at a) 1000 and b) 700 lithic grains per gram.

growth, while three maxima go along with times of ice-sheet decay (Fig. V-5). Moreover, these variance maxima coincide with times when sea level was -40%, i.e., -51 ± 3 m (Fig. V-5), indicating threshold behaviour. The range for this threshold results from the uncertainty of sea level at the last

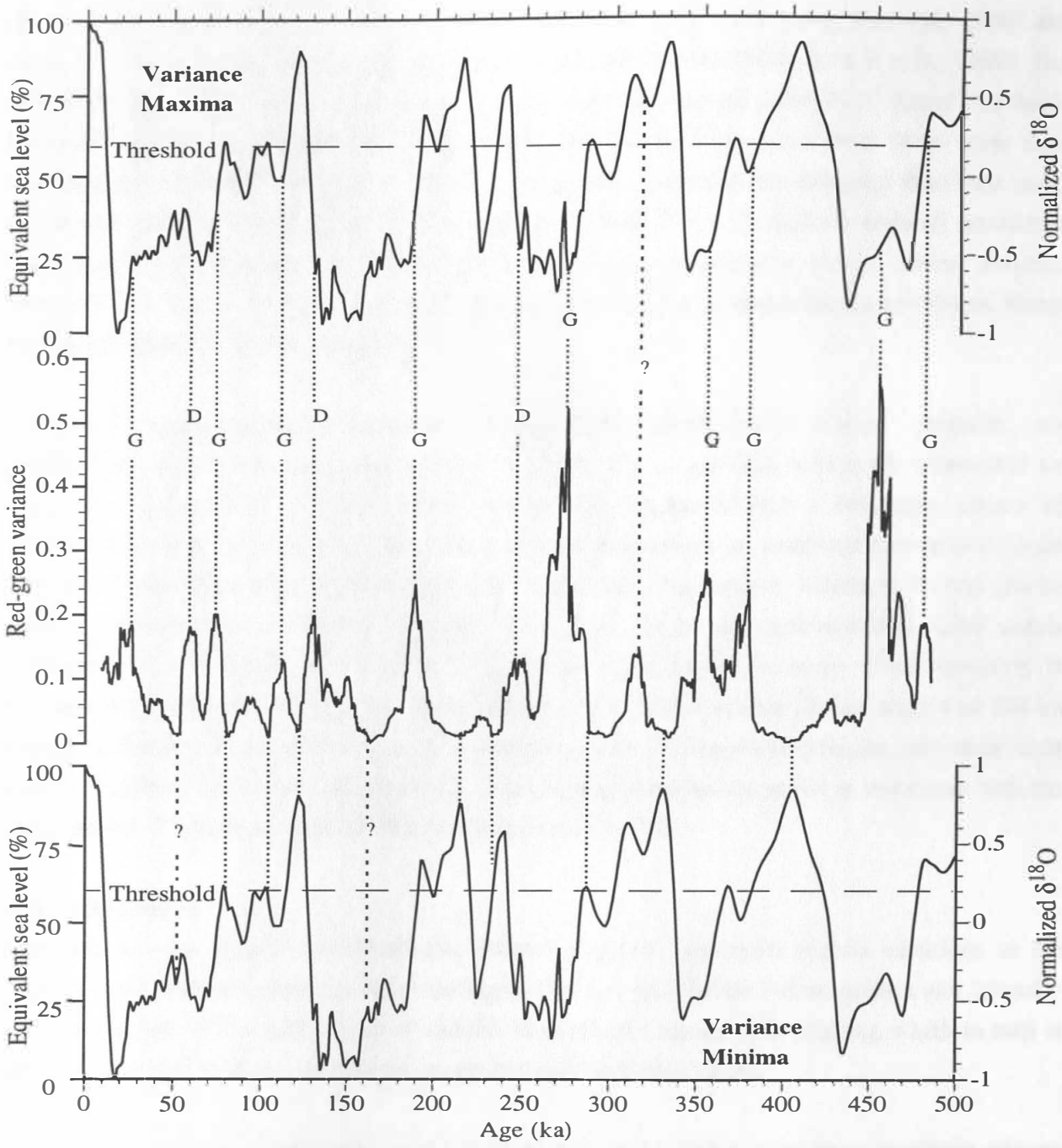

Fig. V-5: Ties between millennial-scale variance (centre) of the red-green color time series and sea level (%) (top/bottom). Sea-level (%) is derived from the normalized SPECMAP (Imbrie et al., 1984; Martinson et al., 1987) oxygen-isotope record (top/bottom). Variance maxima are aligned to the upper panel, variance minima to the lower one. Variance maxima coincide with times of either sea-level rise (ice decay; denoted by D) or sea-level drop (ice growth; denoted by G), as indicated by the dotted lines between the two upper records. An exceptional maximum occurs at 315 ka (short dashed line), when SPECMAP-derived sea level is probably overestimated (see text for details). Variance minima are tied to times with sea level above a threshold of approximately -40% (long dashed line), as indicated by the dotted lines between the two lower records. Two apparent exceptions occur at 53 and 164 ka (short dashed lines), when SPECMAP-derived sea-level is probably underestimated (see text for details).

glacial maximum (between 121 ± 5 m, Fairbanks, 1989 and 130-135 m, Yokoyama et al., 2000) and are in accordance with those derived from ice-core data for the last 100 ky (Schulz et al., 1999). The variance maximum at 315 ka is seemingly at odds with the inferred SPECMAP based threshold. However, according to Berger et al. (1996) sea-level at this time may have been 18 m lower than indicated by SPECMAP, bringing this variance maximum in line with our estimated threshold value. Of the five glacial terminations only Terminations III and II, the glacial-to-interglacial transitions from marine isotope stages 8 to 7, and 6 to 5, respectively, are characterized by variance maxima. Although this suggest different dynamical behaviour across glacial-to-interglacial transitions, future studies are needed to confirm this pattern.

Prominent variance minima, indicating low-amplitude millennial-scale climate variability, are generally associated with peak interglacials (Fig. V-5), that is, intervals with small continental ice mass. This agrees with previous studies, which have suggested that a minimum amount of continental ice is required to sustain prominent climate fluctuations on millennial time scales (Oppo et al., 1998; McManus et al., 1999; Schulz et al., 1999). The two variance minima at 53 and 164 ka seem to contradict our estimated threshold (Fig. V-5). However, radiometrically dated corals (Chappell et al., 1996) indicate that sea level at ~ 50 ka was indeed in the range of our threshold. If the same holds true for the relatively warm interval within glacial marine isotope stage 6 at 164 ka remains speculative but might deserve further investigations. During glacial maxima, millennial-scale climate variability is low, although higher than during peak interglacials, which is consistent with the observations of McManus et al. (1999) and Schulz et al. (1999).

V.6. Conclusions

A red-green color record from Northeast Atlantic deep-sea sediments reveals variations in the amplitude of millennial-scale variability during the last 500 ky. Changes in red-green color intensity are probably linked to varying input of reddish terrigenous material by ice rafting, which in turn is closely connected to climate variations on sub-Milankovitch time scales.

Using sea level as proxy for continental ice mass, our results indicate that large-amplitude climate variations are restricted to times when continental ice volume exceeds a threshold, equivalent to sea level at approximately -40% (or -51 ± 3 m). This value is almost indistinguishable from an earlier estimate, derived for the last 100 ky based on ice-core data. It is remarkable and favourable for future modelling studies that a single threshold value apparently controlled the cessation of large-amplitude millennial scale climate variations over the past five glacial-to-interglacial cycles.

Once continental ice mass exceeds the threshold value, maxima of millennial-scale climate variability are tied to times of changes in ice mass. In contrast, relatively stable ice volume during glacial

maxima goes along with considerable dampening of climate variability. The inferred relationship between ice volume and "agility" of the climate system to undergo short-term fluctuations holds throughout the past 500 ky.

Chapter VI - Comparison of glacial and interglacial conditions between the polar and subpolar North Atlantic Region over the last five climatic cycles

Jan P. Helmke and Henning A. Bauch

VI.1. Abstract

A multiparameter analysis of two sediment cores from the Northeast Atlantic and the Nordic Seas, i.e., the subpolar and polar North Atlantic, suggests that the Nordic Seas have experienced only three intervals of full interglacial conditions during the last 500,000 years, i.e., marine isotope stage (MIS) 11, 5e, and 1. In contrast, the Northeast Atlantic has experienced such conditions more frequently. A comparison of planktic $\delta^{18}O$ from the Northeast Atlantic reveals colder SSTs during MIS 11 than during other peak warm periods (MIS 9, 5e, and 1). The IRD record from the Nordic Seas points at a major temperature gradient in the polar North Atlantic and a reduced advection of warm surface water into the Nordic Seas during interglacial MIS 11. Maximum input of ice-rafted debris (IRD) during the final phase of glaciations and into early terminations was almost coherent between both sites indicating that the subpolar and polar North Atlantic were synchronously affected by the mechanisms that triggered a persistent variability of the glacial climate system. Millennial-scale recurrence periods of IRD maxima at the study areas point at differences in the timing of iceberg discharges between the Laurentide Ice Sheet and European ice sheets.

VI.2. Introduction

A large portion of more recent paleoceanographic research using high northern sediment cores investigated the climatic and environmental conditions of specific glacial and interglacial periods focussing, in particular, on the last glacial period (e.g., Labeyrie et al., 1992; Sarnthein et al., 1995; Fronval and Jansen, 1996; Bauch, 1996; McManus et al., 1998). Comparative analyses of North Atlantic marine sediment records and Greenland ice cores demonstrated that this last glaciation was not a stable climatic regime but punctuated by two modes of abrupt millennial-scale climate change, the so-called "Heinrich events" and "Dansgaard-Oeschger cycles" (Broecker et al., 1992; Bond et al., 1992; Dansgaard et al., 1993). Some of the cold events seem time-coeval between the subpolar North Atlantic and the Nordic Seas, i.e., the polar North Atlantic, even for longer time intervals such as the last interglacial-glacial cycle (McManus et al., 1994; Fronval and Jansen, 1997). But so far, no detailed comparison of climatic conditions for glacial and interglacial periods older than the last peak interglaciation, marine isotope stage (MIS) 5e, has been done for these two regions (Cortijo et al., 1994; Fronval and Jansen, 1997; Bauch et al., 2000b).

Nearly 25 years ago, a first paleoclimatic reconstruction of the Nordic Seas suggested that during the last 450,000 years only MIS 5e and 1 were characterized by a similar strength of warm Atlantic surface water inflow into the Norwegian and Greenland Seas resulting in comparable interglacial conditions in this region (Kellogg, 1976, 1977). More recently, comparisons of peak interglaciations in the Nordic Seas revealed significant differences in the overall water mass pattern, for instance colder conditions during MIS 11 when compared to MIS 5e and 1, suggesting that boundary conditions of peak interglacial climates must have been dissimilar throughout the upper Quaternary (Bauch et al., 1999; 2000a). In contrast, sea-surface temperatures (SST) estimates from about 55°N indicated that interglaciations with comparable peak warm conditions prevailed more frequently in the subpolar North Atlantic over the last five climatic cycles (Ruddiman et al., 1986; McManus et al., 1999).

Taking all the published evidence together implies that major differences in the surface ocean conditions of peak interglacial periods must have existed between the polar and subpolar North Atlantic Region. The purpose of this study is, therefore, to determine the climatic conditions of glacial and interglacial periods over the last five climate cycles in order to unveil possible synchroneities or asynchroneities in the behavior of the glacial-interglacial climate system at high northern latitudes. Using a multiparameter approach, sediment cores were selected that are located in oceanographically crucial areas of the Northeast Atlantic and the Nordic Seas.

VI.3 Core material and methods

Site M23352 from the northwestern Iceland Plateau in the Nordic Seas and Site M23414 from the southern edge of the Rockall Plateau in the Northeast Atlantic were investigated for this study (Fig. VI-1). Site M23352 was selected, as it is located close to the recent Polar Front, which is expected to

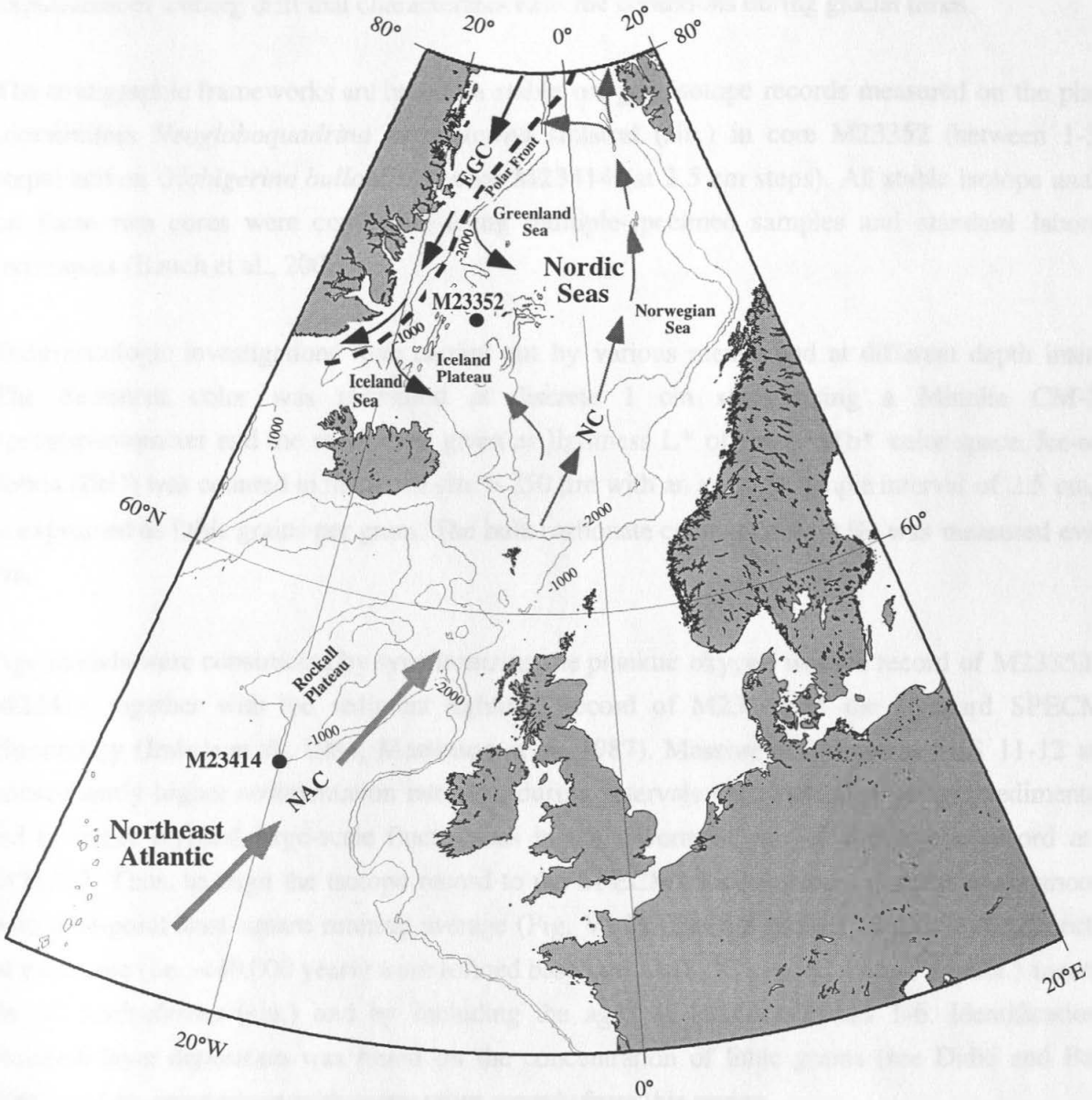

Fig. VI-1: Geographical position of study sites on the Iceland Plateau (M23352: spliced record of trigger box core M23352-2 and kasten core M23352-3; 70°00´N, 12°25´W, water depth 1820 m) and the Rockall Plateau (M23414: spliced record of trigger box core M23414-6, kasten core M23414-9 and gravity core M23414-8; 53°32´N, 20°17´W, water depth 2200 m) and simplified modern surface water circulation of the Northeast Atlantic and the Nordic Seas (Swift, 1986): Gray and black arrows denote warmer and cooler surface currents, respectively; NAC (North Atlantic Current); NC (Norwegian Current), EGC (East Greenland Current). Dashed black line indicates recent position of the Polar Front in the Nordic Seas. Water depth is in m.

have shifted repeatedly over the Iceland Plateau and further south during colder climatic intervals than at present. Accordingly, the Iceland Plateau sediment record should reveal the contrasts of glacial-interglacial climatic conditions in the polar North Atlantic. Site 23414 is located directly below the North Atlantic Current. This region has demonstrated its suitability for recording both the warm water advection that is mostly pronounced during the warmer climate periods and the major expansions of iceberg drift that characterizes extreme conditions during glacial times.

The stratigraphic frameworks are based on stable oxygen isotope records measured on the planktic foraminifers *Neogloboquadrina pachyderma* sinistral (sin.) in core M23352 (between 1-3 cm steps) and on *Globigerina bulloides* in core M23414 (at 2.5 cm steps). All stable isotope analyses on these two cores were conducted using multiple-specimen samples and standard laboratory techniques (Bauch et al., 2000b).

Sedimentologic investigations were carried out by various means and at different depth intervals. The Sediment color was measured at discrete 1 cm steps using a Minolta CM-2002 spectrophotometer and the results are given as lightness L* of the L*a*b* color space. Ice-rafted debris (IRD) was counted in the mesh size > 250 µm with an average sample interval of 2.5 cm, and is expressed as lithic grains per gram. The bulk carbonate content (weight %) was measured every 5 cm.

Age models were constructed by synchronizing the planktic oxygen isotope record of M23352 and M23414 together with the sediment lightness record of M23414 to the standard SPECMAP chronology (Imbrie et al., 1984; Martinson et al., 1987). Massive IRD input in MIS 11-12 and a consequently higher sedimentation rate than during intervals with enhanced pelagic sedimentation led to rather atypical large-scale fluctuations in the lowermost part of the isotope record at site M23352. Thus, to align the isotope record to the SPECMAP chronology, the data were smoothed with a 14-point least-square running average (Fig. VI-2). The age models for the younger sections of each core (i.e., <40,000 years) were refined based on AMS ^{14}C ages (C. Didié, unpubl.) measured on *N. pachyderma* (sin.) and by including the ages of Heinrich events 1-6. Identification of Heinrich layer deposition was based on the concentration of lithic grains (see Didié and Bauch, 2000) and by comparison with many other records from this region.

VI.4. Results

VI.4.1. The Rockall Plateau record

At Site M23414 at the Rockall Plateau all peak interglacial warm periods are characterized by

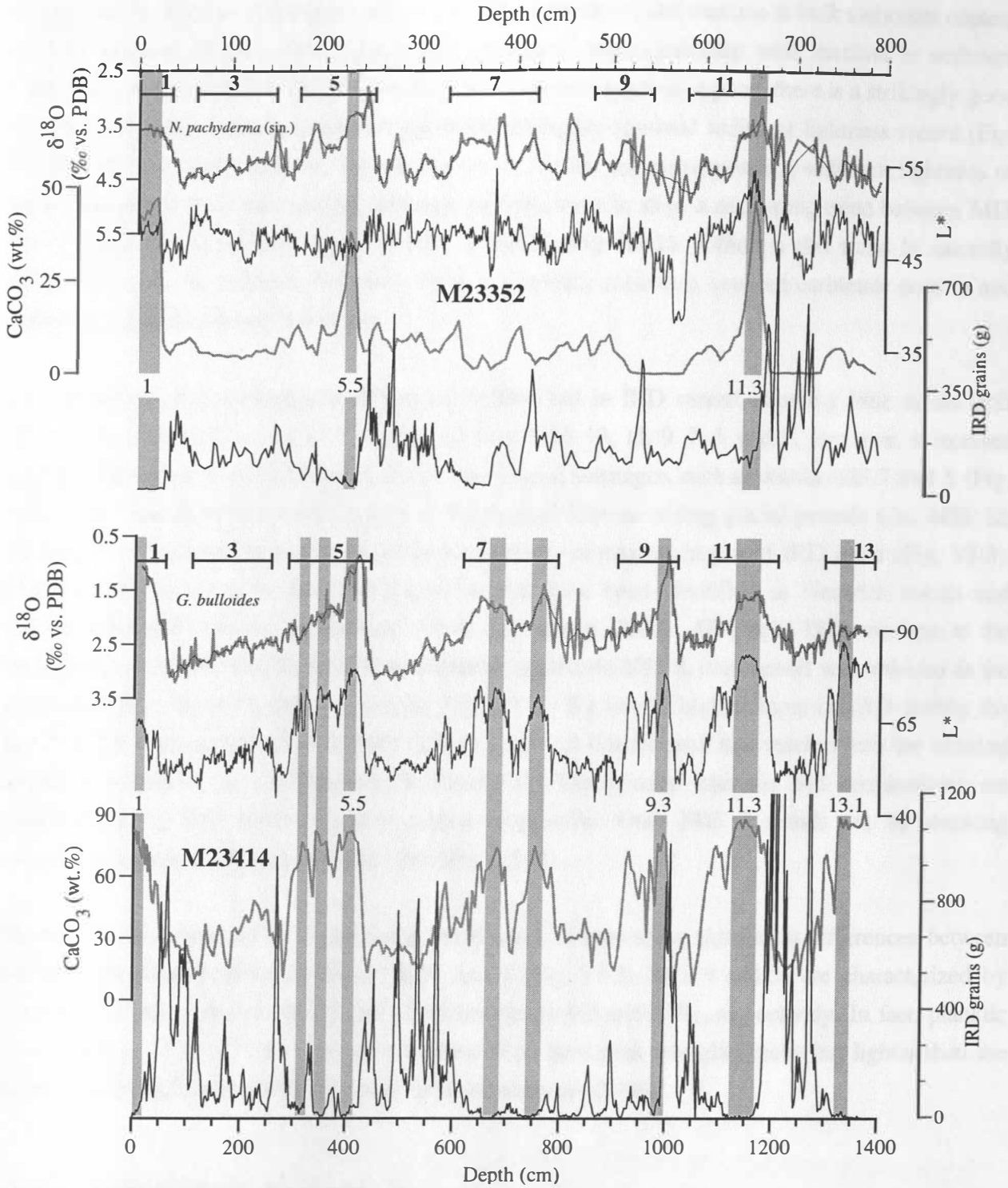

Fig. VI-2: Downcore records of planktic $\delta^{18}O$, sediment lightness, $CaCO_3$ content, and IRD content from the Iceland Plateau (upper panel, data from Henrich, 1998; Bauch and Helmke, 1999; Bauch et al., 2000; Bauch, unpubl.) and the Rockall Plateau (lower panel, data partly from Jung, 1996; Didié and Bauch, 2000), with odd numbered interglacial MIS indicated for reference. Thin black line underlying bosth isotope records (gray line) represents 14-point least square running average of raw isotopic data. Shaded areas denote full-interglacial conditions during MIS 1, 5, 7, 9, 11 and 13. Note that the maximum IRD amount at Termination V (2554 grains (g) at 1220 cm core depth in M23414) is cut off at 1500 grains (g) to enlarge low amplitude fluctuations of IRD input.

minima in planktic oxygen isotope values, no IRD deposition, and maxima in bulk carbonate content ranging between 50 and 90%. These high carbonate values correlate with maxima in sediment lightness, except in MIS 1. Despite the different sample resolution applied, there is a strikingly good correlation between carbonate content and the much higher-resolved sediment lightness record (Fig. VI-2). MIS 13 reveals both the highest carbonate content and corresponding sediment lightness of the entire record. Peak interglacial carbonate contents seem to show a decreasing trend between MIS 13 and MIS 7 but increases again in MIS 5 and 1 (Fig. VI-2). Although this trend is naturally reflected also in the sediment lightness, there is a notable mismatch between carbonate content and sediment lightness for the Holocene.

A pronounced glacial-interglacial difference is observed in IRD record, showing little or no IRD input during the peak interglacial warm phases of MIS 13, 11, 9, 7, 5, and 1. However, it received measureable amounts of IRD during cooler interglacial substages, such as within MIS 7 and 5 (Fig. VI-2). IRD was deposited continuously at the Rockall Plateau during glacial periods (i.e., MIS 12, 10, 6, and 4-2), with millennial-scale recurrence periods of maxima in glacial IRD input (Fig. VI-3). Distinct IRD peaks in the last two glacial periods have been identified as Heinrich events and Heinrich-like IRD events, respectively (Didié and Bauch, 2000). All glacial IRD maxima at the Rockall Plateau, including those of low-amplitude such as in MIS 8, correspond with minima in the sediment lightness and carbonate records (Fig. VI-3). By far the highest input of IRD during the last 500,000 years occurred in late MIS 12 with a distinct double peak that reaches into the ensuing deglacial transition, i.e., Termination V. Nearly all later glacial intervals and terminations are characterized by IRD input of rather similar amplitudes. Only MIS 8 stands out by showing extreme low glacial IRD depositional rates (Fig. VI-3).

Planktic isotope values of *G. bulloides* at the Rockall Plateau show significant differences between the peak interglacial periods MIS 11, 9, 5e, and 1 (Fig. VI-2). MIS 9 and 5e are characterized by values of ~0.9‰, values in MIS 1 and 11 are heavier by 0.3 and 0.7‰, respectively. In fact, planktic isotope values of MIS 11 are heavier than those of all later peak interglaciations but lighter than the preceding interglaciation MIS 13, which reveals values of ~2.1‰.

VI.4.2. The Iceland Plateau record

When compared to the Rockall Plateau, the core sequences on the Iceland Plateau contains generally lower amounts of carbonate (less than 10%), with increased values (30-50%) occurring only in MIS 11, 5e, and 1 (Fig. VI-2). The two younger peak interglacial intervals reveal minimum isotope values associated with strongly reduced or no IRD, as at the Rockall Plateau. However, MIS 11 is characterized by significant IRD (Fig. VI-3). In contrast to the Rockall study site the Iceland Plateau

record does not show any strong correlation between carbonate content and sediment lightness. This is due to the generally low carbonate content of the sediment (Bauch and Helmke, 1999).

The Iceland Plateau received an almost continuous input of IRD, regardless of glacial or interglacial climate mode (Fig. VI-2). Besides MIS 5e and 1, strongly reduced IRD input and IRD-free intervals occurred episodically only in late MIS 7. In comparison with MIS 5e and 1, the reduced IRD deposition during late MIS 7 is associated with relatively low carbonate content (up to 15%) and, because of faunal evidence, seems not representative of a significant warm phase (Bauch, 1997). In general, the glacial IRD record from the Iceland Plateau shows a pattern of millennial-scale variability during MIS 12, 10, 6, and 4-2, but we could not discern a definite recurrence period (Fig. VI-3). Like at the Rockall Plateau, the end of MIS 12 and the ensuing Termination V are marked by highest IRD deposition and a distinctive double peak. After Termination V, IRD maxima are of comparable amplitude during the remaining glacial intervals with steep and short-term increases occurring during Terminations IV-II. In contrast to the Rockall Plateau, the IRD input on the Iceland Plateau during MIS 8 shows an amplitude that is quite comparable to the later glaciations (Fig. VI-3).

Planktic oxygen isotope values of *N. pachyderma* (sin.) show only minor differences between MIS 11, 5, and 1: Mean minimum values of the warm substages during these three interglaciations range between 3.5‰ and 3.2‰ (Fig. VI-2). The extremely light $\delta^{18}O$ spike in early MIS 5e (at ~240 cm core depth) has been identified as meltwater event, and does not represent interglacial conditions (Bauch et al., 2000b). However, meltwater overprints in the planktic $\delta^{18}O$ are a common feature in the Nordic Seas, particularly, below MIS 7, making the establishing of a chronology based on $\delta^{18}O$ alone more difficult if no other means, such as $\delta^{13}C$ records, sedimentologic and faunal evidence, are taken into account (Bauch, 1997).

VI.5. Discussion and conclusions

In accordance with previous results our stable isotope, carbonate, and IRD records from the Iceland Plateau demonstrate that during the last 500,000 years full-interglacial conditions with a significant northward advection of warm Atlantic surface water into the Nordic Seas prevailed only in MIS 11, 5e, and 1 (e.g., Kellogg, 1980; Bauch, 1997; Henrich, 1998). Foraminiferal assemblage data from the Norwegian Sea indicate that SST were significantly lower in MIS 11 than in MIS 1 (Bauch et al., 2000a). The continuous occurrence of IRD on the Iceland Plateau corroborates this finding. The Norwegian Sea revealed a 10,000 years long IRD-free interval during MIS 11 (Bauch et al., 2000a). This implies that a strong frontal system separated the cold water masses in the Greenland and Iceland seas characterized by icebergs from a warmer water mass marked by ice-free conditions further east in the Norwegian Sea. Hence, compared with the present day situation the data would

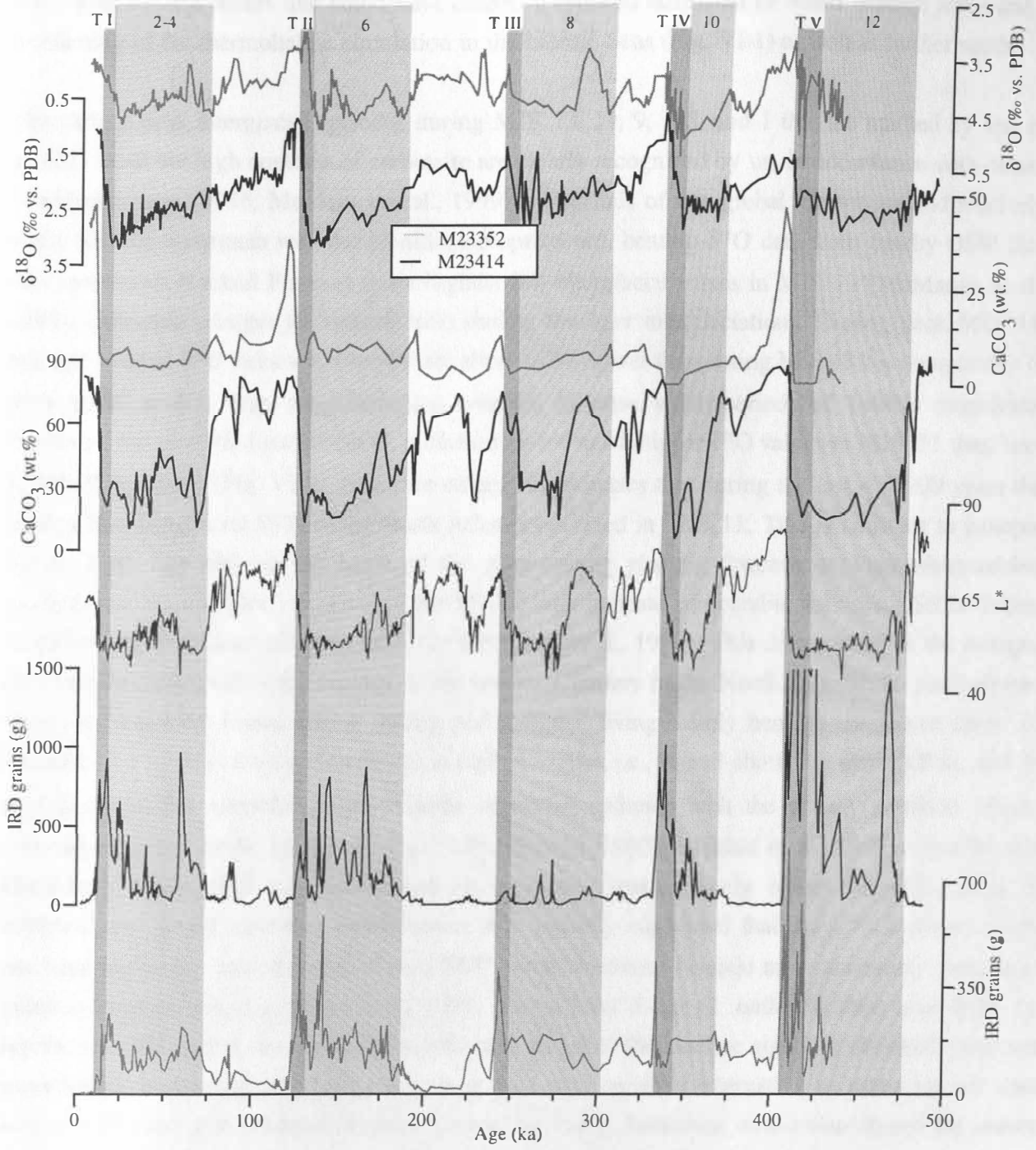

Fig. VI-3: Some records from Figure 2 plotted *vs.* age. Age models are based on spliced standard SPECMAP chronology (Imbrie et al., 1984; Martinson et al., 1987). Glacial MIS and Terminations I-V (T I-V) are shaded in gray and labeled for reference.

suggest a different circulation pattern during MIS 11 compared with MIS 5e and 1 (Bauch et al., 1999; Bauch et al., 2000a). This may point at an eastern expansion of the polar water mass with its

low-saline surface waters that could have caused a reduced advection of warm Atlantic water and a weakening of the thermohaline circulation in the Nordic Seas (Fig. VI-1) as well as further south.

The various peak interglacial episodes during MIS 13, 11, 9, 7, 5, and 1 that are marked by low or no IRD input but high contents of carbonate are clearly recognized by us, in accordance with others (Ruddiman et al., 1986; McManus et al., 1999), as periods of low global ice volume and relatively warm SST. In agreement with our planktic isotope record, benthic $\delta^{18}O$ data from nearby ODP Site 980 (northwest Rockall Plateau) show highest full-interglacial values in MIS 13 (McManus et al., 1999), indicating a larger ice volume than during the later interglaciations. During peak MIS 11, average benthic $\delta^{18}O$ values at Site 980 are about 0.7‰ lower than during MIS 13 but comparable to MIS 9, 5e, and 1, thus suggesting ice volumes in these warm periods of similar magnitude. However, our planktic foraminifer *G. bulloides* yields much higher $\delta^{18}O$ values in MIS 11 than later in MIS 9, 5e, and 1 (Fig. VI-2). As a face value, this indicates that during the last 450,000 years the coldest full-interglacial SSTs in the North Atlantic occurred in MIS 11. This is contrary to isotopic results from Site 980 on the basis of the right-coiling planktic foraminifer *Neogloboquadrina pachyderma* dextral (dex.) as a proxy for SST, which indicate comparable maximum SSTs during all full-interglacial intervals since MIS 12 (McManus et al., 1999). This discrepancy in the isotopic data may be explained by the ecology of the two foraminifers in the North Atlantic. *N. pachyderma* (dex.) is frequently found during spring and summer, living mainly beneath the mixed layer. In contrast, *G. bulloides* lives preferentially in surface waters, i.e., in and above the thermocline, and its abundance in the subpolar North Atlantic seems to coincide with the spring plankton bloom (Hemleben et al., 1989; Duplessy et al., 1991, Ottens, 1992; Schiebel et al., 1997; Schiebel and Hemleben, 2000). SST estimates based on these two species likely reflect the differences in temporal and spatial distribution. Moreover, it is recently suggested that the $\delta^{18}O$ isotopes of *N. pachyderma* (dex.) records mean annual SST in the Northeast Atlantic more accurately than other planktic foraminifers (e.g., Oppo et al., 1998). Regardless, if our *G. bulloides* data from MIS 11 represent a SST signal that more likely reflects a seasonal thermocline signal, it obviously was not recorded by *N. pachyderma* (dex.). In this respect it is certainly interesting to note that our data accord with the results obtained from the Vostok ice core in Antarctica, which also shows the lowest peak interglacial temperatures of the last 450,000 years in MIS 11 (Petit et al., 1997).

The maximum input of IRD towards the end of MIS 12 at both study sites may reflect unusually large discharges of icebergs from the Laurentide and European ice sheets into the polar and subpolar North Atlantic alike. That these high IRD input towards the end of MIS 12 reflects the terminal stage of a strong glaciation is further supported by benthic oxygen isotope data from ODP Sites 980 and 982 (McManus et al., 1999; Venz et al., 1999) and Pleistocene sea-level lowstand

calculations (Rohling et al., 1998), both indicating that MIS 12 was probably characterized by the largest global ice volume during the past 500,000 years. The IRD maxima indicate large amplitude climate variations, although insolation forcing during Termination V was less than during later

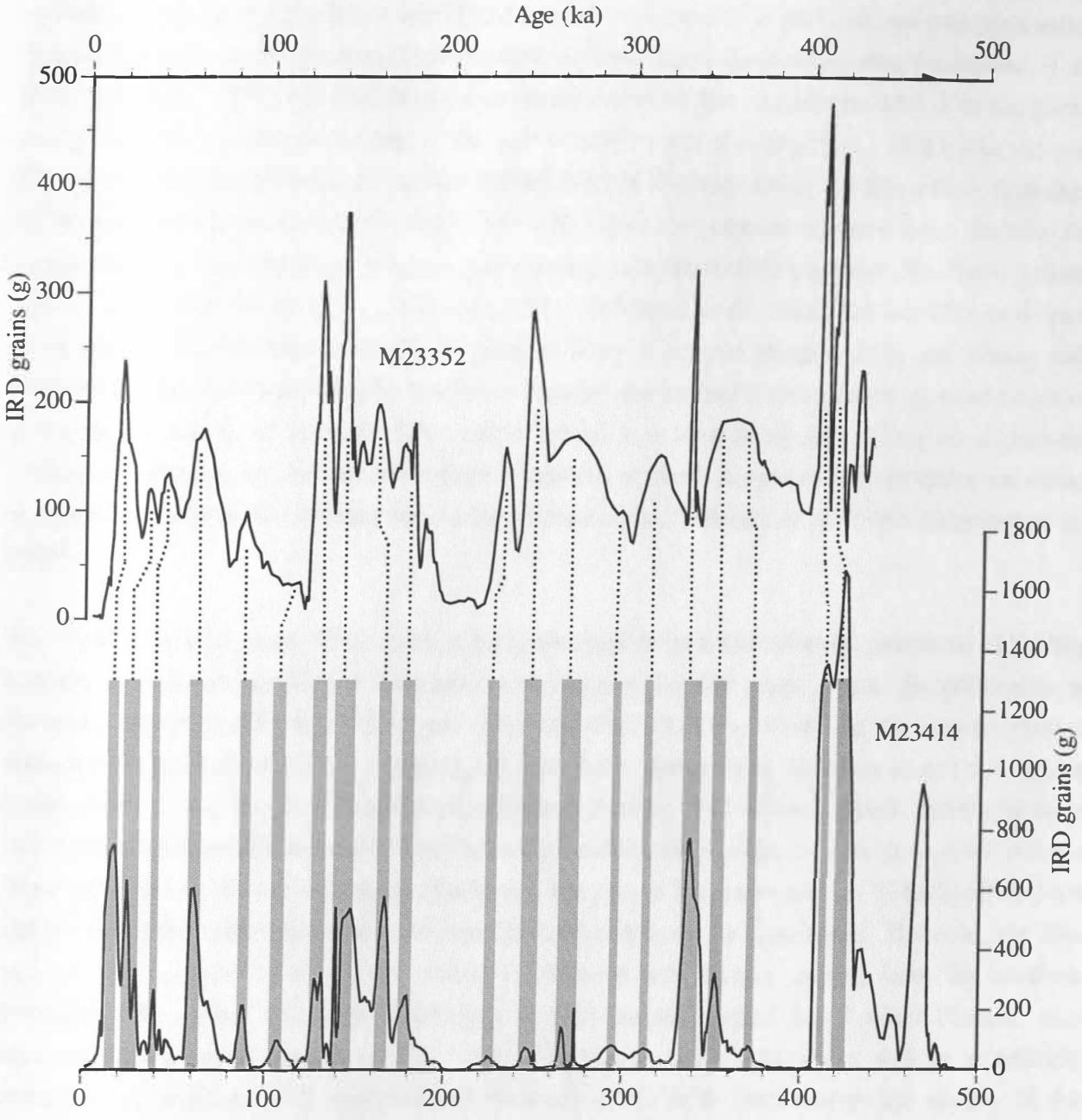

Fig. VI-4: 9-point least square running average of IRD records from M23352 (upper panel) and M23414 (lower panel) *vs.* age. Shaded areas denote major IRD events at the Rockall Plateau during the last 450 ka. Dashed lines indicate corresponding IRD events on the Iceland Plateau.

terminations (Berger, 1978). A maximum input of IRD during Termination V is also reported from Late Quaternary sediments of ODP Site 982 at 57°N (Venz et al., 1999). These authors linked their

IRD record to glacial deep-water production and characterized MIS 12 as an interval of perennial sea ice cover in the Nordic Seas.

Based on the low IRD input to the Rockall Plateau during MIS 8, the iceberg discharge from northern ice sheets is expected to have been less when compared to previous and later glaciations. This finding is in good agreement with benthic isotopes from the Rockall area (McManus et al., 1999; Venz et al., 1999) and with sea-level lowstand estimates that characterize MIS 8 as the glacial period with the smallest ice volume of the past 500,000 years (Rohling et al., 1998). The obvious differences in IRD input between the Iceland and Rockall Plateaus during this time can be explained by the geographical position of the study sites with respect to potential glaciated areas: Because the Laurentide ice sheet is believed to be the major source of massive IRD input into the North Atlantic during the last glacial period (e.g., Broecker, 1994; McManus et al., 1998), the low IRD deposition at the Rockall Plateau during MIS 8 probably indicates a reduced glacier activity and iceberg drift pattern along the northwest Atlantic margin. In contrast, the Iceland Plateau record gives evidence of a continuous supply of icebergs. The reason behind it is most likely the vicinity to a glaciated landmasses, but may be also due to a different behavior of North American and European ice sheets in general, as previously reported for the last climate cycle (Snoeckx et al., 1999; Grousset et al., 2000).

The "cold" climate proxy IRD shows a geographically remarkable coherent pattern of variability between the Iceland and Rockall Plateaus during the past 500,000 years, despite the differences in the total amount of IRD deposited at each core site (Fig. VI-2, Fig. VI-4). At the Rockall Plateau distinct IRD maxima of the last climate cycle have been identified as Heinrich events (Didié and Bauch, 2000), whereas the contemporary Iceland Plateau IRD record reveals millennial-scale variability without a definite periodicity (Didié et al., subm.). Prior to the last glaciation, both records show variations in IRD on millennial time-scales, but due to the uncertainty of SPECMAP-derived age models clear millennial-scale recurrence periods could not be determined. However, the data suggest that comparable short-term climate fluctuations with iceberg calving from the northern hemisphere ice sheets and large discharges of IRD on the Iceland and Rockall Plateaus also occurred during earlier glaciations (Fig. VI-4). Differences in the intervals as well as in periodic recurrence of increased IRD input between the study sites can be explained by the vicinity of the Iceland Plateau to the recent Polar Front (Fig. VI-1). As it can be expected, the Polar Front with its cold and low-saline waters as well as icebergs, shifted repeatedly towards the southeast during glacial periods. Therefore, the Iceland Plateau received an almost continuous IRD sedimentation during the last five climate cycles. The lack of synchroneity in the periods of millennial-scale IRD input between the subpolar and polar North Atlantic indicates differences in ice sheet dynamics between the Laurentide Ice Sheet, the major source of North Atlantic Heinrich events (Bond and

Lotti., 1995), and ice-sheet outlet glaciers draining into the Nordic Seas and iceberg drift on the Iceland Plateau (Dowdeswell et al., 1999, Grousset et al., 2000). Because ice-sheet basins of varying size respond asynchronously to any single external forcing (Johannessen et al., 1989), there is local variability in the drift tracks and sediment-release histories of groups of icebergs (Dowdeswell and Murray, 1990). Thus, the geographical position of our study sites with respect to the northern hemisphere ice sheets during the upper Quaternary caused differences in the recurrence periods of polar and subpolar North Atlantic IRD on millennial time-scales. However, the IRD patterns in the two cores demonstrate that unstable climatic modes with rapid, short-term fluctuations prevailed during glacial intervals, reflecting the overall dynamic nature of the upper Quaternary climate system at high northern.

We conclude that the Nordic Seas have experienced full interglacial conditions only three times during the last 500,000 years (i.e., MIS 11, 5e, and 1), whereas full interglacial periods were more frequent in the Northeast Atlantic. By comparison, planktic $\delta^{18}O$ from the Northeast Atlantic indicate strong discrepancies among interglacial SSTs, i.e., coldest SSTs were found for MIS 11 compared with other peak warm periods (MIS 9, 5e, and 1). The IRD record from the Nordic Seas points at a major temperature gradient in the North Atlantic and a reduced advection of warm surface water into the Nordic Seas during interglacial MIS 11. It would be intriguing to speculate about the effects the reduced heat transfer into the Nordic Seas would have had on the deeper water circulation in the Nordic Seas and the climatic conditions on land. At both sites IRD input was highest during the final phases of glaciations (including early terminations) revealing an almost coherent pattern of IRD deposition between the two study areas with differences in millennial-scale recurrence periods, i.e., in the timing of iceberg discharges between the Laurentide Ice Sheet and European ice sheets. However, the IRD records point at mechanisms that synchronously affected both the Nordic Seas and the North Atlantic and that led to millennial-scale variability of the glacial climate system.

VII - Summary and conclusions

The rationale of this study was to give insight into Late Quaternary climatic variations of the high northern latitudes on glacial-interglacial as well as on millennial time-scales using a wide range of sedimentological, micropaleontological, and geochemical proxy data from Northeast Atlantic and Nordic Seas deep-sea sediments. Four manuscripts that make up the body of this thesis discussed some aspects of the upper Quaternary climate system over the subpolar and polar North Atlantic regions during the last five glacial-interglacial cycles. The paleoceanographic and paleoclimatic conclusions obtained from the results of these manuscripts are summarized below:

In order to determine changes in the Late Quaternary marine carbonate system of the high northern latitudes the carbonate preservation of sediments from the Nordic Seas was studied **(Chapter III):**

- A new method to investigate carbonate corrosion was presented. This method is a combination of weight and lightness measurements as well as SEM-analyses of planktic foraminiferal tests.
- By using this new approach foraminiferal tests from the Nordic Seas revealed distinct glacial-interglacial changes in carbonate preservation with good glacial preservation and increasing corrosion during interglaciations. This pattern is similar to the Late Quaternary carbonate dissolution pattern from the deep Pacific Ocean, but seems to be out of phase with the rest of the Atlantic Ocean.
- Strongest carbonate corrosion was observed in interglacial MIS 11.
- With only few exceptions the samples showed relatively good carbonate preservation. This indicates that deeper waters in the Nordic Seas were almost persistently well-ventilated during last 500,000 years, regardless of the climatic mode.
- The mechanisms that led to the Nordic Seas carbonate preservation pattern cannot be determined definitely: The enhanced calcite corrosion during interglaciations may have been caused by high planktic productivity with an increased downward flux rate of organic material to the sea bottom and, consequently, to more corrosive bottom water due to carbondioxide enrichment. Yet, it may also be linked to global scale variations in the marine carbonate system, e.g., to changes in the alkalinity of the oceans.

Climate variability in the subpolar North Atlantic during the last five climate cycles was investigated using sediment color records. Thus, in a first step it was necessary to unveil the factors that control sediment color **(Chapters IV and V):**

- A detailed investigation of the carbonate fraction from a Northeast Atlantic deep sea sediment core indicated that during the last 500,000 years changes in sediment lightness were controlled mainly by fluctuations of the fine (<20 μm) carbonate fraction.

- There is a strong influence of carbonate corrosion on total sediment lightness: Enhanced corrosion has an effect on the surface structure of the coarse (>20 μm) and, probably, also of the fine carbonate fraction. An increase in carbonate corrosion goes along with an increase in sediment lightness.
- No straightforward correlation between sediment lightness and carbonate content was recognized. Changes in the preservational mode of the carbonate fraction need to be considered before using sediment color data for estimates of carbonate content.
- Changes in the sediment red-green chromaticity during the past half a million years are most likely driven by variations in the iceberg-rafted terrigenous input of reddish minerals containing iron.
- Spectral analysis of the red-green color record revealed persistent millennial-scale climate variability during the upper Quaternary.
- Maxima of climate variability were tied to times of changes in ice mass and coincide to times when sea level was 40% below present-day value indicating threshold behaviour. This single threshold controlled the amplitude of climatic variations on millennial time-scales throughout the investigated period.
- Short-term fluctuations of the climate system were reduced during peak interglacials and also during peak glacial intervals of relatively stable ice volume.

Sedimentological and geochemical proxy records form both study regions were compared in detail to determine climatic conditions of the polar and subpolar North Atlantic during the last five climate cycles (**Chapter VI**):

- In contrast to the more frequent occurrence of warm interglacial conditions in the subpolar North Atlantic full interglacial conditions in the polar North Atlantic occurred only during MIS 1, 5e, and 11.
- A comparison of planktic $\delta^{18}O$ from the Northeast Atlantic suggests colder SSTs during MIS 11 than during other peak warm periods, i.e., MIS 1, 5e, and 9.
- IRD records indicate a major temperature gradient in the polar North Atlantic and a reduced advection of warm surface water into the Nordic Seas during interglacial MIS 11.
- IRD input in the Northeast Atlantic and the Nordic Seas increased almost coherently during glaciations and terminations. A general lack of synchroneity in the reccurrence periods of IRD maxima points at differences in the timing of iceberg discharges between Northern Hemisphere ice sheets.
- Obviously, the subpolar and polar North Atlantic were synchronously affected by the mechanisms that caused a millennial-scale variability of the glacial climate system.

These new results from Northeast Atlantic and Nordic Seas sediments indicate highly dynamic climates during the Late Quaternary with distinct variability on longer, glacial-interglacial as well as on shorter, millennial time-scales. The investigations revealed synchronous influences on the glacial climate system in the polar and subpolar North Atlantic but also pronounced differences in the paleoclimatic and paleoceanographic conditions between the two areas during the last five climate cycles. The findings could shed some light onto the complex interactions of the forcing and feedback mechanisms that commonly are thought to drive climatic variations in the high northern Atlantic region.

References:

Aagaard, K. and Carmarck, E.C., 1994. The Arctic Ocean and climate. In: The Polar Oceans and Their Role in Shaping the Global Environment; Johannesson, O.M. (Ed.), AGU, Washington, D. C., pp. 5-20.

Andrews, J.T. and Freeman, W., 1996. The measurement of sediment color using the colortron spectrophotometer. Arctic and Alpine Research, 28 (4): 524-528.

Andruleit, H., 1995. Coccolithophoriden im Europäischen Nordmeer: Sedimentation und Akkumulation; sowie ihre Entwicklung während der letzten 15.000 Jahre. Reports SFB 313, Univ. Kiel, Vol. 59, pp. 1-110.

Archer, D.E., 1991. Modeling the calcite lysocline. Journal of Geophysical Research, 96: 17037-17050.

Archer, D.E. and Maier-Reimer, E., 1994. Effect of deep-sea sedimentary calcite preservation on atmospheric CO_2 concentration. Nature, 367: 260-263.

Archer, D., Winguth, A., Lea, D. and Mahowald, N., 2000. What caused the glacial/interglacial pCO_2 cycles? Reviews of Geophysics, 38 (2): 159-189.

Arrhenius, G., 1988. Rate of production, dissolution, and accumulation of biogenic solids in the ocean. Palaeogeography, Palaeoclimatology, Palaeoecology, 67: 119-146.

Augstein, E., Hempel, G., Schwarz, A. and Thiede, J., 1984. Die Expedition Arktis 2 des FS "Polarstern" 1984 mit Beiträgen des FS "Valdivia" und des Forschungsflugzeuges "Falcon 20" zum Marginal Ice Zone Experiment 1984 (MIZEX).

Balsam, W.L., 1983. Carbonate dissolution on the Muir Seamount (western North Atlantic): interglacial/glacial changes. Journal of Sedimentological Petrology, 53: 719-731.

Balsam, W.L. and Deaton, B.C., 1996. Determining the composition of late Quaternary marine sediments from NUV, VIS, and NIR diffuse reflectance spectra. Marine Geology, 134: 31-55.

Balsam, W.L., Deaton, B.C. and Damuth, J.E., 1999. Evaluating optical lightness as a proxy for carbonate content in marine sediment cores. Marine Geology, 161: 141-153.

Barnola, J.M., Raynaud, D., Korotkevich, Y.S. and Lorius, C., 1987. Vostok ice core provides 160,000-year record of atmospheric CO_2. Nature, 329: 408-414.

Bassinot, F.C., Beaufort, L., Vincent, E., Labeyrie, L.D., Rostek, F., Müller, P.J., Quidelleur, X. and Lancelot, Y., 1994. Coarse fraction fluctuations in pelagic carbonate sediments from the tropical Indian Ocean: A 1500-kyr record of carbonate dissolution. Paleoceanography, 9 (4): 579-600.

Bauch, H.A., 1996. Monitoring Termination 2 at high latitude: anomalies in the planktic foraminiferal record. Marine Geology, 131: 89-102.

Bauch, H.A., 1997. Paleoceanograpy of the N. Atlantic Ocean (68°-76°N) during the past 450 ky deduced from planktic foraminferal assemblages and stable isotopes. In: Contributions to the Micrppaleontology and paleoceanography of the Northern North Atlantic; Hass, H.C. and Kaminski, M.A. (Eds.), Grzybowski Foundation Special Publication, pp. 83-100.

Bauch, H.A. and Helmke, J.P., 1999. Glacial-interglacial records of the reflectance of sediments from the Norwegian-Greenland-Iceland Sea (Nordic seas). International Journal of Earth Sciences (Geologische Rundschau), 88 (2): 325-336.

Bauch, H.A., Erlenkeuser, H., Fahl, K., Spielhagen, R.F., Weinelt, M.S., Andruleit, H. and Henrich, R., 1999. Evidence for a steeper Eemian than Holocene sea surface temperature gradient between Arctic and sub-Arctic regions. Palaeogeography, Palaeoclimatology, Palaeoecology, 145: 95-117.

Bauch, H.A., Erlenkeuser, H., Jung, S.J.A. and Thiede, J., 2000a. Surface and deep water changes in the subpolar North Atlantic during Termination 2 and the last interglaciation. Paleoceanography, 15 (1): 76-84.

Bauch, H.A., Erlenkeuser, H., Helmke, J.P. and Struck, U., 2000b. A paleoclimatic evaluation of marine oxygen isotope stage 11 in the high Northern Atlantic (Nordic Seas). Global and Planetary Change, 24: 27-39.

References

Baumann, K.-H., Lackschewitz, K.S., Erlenkeuser, H., Henrich, R. and Jünger, B., 1993. Late Quaternary calcium carbonate sedimentation and terrigenous input along the east Greenland continental margin. Marine Geology, 114: 13-36.

Baumann, K.-H., Meggers, H. and Henrich, R., 1996. Variations in surface water mass conditions in the Norwegian-Greenland Sea: Evidence from Pliocene/Pleistocene calcareous plankton records (Sites 644, 907, 909). In: Proceedings of the Ocean Drilling Program, Scientific Results; Thiede, J., Myhre, A.M., Firth, J.V., Johnson, G.L. and Ruddiman, W.F. (Eds.), Vol. 151, College Station, TX, pp. 493-514.

Bendat, J.L. and Piersol, A.G., 1986. Random data. John Wiley & Sons, New York, pp. 1-566.

Berelson, W.M., Hammond, D.E. and Cutter, G.A., 1990. In situ measurements of calcium carbonate dissolution rates in deep-sea sediments. Geochimica et Cosmochimica Acta, 54: 3013-3020.

Berger, A.L., 1978. Long-term variations of caloric insolation resulting from the Earth's orbital elements. Quaternary Research, 9 (2): 139-167.

Berger, W.H., 1968. Planktonic foraminifera: selective solution and paleoclimatic interpretation. Deep-Sea Research, 15: 31-43.

Berger, W.H., 1970. Planktonic foraminifera: Selective solution and the lysocline. Marine Geology, 8: 111-138.

Berger, W.H., 1982. Increase of carbon dioxide in the atmosphere during deglaciation: the coral reef hypothesis. Naturwissenschaften, 69: 87-88.

Berger, W.H., Finkel, R.C., Killingley, J.S. and Marchig, V., 1983. Glacial-Holocene transition in deep-sea sediments: manganese spike in the east equatorial Pacific. Nature, 303: 231-233.

Berger, W.H., 1992. Pacific carbonate cycles revisited: arguments for and against productivity control. In: Centenary of Japanese Micropaleontology; Ishizaki, K. and Saito, T. (Eds.), Terra Scientific Publishing Company, Tokyo, pp. 15-25.

Berger, W.H., Bickert, T., Yasuda, M.K. and Wefer, G., 1996. Reconstruction of atmospheric CO_2 from ice-core data and the deep-sea record of Ontong Java plateau: the Milankovitch chron. Geologische Rundschau, 85: 466-495.

Birgisdottir, L., 1991. Die paläo-ozeanographische Entwicklung der Island-See in den letzten 550.000 Jahren. SFB 313 Reports, Vol. 34, pp. 1-186.

Bond, G.C., Heinrich, H., Broecker, W.S., Labeyrie, L., McManus, J.F., Andrews, J., Huon, S., Jantschik, R., Clasen, S., Simet, C., Tedesco, K., Klas, M., Bonani, G. and Ivy, S., 1992. Evidence for massive discharges of icebergs into the North Atlantic ocean during the last glacial period. Nature, 360: 245-249.

Bond, G.C., Broecker, W.S., Klas, M., Lotti, R. and McManus, J.F., 1992. Abrupt color changes in isotope stage 5 in North Atlantic deep sea cores: implications for rapid change of climate-driven events. In: NATO ASI Series 1; Kukla, G. and Went, E. (Eds.), pp. 185-206.

Bond, G.C., Broecker, W.S., Johnsen, S., McManus, J.F., Labeyrie, L., Jouzel, J. and Bonani, G., 1993. Correlations between climate records from North Atlantic sediments and Greenland ice. Nature, 365: 143-147.

Bond, G.C. and Lotti, R., 1995. Iceberg discharges into the North Atlantic on millennial time scales during the last glaciation. Science, 267: 1005-1010.

Bond, G.C., Showers, W., Cheseby, M., Lotti, R., Almasi, P., deMenocal, P., Priore, P., Cullen, H., Hajdas, I. and Bonani, G., 1997. A pervasive millennial-scale cycle in North Atlantic Holocene and glacial sediments. Science, 278: 1257-1266.

Bond, G.C., Showers, W., Elliot, M., Evans, M., Lotti, R., Hajdas, I., Bonani, G. and Johnson, S., 1999. The North Atlantic's 1-2 ky Climate Rhythm: Relation to Heinrich Events, Dansgaard/Oeschger Cycles and the Little Ice Age. In: Mechanisms of Global Climate Change at Millennial Time Scales; Clark, P.U., Webb, R.S. and Keigwin, L.D. (Eds.), Geophysical Monograph, American Geophysical Union, pp. 35-58.

Boyle, E.A. and Keigwin, L., 1987. North Atlantic thermohaline circulation during the past 20,000 years linked to high latitude surface temperature. Nature, 330: 35-40.

Broecker, W.S. and Peng, T.-H., 1987. The role of $CaCO_3$ compensation in the glacial to interglacial atmospheric CO_2 change. Global Biogeochemical Cycles, 1 (1): 15-29.

References

Broecker, W.S. and Peng, T.-H., 1989. The cause of the glacial to interglacial atmospheric CO_2 change: A polar alkalinity hypothesis. Global Biogeochemical Cycles, 3: 215-239.

Broecker, W.S. and Denton, G.H., 1990. The role of ocean-atmosphere reorganizations in glacial cycles. Quaternary Science Reviews, 9: 305-341.

Broecker, W.S., Bond, G.C. and Klas, M., 1990. A salt oscillator in the glacial Atlantic? The concept. Paleoceanography, 5: 469-477.

Broecker, W.S., 1991. The great ocean conveyor. Oceanography, 4: 79-89.

Broecker, W.S., Bond, G.C., Klas, M., Clark, E. and McManus, J.F., 1992. Origin of the northem Atlantic´s Heinrich events. Climate Dynamics, 6: 265-273.

Broecker, W.S. and Peng, T.-H., 1993. What caused the glacial to interglacial CO_2 change? In: NATO Volume on the Global Carbon Cycle; Heinmann, M. (Ed.), Vol. 15, pp. 95-115.

Broecker, W.S., Lynch-Stieglitz, J., Archer, D.E., Hofmann, M., Maier-Reimer, E., Marchal, O., Stocker, T. and Gruber, N., 1999. How strong is the Harvardton-Bear constraint? Global Biogeochemical Cycles, 13 (4): 817-820.

Catubig, N.R., Archer, D.E., Francois, R., deMenocal, P., Howard, W.R. and Yu, E.-F., 1998. Global deep-sea burial rate of calcium carbonate during the last glacial maximum. Paleoceanography, 13 (3): 298-310.

Chappell, J., Omura, A., Esat, T., McCulloch, M., Pandolfi, J., Ota, Y. and Pillans, B., 1996. Reconcilation of late Quaternary sea levels derived from coral terraces at Huon Peninsula with deep sea oxygen isotope records. Earth and Planetary Science Letters, 141: 227-236.

Chapman, M.R. and Shackleton, N.J., 1998. What level of resolution is attainable in a deep-sea core? Results of a spectrophotometer study. Paleoceanography, 14 (4): 311-315.

Cortijo, E., Duplessy, J.C., Labeyrie, L., Leclaire, H., Duprat, J. and van Weering, T.C.E., 1994. Eemian cooling in the Norwegian Sea and North Atlantic Ocean preceding continental ice-sheet growth, Nature, 372: 446-449.

Cortijo, E., Yiou, P., Labeyrie, L. and Cremer, M., 1995. Sedimentary record of rapid climatic variability in the North Atlantic Ocean during the last glacial cycle. Paleoceanography, 10 (5): 911-926.

Crowley, T.J., 1983. Calcium-carbonate preservation patterns in the central North Atlantic during the last 150,000 years. Marine Geology, 51: 1-14.

Curry, W.B., Duplessy, J.C., Labeyrie, L. and Shackleton, N.J., 1988. Changes in the distribution of $\delta^{13}C$ of deep CO_2 between the last glaciation and the Holocene. Paleoceanography, 3: 317-341.

Dansgaard, W., Johnsen, S.J., Clausen, H.B., Dahl-Jensen, D., Gundestrup, N.S., Hammer, C.U., Hvidberg, C.S., Steffensen, J.P., Sveinbjörnsdottir, A.E., Jouzel, J. and Bond, G.C., 1993. Evidence for general instability of past climate from a 250-kyr-ice-core record. Nature, 364: 218-220.

deMenocal, P., Ortiz, J., Guilderson, T. and Sarnthein, M., 2000. Coherent high- and low-latitude climate during the Holocene warm period. Science, 288: 2198-2202.

Didié, C. and Bauch, H.A., 2000. Species composition and glacial-interglacial variations in the ostracode fauna of the northeast Atlantic. Marine Micropaleontology 40: 105-129.

Didié, C., Bauch, H.A. and Helmke, J.P., subm. Faunal diversity changes of North-Atlantic deep-sea benthic ostracodes of the past 200,000 years. Palaeogeography, Palaeoclimatology, Palaeoecology.

Diester-Haass, L., 1985. Late Quaternary Sedimentation on the Eastern Walvis Ridge, SE Atlantic (HPC 532 and four piston cores). Marine Geology, 65: 145-189.

Dokken, T. and Hald, M., 1996. Rapid climatic shifts during isotope stages 2-4 in the Polar North Atlantic. Geology, 24: 599-602.

Dowdeswell, J.A. and Murray, T., 1990. Modelling rates of sedimentation from icebergs. In: Glaciomarine Environments: Processes and Sediments; Dowdeswell, J.A. and Scourse, J.D. (Eds.), Geological Society, London, pp. 121-137.

Dowdeswell, J.A., Elverhoi, A., Andrews, J.T. and Hebbeln, D., 1999. Asynchrounous deposition of ice-rafted layers in the Nordic seas and the North Atlantic Ocean. Nature, 400: 348-351.

Droxler, A.W., Ferro, E.C., Mucciarone, D.A. and Haddad, G.A., 1996. Simultaeneous Barrier Reef establishment, carbonate bank expansion, and sea floor carbonate dissolution in low latitudes during interglacial stage 11: case of basin to shelf carbonate fractionation? EOS, 77: 427.

Duplessy, J.-C., Labeyrie, L., Juillet-Leclerc, A., Maitre, F., Duprat, J. and Sarnthein, M., 1991. Surface salinity reconstruction of the North Atlantic Ocean during the last glacial maximum. Oceanologica Acta, 14 (4): 311-324.

Emerson, S. and Bender, M., 1981. Carbon fluxes at the sediment-water interface of the deep-sea. Calcium carbonate preservation. Journal of Marine Resarch, 39: 139-162.

Fairbanks, R.G., 1989. A 17,000-year glacio-eustatic sea level record: Influence of glacial melting rates on the Younger Dryas event and deep-ocean circulation. Nature, 342: 637-642.

Farrell, J.W. and Prell, W.L., 1989. Climatic change and $CaCO_3$ preservation: An 800,000 year bathymetric reconstruction from the central equatorial Pacific Ocean. Paleoceanography, 4 (4): 447-466.

Farrell, J.W. and Prell, W.L., 1991. Pacific $CaCO_3$ preservation and $\delta^{18}O$ since 4 Ma: paleoceanic and paleoclimatic implications. Paleoceanography, 6 (4): 485-498.

Fronval, T. and Jansen, E., 1996. Rapid changes in ocean circulation and heat flux in the Nordic seas during the last interglacial period. Nature, 383: 806-810.

Fronval, T. and Jansen, E., 1997. Eemian and early Weichselian (140-60 ka) paleoceanography and paleoclimate in the Nordic seas with comparisons to Holocene conditions. Paleoceanography, 12 (3): 443-462.

Grootes, P.M. and Stuiver, M., 1997. Oxygen 18/16 variability in Greenland snow and ice with 10^{3}- to 10^{5}- year time resolution. Journal of Geophysical Research, C10: 26455-26470.

Grousset, F.E., Labeyrie, L., Sinko, J.A., Cremer, M., Bond, G.C., Duprat, J., Cortijo, E. and Huon, S., 1993. Patterns of ice-rafted detritus in the glacial North-Atlantic (40-55° N). Paleoceanography, 8: 175-192.

Grousset, F.E., Pujol, C., Labeyrie, L., Auffret, G. and Boelaert, A., 2000. Were the North Atlantic Heinrich events triggered by the behaviour of the European ice sheets? Geology, 28 (2): 123-126.

Hagelberg, T.K., Bond, G.C. and deMenocal, P., 1994. Milankovitch band forcing of sub-Milankovitch climate variabilty during the Pleistocene. Paleoceanography, 9 (4): 545-558.

Hales, B., Emerson, S. and Archer, D.E., 1994. Respiration and dissolution in the sediments of the western North Atlantic: estimates from models of *in situ* microelectrode measurements of porewater oxygen and pH. Deep-Sea Research, 4: 695-719.

Harris, S.E., Mix, A.C. and King, T., 1997. Biogenic and terrigenous sedimentation at Ceara Rise, western Tropical Atlantic, supports Pliocene-Pleistocene deep-water linkage between hemispheres. In: Proceedings of the Ocean Drilling Program, Scientific Results; Shackleton, N.J., Curry, W.B., Richter, C. and Bralower, T.J. (Eds.), Vol. 154, College Station, TX, pp. 331-345.

Harris, S.E. and Mix, A.C., 1999. Pleistocene precipitation balance in the Amazon Basin recorded in deep sea sediments. Quaternary Research, 51: 14-26.

Hawley, J.E. and Pytkowicz, R.M., 1969. Solubility of calcium carbonate in seawater at high pressure and 2°C. Geochimica et Cosmochimica Acta, 33: 1557-1561.

Hebbeln, D. and Wefer, G., 1997. Late Quaternary paleoceanography in the Fram Strait. Paleoceanography, 12 (1): 65-79.

Heinrich, H., 1988. Origin and consequences of cyclic ice rafting in the Northeast Atlantic Ocean during the past 130 000 years. Quaternary Research, 29: 142-152.

Helmke, J.P, 1996. Charakterisierung glazial/interglazialer Sedimente des Europäischen Nordmeeres anhand von Graustufenmessungen. Unpublished diploma thesis, Univ. Kiel, pp. 1-61.

Helmke, J.P. and Bauch, H.A., 1999. Karbonatlösungsphänomene im Europäischen Nordmeer: Hinweise auf Veränderungen im glazial-interglazialen Kohlenstoffkreislauf? Zentralblatt für Geologie und Paläontologie I, 5-6: 337-352.

Helmke, J.P. and Bauch, H.A., subm. Glacial-interglacial relationship between carbonate components and sediment reflectance in the North Atlantic. GeoMarine Letters.

References

Hemleben, C., Spindler, M. and Anderson, O.A., 1989. Modern Planktonic Foraminifera. Springer-Verlag, New York, 363 pp.

Henrich, R., 1986. A calcite dissolution pulse in the Norwegian-Greenland Sea during the last deglaciation. Geologische Rundschau, 75: 805-827.

Henrich, R., 1989. Glacial/interglacial cycles in the Norwegian Sea: sedimentology, paleoceanography, and evolution of the late Pliocene to Quaternary Northern Hemisphere climate. In: Proceedings of the Ocean Drilling Program, Scientific Results; Eldholm, O., Thiede, J., Taylor, E., et al. (Eds.), Vol. 104, College Station, TX, pp. 189-232.

Henrich, R., 1992. Beckenanalyse des Europäischen Nordmeeres: Pelagische und glaziomarine Sedimenteinflüsse im Zeitraum 2.6 Ma bis rezent. Unpublished habilitation, Univ. Kiel., pp. 1-344.

Henrich, R. and Baumann, K.-H., 1994. Evolution of the Norwegian Current and the Scandinavian Ice Sheet during the past 2.6 m.y.: evidence from ODP Leg 104 biogenic carbonate and terrigenous records. Palaeogeography, Palaeoclimatology, Palaeoecology, 108: 75-94.

Henrich, R., Wagner, T., Goldschmidt, P. and Michels, K., 1995. Depositional regimes in the Norwegian-Greenland Sea: the last two glacial to interglacial transitions. Geologische Rundschau, 84: 28-48.

Henrich, R., 1998. Dynamics of Atlantic water advection to the Norwegian-Greenland Sea - a time-slice record of carbonate distribution in the last 300 ky. Marine Geology, 145: 95-131.

Hirschleber, H., Theilen, F., Balzer, W., von Bodungen, W. and Thiede, J., 1988. Forschungsschiff Meteor, Reise 7: Berichte der Fahrtleiter, Univ. Kiel.

Honjo, S., 1982. Seasonality and interaction of biogenic and lithogenic particulate flux at the Panama Basin. Science, 218: 883-884.

Honjo, S., 1990. Particle fluxes and modern sedimentation in the polar oceans. In: Polar Oceanography; Smith, W.O.J. (Ed.), Academic Press, pp. 687-737.

Horowitz, L.L., 1974. The effects of spline interpolation on power spectral density. IEEE Trans. Acoust., Speech, Signal, Procecssing, 22: 22-27.

Howard, W.R. and Prell, W.L., 1994. Late Quaternary $CaCO_3$ production and preservation in the Southern Ocean: Implications for oceanic and atmospheric carbon cycling. Paleoceanography, 9 (3): 453-482.

Howard, W.R., 1997. Southern Ocean carbonate deposition during Stage 11: Ecological feedbacks and geochemical consequences. EOS, 78 (17): 180.

Huber, R., Meggers, H., Baumann, K.-H. and Henrich, R., 2000. Recent and Pleistocene carbonate dissolution in sediments of the Norwegian-Greenland Sea. Marine Geology, 165: 123-136.

Imbrie, J., Hays, J.D., Martinson, D.G., McIntyre, A., Mix, A.C., Morley, J.J., Pisias, N.G., Prell, W.L. and Shackleton, N.J., 1984. The Orbital Theory of Pleistocene climate: support from a revised chronology of the marine $\delta^{18}O$ record. In: Milankovitch and Climate; Berger, A.L., Imbrie, J., Hays, J., Kukla, G. and Saltzman, B. (Eds.), D. Reidel Publishing Company, Dordrecht, pp. 269-305.

Jahnke, R.A., Craven, D.B. and Gaillard, J.-F., 1994. The influence of organic matter diagenesis on $CaCO_3$ dissolution at the deep-sea floor. Geochimica et Cosmochimica Acta, 58 (13): 2799-2809.

Jahnke, R.A., Craven, D.B., McCorkle, D.C. and Reimers, C.E., 1997. $CaCO_3$ dissolution in California continental margin sediments: The influence of organic matter remineralization. Geochimica et Cosmochimica Acta, 61 (17): 3587-3604.

Jenkins, G.M. and Watts, D.G., 1968. Spectral Analysis and its Application. Holden-Day, Oakland, CA, pp. 1-525.

Johannessen, T., Raymond, C. and Waddington, E., 1989. Time-scale adjustment of glaciers to changes in mass balance. Journal of Glaciology, 35: 355-369.

Johannessen, T., Jansen, E., Flatoy, A. and Ravelo, A.C., 1994. The relationship between surface water masses, oceanic fronts and paleoclimatic proxies in surface sediments of the Greenland, Iceland, Norwegian Seas. In: Carbon Cycling in the Glacial Ocean: Constraints on the Oceans´ Role in Global Change; Zahn, R., Pedersen, T.F., Kaminski, M.A. and Labeyerie, L. (Eds.), Springer Verlag, Berlin, pp. 61-85.

Jouzel, J., Barkov, N.I., Barnola, J.M., Bender, M., Chappellaz, J., Genthon, C., Kotlyakov, V.M., Lipenkov, V., Lorius, C., Petit, J.R., Raynaud, D., Raisbeck, G., Ritz, C., Sowers, T., Stievenard, M., Yiou, F. and Yiou, P., 1993. Extending the Vostock ice-core record of palaeoclimate to the penultimate glacial period. Nature, 364: 407-412.

Jung, S.J.A., 1996. Wassermassenaustausch zwischen NE-Atlantik und Nordmeer während der letzten 300.000/80.000 Jahre im Abbild stabiler O- und C-Isotope. Reports SFB 313, Univ. Kiel, Vol. 61, pp. 1-104.

Karlin, R., Lyle, M. and Zahn, R., 1992. Carbonate variations in the northeast Pacific during the late Quaternary. Paleoceanography, 7: 43-61.

Keeling, C.D. and Whorf, T.P., 2000. The 1,800-year oceanic tidal cycle: a possible cause of rapid climate change. Proceedings of the National Academy of Sciences, 91: 3814-3819.

Keigwin, L.D., 1987. North Pacific deep water formation during the latest glaciation. Nature, 330: 362-364.

Kellogg, T.B., 1976. Late Quaternary climatic changes: Evidence from deep-sea cores of Norwegian and Greenland Seas. Geological Society of America Memoir, 145: 77-110.

Kellogg, T.B., 1977. Paleoclimatology and paleo-oceanography of the Norwegian and Greenland Seas: The last 450.000 years. Marine Micropaleontology, 2: 235-249.

Kellogg, T.B., 1980. Paleoclimatology and paleo-oceanography of the Norwegian and Greenland Seas: Glacial-interglacial contrasts. Boreas, 9: 115-137.

Labeyrie, L.D., Duplessy, J.C. and Blanc, P.L., 1987. Variations in mode of formation and temperature of oceanic deep water over the past 125.000 years. Nature, 327: 477-482.

Labeyrie, L.D., Duplessy, J.-C., Duprat, J., Juilet-Leclerc, A., Moyes, J., Michel, E., Kallel, N. and Shackleton, N.J., 1992. Changes in the vertical structure of the North Atlantic Ocean between glacial and modern times. Quaternary Science Reviews, 11: 401-414.

Le, J. and Shackleton, N.J., 1992. Carbonate dissolution fluctuations in the western equatorial Pacific during the late Quaternary. Paleoceanography, 7 (1): 21-42.

Lomb, N.R., 1976. Least-square frequency anaylsis of unevenly spaced data. Astrophysics and Space Science, 39: 447-462.

Lotoskaya, A., Ziveri, P., Ganssen, G.M. and van Hinte, J.E., 1998. Calcareous nannofloral response to Termination II at 45°N, 25°W (northeast Atlantic). Marine Micropaleontology, 34: 47-70.

MacAyeal, D.R., 1993. A low-order model of Heinrich event cycle. Paleoceanography, 8: 767-773.

Malmgren, B.A., 1983/84. Ranking of dissolution susceptibility of planktonic foraminifera at high latitudes of the South Atlantic Ocean. Marine Micropaleontology, 8: 183-191.

Manighetti, B. and McCave, I.N., 1995. Late glacial and Holocene palaeocurrents around Rockall Bank, NE Atlantic Ocean. Paleoceanography, 10 (3): 611-626.

Martinson, D.G., Pisias, N.G., Hays, J.D., Imbrie, J., Moore, T.C. and Shackleton, N.J., 1987. Age Dating and the Orbital Theory of the Ice Ages: Development of a High-Resolution 0 to 300,000-Year Chronostratigraphy. Quaternary Research, 27: 1-29.

McCave, I.N. and Tucholke, B.E., 1986. Deep current-controlled sedimentation in the western North Atlantic. In: The Geology of North America; Vogt, P.R. and Tucholke, B.E. (Eds.), Geological Society of America, pp. 451-468.

McManus, J.F., Bond, G.C., Broecker, W.S., Johnsen, S., Labeyrie, L. and Higgins, S., 1994. High-resolution climate records from the North Atlantic during the last interglacial. Nature, 371: 326-329.

McManus, J.F. and Lohmann, G.P., 1998. Evidence for eposodic calcium-carbonate dissolution in the subpolar North Atlantic during the last glaciation. EOS, 79 (17): 179-180.

McManus, J.F., Anderson, R.F., Broecker, W.S., Fleisher, M.Q. and Higgins, S.M., 1998. Radiometrically determined sedimentary fluxes in the sub-polar North Atlantic during the last 140,000 years. Earth and Planetary Science Letters, 155: 29-43.

McManus, J., Oppo, D.W. and Cullen, J.L., 1999. A 0.5-million-year record of millennial-scale climate variability in the North Atlantic. Science, 283: 971-975.

Merrill, R.B. and Beck, J.W., 1995. The ODP color digital imaging system: color logs of Quaternary sediments from the Santa Barbara Basin, Site 893. In: Proceedings of the Ocean Drilling Program, Scientific Results; Kennett, J.P., Baldauf, J.G. and Lyle, M. (Eds.), Vol. 146 (2), College Station, TX, pp. 45-59.

Minolta Corporation, 1994. Precise Color Communication. Osaka, pp. 1-49.

Mix, A.C. and Fairbanks, R.G., 1985. North Atlantic surface-ocean control of Pleistocene deep-ocean circulation and Pleistocene CO_2. Earth and Planetary Science Letters, 73: 231-243.

Mix, A.C., Rugh, W., Pisias, N.G. and Veirs, S., 1992. Color reflectance spectroscopy: a tool for rapid characterization of deep-sea sediments. In: Proceedings of the Ocean Drilling Program, Initial Reports; Mayer, L., Pisias, N. and Janacek, T. (Eds.), Vol. 138, College Station, TX, pp. 67-77.

Mix, A.C., Harris, S.E. and Janecek, T.R., 1995. Estimating Lithology from nonintrusive reflectance spectra: Leg 138. In: Proceedings of the Ocean Drilling Program, Scientific Results; Piasias, N.G., Mayer, L.A., Janecek, T.R., Palmer-Julson, A, and van Andel, T.H. (Eds.), Vol. 138, College Station, TX, pp. 413-427.

Moore, T.C.J., Pisias, N.G. and Heath, G.R., 1978. Climate changes and lags in Pacific carbonate preservation, sea surface temperature, and global ice volume. In: The Fate of Fossil Fuel CO_2 in the Oceans; Anderson, N.R. and Malahof, A. (Eds.), Plenum, New York, pp. 145-167.

Nagao, S. and Nakashima, S., 1992. The factors controlling vertical color variations of North Atlantic Madeira Abyssal Plain sediments. Marine Geology, 109: 83-94.

Nees, S., 1997. High-resolution benthic foraminiferal records of the last glacial termination in the northern North Atlantic. In: Hass, H.C. and Kaminski, M.A. (Eds.), Contributions to the Micropaleontology and paleoceanography of the Northern North Atlantic. Grzybowski Foundation Special Publication 5, pp. 167-197.

Neftel, A., Oeschger, H., Schwander, J., Stauffer, B. and Zumbrunn, R., 1982. Ice core sample measurements give atmospheric CO_2 content during the past 40,000 yr. Nature, 292: 220-223.

Opdyke, B.N. and Walker, J.C.G., 1992. Return of the coral reef hypothesis: Basin to shelf partitioning of $CaCO_3$ and its effect on atmospheric CO_2. Geology, 20: 733-736.

Oppo, D.W. and Fairbanks, R.G., 1987. Variability in the deep and intermediate water circulation of the Atlantic Ocean: Northern hemisphere modulation of the Southern Ocean. Earth and Planetary Science Letters, 86: 1-15.

Oppo, D.W., Horowitz, M. and Lehman, S., 1997. Marine core evidence for reduced deep water production during Termination II followed by a relatively stable substage 5e (Eemian). Paleoceanography, 12: 51-63.

Oppo, D.W., McManus, J.F. and Cullen, J.L., 1998. Abrupt climate events 500,000 to 340,000 years ago: evidence from subpolar North Atlantic sediments. Science, 279: 1335-1338.

Ottens, J.J., 1992. April and August Northeast Atlantic surface water masses reflected in planktic foraminifera. Netherlands Journal of Sea Research, 28: 261-283.

Ortiz, J.D. and Rack, F.R., 1999. Current and future tools for high-resolution climate studies. In: Reconstructing Ocean History: A Window into the Future; Abrantes, F. and Mix, A.C. (Eds.), Kluwer Academic/Plenum Publishers, New York, pp. 343-380.

Ortiz, J.D, Mix, A.C., Harris, S. and O'Connell, S., 1999. Diffuse spectral reflectance as a proxy for percent carbonate content in North Atlantic sediments. Paleoceanography, 14 (2): 171-186.

Peterson, L.C. and Prell, W.L., 1985. Carbonate dissolution in recent sediments of the eastern equatorial Indian Ocean: preservation patterns and carbonate loss above the lysocline. Marine Geology, 64: 259-290.

Petit, J.R., Basile, I., Leruyuet, A., Raynaud, D., Lorius, C., Jouzel, J., Stievenard, M., Lipenkov, V.Y., Barkov, N.I., Kudryashov, B.B., Davis, M., Saltzman, E. and Kotlyakov, V., 1997. Four climate cycles in Vostok ice core. Nature, 387: 359-360.

Pilskaln, C.H. and Honjo, S., 1987. The fecal pellet fraction of biogeochemical particle fluxes to the deep sea. Global Biogeochemical Cycles, 1: 31-48.

Rahmstorf, S., 1994. Rapid climate transitions in a coupled ocean-atmosphere model. Nature, 372: 82.

Rohling, E.J., Fenton, M., Jorissen, F.J., Bertrand, P., Ganssen, G. and Caulet, J.P., 1998. Magnitudes of sea-level lowstands of the past 500.000 years. Nature, 394: 162-165.

Ruddiman, W.F. and McIntyre, A., 1976. Northeast Atlantic paleoclimatic changes over the past 600.000 years. Geological Society of America Memoir, 145: 111-146.

Ruddiman, W.F., Shackleton, N.J. and McIntyre, A., 1986. North Atlantic sea-surface temperatures for the last 1.1 million years. In: North Atlantic Paleoceanography; Summerhayes, C.P. and Shackleton, N.J. (Eds.), Geological Society Special Publication, Vol. 21, pp. 155-173.

Rybicki, G.B. and Press, W.H., 1995. Class of fast methods for processing irregularly sampled otherwise inhomogenous one-dimensional data. Phys. Rev. Lett., 74: 1060-1063.

Sakai, K. and Peltier, W.R., 1997. Dansgaard-Oeschger oscillations in a coupled atmosphere-ocean climate model. Journal of Climate, 10: 949-970.

Sanyal, A., Hemming, N.G., Hanson, G.N. and Broecker, W.S., 1995. Evidence for a higher pH in the glacial ocean from boron isotopes in foraminifera. Nature, 373: 234-236.

Sanyal, A. and Bijma, J., 1999. A comparative study of the northwest Africa and eastern equatorial Pacific upwelling zones as sources of CO_2 during glacial periods based on boron isotope paleo-pH estimation. Paleoceanography, 14 (6): 753-759.

Sarmiento, J.L. and Toggweiler, R., 1984. A new model for the role of the oceans in determining atmospheric pCO_2. Nature, 308: 621-624.

Samthein, M., Jansen, E., Arnold, M., Duplessy, J.C., Erlenkeuser, H., Flatoy, A., Veum, T., Vogelsang, E. and Weinelt, M.S., 1995. Variations in Atlantic surface ocean paleoceanography, 50°-80°N: A time-slice record of the last 30,000 years. Paleoceanography, 10: 1063-1094.

Samthein, M., Stattegger, K., Dreger, D., Erlenkeuser, H., Grootes, P.M., Haupt, B., Jung, S.J.A., Kiefer, T., Kuhnt, W., Pflaumann, U., Schäfer-Neth, C., Schulz, H., Schulz, M., Seidov, D., Simstich, J., van Krefeld, S., Vogelsang, E., Voelker, A.H.L. and Weinelt, M.S., in press. Fundamental modes and abrupt changes in North Atlantic circulation and climate over the last 60 ky - Concepts, reconstruction, and numerical modelling. In: The Northern North Atlantic: A changing environment; Schäfer, P., Ritzrau, W., Schlüter, M and Thiede, J. (Eds.), Springer Verlag, Heidelberg.

Schaaf, M. and Thurow, J., 1994. A fast and easy method to derive highest-resolution time-series datasets from drillcores and rock samples. Sedimentary Geology, 94: 1-10.

Schiebel, R., Bijma, J. and Hemleben, C., 1997. Population dynamics of the planktic foraminifer *Globigerina bulloides* from the eastern North Atlantic. Deep-Sea Research I, 44 (9): 1701-1713.

Schiebel, R. and Hemleben, C., 2000. Interannual variability of planktic foraminiferal populations and test flux in the eastern North Atlantic Ocean (JGOFS). Deep-Sea Research II, 47: 1809-1852.

Schulz, M. and Stattegger, K., 1997. Spectrum: Spectral Analysis of unevenly spaced paleoclimatic time series. Computer & Geosciences, 23 (9): 929-945.

Schulz, M., Berger, W.H., Samthein, M. and Grootes, P.M., 1999. Amplitude variations of 1470-year climate oscillations during the last 100,000 years linked to fluctuations of continental ice mass. Geophysical Research Letters, 26: 3385-3388.

Schulz, M. and Mudelsee, M., subm. Estimating red-noise spectra directly from unevenly spaced paleoclimate time series. Computer & Geosciences.

Smythe, F.W., Ruddiman, W.F. and Lumsden, D.N., 1985. Ice-rafted evidence of long-term North Atlantic circulation. Marine Geology, 64: 131-141.

Snoeckx, H., Grousset, F.E., Revel, M. and Boelaert, A., 1999. European contribution of ice-rafted sand to Heinrich layers H3 and H4. Marine Geology, 158: 197-208.

Sowers, T., Bender, M., Raynaud, D., Korotkevich, Y.S. and Orchardo, J., 1991. The $\delta^{18}O$ of atmospheric O_2 from air inclusions in the Vostok ice core: Timing of CO_2 and ice volume changes during the penultimate deglaciation. Paleoceanography, 6: 679-696.

Stauffer, B., Blunier, T., Dällenbach, A., Indermühle, A., Schwander, J., Stocker, T.F., Tschumi, J., Chappellaz, J., Raynaud, D., Hammer, C.U., and Clausen, H.B., 1998. Atmospheric CO_2 concentration and millennial-scale climate change during the last glacial period. Nature, 392: 59-62.

Struck, U., 1997. Paleoecology of benthic foraminifera in the Norwegian-Greenland Sea during the past 500 ka. In: Hass, C.H. and Kaminski, M.A. (Eds.), Contributions to the

Micropaleontology and Paleoceanography of the Northern North Atlantic, Grzybrowski Foundation Special Publication 5, pp. 51-83.

Stuiver, M., Reimer, P.J., Bard, E., Beck, J.W., Burr, G.S., Hughen, K.A., Kromer, B., McCormac, G., van der Pflicht, J. and Spurk, M., 1998. INTCAL98 Radiocarbon Age Calibration, 24,000-0 cal BP. In: INTCAL 98: Calibration Issue; Stuiver, M. and van der Pflicht, J. (Eds.), Radiocarbon, pp. 1041-1083.

Suess, E. and Altenbach, A.V., 1992. Europäisches Nordmeer, Reise Nr. 17, 15. Juli - 29. August 1991. Meteor-Berichte, 92-3. Universität Hamburg, pp.1 -164.

Swift, J.H., 1986. The Arctic Waters. In: The Nordic Seas; Hurdle, B.G. (Ed.), Springer Verlag, New York, Berlin, Heidelberg, Tokyo, pp. 129-151.

Takahashi, T., 1975. Carbonate chemistry of sea water and the calcite compensation depth in the oceans. In: Dissolution of Deep-sea Carbonates; Sliter, W.V., Bé, A.W. and Berger, W.H. (Eds.), Cushman Foundation Foraminiferal Research, Special Publication, pp. 11-26.

Thunell, R.C., 1976. Calcium carbonate dissolution history in Late Quaternary deep-sea sediments, Western Gulf of Mexico. Quaternary Research, 6: 281-297.

van Geel, B., Raspopov, O.M., Renssen, H., van der Pflicht, J., Dergachev, V.A. and Meijer, H.A.J., 1999. The role of solar forcing upon climate change. Quaternary Science Reviews, 18: 331-338.

van Krefeld, S.A., Knappertsbusch, M., Ottens, J., Ganssen, G.M. and van Hinte, J.E., 1996. Biogenic carbonate and ice-rafted debris (Heinrich layer) accumulation in deep-sea sediments from a Northeast Atlantic piston core. Marine Geology, 131: 21-46.

van Kreveld, S.A., Sarnthein, M., Erlenkeuser, H., Grootes, P.M., Jung, S., Nadeau, M.J., Pflaumann, U. and Voelker, A.H.L., in press. Potential links between surging ice sheets, circulation changes and the Dansgaard-Oeschger cycles in the Irminger Sea. Paleoceanography.

Venz, K.A., Hodell, D.A., Stanton, C. and Warnke, D.A., 1999. A 1.0 Myr record of Glacial North Atlantic Intermediate Water variabiltiy from ODP site 982 in the northeast Atlantic. Paleoceanography, 14: 42-52.

Vidal, L., Schneider, R.R., Marchal, O., Bickert, T., Stocker, T.F. and Wefer, G., 1999. Link between the North and South Atlantic during Heinrich events of the last glacial period. Climate Dynamics, 15: 909-919.

Voelker, A.H.L., Sarnthein, M., Grootes, P.M., Erlenkeuser, H., Laj, C., Mazaud, A., Nadeau, M.-J. and Schleicer, M., 1998. Correlation of marine ^{14}C ages from the Nordic seas with the GISP2 isotope record: implications for radiocarbon calibration beyond 25 ka BP. Radiocarbon, 40 (1): 517-534.

Voelker, A.H.L., 1999. Zur Deutung der Dansgaard-Oeschger Ereignisse in ultra-hochauflösenden Sedimentprofilen aus dem Europäischen Nordmeer. Reports Institut für Geowissenschaften, Univ. Kiel., Vol. 9, pp. 1-278.

Volk, T. and Hoffert, M.I., 1985. Ocean carbon pumps: Analysis of relative strengths and efficiencies in ocean-driven atmospheric CO_2 changes. In: The Carbon cycle and atmospheric CO_2: Natural Variations Archean to present; Sundquist, E.T. and Broecker, W.S. (Eds.), Geopysical Monograph. American Geophysical Union, Washington, D.C., pp. 99-110.

von Bodungen, B., Anita, A., Bauernfeind, E., Haupt, O., Koeve, W., Machado, E., Voss, M., Wunsch, M., Zeller, M. and Zeitschel, B., 1995. Pelagic processes and vertical flux of particles: an overview of a long-term comparative study in the Norwegian Sea and Greenland Sea. Geologische Rundschau, 84: 11-27.

Welch, P.D., 1967. The use of fast Fourier transform for estimation of power spectra: A method based on time averaging over short, modified periodograms. IEEE Transactions on Audio and Electroacoustics, 15 (2): 70-73.

Winton, M., 1993. Deep coupling oscillations of the oceanic thermohaline circulation. In: Ice in the climate system; Peltier, W.R. (Ed.). NATO ASI Series. Springer-Verlag, Berlin, pp. 417-432.

Yokoyama, Y., Lambeck, K., De Deckker, P., Johnston, P. and Fifield, K., 2000. Timing of the last glacial maximum from observed sea-level minima. Nature, 406: 713-716.

Zahn, R., Sarnthein, M. and Erlenkeuser, H., 1987. Benthic isotope evidence for changes of the Mediterranean outflow during the late Quaternary. Paleoceanography, 2: 543-559.

Danksagung

Herrn Prof. Jörn Thiede möchte ich für die Vergabe der Arbeit und die damit gegebene Möglichkeit zur Promotion danken. Dr. Henning Bauch gilt mein Dank für die ausgezeichnete fachliche Betreuung der Dissertation. Stets zeigte er sich engagiert und interessiert am Fortgang der Arbeit, die zahlreichen Diskussionen mit ihm haben mir viele Anregungen für das Anfertigen dieser Arbeit gegeben.

Dr. Abhijit Sanyal bemühte sich in diversen Gesprächen, mir die Grundlagen des marinen Karbonatsystems verständlich zu machen, wofür ich ihm danken möchte. Ohne die hilfreiche Mitarbeit von Dr. Michael Schulz wäre die Zeitserienanalyse der Daten sicher nicht so ergiebig gewesen.

Dr. Christian Hass und Dr. Jeffrey Schuffert haben mit dazu beigetragen, daß das Englisch der in diese Arbeit integrierten Manuskripte verbessert wurde. Insbesondere Jeff hat es sich freundlicherweise aufbürden lassen, ein Großteil der Manuskripte einer kritischen Durchsicht zu unterziehen. Dafür mein Dank an beide. Wenn die Rechner und ich mal wieder nicht zusammenarbeiten konnten, war Dr. Emanuel Söding stets zur Stelle, um diesem Zustand ein Ende zu setzten.

Meine wissenschaftlichen Hilfskräfte Viola Strauß, Ute Reimers, Iris Adomat und insbesondere mein "Langzeit-HiWi" Melanie Wengert haben wesentlich zur sorgfältigen Aufbereitung und Bearbeitung der Proben beigetragen. Dank auch an Jutta Pagel, Dagmar Rau und Regina Surberg für die Durchführung von LECO-, XRF- und ICP-Messungen am GEOMAR, sowie an Dr. Helmut Erlenkeuser für die Durchführung der Isotopenanalysen am Leibniz-Labor.

Für die entspannte und fruchtbare Zusammenarbeit sowie die freundschaftliche Atmosphäre in der "Arbeitsgruppe Bauch" gilt mein herzlicher Dank Claudia und Thomas. Auch Tobi, Sascha, Stefan, Manu und Claudia, den Freunden des Dartspiels am Mittag, sei für willkommene Abwechslung gedankt.

Ein großes Dankeschön geht an meine Mutter und den Rest meiner Familie dafür, daß man mir bei immer mal wieder anstehenden Problemchen und Problemen stets gerne geholfen hat. Zuletzt möchte ich ganz besonders meiner Freundin Carola danken. Ihre liebevolle Unterstützung und Ihre Verständnis während der Enstehungszeit dieser Arbeit haben mir das Leben und Arbeiten sehr viel leichter gemacht.

Appendix

Plate 1: Various surface structures of *N. pachyderma* (sin.) tests from M23352 indicating the three sucessive steps (Step 1-3; see Chapter II) of carbonate corrosion observed at the Nordic Seas Sites M23352 and PS1243. Gray rectangular indicates the part of the foraminiferal chamber that is magnified. The black bar scale equals 100 µm.

Table 1: Bulk, fine (<20 µm), and coarse (>20 µm), carbonate and TOC (bulk carbonate/TOC in weight % of bulk sediment; fine and coarse carbonate/TOC in weight % of bulk carbonate/TOC), sediment lightness L* and red-green chromaticity a* of core M23414-6.

Table 2: Bulk, fine (<20 µm), and coarse (>20 µm) carbonate (bulk carbonate in weight % of bulk sediment; fine and coarse carbonate in weight % of bulk carbonate) of core M23414-9.

Table 3: Bulk, fine (<20 µm), and coarse (>20 µm) TOC (bulk TOC in weight % of bulk sediment; fine and coarse TOC in weight % of bulk TOC) of core M23414-9.

Table 4: Sediment lightness L* and red-green chromaticity a* of core M23414-9.

Table 5: Bulk, fine (<20 µm), and coarse (>20 µm) carbonate (bulk carbonate in weight % of bulk sediment; fine and coarse carbonate in weight % of bulk carbonate) of core M23414-8.

Table 6: Bulk, fine (<20 µm), and coarse (>20 µm) TOC (bulk TOC in weight % of bulk sediment; fine and coarse TOC in weight % of bulk TOC) of core M23414-8.

Table 7: Sediment lightness L* and red-green chromaticity a* of core M23414-8.

Table 8: Stable oxygen and carbon isotopes (planktic foraminifer *G. bulloides*, 125-250 µm) of core M23414-8.

Table 9: Ice-rafted debris (lithic grains >250 µm/gram sediment) of core M23414-8.

Table 10: Age vs. depth relation of M23414 (splice record).

Table 11: Linear sedimentation rates (LSR) and accumulation rates (AR) of M23414 (splice record).

Table 12: Age vs. depth relation of M23352 (splice record).

Table 13: Various weight measurements (mg) and lightness results (L*) of foraminiferal tests (*N. pachyderma* (sin.); size fraction 224-250 µm) from cores PS1243 and M23352.

Table 14: Weight (mg) and lightness (L*) of *N. pachyderma* (sin.) tests from core PS1243 (500 foraminifera from size fraction 125-250 µm).

Table 15: Weight (mg) and lightness (L*) of *N. pachyderma* (sin.) tests from core M23352 (500 foraminifera from size fraction 125-250 µm).

The data will be available through the Pangaea database (http://www.pangaea.de).

Plate 1:

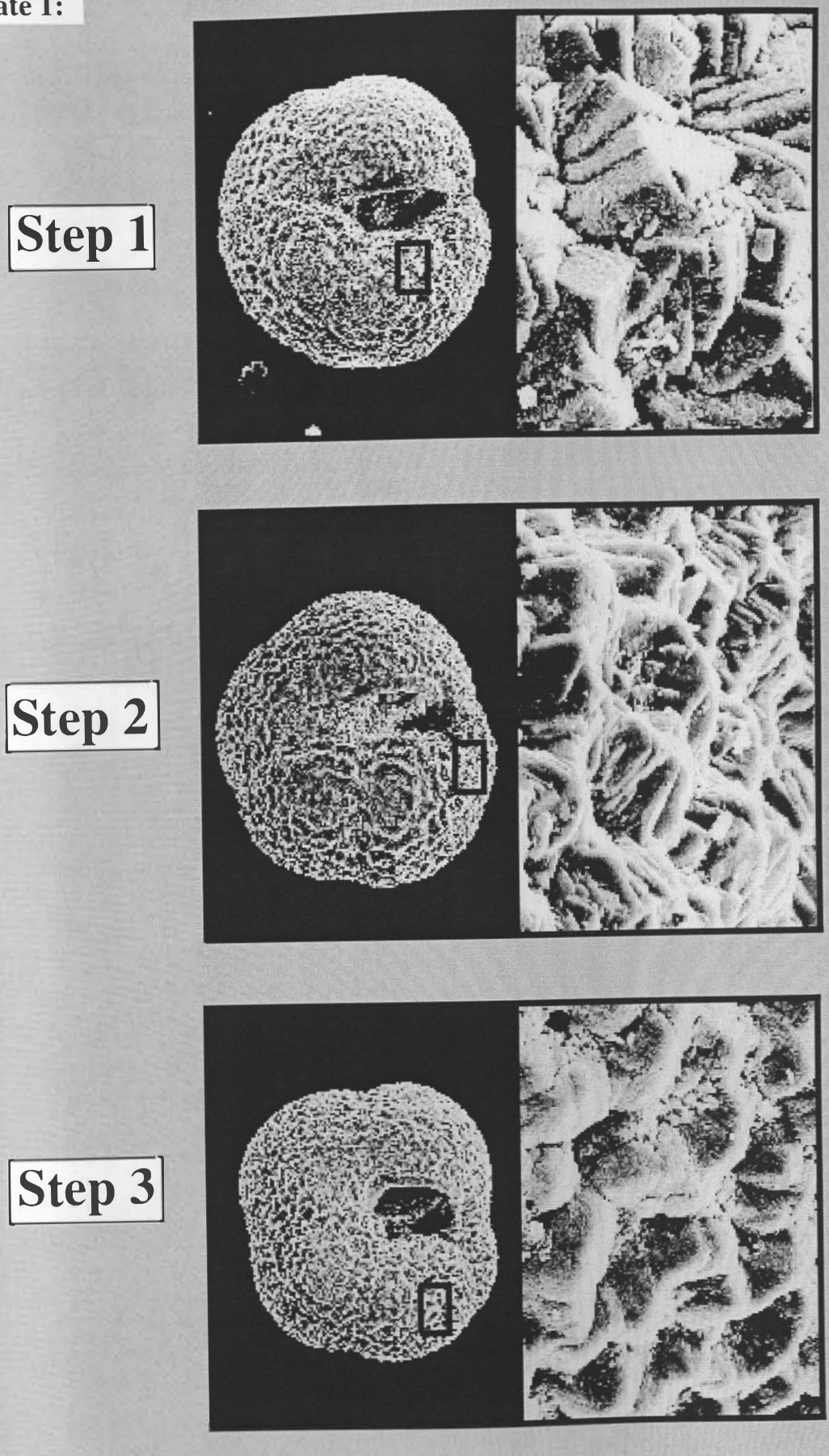

M23414-6 **Carbonate and TOC (weight %); L* and a***

Table 1

Depth (cm)	Bulk $CaCO_3$ (weight %)	Coarse $CaCO_3$ (weight %)	Fine $CaCO_3$ (weight %)
3	75.60	12.78	62.82
7.5	75.40	36.88	38.52
12	74.00	35.05	38.95
17.5	68.50	26.60	41.90
23	65.40	40.08	25.32
28	61.90	19.04	42.86
33	56.60	33.26	23.34
38	46.70	19.68	27.02

Depth (cm)	Bulk TOC (weight %)	Coarse TOC (weight %)	Fine TOC (weight %)
3	0.28	0.05	0.23
7.5	0.29	0.05	0.24
12	0.24	0.05	0.19
17.5	0.17	0.02	0.15
23	0.14	0.06	0.08
28	0.14	0.02	0.12
33	0.17	0.09	0.08
38	0.16	0.02	0.14

Depth (cm)	L*	a*
3	60.88	2.87
4	60.79	2.88
5	60.83	2.94
6	59.74	2.68
7	60.79	2.91
8	61.53	2.88
9	62.38	2.79
10	61.66	3.05
11	61.38	3.06
12	61.11	3.18
13	61.24	3.29
14	60.00	3.35
15	61.75	3.02
16	61.14	3.18
17	60.77	3.19
18	61.19	3.00
19	58.48	3.46
20	55.36	3.36
21	57.67	3.40
22	56.95	3.10
23	52.26	3.79
24	52.25	3.71
25	55.95	3.00
26	60.72	2.43
27	48.87	2.60
28	48.15	2.95
29	48.22	3.11
30	52.10	2.55
31	50.97	2.44
32	52.62	2.47
33	56.42	2.36
34	54.86	3.27

Carbonate (weight %)

Table 2

Depth (cm)	Bulk $CaCO_3$ (weight %)	Coarse $CaCO_3$ (weight %)	Fine $CaCO_3$ (weight %)	Depth (cm)	Bulk $CaCO_3$ (weight %)	Coarse $CaCO_3$ (weight %)	Fine $CaCO_3$ (weight %)
12.5	77.83	52.23	25.60	320	72.88	22.22	50.66
15	83.24	68.44	14.80	325	62.22	21.12	41.10
20	74.83	36.13	38.70	330	49.96	22.81	27.15
25	71.56	31.67	39.89	335	82.10	44.70	37.40
30	70.38	32.40	37.98	340	80.41	33.74	46.67
35	57.51	27.44	30.07	345	75.10	28.71	46.39
40	55.16	31.51	23.65	350	75.48	38.70	36.78
45	29.50	12.26	17.24	355	77.10	29.90	47.20
50	23.13	17.04	6.09	360	65.80	12.16	53.64
55	20.54	12.75	7.79	365	65.80	20.94	44.86
60	28.55	22.25	6.30	370	59.50	12.77	46.73
65	32.25	17.72	14.53	375	68.87	37.94	30.93
70	30.93	14.73	16.20	380	80.42	42.50	37.92
75	25.94	11.69	14.25	385	72.59	27.62	44.97
80	26.04	9.10	16.94	390	75.58	25.64	49.94
85	24.26	11.18	13.08	395	81.33	29.04	52.29
90	24.39	13.85	10.54	400	81.12	31.72	49.40
95	26.51	14.81	11.70	405	82.08	20.98	61.10
100	20.92	18.34	2.58	410	77.72	21.21	56.51
105	18.71	7.29	11.42	415	76.37	21.76	54.61
110	10.00	2.83	7.17	420	62.60		
115	13.71	7.57	6.14	425	40.89	17.85	23.04
120	11.71	5.27	6.44	430	19.62	8.13	11.49
125	22.32	8.63	13.69	435	13.00	4.97	8.03
130	37.00	16.51	20.49	440	22.42	8.76	13.66
135	26.01	11.98	14.03	445	26.50	13.81	12.69
140	23.71	2.19	21.52	450	26.55	15.97	10.58
145	21.02	2.17	18.85	455	28.96	10.39	18.57
150	29.85	10.23	19.62	460	26.75	1.86	24.89
155	36.26	13.74	22.52	465	22.34	7.30	15.04
160	32.41	12.18	20.23	470	26.10	10.91	15.19
165	21.74	12.25	9.49	475	24.79	3.02	21.78
170	16.83	5.22	11.61	480	21.50	2.51	18.99
175	15.46	8.60	6.86	485	22.54	9.52	13.02
180	33.34	14.70	18.64	490	24.94	11.73	13.21
185	34.85	13.89	20.96	495	27.16	9.12	18.04
190	31.87	15.46	16.41	500	23.64	3.51	20.13
195	33.86	12.29	21.57	505	25.35	13.76	11.59
200	38.22	12.34	25.88	510	23.16	5.81	17.35
205	41.34	10.70	30.64	515	22.55	2.35	20.20
210	37.51	17.75	19.76	520	17.10	2.01	15.09
215	40.96	11.29	29.67	525	18.32	4.39	13.93
220	48.33	10.69	37.64	530	15.32	10.21	5.11
225	46.71	16.19	30.52	535	15.66	7.35	8.31
230	43.99	29.83	14.16	540	22.35	16.50	5.85
235	38.69	11.78	26.91	545	22.28	9.77	12.51
240	42.76	15.66	27.10	550	29.73	12.20	17.53
245	43.86	11.18	32.68	555	26.30	9.49	16.81
250	31.12	17.04	14.08	560	36.14	9.62	26.52
255	32.06	13.26	18.80	565	24.58	10.92	13.66
260	26.72	10.21	16.51	570	39.07	33.05	6.02
265	25.12	13.52	11.60	575	51.16	33.05	18.11
270	38.87	26.46	12.41	580	57.28	19.49	37.79
275	10.72	4.58	6.14	585	42.49	18.74	23.75
280	21.99	12.80	9.19	590	30.23	17.45	12.78
285	42.76	28.33	14.43	595	33.22	23.05	10.17
290	59.10	19.39	39.71	600	40.37	21.50	18.87
295	63.25	14.78	48.47	605	37.55	17.78	19.77
300	64.25	22.45	41.80	610	35.39	19.25	16.14
305	67.16	20.56	46.60	615	42.06	26.03	16.03
310	76.85	13.14	63.71	620	49.72	21.81	27.91
315	72.74	20.17	52.57	625	26.22	2.08	24.14

Table 2 continued

Depth (cm)	Bulk $CaCO_3$ (weight %)	Coarse $CaCO_3$ (weight %)	Fine $CaCO_3$ (weight %)
630	53.27	23.48	29.79
635	44.92	1.91	43.01
640	65.74	18.31	47.43
645	66.59	25.98	40.61
650	51.96	6.25	45.71
655	62.84	41.97	20.87
660	64.19	26.05	38.14
665	65.92	23.77	42.15
670	69.86	23.75	46.11
675	74.17	25.27	48.90
680	71.18	29.78	41.40
685	57.54	12.04	45.50
690	64.88	24.34	40.54
695	41.41	13.68	27.73
700	23.82	8.88	14.94
705	23.02	13.47	9.55
710	36.63	20.46	16.17
715	46.55	22.25	24.30
720	47.16	24.62	22.54
725	48.01	11.53	36.48
730	52.43	13.55	38.88
735	65.16	22.45	42.71
740	68.19	21.19	47.00
745	75.24	19.80	55.44
750	69.10	13.99	55.11
755	65.24		
760	63.56	19.76	43.80
765	56.97	17.72	39.25
770	54.25	36.62	17.63
775	64.67	55.06	9.61
780	53.03	28.41	24.62
785	34.92	16.42	18.50
790	29.22	9.63	19.59
795	36.94	17.87	19.07
800	36.92	20.95	15.97
805	28.01	14.53	13.48
810	29.84	16.61	13.23
815	30.75	13.40	17.35
820	30.30	12.59	17.71
825	30.00	16.50	13.50
830	31.78	13.74	18.04
835	31.06	11.72	19.34
840	39.99	12.33	27.66
845	34.20	12.00	22.20
850	31.39	11.65	19.74
855	15.71	10.84	4.87
860	32.71	12.21	20.50
865	30.37	12.11	18.26
870	27.00	16.20	10.80
875	32.58	14.77	17.81
880	34.82	16.54	18.28
885	30.86	24.70	6.16
890	17.35	8.60	8.75

TOC (weight %)

Table 3

Depth (cm)	Bulk TOC (weight %)	Coarse TOC (weight %)	Fine TOC (weight %)	Depth (cm)	Bulk TOC (weight %)	Coarse TOC (weight %)	Fine TOC (weight %)
12.5	0.13	0.08	0.05	320	0.10	0.00	0.10
15	0.16	0.13	0.03	325	0.13	0.03	0.10
20	0.14	0.02	0.12	330	0.10	0.04	0.06
25	0.14	0.07	0.07	335	0.05	0.00	0.05
30	0.17	0.04	0.13	340	0.05	0.00	0.05
35	0.16	0.04	0.12	345	0.06	0.00	0.06
40	0.28	0.22	0.06	350	0.07	0.00	0.07
45	0.15	0.04	0.11	355	0.15	0.07	0.08
50	0.13	0.08	0.05	360	0.21	0.12	0.09
55	0.18	0.10	0.08	365	0.12	0.04	0.08
60	0.12	0.06	0.06	370	0.13	0.09	0.04
65	0.24	0.04	0.20	375	0.14	0.00	0.14
70	0.21	0.00	0.21	380	0.06	0.00	0.06
75	0.27	0.16	0.11	385	0.08	0.00	0.08
80	0.21	0.12	0.09	390	0.06	0.00	0.06
85	0.16	0.06	0.10	395	0.06	0.00	0.06
90	0.22	0.09	0.13	400	0.05	0.03	0.02
95	0.16	0.12	0.04	405	0.17	0.05	0.12
100	0.17	0.13	0.04	410	0.09	0.02	0.07
105	0.15	0.05	0.10	415	0.10	0.01	0.09
110	0.17	0.06	0.11	420	0.10		
115	0.15	0.09	0.06	425	0.19	0.12	0.07
120	0.16	0.04	0.12	430	0.14	0.04	0.10
125	0.18	0.08	0.10	435	0.13	0.06	0.07
130	0.21	0.05	0.16	440	0.17	0.08	0.09
135	0.21	0.02	0.19	445	0.11	0.01	0.10
140	0.21	0.07	0.14	450	0.15	0.05	0.10
145	0.21	0.04	0.17	455	0.17	0.04	0.13
150	0.22	0.05	0.17	460	0.26	0.05	0.21
155	0.20	0.04	0.16	465	0.24	0.06	0.18
160	0.24	0.09	0.15	470	0.33	0.09	0.24
165	0.20	0.13	0.07	475	0.48	0.12	0.36
170	0.33	0.17	0.16	480	0.47	0.12	0.35
175	0.19	0.12	0.07	485	0.44	0.24	0.20
180	0.17	0.07	0.10	490	0.12	0.00	0.12
185	0.18	0.00	0.18	495	0.19	0.05	0.14
190	0.16	0.02	0.14	500	0.22	0.04	0.18
195	0.18	0.07	0.11	505	0.20	0.14	0.06
200	0.20	0.00	0.20	510	0.19	0.00	0.19
205	0.20	0.04	0.16	515	0.22	0.06	0.16
210	0.22	0.13	0.09	520	0.22	0.08	0.14
215	0.21	0.06	0.15	525	0.20	0.06	0.14
220	0.21	0.08	0.13	530	0.24	0.18	0.06
225	0.23	0.15	0.08	535	0.20	0.07	0.13
230	0.16	0.03	0.13	540	0.18	0.08	0.10
235	0.17	0.05	0.12	545	0.14	0.00	0.14
240	0.19	0.03	0.16	550	0.13	0.06	0.07
245	0.20	0.00	0.20	555	0.16	0.03	0.13
250	0.22	0.11	0.11	560	0.19	0.12	0.07
255	0.26	0.06	0.20	565	0.25	0.15	0.10
260	0.32	0.13	0.19	570	0.16	0.12	0.04
265	0.22	0.06	0.16	575	0.10	0.04	0.06
270	0.27	0.16	0.11	580	0.19	0.14	0.05
275	0.12	0.05	0.07	585	0.15	0.10	0.05
280	0.10	0.02	0.08	590	0.16	0.11	0.05
285	0.14	0.00	0.14	595	0.16	0.10	0.06
290	0.07	0.00	0.07	600	0.17	0.09	0.08
295	0.09	0.00	0.09	605	0.19	0.13	0.06
300	0.10	0.00	0.10	610	0.14	0.01	0.13
305	0.09	0.00	0.09	615	0.10	0.03	0.07
310	0.09	0.05	0.04	620	0.12	0.02	0.10
315	0.12	0.00	0.12	625	0.14	0.05	0.09

Table 3 continued

Depth (cm)	Bulk TOC (weight %)	Coarse TOC (weight %)	Fine TOC (weight %)
630	0.10	0.00	0.10
635	0.13	0.03	0.10
640	0.11	0.01	0.10
645	0.14	0.07	0.07
650	0.11	0.02	0.09
655	0.12	0.09	0.03
660	0.13	0.09	0.04
665	0.10	0.03	0.07
670	0.07	0.00	0.07
675	0.08	0.06	0.02
680	0.08	0.03	0.05
685	0.08	0.01	0.07
690	0.07	0.00	0.07
695	0.10	0.01	0.09
700	0.12	0.04	0.08
705	0.11	0.02	0.09
710	0.12	0.07	0.05
715	0.10	0.01	0.09
720	0.14	0.05	0.09
725	0.14	0.06	0.08
730	0.10	0.02	0.08
735	0.08	0.00	0.08
740	0.09	0.01	0.08
745	0.08	0.01	0.07
750	0.06	0.00	0.06
755	0.12	0.12	0.00
760	0.12	0.05	0.07
765	0.15	0.07	0.08
770	0.10	0.03	0.07
775	0.14	0.03	0.11
780	0.17	0.05	0.12
785	0.17	0.08	0.09
790	0.17	0.08	0.09
795	0.14	0.02	0.12
800	0.20	0.08	0.12
805	0.16	0.03	0.13
810	0.16	0.03	0.13
815	0.24	0.10	0.14
820	0.23	0.10	0.13
825	0.24	0.12	0.12
830	0.19	0.03	0.16
835	0.13	0.00	0.13
840	0.13	0.00	0.13
845	0.14	0.05	0.09
850	0.12	0.05	0.07
855	0.36	0.10	0.26
860	0.21	0.00	0.21
865	0.25	0.08	0.17
870	0.27	0.19	0.08
875	0.20	0.06	0.14
880	0.18	0.05	0.13
885	0.17	0.10	0.07
890	0.17	0.09	0.08

Sediment L* and a*

Table 4

Depth (cm)	L*	a*	Depth (cm)	L*	a*	Depth (cm)	L*	a*	Depth (cm)	L*	a*
15	49.48	1.90	77	52.64	3.64	146	55.19	2.26	208	58.42	1.09
16	51.66	2.64	78	53.02	3.56	147	53.45	2.21	209	54.44	1.17
17	60.60	2.95	79	54.99	3.30	148	56.09	1.99	210	55.76	1.28
18	62.22	2.83	80	53.63	3.25	149	55.23	1.75	211	55.30	0.60
19	63.78	2.79	81	53.00	3.19	150	55.93	1.76	212	53.71	1.04
20	63.69	3.13	82	53.57	2.96	151	56.29	1.93	213	51.38	1.26
21	62.25	3.41	83	56.32	1.93	152	54.07	1.75	214	52.49	0.78
22	61.61	3.33	84	52.50	2.72	153	56.37	1.56	215	58.48	0.99
23	61.14	3.26	85	52.34	3.29	154	55.84	1.42	216	57.61	0.71
24	57.75	3.38	86	51.83	3.16	155	56.77	1.14	217	58.13	0.84
25	55.58	3.20	87	50.50	3.54	156	57.34	1.53	218	59.36	0.86
26	55.26	2.73	88	51.74	3.02	157	54.79	1.45	220	59.63	0.82
27	54.84	2.24	89	50.40	3.51	158	54.41	1.58	221	58.65	0.99
28	54.93	2.22	90	50.49	3.08	159	55.03	1.46	222	59.50	0.67
29	58.96	3.01	91	52.66	2.94	160	54.57	1.13	223	59.95	0.78
30	62.39	2.52	92	51.69	3.61	161	54.72	1.19	224	61.19	0.94
31	62.35	2.61	93	52.90	3.49	162	57.40	1.16	225	61.45	0.97
32	58.84	2.80	94	52.86	3.58	163	52.81	1.20	226	62.52	0.97
33	57.68	2.81	95	52.70	3.64	164	53.71	1.45	227	63.13	0.85
34	60.02	2.84	96	52.26	3.52	165	54.54	1.37	228	62.39	1.03
35	60.40	2.87	97	52.13	3.58	166	51.36	1.33	229	61.89	0.88
36	61.42	2.72	98	53.69	2.93	167	50.86	1.22	230	62.06	1.12
37	62.18	2.65	99	53.93	3.53	168	51.44	1.26	231	59.85	1.38
38	62.50	2.69	100	52.61	3.17	169	52.38	1.38	232	60.15	1.31
39	59.53	2.87	101	52.30	2.91	170	51.42	1.71	234	59.73	1.11
40	54.75	3.07	102	53.18	2.71	171	52.51	1.52	235	57.62	1.32
41	52.74	2.91	103	49.59	2.52	172	51.66	1.55	236	57.86	1.38
42	54.23	2.99	111	48.42	2.77	173	51.32	1.53	237	57.11	1.43
43	51.24	2.92	112	48.66	3.00	174	53.14	1.75	238	58.68	1.16
44	50.96	3.19	113	49.91	3.49	175	52.62	1.63	239	58.06	1.28
45	50.76	3.32	114	49.25	3.39	176	52.58	1.94	240	59.47	1.11
46	51.72	3.43	115	49.22	3.25	177	52.25	1.75	241	58.23	1.16
47	51.68	3.41	116	48.95	3.30	178	54.52	1.86	242	56.76	1.11
48	51.96	3.37	117	46.66	2.90	179	53.32	1.90	243	59.15	1.09
49	53.41	3.34	118	49.85	3.51	180	54.55	1.77	244	55.88	1.00
50	53.29	2.64	119	52.33	2.91	181	55.44	1.83	245	59.55	1.09
51	50.91	3.50	120	48.88	2.67	182	53.67	1.77	246	60.68	1.26
52	53.57	3.37	121	51.10	2.91	183	56.67	1.61	247	60.67	1.28
53	53.21	3.39	122	52.70	2.66	184	56.56	1.51	248	59.07	1.20
54	54.87	3.66	123	54.82	2.56	185	53.67	1.49	249	55.03	1.18
55	51.76	3.82	124	55.28	2.53	186	56.49	1.50	250	55.43	1.29
56	50.39	3.75	125	56.02	2.30	187	56.71	1.21	251	59.84	1.26
57	50.06	3.53	126	55.10	2.19	188	57.59	1.28	252	57.03	1.24
58	48.36	3.46	127	54.70	2.21	189	58.14	1.21	253	55.04	1.24
59	49.56	3.42	128	54.60	2.05	190	55.66	1.37	254	53.12	1.03
60	50.65	3.48	129	54.89	2.27	191	55.55	1.38	255	52.53	1.09
61	52.67	2.63	130	54.89	2.21	192	58.23	1.18	256	52.96	0.90
62	51.72	3.80	131	55.33	2.28	193	58.32	1.18	257	49.99	1.14
63	54.46	3.07	132	55.19	2.29	194	55.02	1.57	258	45.76	0.21
64	52.68	3.65	133	54.69	2.42	195	55.85	1.50	259	44.42	0.26
65	52.29	3.31	134	54.97	2.20	196	55.27	1.36	260	51.12	1.78
66	51.55	3.94	135	53.61	2.45	197	55.26	1.48	261	51.48	1.67
67	51.70	3.86	136	53.75	2.59	198	57.84	1.25	262	52.49	1.60
68	50.97	4.05	137	53.81	2.44	199	52.37	1.32	263	51.41	2.06
69	51.23	4.10	138	56.05	2.36	200	58.97	1.29	264	53.48	1.41
70	51.44	3.37	139	56.16	2.29	201	53.40	1.40	265	52.37	1.33
71	52.92	3.43	140	56.47	2.35	202	56.76	1.17	266	51.50	2.07
72	51.61	3.72	141	57.71	2.16	203	57.70	1.08	267	52.17	2.14
73	53.49	3.04	142	58.16	2.15	204	57.58	0.93	268	53.63	2.38
74	52.61	3.50	143	57.73	2.07	205	56.73	1.08	269	50.84	1.68
75	53.21	3.75	144	53.78	2.26	206	57.19	1.13	270	50.54	1.69
76	52.89	3.73	145	53.35	2.16	207	58.91	1.02	271	51.48	1.99

Table 4 contin.

Depth (cm)	L*	a*	Depth (cm)	L*	a*	Depth (cm)	L*	a*	Depth (cm)	L*	a*
272	51.12	2.15	337	70.92	0.47	399	79.30	0.74	461	53.87	2.06
273	51.60	2.35	338	73.56	0.16	400	78.97	0.77	462	53.56	2.01
274	50.78	2.38	339	73.68	0.08	401	76.93	0.89	463	53.54	1.82
275	50.26	2.69	340	73.86	-0.01	402	78.79	0.82	464	52.40	1.86
276	49.82	2.58	341	74.29	0.09	403	78.65	0.83	465	51.89	1.58
277	50.18	2.57	342	74.33	0.10	404	78.99	0.77	466	52.93	1.42
278	50.59	2.75	343	74.00	0.25	405	78.45	0.83	467	52.64	1.17
279	50.77	2.65	344	73.17	0.27	406	78.72	0.81	468	52.24	1.17
280	50.97	2.56	345	70.16	0.66	407	78.89	0.91	469	51.27	1.36
281	52.08	2.46	346	70.10	0.73	408	79.14	0.81	470	51.61	1.24
282	52.99	2.46	347	70.99	0.60	409	78.06	1.01	471	53.19	1.12
283	53.25	2.20	348	72.08	0.72	410	77.94	0.92	472	51.67	1.26
284	55.67	2.59	349	71.67	0.73	411	78.51	0.80	473	51.99	1.34
285	57.78	2.35	350	70.99	0.80	412	77.74	0.96	474	50.83	1.33
286	56.30	2.45	351	70.74	0.59	413	77.44	0.93	475	49.76	1.65
287	61.23	2.32	352	72.15	0.66	414	77.00	0.88	476	48.80	1.52
288	63.04	2.29	353	71.38	0.70	415	75.88	0.98	477	50.42	1.29
289	61.49	2.50	354	70.87	0.55	416	76.45	1.04	478	50.37	1.33
290	61.33	2.38	355	72.65	0.46	417	74.87	1.18	479	49.28	1.53
291	63.37	1.99	356	72.15	0.69	418	70.54	1.53	480	49.24	1.45
292	66.18	1.75	357	71.50	0.76	419	68.42	0.87	481	49.94	1.38
293	68.28	1.40	358	72.15	0.86	420	62.02	1.07	482	50.56	1.26
294	68.64	1.48	359	73.48	0.85	421	63.63	2.14	483	50.43	1.51
295	67.61	1.72	360	71.65	1.12	422	61.69	2.08	484	51.20	2.02
296	61.20	2.37	361	70.22	1.19	423	64.92	2.12	485	52.41	1.82
297	68.87	1.50	362	70.24	1.21	424	60.17	3.28	486	52.30	2.04
298	69.21	1.66	363	67.86	1.06	425	58.45	3.02	487	52.49	2.09
299	65.67	2.04	364	70.12	1.23	426	60.49	3.01	488	51.83	2.16
300	62.23	2.12	365	68.96	1.47	427	55.36	3.57	489	52.48	1.95
301	63.76	2.18	366	69.67	1.31	428	53.67	3.67	490	52.92	1.90
302	64.72	1.57	367	68.71	1.48	429	51.09	3.69	491	52.47	1.79
303	68.43	0.66	368	69.33	1.48	430	53.75	3.91	492	52.51	1.99
304	68.33	0.72	369	68.90	1.64	431	52.36	4.19	493	53.96	2.14
305	72.67	0.23	370	68.52	1.67	432	52.39	3.97	494	53.76	2.08
306	70.78	0.28	371	67.22	1.85	433	52.07	4.09	495	54.22	1.90
307	67.22	0.18	372	69.25	1.75	434	51.92	3.77	496	53.63	2.13
308	62.35	0.56	373	69.41	1.61	435	50.20	3.24	497	53.46	2.11
312	62.66	0.26	374	67.15	1.96	436	50.66	2.77	498	54.45	2.12
313	70.48	0.27	375	63.81	2.41	437	50.91	3.15	499	53.72	1.96
314	70.79	0.26	376	63.48	2.67	438	52.96	3.47	500	53.90	2.11
315	73.67	0.18	377	67.49	2.12	439	53.69	3.73	501	54.79	2.37
316	72.34	0.37	378	66.54	2.20	440	53.09	3.57	502	54.62	2.20
317	72.75	0.31	379	70.15	1.78	441	54.49	3.79	503	53.51	2.29
318	71.31	0.56	380	73.95	1.02	442	55.07	3.21	504	55.05	2.41
319	70.90	0.65	381	69.59	1.57	443	54.88	3.36	505	54.26	2.37
320	70.66	0.62	382	69.32	1.71	444	56.45	3.07	506	54.12	2.39
321	70.90	0.64	383	71.37	1.34	445	56.21	3.19	507	54.95	2.37
322	69.78	0.68	384	71.49	1.29	446	57.02	2.97	508	54.25	2.27
323	69.63	0.66	385	73.39	1.19	447	54.04	2.39	509	54.13	2.38
324	68.31	0.90	386	73.81	1.21	448	55.18	2.68	510	53.19	2.17
325	65.57	1.05	387	73.45	1.13	449	54.62	2.94	511	52.96	2.42
326	67.44	1.14	388	72.19	1.52	450	54.88	2.66	512	53.09	2.29
327	64.77	1.26	389	73.68	1.17	451	52.85	2.51	513	54.61	2.24
328	64.11	1.30	390	70.89	1.73	452	55.59	2.64	514	53.74	2.23
329	60.94	1.09	391	73.62	1.30	453	54.46	2.65	515	53.71	2.15
330	61.74	1.47	392	75.88	0.93	454	54.69	2.26	516	51.95	2.10
331	59.61	1.66	393	75.94	0.92	455	54.34	2.16	517	52.87	2.04
332	61.25	1.57	394	75.61	0.94	456	55.60	2.20	518	52.82	2.07
333	63.00	1.31	395	77.95	0.78	457	55.31	2.31	521	51.24	2.14
334	67.75	1.00	396	78.07	0.72	458	54.53	2.22	522	51.70	2.06
335	66.63	0.89	397	74.83	1.18	459	54.58	2.06	523	52.88	2.54
336	71.89	0.44	398	78.98	0.70	460	54.68	2.03	524	53.16	2.48

Table 4 contin.

Depth (cm)	L*	a*	Depth (cm)	L*	a*	Depth (cm)	L*	a*	Depth (cm)	L*	a*
525	52.82	2.42	587	58.10	1.19	652	67.26	1.17	714	59.81	1.94
526	53.67	2.50	589	52.38	1.13	653	65.12	1.58	715	59.83	2.06
527	51.98	2.25	590	53.86	1.51	654	65.21	1.20	716	60.21	2.03
528	53.15	1.72	591	55.29	1.54	655	60.28	1.60	717	59.40	1.76
529	52.75	1.71	592	55.39	1.41	656	67.00	1.08	721	57.85	1.70
530	51.05	1.92	593	56.42	1.33	657	70.49	1.01	722	59.46	1.66
531	52.04	2.13	594	54.88	1.19	658	68.92	0.81	723	57.28	1.75
532	52.54	2.13	595	54.66	1.41	659	70.09	0.78	724	61.71	1.89
533	51.90	1.75	596	56.31	1.45	660	68.62	0.87	725	63.56	1.77
534	51.91	1.86	597	58.27	1.43	661	68.31	0.92	726	62.21	1.80
535	51.72	1.96	598	57.14	1.30	662	69.15	0.78	727	64.11	1.74
536	52.06	1.92	599	57.37	1.46	663	71.06	0.67	728	64.01	1.62
537	53.51	1.66	600	57.14	1.76	664	69.18	0.91	729	64.45	1.46
538	53.94	1.33	601	55.90	1.80	665	72.34	0.59	730	65.06	1.48
539	52.53	2.04	602	57.32	1.67	666	72.96	0.51	731	66.82	1.26
540	52.50	1.99	603	58.74	1.78	667	73.87	0.45	732	66.36	1.44
541	52.61	2.10	604	58.41	1.66	668	74.24	0.39	733	65.29	1.48
542	53.91	2.12	605	55.12	1.76	669	73.80	0.45	734	67.88	1.28
543	55.65	1.91	606	56.21	2.01	670	73.52	0.51	735	67.61	1.30
544	53.83	2.29	607	56.88	2.01	671	72.64	0.60	736	65.68	1.44
545	53.66	2.22	608	56.29	1.99	672	72.53	0.57	737	68.00	1.22
546	55.24	2.07	609	56.32	2.10	673	72.52	0.36	738	67.04	1.36
547	55.20	2.15	610	57.09	2.31	674	73.71	0.42	739	69.81	1.04
548	56.23	2.02	611	56.75	2.29	675	73.49	0.47	740	70.38	0.95
549	55.70	2.09	612	56.57	2.28	676	72.52	0.53	741	69.00	1.02
550	56.94	1.87	613	57.05	2.82	677	71.12	0.48	742	70.75	0.85
551	56.01	1.68	614	56.88	2.76	678	73.06	0.30	743	70.43	0.86
552	57.86	1.97	615	59.42	2.89	679	70.73	0.48	744	71.50	0.79
553	54.98	1.89	616	59.85	2.85	680	71.30	0.49	745	69.96	0.91
554	55.74	1.77	617	60.28	2.80	681	69.06	0.62	746	71.68	0.83
555	54.77	1.88	618	60.12	2.62	682	69.51	0.71	747	72.38	0.59
556	54.71	1.93	621	61.87	2.98	683	66.68	0.87	748	71.77	0.70
557	54.53	1.88	622	60.68	3.09	684	72.71	0.49	749	70.44	0.83
558	57.79	1.97	623	58.85	3.13	685	70.69	0.51	750	69.79	0.83
559	59.85	1.75	624	52.81	3.29	686	66.84	0.72	751	70.00	0.79
560	58.19	1.82	625	53.98	3.34	687	66.32	0.79	752	69.00	1.07
561	59.25	1.67	626	55.90	3.32	688	66.52	0.80	753	68.34	1.20
562	57.50	1.59	627	54.55	3.53	689	65.62	1.01	754	69.70	0.79
563	50.58	1.28	628	57.54	3.13	690	63.53	1.03	755	67.57	1.08
564	51.55	1.45	629	70.09	1.45	691	65.44	1.00	756	65.00	1.89
565	48.79	1.29	630	67.51	1.66	692	63.48	1.20	757	66.10	1.88
566	50.94	1.39	631	71.62	1.24	693	68.34	0.74	758	66.52	1.50
567	54.94	1.48	632	70.48	1.27	694	59.45	1.27	759	68.42	1.18
568	56.36	1.55	633	71.95	1.14	695	60.65	1.19	760	66.46	1.02
569	56.48	1.55	634	71.35	1.24	696	61.21	1.25	761	66.87	1.21
570	58.81	1.59	635	72.39	1.01	697	60.66	1.43	762	65.28	1.11
571	60.98	1.53	636	73.74	0.64	698	57.52	1.35	763	66.13	1.00
572	62.19	1.48	637	68.67	1.31	699	54.89	1.57	764	66.44	1.15
573	60.77	1.66	638	72.79	1.00	700	60.03	1.51	765	67.04	1.05
574	63.52	1.21	639	74.73	0.63	701	55.30	1.38	766	64.02	1.22
575	66.35	1.13	640	74.15	0.74	702	50.13	1.75	767	59.80	1.14
576	66.56	1.12	641	74.55	0.75	703	54.06	1.80	768	57.06	1.24
577	64.80	1.30	642	73.95	0.50	704	53.13	1.81	769	56.88	1.28
578	63.91	1.19	643	72.98	0.81	705	54.60	2.04	770	58.03	1.00
579	62.72	1.21	644	69.96	1.35	706	55.71	2.23	771	58.50	0.72
580	63.84	1.35	645	70.50	1.10	707	56.18	2.12	772	58.99	0.91
581	57.27	1.41	646	69.87	1.40	708	59.03	1.96	773	58.33	0.48
582	57.87	1.43	647	71.85	1.05	709	57.86	2.07	774	48.15	1.30
583	58.00	1.40	648	66.44	1.39	710	57.89	1.91	775	51.58	0.92
584	59.59	1.38	649	66.39	1.48	711	55.59	1.73	776	54.79	1.17
585	63.56	0.85	650	67.35	1.41	712	50.66	1.34	777	55.26	1.58
586	61.09	1.32	651	64.58	1.51	713	59.97	1.97	778	56.57	1.45

Table 4 contin.

Depth (cm)	L*	a*	Depth (cm)	L*	a*
779	57.84	1.95	843	55.20	1.07
780	57.52	1.93	844	54.08	0.80
781	57.22	1.84	845	52.31	0.61
782	57.37	1.88	846	52.45	0.16
783	57.31	1.92	847	52.03	0.26
784	56.45	1.85	848	52.24	0.23
785	56.13	1.73	849	52.52	0.04
786	56.84	1.86	850	52.31	0.09
787	55.73	1.75	851	51.89	-0.02
788	54.68	2.08	852	50.80	-0.08
789	54.39	1.73	853	49.19	0.03
790	54.91	1.59	854	47.55	-0.29
791	54.76	0.95	855	46.15	-0.52
792	54.90	0.79	856	43.52	-0.48
793	54.55	1.20	857	51.27	0.96
794	56.14	1.68	858	46.05	0.06
795	56.01	1.62	859	51.63	1.20
796	55.82	1.54	860	52.60	1.55
797	55.52	1.59	861	52.46	1.63
798	55.89	1.59	862	48.87	0.44
799	55.11	1.43	863	52.73	1.73
800	55.36	1.57	864	52.64	1.71
801	55.71	1.44	865	53.22	1.84
802	54.82	1.29	866	53.22	1.70
803	53.84	0.98	867	51.60	1.41
804	55.35	1.21	868	53.00	1.83
805	55.22	1.14	869	53.69	1.92
806	53.91	0.95	870	54.49	1.78
807	51.52	0.67	871	53.85	1.82
808	51.14	0.88	872	53.61	2.06
809	49.89	1.00	873	53.33	1.85
810	49.98	0.93	874	55.03	1.70
811	50.75	0.94	875	56.08	1.80
812	50.21	0.75	876	56.08	1.86
813	54.30	1.08	877	45.45	1.54
814	54.58	1.10	878	56.17	1.79
815	52.94	0.81	879	55.05	1.76
816	54.20	0.95	880	54.17	1.71
817	53.95	0.73	881	52.10	1.71
818	53.23	0.86	882	53.61	1.73
819	53.56	0.64	883	52.07	1.70
821	52.82	0.75	884	53.04	1.62
822	51.29	0.18	885	52.19	1.79
824	51.51	0.43	886	52.15	1.56
825	50.67	0.12	887	50.60	1.49
826	51.35	-0.02	888	50.68	1.48
827	51.47	0.12	889	51.77	1.40
828	51.32	0.14	890	51.72	1.65
829	51.50	0.25	891	53.76	1.60
830	53.10	0.60	892	51.51	1.28
831	53.30	0.53			
832	53.97	0.73			
833	53.84	0.85			
834	53.49	0.96			
835	52.46	0.48			
836	52.90	0.72			
837	52.41	0.36			
838	55.42	1.16			
839	55.50	1.04			
840	55.80	1.22			
841	53.75	0.92			
842	54.81	1.00			

Carbonate (weight %)

Table 5

Depth (cm)	Bulk $CaCO_3$ (weight %)	Coarse $CaCO_3$ (weight %)	Fine $CaCO_3$ (weight %)	Depth (cm)	Bulk $CaCO_3$ (weight %)	Coarse $CaCO_3$ (weight %)	Fine $CaCO_3$ (weight %)
720	62.72	29.15	33.57	1035	73.69	15.73	57.96
725	57.53	29.78	27.75	1040	76.64	20.42	56.22
730	54.58	22.13	32.45	1045	83.33	15.28	68.05
735	21.92	12.93	8.99	1050	86.50	30.26	56.24
740	33.47	15.88	17.59	1055	87.41	12.48	74.93
745	28.74	14.37	14.37	1060	83.37	12.82	70.55
750	34.86	17.55	17.31	1065	88.12	25.77	62.35
755	32.73	22.75	9.98	1070	85.04	15.38	69.66
760	27.97	18.07	9.90	1075	84.50	12.27	72.23
765	30.69	21.87	8.82	1080	81.78	9.60	72.18
770	28.87	18.71	10.16	1085	79.55	12.21	67.34
775	31.79	22.22	9.57	1090	85.10	16.55	68.55
780	35.15	21.75	13.40	1095	71.50	17.88	53.62
785	35.12	9.88	25.24	1100	76.62	11.34	65.28
790	25.76	9.88	15.88	1105	69.18	8.99	60.19
795	35.42	15.71	19.71	1110	49.10	6.78	42.32
800	27.94	21.25	6.69	1115	34.07	5.41	28.66
805	33.83	19.81	14.02	1120	28.99	6.46	22.53
810	28.50	20.21	8.29	1125	16.04	3.75	12.29
815	13.76	13.76	0.00	1130	24.30	4.38	19.92
820	14.29	6.09	8.20	1135	19.32	4.01	15.31
825	21.11	7.69	13.42	1140	16.47	5.82	10.65
830	34.33	12.36	21.97	1145	15.00	5.35	9.65
835	49.54	14.66	34.88	1150	16.30	9.91	6.39
840	67.50	14.41	53.09	1155	17.25	5.91	11.34
845	72.52	14.35	58.17	1160	19.84	14.72	5.12
850	63.55	16.88	46.67	1165	27.88	15.29	12.59
855	62.22	21.10	41.12	1170	11.89	3.19	8.70
860	54.41	17.05	37.36	1175	21.98	9.02	12.96
865	49.25	20.14	29.11	1180	27.57	4.88	22.69
870	60.74	21.09	39.65	1185	32.39	3.88	28.51
875	59.77	16.46	43.31	1190	34.17	9.23	24.94
880	30.37	12.28	18.09	1195	13.25	2.89	10.36
885	68.33	23.19	45.14	1200	35.09		
890	59.05	23.29	35.76	1205	41.42	9.13	32.29
895	45.75	20.23	25.52	1210	24.23	6.56	17.67
900	76.21	22.04	54.17	1215	68.25	9.11	59.14
905	72.43	19.95	52.48	1220	71.08	8.67	62.41
910	81.04	13.15	67.89	1225	61.61	8.93	52.68
915	77.05	15.30	61.75	1230	56.90	6.67	50.23
920	52.33	13.42	38.91	1235	42.13	4.54	37.59
925	33.55	9.47	24.08	1240	81.86	6.05	75.81
930	5.83	2.06	3.77	1245	89.25	8.60	80.65
935	8.99	3.22	5.77	1250	83.99	7.23	76.76
940	23.02	11.40	11.62	1255	88.12	8.55	79.57
945	24.15	8.02	16.13	1260	83.41	17.16	66.25
950	29.99	7.80	22.19	1265	85.91	10.25	75.66
955	32.16	8.96	23.20	1270	85.75	14.58	71.17
960	31.57	2.64	28.93	1275	84.75	14.73	71.02
965	16.48	3.49	12.99	1280	84.41	20.49	63.92
970	6.98	5.46	1.52	1285	86.16	14.49	71.67
980	24.44	10.60	13.84	1290	92.66	14.05	78.61
985	41.16	15.95	25.21	1295	85.16	11.14	74.02
990	54.07	19.82	34.25	1320	85.04	19.40	65.64
995	62.45	43.13	19.32	1325	86.25	23.11	63.14
1000	61.50	17.17	44.33	1330	86.53		
1005	72.70	22.18	50.52				
1010	75.35	16.01	59.34				
1015	69.44	13.40	56.04				
1020	72.15	15.16	56.99				
1025	59.76	13.96	45.80				
1030	54.18	12.70	41.48				

TOC (weight %)

Table 6

Depth (cm)	Bulk TOC (weight %)	Coarse TOC (weight %)	Fine TOC (weight %)	Depth (cm)	Bulk TOC (weight %)	Coarse TOC (weight %)	Fine TOC (weight %)
720	0.15	0.03	0.12	1030	0.00	0.00	0.00
725	0.10	0.04	0.06	1035	0.12	0.01	0.11
730	0.18	0.09	0.09	1040	0.09	0.02	0.07
735	0.16	0.12	0.04	1045	0.10	0.01	0.09
740	0.20	0.06	0.14	1050	0.14	0.04	0.10
745	0.21	0.07	0.14	1055	0.06	0.01	0.05
750	0.19	0.08	0.11	1060	0.12	0.01	0.11
755	0.26	0.12	0.14	1065	0.07	0.02	0.05
760	0.30	0.12	0.18	1070	0.09	0.01	0.08
765	0.25	0.10	0.15	1075	0.11	0.01	0.10
770	0.27	0.13	0.14	1080	0.11	0.01	0.10
775	0.26	0.14	0.12	1085	0.08	0.01	0.07
780	0.18	0.09	0.09	1090	0.08	0.01	0.07
785	0.15	0.03	0.12	1095	0.10	0.02	0.08
790	0.26	0.08	0.18	1100	0.14	0.03	0.11
795	0.25	0.09	0.16	1105	0.14	0.01	0.13
800	0.26	0.20	0.06	1110	0.27	0.02	0.25
805	0.21	0.10	0.11	1115	0.21	0.05	0.16
810	0.20	0.10	0.10	1120	0.27	0.05	0.22
815	0.19	0.13	0.06	1125	0.19	0.03	0.16
820	0.21	0.03	0.18	1130	0.16	0.03	0.13
825	0.15	0.02	0.13	1135	0.20	0.00	0.20
830	0.13	0.02	0.11	1140	0.19	0.03	0.16
835	0.15	0.02	0.13	1145	0.18	0.07	0.11
840	0.19	0.01	0.18	1150	0.16	0.04	0.12
845	0.13	0.01	0.12	1155	0.31	0.06	0.25
850	0.14	0.02	0.12	1160	0.18	0.05	0.13
855	0.13	0.02	0.11	1165	0.18	0.04	0.14
860	0.24	0.02	0.22	1170	0.09	0.01	0.08
865	0.13	0.02	0.11	1175	0.16	0.02	0.14
870	0.13	0.01	0.12	1180	0.17	0.01	0.16
875	0.13	0.02	0.11	1185	0.14	0.01	0.13
880	0.12	0.01	0.11	1190	0.13	0.02	0.11
885	0.15	0.02	0.13	1195	0.15	0.02	0.13
890	0.11	0.02	0.09	1200	0.17		
895	0.13	0.02	0.11	1205	0.13	0.02	0.11
900	0.14	0.03	0.11	1210	0.14	0.03	0.11
905	0.33	0.02	0.31	1215	0.09	0.02	0.07
910	0.12	0.02	0.10	1220	0.06	0.01	0.05
915	0.09	0.01	0.08	1225	0.08	0.01	0.07
920	0.30	0.03	0.27	1230	0.06	0.01	0.05
925	0.14	0.02	0.12	1235	0.20	0.01	0.19
930	0.17	0.03	0.14	1240	0.05	0.01	0.04
935	0.15	0.04	0.11	1245	0.05	0.01	0.04
940	0.12	0.04	0.08	1250	0.06	0.01	0.05
945	0.15	0.03	0.12	1255	0.04	0.01	0.03
950	0.22	0.02	0.20	1260	0.09	0.02	0.07
955	0.21	0.03	0.18	1265	0.05	0.01	0.04
960	0.34	0.02	0.32	1270	0.07	0.01	0.06
965	0.06	0.06	0.00	1275	0.08	0.01	0.07
970	0.33	0.04	0.29	1280	0.10	0.02	0.08
980	0.21	0.04	0.17	1285	0.05	0.01	0.04
985	0.12	0.02	0.10	1290	0.05	0.01	0.04
990	0.12	0.03	0.09	1295	0.06	0.01	0.05
995	0.14	0.03	0.11	1320	0.06	0.02	0.04
1000	0.09	0.05	0.04	1325	0.08	0.01	0.07
1005	0.06	0.01	0.05	1330	0.06		
1010	0.14	0.01	0.13				
1015	0.10	0.01	0.09				
1020	0.10	0.01	0.09				
1025	0.10	0.02	0.08				

Sediment L* and a*

Table 7

Depth (cm)	L*	a*	Depth (cm)	L*	a*	Depth (cm)	L*	a*	Depth (cm)	L*	a*
14	62.94	3.65	76	53.45	3.69	139	51.91	1.91	201	59.15	2.09
15	61.91	3.49	77	54.77	3.82	140	51.81	1.93	202	58.14	1.95
16	65.17	2.35	78	55.20	3.95	141	52.51	2.05	203	54.89	1.69
17	56.00	3.34	79	54.47	4.19	142	53.81	2.14	204	58.00	1.76
18	60.17	3.60	80	54.20	3.70	143	54.37	2.12	205	56.72	1.79
19	58.28	3.88	81	53.91	3.68	144	52.44	2.20	206	54.90	1.81
20	57.66	3.62	82	52.07	3.71	145	53.31	2.10	209	54.52	1.98
21	54.41	3.20	83	51.70	3.27	146	53.59	2.30	210	55.21	2.00
22	55.79	2.83	84	51.70	3.87	147	53.76	2.17	211	55.36	1.52
23	55.78	3.18	85	52.34	3.96	148	53.80	2.01	212	55.13	1.95
24	57.45	3.51	86	51.08	3.44	149	55.62	2.18	213	55.25	1.89
25	59.90	3.19	87	51.58	3.43	150	55.11	1.82	214	56.75	1.80
26	60.97	3.44	88	50.22	3.33	151	56.64	1.98	215	50.67	1.81
27	60.33	3.35	89	49.94	3.36	152	54.37	1.74	216	50.06	1.59
28	59.28	3.31	90	50.49	3.24	153	53.85	1.93	217	54.33	1.62
29	56.07	3.34	91	50.06	2.88	154	55.26	1.76	218	44.74	1.48
30	57.57	2.98	92	48.59	2.74	155	56.14	1.83	219	49.62	0.79
31	60.80	3.10	93	47.62	2.86	156	55.25	1.65	220	52.84	0.78
32	52.20	3.42	94	46.46	3.04	157	53.76	1.91	221	50.38	1.39
33	55.12	3.78	95	47.34	3.31	158	55.46	1.71	222	51.24	1.95
34	55.24	3.66	96	49.53	3.21	159	56.67	1.78	223	50.25	2.39
35	54.33	4.00	97	50.05	3.04	160	56.75	1.78	224	50.34	2.35
36	52.14	3.81	98	51.43	3.37	161	57.54	1.69	225	50.56	2.24
37	50.17	3.60	99	51.60	2.90	162	57.46	1.43	226	51.93	2.04
38	49.91	3.69	100	53.65	2.63	163	57.51	1.50	227	52.57	2.39
39	57.08	3.54	101	55.61	2.66	164	58.70	1.50	228	51.65	2.55
40	57.12	3.89	102	54.58	2.48	165	57.56	1.31	229	52.66	2.41
41	49.48	3.98	103	54.87	2.48	166	56.82	1.29	230	51.14	2.33
42	50.06	3.93	104	54.49	2.58	167	57.84	1.46	231	52.14	2.18
43	51.66	4.24	105	50.20	2.54	168	53.86	1.52	232	52.23	2.31
44	51.47	4.15	106	54.23	2.60	169	56.05	1.38	233	52.70	2.32
45	52.68	4.36	107	55.17	2.66	170	57.24	1.64	234	51.55	1.89
46	50.29	4.52	109	51.81	2.62	171	58.02	1.61	235	50.96	2.29
47	52.63	4.18	110	53.46	2.65	172	56.39	1.54	236	49.42	2.37
48	53.21	4.25	111	54.25	2.69	173	56.40	1.33	237	50.14	2.90
49	53.13	4.33	112	53.26	2.82	174	55.75	1.43	238	51.53	2.74
50	51.39	4.62	113	53.42	2.86	175	54.57	1.36	239	50.12	2.66
51	51.56	4.70	114	52.35	2.90	176	54.25	1.37	240	49.62	2.86
52	51.34	4.53	115	54.31	2.62	177	60.62	1.26	241	49.54	2.67
53	50.53	4.42	116	55.12	2.34	178	60.51	1.25	242	49.08	3.01
54	50.46	4.69	117	56.39	2.53	179	61.15	1.34	243	51.52	2.98
55	51.22	4.60	118	51.09	2.51	180	59.62	1.08	244	52.43	2.84
56	51.50	4.29	119	54.93	2.05	181	60.14	1.27	245	53.61	2.52
57	51.76	3.73	120	54.79	2.08	182	60.50	1.17	246	56.32	3.03
58	51.68	3.60	121	51.50	2.10	183	61.64	1.30	247	59.08	2.92
59	51.87	3.56	122	55.56	2.19	184	60.46	1.70	248	63.24	2.92
60	51.12	3.68	123	55.03	2.41	185	61.50	1.70	249	64.21	2.91
61	50.47	3.77	124	57.32	2.30	186	61.06	1.27	250	64.49	2.73
62	51.25	3.40	125	54.13	2.01	187	60.26	1.55	251	61.65	2.72
63	51.52	3.50	126	53.91	1.86	188	61.28	1.51	252	60.85	2.71
64	50.79	3.45	127	53.95	1.73	189	60.47	1.42	253	64.17	2.81
65	52.91	2.74	128	55.29	1.81	190	60.77	1.63	254	63.38	2.86
66	51.30	2.49	129	53.97	1.69	191	60.45	1.61	255	64.22	2.59
67	49.84	2.49	130	55.19	1.70	192	56.73	1.76	256	67.15	2.75
68	52.79	3.57	131	55.51	1.51	193	58.82	1.79	257	65.65	2.46
69	51.39	3.44	132	56.49	1.60	194	56.70	1.67	258	67.31	2.12
70	51.05	3.18	133	56.22	1.42	195	57.81	1.91	259	67.58	1.98
71	51.90	3.47	134	55.03	1.61	196	57.56	1.70	260	67.63	2.12
72	52.32	3.39	135	54.75	1.70	197	57.55	1.76	261	69.06	2.10
73	52.36	3.15	136	52.68	1.53	198	57.51	1.55	262	68.04	2.55
74	52.77	3.24	137	51.92	1.76	199	54.51	1.60	263	65.90	2.26
75	52.68	3.78	138	51.90	1.98	200	57.87	1.64	264	68.81	2.53

Table 7 contin.

Depth (cm)	L*	a*	Depth (cm)	L*	a*	Depth (cm)	L*	a*	Depth (cm)	L*	a*
265	71.21	2.36	327	74.04	1.34	390	79.13	1.67	452	54.23	2.24
266	66.84	2.31	328	73.13	1.33	391	78.95	1.71	453	54.21	1.87
267	67.86	2.05	329	73.17	1.33	392	78.88	1.72	454	52.34	1.99
268	69.85	2.11	330	71.78	1.57	393	78.50	1.76	455	51.51	1.92
269	70.29	1.62	331	72.49	1.39	394	78.90	1.79	456	51.73	1.86
270	72.24	2.10	332	73.22	1.41	395	78.04	1.80	457	52.01	1.65
271	71.07	1.23	333	72.07	1.52	396	77.82	2.09	458	51.25	1.64
272	73.37	0.91	334	71.87	1.75	397	77.05	1.50	459	49.79	1.86
273	74.14	0.89	335	71.92	1.71	398	77.12	1.51	460	50.96	1.93
274	74.38	0.77	336	72.48	1.76	399	74.54	1.64	461	52.02	1.84
275	73.82	0.77	337	70.54	1.74	400	71.66	1.30	462	50.05	1.58
276	73.67	1.00	338	70.30	1.79	401	65.40	1.47	463	50.05	1.59
277	73.42	0.91	339	69.76	1.79	402	66.60	1.59	464	49.59	1.45
278	73.56	1.01	340	70.46	1.89	403	61.65	1.82	465	49.40	1.47
279	73.72	0.95	341	70.56	1.97	404	67.04	1.63	466	48.68	1.68
280	74.23	1.00	342	67.77	1.93	405	61.66	2.86	467	48.59	1.49
281	74.01	1.21	343	67.68	2.46	406	63.94	2.61	468	48.14	1.59
282	73.76	1.22	344	68.94	2.48	407	64.96	3.09	469	47.44	1.62
283	73.05	1.17	345	71.13	2.27	408	68.86	3.13	470	48.28	1.75
284	71.88	1.34	346	67.70	2.30	409	70.16	3.15	471	47.51	1.53
285	70.29	1.39	347	66.82	2.75	410	71.14	3.09	472	47.33	1.72
286	71.39	1.49	348	67.63	2.57	411	63.78	3.20	473	47.90	1.59
287	71.07	1.67	349	62.20	2.53	412	64.39	3.27	474	48.97	1.67
288	71.41	1.97	350	65.53	3.04	413	62.17	3.32	475	48.87	1.95
289	70.60	1.89	351	64.46	2.47	414	60.91	3.40	476	49.92	2.02
290	70.60	1.82	352	66.19	2.53	415	60.77	3.48	477	51.04	1.80
291	69.54	1.95	353	71.63	2.82	416	59.25	3.57	478	51.47	2.34
292	64.90	1.99	354	65.39	2.97	417	58.37	3.40	479	51.66	2.33
293	64.24	2.09	355	73.61	2.09	418	56.52	3.55	480	50.60	2.33
294	65.47	1.97	356	71.84	2.05	419	53.06	3.23	481	51.17	2.25
295	62.87	2.24	357	72.31	2.41	420	53.93	3.70	482	52.31	2.30
296	65.33	1.87	358	72.41	2.05	421	54.16	3.32	483	52.95	2.30
297	66.58	2.64	359	72.66	2.05	422	54.51	3.97	484	53.35	2.22
298	64.15	2.07	360	73.86	1.87	423	51.23	3.95	485	53.55	2.35
299	56.96	1.90	361	74.24	1.76	424	49.41	3.81	486	53.13	2.48
300	59.56	1.70	362	74.01	1.82	425	53.03	3.85	487	53.09	2.69
301	61.60	1.51	363	74.67	1.95	426	54.16	3.88	488	54.53	2.59
302	65.21	1.36	364	73.99	1.92	427	55.05	3.52	489	54.11	2.50
303	70.55	1.16	365	72.87	1.94	428	54.35	3.56	490	53.76	2.57
304	68.95	1.20	366	74.05	1.98	429	55.25	3.64	491	53.18	2.41
305	69.87	1.32	367	73.94	1.97	430	55.36	3.63	492	52.30	2.63
306	70.62	1.27	368	73.58	1.92	431	57.23	3.69	493	52.61	2.75
307	66.01	1.26	369	75.41	1.96	432	57.75	3.91	494	50.80	2.69
308	49.83	0.85	370	74.70	1.88	433	56.59	3.67	495	51.13	2.64
309	68.21	0.98	371	75.47	1.74	434	56.71	3.54	496	51.96	2.49
310	69.38	0.93	372	75.95	1.81	435	55.15	3.52	497	51.26	2.41
311	70.63	0.87	373	77.29	1.67	436	54.04	3.24	498	51.43	2.47
312	70.98	0.66	374	76.95	1.60	437	53.12	3.46	499	53.67	2.54
313	71.58	0.75	375	78.15	1.61	438	53.89	3.39	500	51.89	2.84
314	72.18	0.68	376	77.07	1.67	439	54.86	3.42	501	52.08	2.81
315	73.43	0.60	378	78.76	1.55	440	55.04	2.88	502	52.65	2.74
316	73.37	0.57	379	79.05	1.55	441	54.54	2.61	503	51.90	2.84
317	75.04	0.84	380	79.08	1.60	442	55.79	2.49	504	51.60	2.89
318	74.59	0.95	381	76.35	1.63	443	53.15	2.82	505	51.34	2.71
319	65.74	1.45	382	79.29	1.74	444	54.44	2.46	506	52.30	2.50
320	66.56	1.35	383	79.58	1.59	445	55.06	2.48	507	53.07	2.36
321	68.86	1.74	384	79.62	1.55	446	53.54	2.37	508	51.61	2.56
322	70.14	1.58	385	78.24	1.72	447	51.90	2.34	509	52.65	2.55
323	70.05	1.58	386	78.89	1.54	448	52.71	2.20	510	51.98	2.72
324	71.41	1.50	387	79.37	1.60	449	52.43	2.30	511	52.29	2.66
325	73.29	1.38	388	77.36	1.65	450	52.87	2.21	512	49.34	2.68
326	73.14	1.49	389	79.29	1.70	451	55.01	1.99	513	47.84	2.20

Table 7 contin.

Depth (cm)	L*	a*	Depth (cm)	L*	a*	Depth (cm)	L*	a*	Depth (cm)	L*	a*
514	49.19	2.41	578	57.00	1.73	640	64.14	1.59	703	56.41	1.56
515	51.47	2.66	579	56.41	1.63	641	64.26	1.91	704	65.28	1.90
516	50.83	2.59	580	53.91	1.27	642	65.93	1.46	705	63.91	1.64
517	50.78	2.47	581	52.36	1.61	643	69.16	1.55	706	68.92	1.50
518	51.71	2.11	582	52.50	1.65	644	68.39	1.37	707	68.57	1.48
519	48.07	2.55	583	52.80	1.70	645	67.41	1.33	708	69.32	1.41
520	51.61	2.47	584	53.52	1.73	646	69.43	1.26	709	70.31	1.41
521	49.89	2.53	585	54.15	1.50	647	70.43	1.24	710	66.18	1.39
522	51.79	2.53	586	56.16	1.41	648	70.25	1.24	711	70.67	1.36
524	51.46	2.68	587	56.52	1.78	649	72.49	1.36	712	71.34	1.42
525	51.06	2.31	588	56.13	1.92	650	72.63	1.08	713	71.08	1.55
526	51.35	1.94	589	56.89	1.99	651	73.86	1.38	714	70.94	1.62
527	51.02	1.87	590	55.17	2.01	652	73.21	1.21	715	70.41	1.59
528	50.96	1.80	591	54.90	1.89	653	70.80	1.07	716	70.36	1.53
529	51.49	2.06	592	56.87	2.06	654	73.58	1.09	717	69.18	1.45
530	51.65	2.09	593	55.66	2.08	655	73.62	1.11	719	61.09	1.50
531	51.17	2.30	594	54.35	2.14	656	73.75	1.10	720	67.95	1.46
532	51.90	2.65	595	53.52	1.98	657	72.78	1.13	721	69.02	1.57
534	53.77	2.62	596	55.07	2.40	658	71.56	1.22	722	69.16	1.42
535	53.71	2.56	597	53.21	2.58	659	72.25	1.24	723	71.21	1.34
536	54.28	2.43	598	56.03	2.66	660	72.68	1.16	724	69.88	1.37
537	53.97	2.82	599	55.13	2.51	661	71.21	1.34	725	68.84	1.32
538	55.33	2.88	600	54.94	2.82	662	72.12	1.40	726	68.83	1.45
539	55.95	2.65	601	55.22	3.22	663	68.68	1.53	727	64.59	1.37
540	56.33	2.94	602	55.64	3.32	664	67.27	1.44	728	60.15	1.78
541	57.43	2.73	603	55.49	3.43	665	65.40	1.58	729	58.65	1.57
542	57.15	2.64	604	57.08	3.37	666	67.31	1.51	730	63.43	1.42
543	58.83	2.59	605	58.90	3.31	667	66.14	1.36	731	61.62	1.77
544	58.94	2.52	606	59.23	3.42	668	66.73	1.56	732	50.32	1.81
545	58.77	2.34	607	59.89	3.38	669	66.82	1.62	733	51.23	1.82
546	56.63	2.35	608	61.06	3.44	670	64.70	1.93	734	52.37	1.71
547	54.11	2.23	609	58.95	3.00	671	61.77	1.67	735	49.74	1.03
548	54.45	2.22	610	59.04	2.85	672	57.75	2.22	736	53.30	1.25
549	56.52	2.06	611	52.27	2.18	673	53.52	1.96	737	48.08	1.70
550	57.16	2.35	612	52.19	1.98	674	58.05	1.99	738	49.31	1.82
551	59.80	2.40	613	53.74	1.91	675	51.60	1.85	739	54.70	2.11
552	59.39	2.35	614	60.13	1.88	676	53.35	1.87	740	53.69	1.69
553	59.42	2.27	615	62.94	1.94	678	50.59	2.02	741	50.71	2.50
554	55.57	2.03	616	65.71	2.05	679	51.72	2.40	742	55.64	2.38
555	53.56	2.22	617	67.14	2.23	680	53.34	2.03	743	56.07	2.34
556	55.01	2.12	618	68.48	2.10	681	52.67	2.29	744	54.82	2.31
557	55.44	2.34	619	69.17	1.95	682	51.37	2.61	745	56.12	2.10
558	52.86	1.82	620	70.90	1.96	683	52.04	2.39	746	57.37	1.15
559	53.58	1.82	621	53.57	1.86	684	54.93	2.40	747	55.14	1.91
560	55.95	2.05	622	71.71	1.66	685	55.57	2.45	748	51.97	2.16
561	57.56	2.42	623	72.07	1.83	686	56.60	2.55	749	52.21	1.81
562	57.97	2.30	624	72.97	1.53	687	57.81	2.52	750	53.26	2.05
563	58.38	2.39	625	72.67	1.61	688	60.66	2.49	751	54.09	2.01
564	57.88	2.17	626	71.64	1.74	689	57.80	2.29	752	55.83	1.95
565	61.03	1.90	627	70.35	1.80	690	56.14	2.39	753	54.97	1.97
566	62.38	1.62	628	71.21	1.59	691	57.27	2.54	754	54.83	1.76
567	64.21	1.73	629	71.21	1.74	692	57.79	2.59	756	53.60	1.68
568	65.38	1.67	630	69.66	1.75	693	58.77	2.35	757	52.74	1.74
569	65.96	1.66	631	70.52	1.63	694	60.33	2.36	758	50.80	1.48
570	67.35	1.62	632	68.83	1.89	695	62.43	2.30	759	51.96	1.85
571	63.39	1.63	633	63.41	1.49	696	58.96	2.10	760	51.98	1.61
572	62.94	1.61	634	71.15	2.19	697	62.77	2.12	761	51.37	1.35
573	61.82	1.57	635	70.31	2.47	698	63.49	2.02	762	51.77	1.31
574	60.26	1.69	636	60.12	2.39	699	64.20	1.90	763	51.31	1.32
575	58.27	1.74	637	65.56	2.11	700	66.85	2.09	764	51.14	1.15
576	57.35	1.77	638	62.41	2.22	701	64.52	2.02	765	50.80	0.94
577	55.88	1.86	639	61.15	1.87	702	65.02	1.78	766	51.15	1.40

Table 7 contin.

Depth (cm)	L*	a*	Depth (cm)	L*	a*	Depth (cm)	L*	a*	Depth (cm)	L*	a*
767	51.11	0.73	830	49.53	3.94	892	67.52	1.64	954	55.47	3.10
768	50.05	0.88	831	54.06	4.00	893	67.56	2.00	955	56.74	2.78
769	50.64	1.17	832	56.99	3.98	894	64.44	2.18	956	55.63	2.71
770	51.09	0.82	833	58.29	3.78	895	62.99	2.06	957	55.87	2.83
771	50.55	0.71	834	58.51	3.67	896	60.94	2.21	958	55.89	2.73
772	51.25	0.65	835	55.04	3.41	897	65.41	2.46	959	55.54	2.81
773	50.42	0.86	836	59.43	3.38	898	66.44	2.36	960	55.55	2.74
774	51.99	0.52	837	59.25	3.37	899	68.33	2.10	961	53.41	2.83
775	50.65	0.79	838	61.43	3.34	900	69.59	2.08	962	55.37	2.66
776	52.11	1.21	839	69.17	3.33	901	69.53	2.11	963	54.26	2.43
777	51.61	0.70	840	67.35	1.39	902	72.33	1.89	964	51.46	1.78
778	54.06	1.23	841	71.79	1.66	903	74.43	2.08	965	51.70	2.11
779	52.20	1.46	842	72.55	1.27	904	69.60	1.74	967	51.27	1.49
780	53.14	0.98	843	73.04	1.38	905	70.03	2.14	968	49.53	1.06
781	54.57	1.54	844	72.72	1.24	906	73.54	1.58	969	51.12	0.46
782	52.29	1.57	845	73.25	1.25	907	77.68	1.77	970	48.41	1.16
783	52.53	1.12	846	72.21	1.26	908	77.90	1.55	971	48.32	1.62
784	53.03	1.32	847	72.91	1.43	909	77.99	1.43	972	45.96	1.48
785	51.71	1.12	848	71.50	1.41	910	77.73	1.52	973	48.76	1.65
786	51.40	0.99	849	71.88	1.44	911	77.13	1.59	974	49.74	1.55
787	51.38	0.70	850	70.23	1.51	912	76.78	1.47	975	50.01	1.68
789	50.04	0.53	851	70.05	1.53	913	76.96	1.59	976	50.42	2.00
790	48.10	0.29	852	70.69	1.26	914	76.40	1.53	977	50.41	2.21
791	48.60	0.28	853	69.43	1.35	915	75.40	1.62	978	51.47	2.00
792	44.93	0.22	854	68.67	1.63	916	73.96	1.66	979	50.68	2.74
793	47.97	-0.05	855	68.78	1.68	917	73.46	1.49	980	50.66	3.10
794	49.75	-0.05	856	68.17	1.71	918	72.16	1.37	981	50.66	3.01
795	50.93	0.69	857	68.09	1.96	919	66.20	1.57	982	52.49	3.30
796	51.40	1.15	858	66.76	1.93	920	65.81	1.41	983	51.75	3.59
797	51.84	1.72	859	67.20	1.85	921	64.56	1.36	984	53.97	3.41
798	51.19	1.62	860	65.59	2.16	922	64.07	1.42	985	53.23	3.28
799	52.12	2.04	861	53.43	2.28	923	63.02	1.17	986	58.13	3.33
800	52.88	2.02	862	63.42	2.22	924	58.35	1.51	987	59.50	3.48
801	52.40	2.09	863	63.82	2.34	925	60.98	1.70	988	61.02	3.06
802	54.07	2.00	864	63.05	2.19	926	59.98	1.71	989	60.91	3.22
803	55.01	1.90	865	60.63	2.12	927	57.19	1.60	990	59.33	2.98
804	54.31	2.18	866	59.90	2.43	928	54.59	1.66	991	58.22	2.63
805	54.14	2.19	867	59.85	2.52	929	58.64	1.88	992	61.19	2.91
806	54.18	2.11	868	59.44	2.55	930	53.47	2.56	993	62.09	2.61
807	55.71	1.95	869	62.12	2.37	931	49.53	2.41	994	60.00	2.15
808	55.20	2.06	870	66.49	2.18	932	48.49	2.52	995	64.70	2.54
809	53.94	2.01	871	68.60	1.95	933	50.12	2.76	996	64.21	2.82
810	54.60	2.05	872	68.59	1.70	934	49.75	2.36	997	65.11	2.45
811	52.52	1.77	873	73.23	1.71	935	50.57	1.41	998	63.41	2.46
812	54.44	1.52	874	70.57	1.70	936	50.45	2.45	999	65.64	2.43
813	52.53	1.92	875	71.77	1.47	937	49.38	2.52	1000	66.93	2.50
814	49.48	1.98	876	71.16	1.66	938	49.23	3.03	1001	68.62	2.75
815	49.26	1.55	877	70.83	1.44	939	48.38	2.64	1002	67.61	2.59
816	52.49	1.29	878	68.64	1.79	940	51.85	2.37	1003	67.58	2.02
817	51.44	1.41	879	61.98	2.00	941	52.68	2.92	1004	62.51	2.19
818	49.01	1.41	880	60.59	2.31	942	52.35	2.92	1005	67.96	1.59
819	48.76	1.33	881	63.20	2.30	943	52.19	2.89	1006	70.19	1.43
820	48.40	2.16	882	63.76	2.19	944	52.61	2.84	1007	72.97	1.33
821	48.94	1.93	883	61.99	2.41	945	53.87	2.87	1008	74.62	1.41
822	49.33	2.88	884	65.46	2.10	946	52.65	2.77	1009	74.21	1.46
823	48.80	2.82	885	68.44	1.83	947	54.12	2.48	1010	74.46	1.34
824	49.68	2.87	886	67.27	1.76	948	52.57	2.80	1011	72.88	1.48
825	50.12	3.48	887	68.61	1.40	949	48.14	3.05	1012	73.77	1.76
826	49.86	3.11	888	68.84	1.20	950	52.83	2.77	1013	74.60	1.83
827	50.48	3.58	889	67.38	1.27	951	53.53	2.96	1014	72.84	1.43
828	46.05	4.10	890	68.16	1.37	952	53.59	3.12	1015	72.42	2.09
829	47.28	4.07	891	70.95	1.31	953	55.11	3.10	1016	70.23	0.57

Table 7 contin.

Depth (cm)	L*	a*	Depth (cm)	L*	a*	Depth (cm)	L*	a*	Depth (cm)	L*	a*
1017	68.29	1.43	1079	81.68	0.83	1141	51.29	1.75	1204	57.83	2.29
1018	70.65	1.50	1080	81.54	0.95	1142	54.62	1.73	1205	58.42	2.05
1019	72.68	1.23	1081	81.80	1.09	1143	51.55	2.00	1206	59.05	2.27
1020	73.00	1.49	1082	79.54	1.11	1144	52.54	2.13	1207	59.30	2.41
1021	72.34	1.43	1083	78.92	1.13	1145	52.20	1.99	1208	58.17	2.27
1022	72.67	1.36	1084	79.53	1.21	1146	52.27	2.11	1209	57.12	2.32
1023	72.43	1.53	1085	79.54	0.97	1147	52.65	2.28	1210	58.06	2.15
1024	73.47	1.67	1086	78.95	0.71	1148	51.68	2.45	1211	52.59	1.84
1025	71.13	2.01	1087	78.55	0.97	1149	51.01	2.36	1212	50.92	2.04
1026	70.41	2.03	1088	75.63	0.82	1150	51.56	2.71	1213	52.63	1.86
1027	68.58	1.60	1089	77.50	0.95	1151	51.93	2.33	1214	54.28	1.80
1028	68.77	3.14	1090	77.32	0.91	1152	51.25	2.37	1215	54.15	1.83
1029	66.15	3.26	1091	76.76	1.07	1153	51.32	2.19	1216	53.61	2.31
1030	66.59	2.91	1092	76.53	1.34	1154	51.17	2.08	1217	65.84	2.01
1031	63.84	2.82	1093	76.32	1.18	1155	51.32	1.79	1218	66.65	2.21
1032	72.08	2.08	1094	75.24	0.94	1156	48.60	0.12	1219	70.77	1.78
1033	67.37	1.56	1095	74.17	0.91	1157	43.53	2.50	1220	73.98	1.65
1034	66.81	1.28	1096	71.92	1.17	1158	53.38	2.39	1221	73.43	1.47
1035	68.09	1.26	1097	75.18	1.34	1159	53.28	2.37	1222	73.81	1.45
1036	74.05	1.31	1098	74.63	1.29	1160	51.24	2.33	1223	73.18	1.23
1037	74.02	1.40	1099	76.25	1.35	1162	52.45	2.40	1224	74.16	1.51
1038	74.24	1.46	1100	72.19	1.64	1163	52.70	2.79	1225	72.60	1.49
1039	75.02	1.48	1101	70.49	1.45	1164	55.10	3.25	1226	71.43	1.78
1040	74.33	1.20	1102	71.41	1.31	1165	52.58	3.59	1227	73.15	1.87
1041	74.03	1.21	1103	70.07	1.58	1166	55.11	3.70	1228	72.45	1.85
1042	73.65	1.23	1104	70.09	1.55	1167	55.99	3.57	1229	71.22	2.51
1043	76.37	1.13	1105	69.35	1.65	1168	52.86	3.22	1230	68.05	2.41
1044	75.92	0.88	1106	67.61	1.76	1169	52.90	2.85	1231	65.11	2.21
1045	75.30	1.00	1107	67.55	1.70	1170	51.40	3.29	1232	60.76	2.46
1046	75.84	1.20	1108	66.79	1.71	1171	52.69	3.32	1233	64.26	1.56
1047	78.09	0.81	1109	65.90	1.26	1172	54.28	3.45	1234	58.80	1.30
1048	80.93	0.76	1110	67.09	1.97	1173	55.02	3.11	1235	62.50	1.34
1049	80.76	0.76	1111	63.04	1.30	1174	55.09	3.32	1236	68.46	1.40
1050	81.54	0.69	1112	59.63	1.18	1175	51.35	2.92	1237	73.15	2.34
1051	81.90	0.64	1113	56.30	1.73	1176	53.12	2.71	1238	72.05	1.05
1052	82.09	0.63	1114	56.07	1.74	1177	52.34	2.85	1239	78.09	0.70
1053	82.80	0.59	1115	56.48	1.68	1178	51.11	2.36	1240	83.73	0.73
1054	82.72	0.61	1116	53.17	1.61	1179	51.41	2.06	1241	82.21	1.15
1055	83.03	0.61	1117	53.45	1.68	1180	50.58	0.30	1242	82.67	0.61
1056	82.18	0.67	1118	54.80	1.73	1181	48.22	2.28	1243	84.60	0.53
1057	82.76	0.72	1119	51.85	2.09	1182	50.31	2.57	1244	85.91	0.51
1058	82.08	0.67	1120	50.22	2.03	1183	51.09	2.37	1245	85.83	0.48
1059	82.34	0.69	1121	49.20	1.58	1184	50.76	1.88	1246	86.98	0.63
1060	83.01	0.74	1122	49.30	1.78	1185	51.70	1.61	1247	84.43	0.71
1061	83.30	0.68	1123	50.23	1.48	1186	53.35	1.84	1248	86.63	0.47
1062	83.09	0.68	1124	51.43	1.80	1187	55.25	2.09	1249	86.11	0.66
1063	82.66	0.70	1125	48.96	1.82	1188	53.80	2.37	1250	86.09	0.57
1064	82.69	0.68	1126	50.09	2.13	1189	59.66	2.19	1251	85.84	0.60
1065	82.96	0.52	1127	48.87	2.16	1190	61.23	2.24	1253	84.88	0.45
1066	82.59	0.49	1128	49.37	2.07	1191	62.02	1.82	1254	83.25	0.18
1067	83.48	0.61	1129	50.64	1.89	1192	58.96	1.64	1255	82.23	0.77
1068	82.88	0.63	1130	52.21	1.82	1193	55.47	2.53	1256	84.11	0.26
1069	82.84	0.69	1131	50.96	1.79	1194	60.34	2.54	1257	79.89	1.00
1070	82.79	0.60	1132	50.70	1.92	1195	59.93	1.52	1258	80.37	1.18
1071	82.82	0.60	1133	51.39	2.04	1196	52.12	1.18	1259	78.29	1.28
1072	82.59	0.60	1134	51.49	1.85	1197	51.70	0.78	1260	76.42	0.79
1073	82.15	0.56	1135	51.95	1.71	1198	51.03	0.89	1261	74.40	0.33
1074	82.40	0.69	1136	51.27	1.52	1199	46.28	1.14	1262	78.31	0.10
1075	81.96	0.78	1137	52.15	1.48	1200	49.98	1.77	1263	78.86	0.11
1076	82.50	0.81	1138	50.85	1.52	1201	51.83	1.62	1264	81.44	0.23
1077	82.02	0.90	1139	54.64	1.38	1202	55.93	1.88	1265	81.58	0.10
1078	81.72	0.73	1140	53.09	1.72	1203	56.98	2.12	1266	81.03	0.87

Table 7 contin.

Depth (cm)	L*	a*
1267	82.33	0.13
1268	78.62	-0.05
1269	82.60	-0.04
1270	82.76	-0.02
1271	80.59	0.09
1272	81.69	0.17
1273	80.87	0.12
1274	80.34	0.21
1275	80.90	0.24
1276	79.22	0.35
1277	77.57	0.31
1278	77.32	0.25
1279	77.58	0.05
1280	77.73	0.17
1281	77.77	0.31
1282	77.73	0.25
1283	77.80	0.34
1284	79.95	0.17
1285	80.78	0.10
1286	80.18	0.09
1287	80.88	0.05
1288	81.16	0.07
1289	81.26	-0.03
1290	81.71	-0.01
1291	80.43	0.09
1292	80.25	0.08
1293	79.62	0.06
1294	80.35	0.13
1295	78.94	0.11
1296	78.60	0.10

Table 8

Depth (cm)	$\delta^{18}O$ vs. PDB (‰)	$\delta^{13}C$ vs. PDB (‰)	Depth (cm)	$\delta^{18}O$ vs. PDB (‰)	$\delta^{13}C$ vs. PDB (‰)	Depth (cm)	$\delta^{18}O$ vs. PDB (‰)	$\delta^{13}C$ vs. PDB (‰)
800	2.57	-1.23	955	2.44	-0.99	1112.5	2.09	-0.81
802.5	2.55	-1.43	957.5	2.40	-1.23	1115	2.19	-0.68
805	2.21	-1.27	960	2.28	-1.45	1117.5	2.19	-0.81
807.5	2.30	-1.44	962.5	2.24	-1.40	1120	2.27	-0.99
810	2.23	-1.39	965	2.54	-1.43	1122.5	2.44	-0.22
812.5	2.30	-1.54	967.5	2.30	-1.26	1125	2.39	-0.59
815	2.42	-1.61	970	2.58	-0.95	1127.5	2.16	-0.25
817.5	1.97	-0.77	972.5	2.53	-0.83	1130	2.14	-0.26
820	2.46	-0.76	975	2.28	-0.79	1132.5	2.20	-0.12
822.5	2.62	-1.10	977.5	2.43	-0.82	1135	2.23	0.03
825	2.53	-1.08	980	2.55	-0.83	1137.5	2.58	-0.53
827.5	2.57	-0.98	982.5	2.44	-0.81	1140	2.17	-0.28
830	2.16	-1.10	987.5	2.55	-0.35	1142.5	2.33	-0.37
832.5	2.18	-0.92	990	2.31	-0.69	1145	2.50	-0.54
835	2.27	-1.09	992.5	2.30	-0.31	1147.5	2.58	-0.32
837.5	2.28	-0.64	995	2.55	-0.36	1150	2.08	-0.09
840	2.37	-0.53	997.5	2.47	-0.60	1152.5	2.65	-0.44
842.5	2.27	-0.52	1000	2.37	-0.33	1155	2.20	-0.31
845	2.17	-0.73	1002.5	2.31	-0.41	1157.5	2.50	-0.20
847.5	2.31	-0.57	1005	2.72	0.07	1160	2.87	-0.59
850	2.17	-0.75	1007.5	2.44	-0.04	1162.5	2.71	-0.99
852.5	2.26	-0.77	1010	2.41	-0.03	1165	2.60	-1.09
855	1.94	-0.89	1012.5	2.26	-0.03	1167.5	2.69	-1.24
857.5	1.89	-0.92	1015	1.96	-0.16	1170	2.64	-1.08
860	2.27	-0.72	1017.5	2.20	-0.10	1172.5	2.58	-1.24
862.5	2.12	-1.00	1020	2.18	-0.10	1175	2.47	-1.04
865	2.05	-0.87	1022.5	2.35	-0.05	1177.5	2.51	-1.44
867.5	2.16	-0.66	1025	2.07	-0.26	1180	2.53	-0.90
870	2.09	-0.55	1027.5	2.08	-0.59	1182.5	2.65	-0.96
872.5	1.89	-0.48	1030	2.04	-0.39	1185	2.76	-0.84
875	2.02	-0.29	1032.5	2.12	-0.16	1187.5	2.45	-1.16
877.5	2.07	-0.33	1035	2.19	-0.32	1190	2.55	-0.67
880	2.10	-0.37	1037.5	2.30	-0.15	1192.5	2.47	-1.01
882.5	2.34	-0.12	1040	2.16	-0.01	1195	2.51	-0.68
885	2.17	-0.16	1042.5	2.04	0.14	1197.5	2.43	-0.79
887.5	2.39	-0.27	1045	1.95	0.13	1200	2.84	-0.79
890	2.08	-0.54	1047.5	1.91	0.29	1202.5	2.48	-0.69
892.5	1.82	-0.51	1050	1.83	0.19	1205	2.33	-0.83
895	1.93	-0.61	1052.5	1.50	0.11	1207.5	2.29	-0.76
897.5	1.88	-0.64	1055	1.64	0.14	1210	2.46	-0.45
900	2.04	-0.34	1057.5	1.85	0.18	1212.5	2.68	-0.32
902.5	1.71	-0.68	1060	1.77	0.23	1215	2.39	-0.05
905	1.63	-0.55	1062.5	1.56	0.20	1217.5	2.56	0.16
907.5	1.38	-0.57	1065	1.56	0.16	1220	2.35	0.13
910	1.34	-0.47	1067.5	1.63	0.13	1222.5	2.20	-0.05
912.5	1.26	-0.61	1070	1.66	-0.09	1225	2.27	-0.25
915	1.25	-0.81	1072.5	1.66	0.19	1227.5	2.18	-0.06
917.5	1.24	-0.81	1075	1.65	0.04	1230	1.99	-0.14
920	0.76	-1.27	1077.5	1.59	0.07	1232.5	2.09	-0.33
922.5	0.90	-1.40	1080	1.66	-0.32	1235	2.08	-0.15
925	1.28	-1.26	1082.5	1.67	-0.24	1237.5	2.39	0.25
927.5	1.07	-1.22	1085	1.49	-0.38	1240	2.55	0.36
930	1.96	-0.73	1087.5	1.59	-0.36	1242.5	2.40	0.38
932.5	1.81	-1.03	1090	1.51	-0.51	1245	2.40	0.36
935	2.00	-0.87	1092.5	1.50	-0.55	1247.5	2.18	0.19
937.5	2.28	-0.63	1095	1.90	-0.46	1250	2.10	0.17
940	2.29	-1.16	1097.5	1.57	-0.35	1252.5	2.24	0.14
942.5	2.85	-1.09	1100	1.64	-0.45	1255	2.20	0.08
945	2.79	-1.17	1102.5	1.97	-0.88	1257.5	2.12	0.02
947.5	2.59	-1.41	1105	1.96	-0.85	1260	2.24	0.33
950	2.56	-1.67	1107.5	1.92	-0.93	1262.5	2.37	0.62
952.5	2.24	-1.29	1110	2.12	-0.90	1265	2.38	0.42

Table 8 continued

Depth (cm)	$\delta^{18}O$ vs. PDB (‰)	$\delta^{13}C$ vs. PDB (‰)
1267.5	2.24	0.48
1270	2.26	0.43
1272.5	2.24	0.62
1275	2.35	0.63
1277.5	2.15	0.47
1280	2.11	0.52
1282.5	2.28	0.68
1285	2.11	0.42
1287.5	2.23	0.49
1290	2.24	0.34
1292.5	2.22	0.44
1295	2.32	0.43
1297.5	2.24	0.39
1317.5	2.05	-0.12
1320	1.88	-0.15
1325	2.01	-0.20
1330	2.01	0.17

IRD (grains/gram)

Table 9

Depth (cm)	IRD >250 microns grains (gram)	Depth (cm)	IRD >250 microns grains (gram)	Depth (cm)	IRD >250 microns grains (gram)	Depth (cm)	IRD >250 microns grains (gram)
822.5	287.41	977.5	274.82	1137.5	1698.47	1292.5	2.55
825	207.37	982.5	157.79	1140	1500.00	1295	2.10
827.5	94.06	987.5	270.93	1142.5	1453.76	1297.5	2.51
830	51.59	990	105.15	1145	2554.40		
832.5	40.09	992.5	50.82	1147.5	992.25		
835	68.11	995	77.71	1150	458.81		
837.5	18.71	997.5	82.88	1152.5	917.65		
840	8.13	1000	58.10	1155	200.93		
842.5	4.22	1002.5	98.22	1157.5	275.18		
845	5.58	1005	56.23	1160	321.29		
847.5	19.94	1007.5	46.33	1162.5	471.39		
850	37.25	1010	46.44	1165	587.16		
852.5	36.88	1012.5	27.00	1167.5	39.05		
855	37.52	1015	82.98	1170	52.16		
857.5	80.54	1017.5	44.32	1172.5	89.03		
860	64.23	1020	44.79	1175	231.23		
862.5	119.74	1022.5	44.23	1177.5	135.18		
865	60.65	1025	89.40	1180	227.05		
867.5	62.37	1027.5	98.43	1182.5	159.06		
870	49.24	1030	66.22	1185	129.40		
872.5	40.25	1032.5	53.67	1187.5	72.42		
875	32.89	1035	58.66	1190	121.98		
877.5	48.52	1037.5	10.04	1192.5	207.63		
880	82.24	1040	18.09	1195	1271.05		
882.5	63.11	1042.5	6.18	1197.5	1428.15		
885	86.36	1045	16.06	1200	931.60		
887.5	29.25	1047.5	3.79	1202.5	240.11		
890	84.99	1050	0.82	1205	275.14		
892.5	75.96	1052.5	6.38	1207.5	179.32		
895	74.29	1055	5.88	1210	228.05		
897.5	42.54	1057.5	0.79	1212.5	135.42		
900	37.72	1060	10.18	1215	25.75		
902.5	29.33	1062.5	0.00	1217.5	36.56		
905	15.26	1065	0.00	1220	34.80		
907.5	13.19	1067.5	10.34	1222.5	41.85		
910	51.09	1070	6.90	1225	111.76		
912.5	61.08	1072.5	1.15	1227.5	49.31		
915	72.20	1075	6.07	1230	83.71		
917.5	46.42	1077.5	3.62	1232.5	95.20		
920	250.69	1080	4.60	1235	80.64		
922.5	495.24	1082.5	7.20	1237.5	43.91		
925	875.19	1085	1.44	1240	28.58		
927.5	631.41	1087.5	4.56	1242.5	10.02		
930	607.06	1090	10.91	1245	13.62		
932.5	1014.96	1092.5	11.76	1247.5	8.45		
935	488.85	1095	19.06	1250	12.96		
937.5	464.47	1097.5	36.49	1252.5	17.52		
940	351.95	1100	58.26	1255	8.13		
942.5	550.26	1102.5	37.99	1257.5	19.59		
945	520.85	1105	83.19	1260	28.07		
947.5	366.74	1107.5	132.28	1262.5	9.21		
950	83.76	1110	270.94	1265	6.18		
952.5	71.95	1112.5	572.67	1267.5	12.40		
955	38.85	1115	1030.94	1270	4.68		
957.5	86.72	1117.5	461.56	1272.5	6.64		
960	153.34	1120	545.57	1275	3.71		
962.5	93.25	1122.5	1471.24	1277.5	4.64		
965	237.42	1125	671.34	1280	5.80		
967.5	183.01	1127.5	1405.03	1282.5	3.41		
970	121.64	1130	2387.63	1285	2.70		
972.5	425.16	1132.5	892.02	1287.5	1.50		
975	309.12	1135	532.85	1290	8.50		

M23414
(composite core)

Age vs. Depth

Table 10

Depth (cm)	Age Cal. (ka)	Depth (cm)	Age Cal. (ka)	Depth (cm)	Age Cal. (ka)	Depth (cm)	Age Cal. (ka)	Depth (cm)	Age Cal. (ka)
0	3.28	62	15.72	124	29.79	186	40.58	248	51.13
1	3.39	63	16.06	125	29.98	187	40.69	249	51.56
2	3.49	64	16.40	126	30.18	188	40.80	250	52.00
3	3.60	65	16.76	127	30.37	189	40.90	251	52.47
4	3.71	66	17.13	128	30.56	190	41.01	252	53.30
5	4.18	67	17.49	129	30.75	191	41.11	253	53.42
6	4.47	68	17.86	130	30.94	192	41.22	254	53.89
7	4.85	69	18.22	131	31.14	193	41.33	255	54.37
8	5.23	70	18.59	132	31.33	194	41.43	256	54.84
9	5.61	71	18.95	133	31.52	195	41.54	257	55.31
10	5.99	72	19.31	134	31.71	196	41.65	258	55.79
11	6.34	73	19.68	135	31.90	197	41.75	259	56.26
12	6.75	74	20.04	136	32.10	198	41.86	260	56.73
13	7.13	75	20.41	137	32.29	199	41.97	261	57.21
14	7.51	76	20.77	138	32.48	200	42.07	262	57.68
15	7.89	77	21.14	139	32.67	201	42.18	263	58.15
16	8.27	78	21.50	140	32.86	202	42.28	264	58.63
17	8.65	79	21.63	141	33.06	203	42.39	265	59.10
18	9.03	80	21.76	142	33.25	204	42.50	266	59.49
19	9.41	81	21.88	143	33.44	205	42.60	267	59.88
20	9.79	82	22.01	144	33.63	206	42.71	268	60.26
21	9.87	83	22.14	145	33.82	207	42.82	269	60.65
22	9.94	84	22.27	146	34.02	208	42.92	270	61.04
23	10.01	85	22.39	147	34.21	209	43.03	271	61.43
24	10.08	86	22.52	148	34.40	210	43.13	272	61.82
25	10.15	87	22.65	149	34.59	211	43.24	273	62.21
26	10.22	88	22.78	150	34.78	212	43.35	274	62.59
27	10.29	89	22.91	151	34.98	213	43.45	275	62.98
28	10.36	90	23.03	152	35.17	214	43.56	276	63.37
29	10.44	91	23.16	153	35.36	215	43.67	277	63.76
30	10.51	92	23.29	154	35.55	216	43.77	278	64.15
31	10.58	93	23.42	155	35.74	217	43.88	279	64.54
32	10.65	94	23.54	156	35.94	218	43.99	280	64.92
33	10.72	95	23.67	157	36.13	219	44.09	281	65.31
34	10.79	96	23.80	158	36.32	220	44.20	282	65.70
35	10.86	97	24.05	159	36.51	221	44.30	283	66.04
36	10.93	98	24.30	160	36.70	222	44.41	284	66.38
37	11.00	99	24.55	161	36.90	223	44.52	285	66.72
38	11.08	100	24.80	162	37.09	224	44.62	286	67.05
39	11.15	101	25.05	163	37.28	225	44.73	287	67.39
40	11.22	102	25.30	164	37.47	226	44.84	288	67.73
41	11.29	103	25.55	165	37.66	227	44.94	289	68.07
42	11.36	104	25.80	166	37.86	228	45.05	290	68.41
43	11.43	105	26.05	167	38.05	229	45.16	291	68.75
44	11.50	106	26.30	168	38.24	230	45.26	292	69.08
45	11.57	107	26.49	169	38.43	231	45.37	293	69.42
46	11.64	108	26.69	170	38.62	232	45.47	294	69.76
47	11.72	109	26.88	171	38.82	233	45.58	295	70.10
48	11.79	110	27.17	172	39.01	234	45.69	296	70.44
49	11.86	111	27.36	173	39.20	235	45.79	297	70.78
50	11.93	112	27.54	174	39.31	236	45.90	298	71.12
51	12.00	113	27.72	175	39.41	237	46.34	299	71.45
52	12.34	114	27.90	176	39.52	238	46.77	300	71.79
53	12.68	115	28.08	177	39.63	239	47.17	301	72.13
54	13.02	116	28.26	178	39.73	240	47.64	302	72.47
55	13.35	117	28.44	179	39.84	241	48.08	303	72.81
56	13.69	118	28.63	180	39.94	242	48.51	304	73.15
57	14.03	119	28.82	181	40.05	243	48.95	305	73.48
58	14.37	120	29.02	182	40.16	244	49.39	306	73.82
59	14.71	121	29.21	183	40.26	245	49.82	307	74.16
60	15.05	122	29.41	184	40.37	246	50.26	308	74.50
61	15.38	123	29.60	185	40.48	247	50.69	309	74.84

M23414
(composite core)

Age vs. Depth

Table 10 continued

Depth (cm)	Age Cal. (ka)	Depth (cm)	Age Cal. (ka)	Depth (cm)	Age Cal. (ka)	Depth (cm)	Age Cal. (ka)	Depth (cm)	Age Cal. (ka)
310	75.18	372	105.88	434	134.33	496	150.07	558	154.50
311	75.52	373	106.29	435	135.00	497	150.14	559	154.57
312	75.85	374	106.71	436	137.00	498	150.21	560	154.64
313	76.19	375	107.12	437	137.40	499	150.29	561	154.71
314	76.53	376	107.53	438	137.80	500	150.36	562	154.79
315	76.86	377	107.94	439	138.20	501	150.43	563	154.86
316	77.19	378	108.35	440	138.60	502	150.50	564	154.93
317	77.52	379	108.76	441	139.00	503	150.57	565	155.00
318	77.88	380	109.18	442	139.22	504	150.64	566	155.33
319	78.22	381	109.59	443	139.44	505	150.71	567	155.67
320	78.56	382	110.00	444	139.67	506	150.79	568	156.00
321	79.00	383	110.47	445	139.89	507	150.86	569	156.33
322	79.50	384	110.93	446	140.11	508	150.93	570	156.67
323	80.00	385	111.40	447	140.33	509	151.00	571	157.00
324	80.50	386	111.87	448	140.56	510	151.07	572	159.00
325	81.00	387	112.33	449	140.78	511	151.14	573	161.00
326	81.50	388	112.80	450	141.00	512	151.21	574	163.00
327	82.00	389	113.27	451	141.50	513	151.29	575	165.00
328	82.40	390	113.73	452	142.00	514	151.36	576	166.00
329	82.80	391	114.20	453	142.25	515	151.43	577	167.00
330	83.20	392	114.67	454	142.50	516	151.50	578	168.00
331	83.60	393	115.13	455	142.75	517	151.57	579	169.00
332	84.00	394	115.60	456	143.00	518	151.64	580	170.50
333	85.40	395	116.07	457	143.25	519	151.71	581	172.00
334	86.80	396	116.53	458	143.50	520	151.79	582	172.50
335	88.20	397	117.00	459	143.75	521	151.86	583	173.00
336	89.60	398	117.36	460	144.00	522	151.93	584	173.50
337	91.00	399	117.71	461	144.25	523	152.00	585	174.00
338	91.60	400	118.07	462	144.50	524	152.07	586	174.50
339	92.20	401	118.43	463	144.75	525	152.14	587	175.00
340	92.80	402	118.79	464	145.00	526	152.22	588	175.50
341	93.40	403	119.14	465	145.25	527	152.29	589	176.00
342	94.00	404	119.50	466	145.50	528	152.36	590	176.50
343	94.60	405	119.86	467	145.75	529	152.43	591	177.00
344	95.20	406	120.21	468	146.00	530	152.50	592	177.50
345	95.80	407	120.57	469	146.23	531	152.57	593	178.00
346	96.40	408	120.93	470	146.46	532	152.64	594	178.50
347	97.00	409	121.29	471	146.69	533	152.71	595	179.00
348	97.30	410	121.64	472	146.92	534	152.79	596	179.14
349	97.60	411	122.00	473	147.15	535	152.86	597	179.29
350	97.90	412	122.37	474	147.38	536	152.93	598	179.43
351	98.20	413	122.74	475	147.62	537	153.00	599	179.57
352	98.50	414	123.11	476	147.85	538	153.07	600	179.71
353	98.80	415	123.47	477	148.08	539	153.14	601	179.86
354	99.10	416	123.84	478	148.31	540	153.21	602	180.00
355	99.40	417	124.21	479	148.54	541	153.29	603	180.14
356	99.70	418	124.58	480	148.77	542	153.36	604	180.29
357	100.00	419	124.95	481	149.00	543	153.43	605	180.43
358	100.38	420	125.32	482	149.07	544	153.50	606	180.57
359	100.75	421	125.68	483	149.14	545	153.57	607	180.71
360	101.13	422	126.05	484	149.21	546	153.64	608	180.86
361	101.50	423	126.42	485	149.29	547	153.71	609	181.00
362	101.88	424	126.79	486	149.36	548	153.79	610	181.14
363	102.25	425	127.16	487	149.43	549	153.86	611	181.29
364	102.63	426	127.53	488	149.50	550	153.93	612	181.43
365	103.00	427	127.89	489	149.57	551	154.00	613	181.57
366	103.41	428	128.26	490	149.64	552	154.07	614	181.71
367	103.82	429	128.63	491	149.71	553	154.14	615	181.86
368	104.24	430	129.00	492	149.79	554	154.21	616	182.00
369	104.65	431	131.00	493	149.86	555	154.29	617	182.14
370	105.06	432	133.00	494	149.93	556	154.36	618	182.29
371	105.47	433	133.67	495	150.00	557	154.43	619	182.43

M23414
(composite core)

Age vs. Depth

Table 10 continued

Depth (cm)	Age Cal. (ka)	Depth (cm)	Age Cal. (ka)	Depth (cm)	Age Cal. (ka)	Depth (cm)	Age Cal. (ka)	Depth (cm)	Age Cal. (ka)
620	182.57	682	215.70	744	237.48	806	252.07	868	269.20
621	182.71	683	216.05	745	237.87	807	252.17	869	269.40
622	182.86	684	216.40	746	238.26	808	252.28	870	269.60
623	183.00	685	216.75	747	238.65	809	252.38	871	269.80
624	183.14	686	217.10	748	239.04	810	252.48	872	270.00
625	183.29	687	217.45	749	239.43	811	252.59	873	270.20
626	183.43	688	217.80	750	239.83	812	252.69	874	270.40
627	183.57	689	218.15	751	240.22	813	252.79	875	270.60
628	183.71	690	218.50	752	240.61	814	252.90	876	270.80
629	183.86	691	218.85	753	241.00	815	253.00	877	271.00
630	184.00	692	219.20	754	241.15	816	253.40	878	271.20
631	185.25	693	219.55	755	241.30	817	253.80	879	271.40
632	186.50	694	219.90	756	241.45	818	254.20	880	271.60
633	187.75	695	220.25	757	241.60	819	254.60	881	271.80
634	189.00	696	220.60	758	241.75	820	255.00	882	272.00
635	189.33	697	220.95	759	241.90	821	255.80	883	272.07
636	189.67	698	221.30	760	242.05	822	256.60	884	272.14
637	190.00	699	221.65	761	242.20	823	257.40	885	272.21
638	190.33	700	222.00	762	242.35	824	258.20	886	272.28
639	190.67	701	222.38	763	242.50	825	259.00	887	272.34
640	191.00	702	222.75	764	242.65	826	259.33	888	272.41
641	191.33	703	223.13	765	242.80	827	259.67	889	272.48
642	191.67	704	223.50	766	242.95	828	260.00	890	272.55
643	192.00	705	223.88	767	243.10	829	269.33	891	272.62
644	192.33	706	224.25	768	243.25	830	260.67	892	272.69
645	192.67	707	224.63	769	243.40	831	261.00	893	272.76
646	193.00	708	225.00	770	243.55	832	261.21	894	272.83
647	193.53	709	225.32	771	243.70	833	261.43	895	272.90
648	194.07	710	225.64	772	243.85	834	261.64	896	272.97
649	194.60	711	225.95	773	244.00	835	261.86	897	273.03
650	195.13	712	226.27	774	244.57	836	262.07	898	273.10
651	195.67	713	226.59	775	245.14	837	262.29	899	273.17
652	196.20	714	226.91	776	245.71	838	262.50	900	273.24
653	196.73	715	227.23	777	246.29	839	262.71	901	273.31
654	197.27	716	227.55	778	246.86	840	262.93	902	273.38
655	197.80	717	227.86	779	247.43	841	263.14	903	273.45
656	198.33	718	228.18	780	248.00	842	263.36	904	273.52
657	198.87	719	228.50	781	248.33	843	263.57	905	273.59
658	199.40	720	228.82	782	248.67	844	263.79	906	273.66
659	199.93	721	229.14	783	249.00	845	264.00	907	273.72
660	200.47	722	229.45	784	249.33	846	264.24	908	273.79
661	201.00	723	229.77	785	249.67	847	264.47	909	273.86
662	203.50	724	230.01	786	250.00	848	264.71	910	273.93
663	206.00	725	230.34	787	250.10	849	264.94	911	274.00
664	206.71	726	230.68	788	250.21	850	265.18	912	274.50
665	207.43	727	231.05	789	250.31	851	265.41	913	275.00
666	208.14	728	231.36	790	250.41	852	265.65	914	275.50
667	208.86	729	231.68	791	250.52	853	265.88	915	276.00
668	209.57	730	232.00	792	250.62	854	266.12	916	276.50
669	210.29	731	232.39	793	250.72	855	266.35	917	277.00
670	211.00	732	232.78	794	250.83	856	266.59	918	278.00
671	211.40	733	233.17	795	250.93	857	266.82	919	278.75
672	211.80	734	233.57	796	251.03	858	267.06	920	279.50
673	212.20	735	233.96	797	251.14	859	267.29	921	280.25
674	212.60	736	234.35	798	251.24	860	267.53	922	281.00
675	213.00	737	234.74	799	251.34	861	267.76	923	282.00
676	213.40	738	235.13	800	251.45	862	268.00	924	283.25
677	213.80	739	235.52	801	251.55	863	268.20	925	284.50
678	214.20	740	235.91	802	251.66	864	268.40	926	285.75
679	214.60	741	236.30	803	251.76	865	268.60	927	287.00
680	215.00	742	236.70	804	251.86	866	268.80	928	287.71
681	215.35	743	237.09	805	251.97	867	269.00	929	288.41

Age vs. Depth

Table 10 continued

Depth (cm)	Age Cal. (ka)	Depth (cm)	Age Cal. (ka)	Depth (cm)	Age Cal. (ka)	Depth (cm)	Age Cal. (ka)	Depth (cm)	Age Cal. (ka)
930	289.12	992	331.00	1054	352.71	1116	379.25	1178	417.24
931	289.82	993	331.44	1055	353.00	1117	380.88	1179	417.60
932	290.53	994	331.89	1056	353.43	1118	382.50	1180	417.96
933	291.24	995	332.33	1057	353.86	1119	384.13	1181	418.32
934	291.94	996	332.78	1058	354.29	1120	385.75	1182	418.68
935	292.65	997	333.22	1059	354.71	1121	387.38	1183	419.04
936	293.35	998	333.67	1060	355.14	1122	389.00	1184	419.40
937	294.06	999	334.11	1061	355.57	1123	389.73	1185	419.76
938	294.76	1000	334.56	1062	356.00	1124	390.45	1186	420.12
939	295.47	1001	335.00	1063	356.43	1125	391.18	1187	420.48
940	296.18	1002	335.44	1064	356.86	1126	391.91	1188	420.84
941	296.88	1003	335.89	1065	357.29	1127	392.64	1189	421.20
942	297.59	1004	336.33	1066	357.71	1128	393.36	1190	421.56
943	298.29	1005	336.78	1067	358.14	1129	394.09	1191	421.92
944	299.00	1006	337.22	1068	358.57	1130	394.82	1192	422.28
945	303.00	1007	337.67	1069	359.00	1131	395.55	1193	422.64
946	303.64	1008	338.11	1070	359.33	1132	396.27	1194	423.00
947	304.27	1009	338.56	1071	359.67	1133	397.00	1195	424.20
948	304.91	1010	339.00	1072	360.00	1134	397.73	1196	425.40
949	305.55	1011	339.60	1073	360.33	1135	398.45	1197	426.60
950	306.18	1012	340.20	1074	360.67	1136	399.18	1198	427.80
951	306.82	1013	340.80	1075	361.00	1137	399.91	1199	429.00
952	307.45	1014	341.40	1076	361.33	1138	400.64	1200	430.20
953	308.09	1015	342.00	1077	361.67	1139	401.36	1201	431.40
954	308.73	1016	342.26	1078	362.00	1140	402.09	1202	432.60
955	309.36	1017	342.52	1079	362.33	1141	402.82	1203	433.80
956	310.00	1018	342.78	1080	362.67	1142	403.55	1204	435.00
957	310.39	1019	343.04	1081	363.00	1143	404.27	1205	435.44
958	310.78	1020	343.30	1082	363.33	1144	405.00	1206	435.89
959	311.17	1021	343.57	1083	363.67	1145	405.36	1207	436.33
960	311.57	1022	343.83	1084	364.00	1146	405.72	1208	436.78
961	311.96	1023	344.09	1085	364.33	1147	406.08	1209	437.22
962	312.35	1024	344.35	1086	364.67	1148	406.44	1210	437.67
963	312.74	1025	344.61	1087	365.00	1149	406.80	1211	438.11
964	313.13	1026	344.87	1088	365.33	1150	407.16	1212	438.56
965	313.52	1027	345.13	1089	365.67	1151	407.52	1213	439.00
966	313.91	1028	345.39	1090	366.00	1152	407.88	1214	439.44
967	314.30	1029	345.65	1091	366.33	1153	408.24	1215	439.89
968	314.70	1030	345.91	1092	366.67	1154	408.60	1216	440.33
969	315.09	1031	346.17	1093	367.00	1155	408.96	1217	440.78
970	315.48	1032	346.43	1094	367.33	1156	409.32	1218	441.22
971	315.87	1033	346.70	1095	367.67	1157	409.68	1219	441.67
972	316.26	1034	346.96	1096	368.00	1158	410.04	1220	442.11
973	316.65	1035	347.22	1097	368.44	1159	410.40	1221	442.56
974	317.04	1036	347.48	1098	368.89	1160	410.76	1222	443.00
975	317.43	1037	347.74	1099	369.33	1161	411.12	1223	443.44
976	317.83	1038	348.00	1100	369.78	1162	411.48	1224	443.89
977	318.22	1039	348.29	1101	370.22	1163	411.84	1225	444.33
978	318.61	1040	348.59	1102	370.67	1164	412.20	1226	444.78
979	319.00	1041	348.88	1103	371.11	1165	412.56	1227	445.22
980	319.92	1042	349.18	1104	371.56	1166	412.92	1228	445.67
981	320.85	1043	349.47	1105	372.00	1167	413.28	1229	446.11
982	321.77	1044	349.76	1106	372.44	1168	413.64	1230	446.56
983	322.69	1045	350.06	1107	372.89	1169	414.00	1231	447.00
984	323.62	1046	350.35	1108	373.33	1170	414.36	1232	447.44
985	324.54	1047	350.65	1109	373.78	1171	414.72	1233	447.89
986	325.46	1048	350.94	1110	374.22	1172	415.08	1234	448.33
987	326.38	1049	351.29	1111	374.67	1173	415.44	1235	448.78
988	327.31	1050	351.53	1112	375.11	1174	415.80	1236	449.22
989	328.23	1051	351.82	1113	375.56	1175	416.16	1237	449.67
990	329.15	1052	352.12	1114	376.00	1176	416.52	1238	450.11
991	330.08	1053	352.41	1115	377.63	1177	416.88	1239	450.56

M23414
(composite core)

Table 10 continued

Depth (cm)	Age Cal. (ka)	Depth (cm)	Age Cal. (ka)	Depth (cm)	Age Cal. (ka)
1240	451.00	1302	478.28	1364	486.69
1241	451.26	1303	478.41	1365	486.83
1242	451.53	1304	478.55	1366	486.97
1243	451.79	1305	478.69	1367	487.10
1244	452.05	1306	478.83	1368	487.24
1245	452.32	1307	478.97	1369	487.38
1246	452.59	1308	479.10	1370	487.52
1247	452.85	1309	479.24	1371	487.66
1248	453.12	1310	479.38	1372	487.79
1249	453.38	1311	479.52	1373	487.93
1250	453.65	1312	479.66	1374	488.07
1251	453.91	1313	479.79	1375	488.21
1252	454.18	1314	479.93	1376	488.34
1253	454.44	1315	480.07	1377	488.48
1254	454.71	1316	480.21	1378	488.62
1255	454.97	1317	480.34	1379	488.76
1256	455.24	1318	480.48		
1257	455.50	1319	480.62		
1258	455.76	1320	480.76		
1259	456.03	1321	480.90		
1260	456.29	1322	481.03		
1261	456.56	1323	481.17		
1262	456.82	1324	481.31		
1263	457.09	1325	481.45		
1264	457.35	1326	481.59		
1265	457.62	1327	481.72		
1266	457.98	1329	482.00		
1267	458.15	1329	482.00		
1268	458.41	1330	482.14		
1269	458.68	1331	482.28		
1270	458.94	1332	482.41		
1271	459.21	1333	482.55		
1272	459.47	1334	482.69		
1273	459.74	1335	482.76		
1274	460.00	1336	482.83		
1275	461.25	1337	482.97		
1276	462.50	1338	483.10		
1277	463.75	1339	483.24		
1278	465.00	1340	483.38		
1279	466.25	1341	483.52		
1280	467.50	1342	483.66		
1281	468.75	1343	483.79		
1282	470.00	1344	483.93		
1283	470.44	1345	484.07		
1284	470.89	1346	484.21		
1285	471.33	1347	484.34		
1286	471.78	1348	484.48		
1287	472.22	1349	484.62		
1288	472.67	1350	484.76		
1289	473.11	1351	484.90		
1290	473.56	1352	485.03		
1291	474.00	1353	485.17		
1292	474.44	1354	485.31		
1293	474.89	1355	485.45		
1294	475.33	1356	485.59		
1295	475.78	1357	485.72		
1296	476.22	1358	485.86		
1297	476.67	1359	486.00		
1298	477.11	1360	486.14		
1299	477.56	1361	486.28		
1300	478.00	1362	486.41		
1301	478.14	1363	486.55		

M23414
(splice record)

Sedimentation rates and linear accumulation rates

Tab. 11

Depth (cm)	Age (ka)	LSR (cm/ky)	AR (g/cm²/ky)	Depth (cm)	Age (ka)	LSR (cm/ky)	AR (g/cm²/ky)	Depth (cm)	Age (ka)	LSR (cm/ky)	AR (g/cm²/ky)
4	3.71	2.09	2.96	65	16.76	2.75	4.13	133	31.52	5.21	8.14
5	4.18	3.55	5.01	66	17.13	2.75	4.12	134	31.71	5.21	8.14
6	4.47	2.63	3.72	67	17.49	2.75	4.11	135	31.90	5.21	8.11
7	4.85	2.63	3.72	68	17.86	2.75	4.10	136	32.10	5.21	8.08
8	5.23	2.63	3.72	69	18.22	2.75	4.11	137	32.29	5.21	8.08
9	5.61	2.63	3.72	70	18.59	2.75	4.10	138	32.48	5.21	8.10
10	5.99	2.86	4.04	71	18.95	2.75	4.10	139	32.67	5.21	8.25
11	6.34	2.44	3.45	72	19.31	2.75	4.12	140	32.86	5.21	8.40
12	6.75	2.63	3.72	73	19.68	2.75	4.13	141	33.06	5.21	8.27
13	7.13	2.63	3.72	74	20.04	2.75	4.13	142	33.25	5.21	8.12
14	7.51	2.63	3.72	75	20.41	2.75	4.06	143	33.44	5.21	8.08
15	7.89	2.63	3.72	76	20.77	2.75	4.00	144	33.63	5.21	8.10
16	8.27	2.63	3.72	77	21.14	2.75	4.05	145	33.82	5.21	8.13
17	8.65	2.63	3.72	78	21.50	7.83	11.71	146	34.02	5.21	8.19
18	9.03	2.63	3.72	79	21.63	7.83	11.72	147	34.21	5.21	8.24
19	9.41	2.63	3.72	80	21.76	7.83	11.73	148	34.40	5.21	8.16
20	9.79	12.48	17.64	81	21.88	7.83	11.79	149	34.59	5.21	8.12
21	9.87	14.06	19.87	82	22.01	7.83	11.85	150	34.78	5.21	8.07
22	9.94	14.06	19.87	83	22.14	7.83	11.95	151	34.98	5.21	8.10
23	10.01	14.06	20.17	84	22.27	7.83	12.05	152	35.17	5.21	8.12
24	10.08	14.06	20.48	85	22.39	7.83	12.63	153	35.36	5.21	8.14
25	10.15	14.06	20.41	86	22.52	7.83	13.10	154	35.55	5.21	8.16
26	10.22	14.06	20.33	87	22.65	7.83	12.82	155	35.74	5.21	8.20
27	10.29	14.06	20.54	88	22.78	7.83	12.19	156	35.94	5.21	8.23
28	10.36	14.06	20.75	89	22.91	7.83	11.64	157	36.13	5.21	8.27
29	10.44	14.06	21.27	90	23.03	7.83	11.62	158	36.32	5.21	8.30
30	10.51	14.06	21.78	91	23.16	7.83	11.60	159	36.51	5.21	8.27
31	10.58	14.06	21.23	92	23.29	7.83	11.58	160	36.70	5.21	8.23
32	10.65	14.06	21.00	93	23.42	7.83	11.56	161	36.90	5.21	8.19
33	10.72	14.06	20.78	94	23.54	7.83	11.53	162	37.09	5.21	8.16
34	10.79	14.06	20.64	95	23.67	7.83	11.50	163	37.28	5.21	8.10
35	10.86	14.06	20.59	96	23.80	4.00	5.86	164	37.47	5.21	8.01
36	10.93	14.06	20.56	97	24.05	4.00	5.84	165	37.66	5.21	7.90
37	11.00	14.06	20.74	98	24.30	4.00	5.82	166	37.86	5.21	7.91
38	11.08	14.06	20.92	99	24.55	4.00	5.82	167	38.05	5.21	7.97
39	11.15	14.06	20.86	100	24.80	4.00	5.84	168	38.24	5.21	8.09
40	11.22	14.06	20.84	101	25.05	4.00	5.86	169	38.43	5.21	8.18
41	11.29	14.06	20.82	102	25.30	4.00	5.87	170	38.62	5.21	8.26
42	11.36	14.06	20.80	103	25.55	4.00	5.89	171	38.82	5.21	8.32
43	11.43	14.06	20.79	104	25.80	4.00	5.90	172	39.01	5.21	8.30
44	11.50	14.06	20.77	105	26.05	4.00	5.91	173	39.20	9.40	14.89
45	11.57	14.06	20.75	106	26.30	5.15	7.57	174	39.31	9.40	14.86
46	11.64	14.06	20.74	107	26.49	5.15	7.53	175	39.41	9.40	14.83
47	11.72	14.06	20.88	108	26.69	5.15	7.54	176	39.52	9.40	14.81
48	11.79	14.06	21.03	109	26.88	5.15	7.57	177	39.63	9.40	14.79
49	11.86	14.06	21.18	117	28.44	5.15	8.04	178	39.73	9.40	14.80
50	11.93	14.06	21.32	118	28.63	5.15	7.87	179	39.84	9.40	14.80
51	12.00	2.95	4.48	119	28.82	5.15	7.81	180	39.94	9.40	14.74
52	12.34	2.95	4.48	120	29.02	5.15	7.84	181	40.05	9.40	14.70
53	12.68	2.95	4.48	121	29.21	5.15	7.87	182	40.16	9.40	15.41
54	13.02	2.95	4.48	122	29.41	5.15	7.84	183	40.26	9.40	16.11
55	13.35	2.95	4.47	123	29.60	5.21	7.90	184	40.37	9.40	15.35
56	13.69	2.95	4.46	124	29.79	5.21	7.91	185	40.48	9.40	14.58
57	14.03	2.95	4.45	125	29.98	5.21	7.93	186	40.58	9.40	14.63
58	14.37	2.95	4.44	126	30.18	5.21	7.98	187	40.69	9.40	14.69
59	14.71	2.95	4.48	127	30.37	5.21	8.03	188	40.80	9.40	14.65
60	15.05	2.95	4.52	128	30.56	5.21	8.02	189	40.90	9.40	14.62
61	15.38	2.95	4.56	129	30.75	5.21	8.02	190	41.01	9.40	14.69
62	15.72	2.95	4.59	130	30.94	5.21	8.02	191	41.11	9.40	14.76
63	16.06	2.95	4.56	131	31.14	5.21	8.03	192	41.22	9.40	14.82
64	16.40	2.75	4.20	132	31.33	5.21	8.08	193	41.33	9.40	14.87

Tab. 11 cont.

Depth (cm)	Age (ka)	LSR (cm/ky)	AR (g/cm²/ky)	Depth (cm)	Age (ka)	LSR (cm/ky)	AR (g/cm²/ky)	Depth (cm)	Age (ka)	LSR (cm/ky)	AR (g/cm²/ky)
194	41.43	9.40	14.85	257	55.31	2.11	3.14	321	79.00	2.00	3.00
195	41.54	9.40	14.82	258	55.79	2.11	3.20	322	79.50	2.00	2.97
196	41.65	9.40	14.79	259	56.26	2.11	3.20	323	80.00	2.00	3.00
197	41.75	9.40	14.75	260	56.73	2.11	3.50	324	80.50	2.00	2.99
198	41.86	9.40	14.66	261	57.21	2.11	3.33	325	81.00	2.00	3.00
199	41.97	9.40	14.58	262	57.68	2.11	3.43	326	81.50	2.00	3.01
200	42.07	9.40	14.62	263	58.15	2.11	3.51	327	82.00	2.50	3.77
201	42.18	9.40	14.66	264	58.63	2.11	3.66	328	82.40	2.50	3.78
202	42.28	9.40	14.57	265	59.10	2.58	4.68	329	82.80	2.50	3.76
203	42.39	9.40	14.49	266	59.49	2.58	3.88	330	83.20	2.50	3.74
204	42.50	9.40	14.56	267	59.88	2.58	5.09	331	83.60	2.50	3.73
205	42.60	9.40	14.59	268	60.26	2.58	5.28	332	84.00	0.71	1.09
206	42.71	9.40	14.63	269	60.65	2.58	4.64	333	85.40	0.71	1.12
207	42.82	9.40	14.52	270	61.04	2.58	3.78	334	86.80	0.71	1.13
208	42.92	9.40	14.67	271	61.43	2.58	3.79	335	88.20	0.71	1.13
209	43.03	9.40	14.86	272	61.82	2.58	3.79	336	89.60	0.71	1.11
210	43.13	9.40	15.04	273	62.21	2.58	3.80	337	91.00	1.67	2.62
211	43.24	9.40	15.23	274	62.59	2.58	3.83	338	91.60	1.67	2.62
212	43.35	9.40	15.13	275	62.98	2.58	3.92	339	92.20	1.67	2.62
213	43.45	9.40	15.04	276	63.37	2.58	4.02	340	92.80	1.67	2.61
214	43.56	9.40	14.88	277	63.76	2.58	4.04	341	93.40	1.67	2.60
215	43.67	9.40	14.80	278	64.15	2.58	4.05	342	94.00	1.67	2.59
216	43.77	9.40	14.75	279	64.54	2.58	4.07	343	94.60	1.67	2.55
217	43.88	9.40	14.72	280	64.92	2.58	4.11	344	95.20	1.67	2.51
218	43.99	9.40	14.72	281	65.31	2.58	4.15	345	95.80	1.67	2.52
219	44.09	9.40	14.72	282	65.70	2.95	4.81	346	96.40	1.67	2.57
220	44.20	9.40	14.65	283	66.04	2.95	4.86	347	97.00	3.33	5.22
221	44.30	9.40	14.57	284	66.38	2.95	4.88	348	97.30	3.33	5.22
222	44.41	9.40	14.49	285	66.72	2.95	4.89	349	97.60	3.33	5.22
223	44.52	9.40	14.46	286	67.05	2.95	4.89	350	97.90	3.33	5.22
224	44.62	9.40	14.43	287	67.39	2.95	4.86	351	98.20	3.33	5.24
226	44.84	9.40	14.39	288	67.73	2.95	4.83	352	98.50	3.33	5.25
227	44.94	9.40	14.39	289	68.07	2.95	4.77	353	98.80	3.33	5.27
228	45.05	9.40	14.38	290	68.41	2.95	4.70	354	99.10	3.33	5.21
229	45.16	9.40	14.36	291	68.75	2.95	4.63	355	99.40	3.33	5.15
230	45.26	9.40	14.32	292	69.08	2.95	4.58	356	99.70	3.33	5.08
231	45.37	9.40	14.29	293	69.42	2.95	4.56	357	100.00	2.67	4.05
232	45.47	9.40	14.27	294	69.76	2.95	4.53	358	100.38	2.67	4.07
233	45.58	9.40	14.27	295	70.10	2.95	4.51	359	100.75	2.67	4.09
234	45.69	9.40	14.31	296	70.44	2.95	4.50	360	101.13	2.67	4.11
235	45.79	9.40	14.43	297	70.78	2.95	4.50	361	101.50	2.67	4.11
236	45.90	2.30	3.55	298	71.12	2.95	4.49	362	101.88	2.67	4.10
237	46.34	2.30	3.55	299	71.45	2.95	4.49	363	102.25	2.67	4.10
238	46.77	2.30	3.57	300	71.79	2.95	4.47	364	102.63	2.67	4.11
240	47.64	2.30	3.59	301	72.13	2.95	4.46	365	103.00	2.43	3.74
241	48.08	2.30	3.56	302	72.47	2.95	4.46	366	103.41	2.43	3.75
242	48.51	2.30	3.54	303	72.81	2.95	4.45	367	103.82	2.43	3.76
243	48.95	2.30	3.54	304	73.15	2.95	4.45	368	104.24	2.43	3.77
244	49.39	2.30	3.54	305	73.48	2.95	4.45	369	104.65	2.43	3.78
245	49.82	2.30	3.54	306	73.82	2.95	4.44	370	105.06	2.43	3.78
246	50.26	2.30	3.54	307	74.16	2.95	4.44	371	105.47	2.43	3.79
247	50.69	2.30	3.54	308	74.50	2.95	4.43	372	105.88	2.43	3.80
248	51.13	2.30	3.53	309	74.84	2.95	4.43	373	106.29	2.43	3.80
249	51.56	2.30	3.52	310	75.18	2.95	4.45	374	106.71	2.43	3.80
250	52.00	2.11	3.24	311	75.52	2.95	4.46	375	107.12	2.43	3.82
251	52.47	2.11	3.24	312	75.85	2.95	4.47	376	107.53	2.43	3.81
252	52.95	2.11	3.23	313	76.19	2.95	4.48	377	107.94	2.43	3.81
253	53.42	2.11	3.22	314	76.53	2.95	4.48	378	108.35	2.43	3.81
254	53.89	2.11	3.20	318	77.88	2.95	4.50	379	108.76	2.43	3.81
255	54.37	2.11	3.18	319	78.22	2.95	4.49	380	109.18	2.43	3.79
256	54.84	2.11	3.16	320	78.56	2.28	3.45	381	109.59	2.43	3.76

Tab. 11 cont.

Depth (cm)	Age (ka)	LSR (cm/ky)	AR (g/cm²/ky)	Depth (cm)	Age (ka)	LSR (cm/ky)	AR (g/cm²/ky)	Depth (cm)	Age (ka)	LSR (cm/ky)	AR (g/cm²/ky)
382	110.00	2.14	3.31	443	139.44	4.50	7.07	505	150.71	14.00	22.12
383	110.47	2.14	3.30	444	139.67	4.50	7.07	506	150.79	14.00	21.95
384	110.93	2.14	3.30	445	139.89	4.50	7.06	507	150.86	14.00	21.75
385	111.40	2.14	3.29	446	140.11	4.50	7.05	508	150.93	14.00	21.52
386	111.87	2.14	3.27	447	140.33	4.50	7.05	509	151.00	14.00	21.33
387	112.33	2.14	3.25	448	140.56	4.50	7.05	510	151.07	14.00	21.29
388	112.80	2.14	3.26	449	140.78	4.50	7.06	511	151.14	14.00	21.37
389	113.27	2.14	3.27	451	141.50	2.00	3.13	512	151.21	14.00	21.59
390	113.73	2.14	3.27	452	142.00	4.00	6.24	513	151.29	14.00	21.62
391	114.20	2.14	3.26	453	142.25	4.00	6.35	514	151.36	14.00	21.53
392	114.67	2.14	3.24	454	142.50	4.00	6.43	515	151.43	14.00	21.43
393	115.13	2.14	3.24	455	142.75	4.00	6.43	516	151.50	14.00	21.34
394	115.60	2.14	3.24	456	143.00	4.00	6.43	517	151.57	14.00	21.24
395	116.07	2.14	3.24	457	143.25	4.00	6.41	518	151.64	14.00	21.14
396	116.53	2.14	3.24	458	143.50	4.00	6.38	519	151.71	14.00	21.25
397	117.00	2.80	4.21	459	143.75	4.00	6.40	520	151.79	14.00	21.33
398	117.36	2.80	4.20	460	144.00	4.00	6.47	521	151.86	14.00	21.30
399	117.71	2.80	4.20	461	144.25	4.00	6.40	522	151.93	14.00	21.21
400	118.07	2.80	4.20	462	144.50	4.00	6.35	523	152.00	14.00	21.14
401	118.43	2.80	4.20	463	144.75	4.00	6.37	524	152.07	14.00	20.94
402	118.79	2.80	4.20	464	145.00	4.00	6.35	527	152.29	14.00	20.87
403	119.14	2.80	4.20	465	145.25	4.00	6.31	528	152.36	14.00	21.04
404	119.50	2.80	4.19	466	145.50	4.00	6.25	529	152.43	14.00	21.20
405	119.86	2.80	4.20	467	145.75	4.00	6.26	530	152.50	14.00	21.39
406	120.21	2.80	4.21	468	146.00	4.33	6.92	531	152.57	14.00	21.59
407	120.57	2.80	4.24	469	146.23	4.33	6.87	532	152.64	14.00	21.67
408	120.93	2.80	4.25	470	146.46	4.33	6.81	533	152.71	14.00	21.67
409	121.29	2.80	4.23	471	146.69	4.33	6.84	534	152.79	14.00	21.67
410	121.64	2.80	4.25	472	146.92	4.33	6.86	535	152.86	14.00	21.71
411	122.00	2.71	4.14	473	147.15	4.33	6.87	536	152.93	14.00	21.80
412	122.37	2.71	4.18	474	147.38	4.33	6.85	537	153.00	14.00	21.92
413	122.74	2.71	4.19	475	147.62	4.33	6.85	538	153.07	14.00	21.87
414	123.11	2.71	4.17	476	147.85	4.33	6.87	539	153.14	14.00	21.92
415	123.47	2.71	4.16	477	148.08	4.33	6.85	540	153.21	14.00	22.20
416	123.84	2.71	4.15	478	148.31	4.33	6.80	541	153.29	14.00	22.36
417	124.21	2.71	4.14	479	148.54	4.33	6.78	542	153.36	14.00	22.40
418	124.58	2.71	4.16	480	148.77	4.33	6.78	543	153.43	14.00	22.32
419	124.95	2.71	4.16	481	149.00	14.00	21.98	544	153.50	14.00	22.15
420	125.32	2.71	4.18	482	149.07	14.00	22.02	545	153.57	14.00	21.90
421	125.68	2.71	4.21	483	149.14	14.00	22.04	546	153.64	14.00	21.61
422	126.05	2.71	4.23	484	149.21	14.00	22.00	547	153.71	14.00	21.52
423	126.42	2.71	4.23	485	149.29	14.00	21.92	548	153.79	14.00	21.46
424	126.79	2.71	4.25	486	149.36	14.00	21.85	549	153.86	14.00	21.62
425	127.16	2.71	4.29	487	149.43	14.00	21.48	550	153.93	14.00	21.81
426	127.53	2.71	4.25	488	149.50	14.00	21.19	551	154.00	14.00	22.09
427	127.89	2.71	4.23	489	149.57	14.00	21.32	552	154.07	14.00	22.37
428	128.26	2.71	4.22	490	149.64	14.00	21.39	553	154.14	14.00	22.65
429	128.63	2.71	4.23	491	149.71	14.00	21.21	554	154.21	14.00	22.60
430	129.00	0.50	0.78	492	149.79	14.00	21.15	555	154.29	14.00	22.37
431	131.00	0.50	0.77	493	149.86	14.00	21.26	556	154.36	14.00	22.20
432	133.00	1.50	2.32	494	149.93	14.00	21.28	557	154.43	14.00	22.06
433	133.67	1.50	2.38	495	150.00	14.00	21.18	558	154.50	14.00	22.00
434	134.33	1.50	2.38	496	150.07	14.00	21.31	559	154.57	14.00	21.95
435	135.00	0.50	0.81	497	150.14	14.00	21.66	560	154.64	14.00	21.90
436	137.00	2.50	4.07	498	150.21	14.00	21.90	561	154.71	14.00	21.86
437	137.40	2.50	4.04	499	150.29	14.00	22.07	562	154.79	14.00	21.89
438	137.80	2.50	4.00	500	150.36	14.00	22.17	563	154.86	14.00	21.74
439	138.20	2.50	3.97	501	150.43	14.00	22.24	564	154.93	14.00	21.36
440	138.60	2.50	3.94	502	150.50	14.00	22.06	565	155.00	3.00	4.54
441	139.00	4.50	7.06	503	150.57	14.00	21.87	566	155.33	3.00	4.57
442	139.22	4.50	7.06	504	150.64	14.00	22.02	567	155.67	3.00	4.59

Tab. 11 cont.

Depth (cm)	Age (ka)	LSR (cm/ky)	AR (g/cm²/ky)	Depth (cm)	Age (ka)	LSR (cm/ky)	AR (g/cm²/ky)	Depth (cm)	Age (ka)	LSR (cm/ky)	AR (g/cm²/ky)
568	156.00	3.00	4.64	632	186.50	0.80	1.26	693	219.55	2.86	4.42
569	156.33	3.00	4.68	633	187.75	0.80	1.23	694	219.90	2.86	4.42
570	156.67	3.00	4.70	634	189.00	3.00	4.62	695	220.25	2.86	4.42
571	157.00	0.50	0.79	635	189.33	3.00	4.62	696	220.60	2.86	4.43
572	159.00	0.50	0.79	636	189.67	3.00	4.63	697	220.95	2.86	4.44
573	161.00	0.50	0.79	637	190.00	3.00	4.63	698	221.30	2.86	4.45
574	163.00	0.50	0.79	638	190.33	3.00	4.63	699	221.65	2.86	4.48
575	165.00	1.00	1.57	639	190.67	3.00	4.63	700	222.00	2.67	4.22
576	166.00	1.00	1.58	640	191.00	3.00	4.65	701	222.38	2.67	4.24
577	167.00	1.00	1.58	641	191.33	3.00	4.66	702	222.75	2.67	4.26
578	168.00	1.00	1.59	642	191.67	3.00	4.68	703	223.13	2.67	4.25
579	169.00	0.67	1.05	643	192.00	3.00	4.66	704	223.50	2.67	4.24
580	170.50	0.67	1.04	644	192.33	3.00	4.63	705	223.88	2.67	4.22
581	172.00	2.00	3.13	645	192.67	3.00	4.60	706	224.25	2.67	4.20
582	172.50	2.00	3.16	646	193.00	1.88	2.85	707	224.63	2.67	4.21
583	173.00	2.00	3.30	647	193.53	1.87	2.86	708	225.00	3.14	4.98
584	173.50	2.00	3.45	648	194.07	1.88	2.88	709	225.32	3.14	4.98
585	174.00	2.00	3.39	649	194.60	1.88	2.91	710	225.64	3.14	4.98
586	174.50	2.00	3.25	650	195.13	1.87	2.93	711	225.95	3.14	4.97
587	175.00	2.00	3.21	651	195.67	1.88	2.92	712	226.27	3.14	4.97
588	175.50	2.00	3.22	652	196.20	1.88	2.93	713	226.59	3.14	4.96
589	176.00	2.00	3.22	653	196.73	1.87	2.95	714	226.91	3.14	4.96
590	176.50	2.00	3.21	654	197.27	1.88	2.95	715	227.23	3.14	4.95
591	177.00	2.00	3.21	655	197.80	1.88	2.95	716	227.55	3.14	4.95
592	177.50	2.00	3.24	656	198.33	1.87	2.95	717	227.86	3.14	4.94
593	178.00	2.00	3.26	657	198.87	1.88	2.95	718	228.18	3.14	4.95
595	179.00	7.00	11.35	658	199.40	1.88	2.95	719	228.50	3.14	4.95
596	179.14	7.00	11.31	659	199.93	1.87	2.95	720	228.82	3.14	4.93
597	179.29	7.00	11.27	660	200.47	1.88	2.96	721	229.14	3.14	4.83
598	179.43	7.00	11.24	661	201.00	0.40	0.63	722	229.45	3.14	4.81
599	179.57	7.00	11.23	662	203.50	0.40	0.63	723	229.77	3.14	4.79
600	179.71	7.00	11.23	663	206.00	1.40	2.16	727	231.05	3.14	4.72
601	179.86	7.00	11.18	664	206.71	1.40	2.15	728	231.36	3.14	4.70
602	180.00	7.00	11.11	665	207.43	1.40	2.15	729	231.68	3.14	4.69
603	180.14	7.00	11.05	666	208.14	1.40	2.14	730	232.00	2.56	3.84
604	180.29	7.00	11.06	667	208.86	1.40	2.13	731	232.39	2.56	3.99
605	180.43	7.00	11.06	668	209.57	1.40	2.12	732	232.78	2.56	4.02
606	180.57	7.00	11.07	669	210.29	1.40	2.11	733	233.17	2.56	4.02
607	180.71	7.00	11.08	670	211.00	2.50	3.75	734	233.57	2.56	4.02
608	180.86	7.00	11.09	671	211.40	2.50	3.76	735	233.96	2.56	4.01
609	181.00	7.00	11.09	672	211.80	2.50	3.78	736	234.35	2.56	4.00
610	181.14	7.00	11.11	673	212.20	2.50	3.77	737	234.74	2.56	3.98
611	181.29	7.00	11.08	674	212.60	2.50	3.76	738	235.13	2.56	3.95
612	181.43	7.00	11.06	675	213.00	2.50	3.76	739	235.52	2.56	3.95
613	181.57	7.00	11.05	676	213.40	2.50	3.77	740	235.91	2.56	3.98
614	181.71	7.00	11.05	677	213.80	2.50	3.78	741	236.30	2.56	4.01
615	181.86	7.00	11.05	678	214.20	2.50	3.78	742	236.70	2.56	3.98
616	182.00	7.00	11.08	679	214.60	2.50	3.79	743	237.09	2.56	3.95
617	182.14	7.00	11.10	680	215.00	2.86	4.34	744	237.48	2.56	3.94
618	182.29	7.00	11.09	681	215.35	2.86	4.35	745	237.87	2.56	3.93
619	182.43	7.00	11.08	682	215.70	2.86	4.36	746	238.26	2.56	3.92
620	182.57	7.00	11.09	683	216.05	2.86	4.36	747	238.65	2.56	3.92
621	182.71	7.00	11.14	684	216.40	2.86	4.37	748	239.04	2.56	3.92
622	182.86	7.00	11.18	685	216.75	2.86	4.37	749	239.43	2.56	3.93
623	183.00	7.00	11.14	686	217.10	2.86	4.38	750	239.83	2.56	3.93
624	183.14	7.00	11.09	687	217.45	2.86	4.39	751	240.22	2.56	3.93
627	183.57	7.00	11.13	688	217.80	2.86	4.39	752	240.61	2.56	3.92
628	183.71	7.00	11.19	689	218.15	2.86	4.40	753	241.00	6.67	10.14
629	183.86	7.00	11.33	690	218.50	2.86	4.41	754	241.15	6.67	10.05
630	184.00	0.80	1.32	691	218.85	2.86	4.41	755	241.30	6.67	10.00
631	185.25	0.80	1.29	692	219.20	2.86	4.41	756	241.45	6.67	9.95

Tab. 11 cont.

Depth (cm)	Age (ka)	LSR (cm/ky)	AR (g/cm²/ky)	Depth (cm)	Age (ka)	LSR (cm/ky)	AR (g/cm²/ky)	Depth (cm)	Age (ka)	LSR (cm/ky)	AR (g/cm²/ky)
757	241.60	6.67	9.90	818	254.20	2.50	4.08	887	272.34	14.50	21.94
758	241.75	6.67	9.86	819	254.60	2.50	4.11	888	272.41	14.50	21.92
759	241.90	6.67	9.86	820	255.00	1.25	2.05	889	272.48	14.50	21.91
760	242.05	6.67	9.97	821	255.80	1.25	2.04	890	272.55	14.50	21.88
761	242.20	6.67	10.09	822	256.60	1.25	2.04	891	272.62	14.50	21.86
762	242.35	6.67	10.26	823	257.40	1.25	2.04	892	272.69	14.50	21.81
763	242.50	6.67	10.43	824	258.20	1.25	2.04	893	272.76	14.50	21.73
764	242.65	6.67	10.38	825	259.00	3.00	4.90	894	272.83	14.50	21.68
765	242.80	6.67	10.36	827	259.67	3.00	4.93	895	272.90	14.50	21.50
766	242.95	6.67	10.36	828	260.00	3.00	4.90	896	272.97	14.50	21.39
767	243.10	6.67	10.45	830	260.67	3.00	4.83	897	273.03	14.50	21.30
768	243.25	6.67	10.52	831	261.00	4.67	7.53	898	273.10	14.50	21.30
769	243.40	6.67	10.55	832	261.21	4.67	7.54	899	273.17	14.50	21.36
770	243.55	6.67	10.60	833	261.43	4.67	7.55	900	273.24	14.50	21.67
771	243.70	6.67	10.68	834	261.64	4.67	7.58	901	273.31	14.50	22.01
772	243.85	6.67	10.69	835	261.86	4.67	7.62	902	273.38	14.50	22.25
773	244.00	1.75	2.81	836	262.07	4.67	7.63	903	273.45	14.50	22.44
774	244.57	1.75	2.81	837	262.29	4.67	7.63	904	273.52	14.50	22.44
775	245.14	1.75	2.82	838	262.50	4.67	7.63	905	273.59	14.50	22.45
776	245.71	1.75	2.83	839	262.71	4.67	7.64	906	273.66	14.50	22.76
777	246.29	1.75	2.82	840	262.93	4.67	7.66	907	273.72	14.50	23.12
778	246.86	1.75	2.81	841	263.14	4.67	7.68	908	273.79	14.50	23.40
779	247.43	1.75	2.81	842	263.36	4.67	7.68	909	273.86	14.50	23.68
780	248.00	3.00	4.89	843	263.57	4.67	7.67	910	273.93	14.50	23.99
781	248.33	3.00	4.95	844	263.79	4.67	7.67	911	274.00	2.00	3.35
782	248.67	3.00	4.88	845	264.00	4.25	7.00	912	274.50	2.00	3.36
783	249.00	3.00	4.89	846	264.24	4.25	7.01	913	275.00	2.00	3.36
784	249.33	3.00	4.87	847	264.47	4.25	7.06	914	275.50	2.00	3.33
785	249.67	3.00	4.93	848	264.71	4.25	7.14	915	276.00	2.00	3.30
786	250.00	9.67	16.71	849	264.94	4.25	7.24	916	276.50	2.00	3.28
787	250.10	9.67	16.67	850	265.18	4.25	7.30	917	277.00	1.00	1.63
788	250.21	9.67	16.64	851	265.41	4.25	7.34	918	278.00	1.33	2.16
789	250.31	9.67	16.58	852	265.65	4.25	7.39	919	278.75	1.33	2.15
790	250.41	9.67	16.53	853	265.88	4.25	7.61	920	279.50	1.33	2.13
791	250.52	9.67	16.48	854	266.12	4.25	7.77	921	280.25	1.33	2.12
792	250.62	9.67	16.44	855	266.35	4.25	7.99	922	281.00	1.00	1.57
793	250.72	9.67	16.39	856	266.59	4.25	8.22	923	282.00	0.80	1.24
794	250.83	9.67	16.39	857	266.82	4.25	8.41	924	283.25	0.80	1.24
795	250.93	9.67	16.67	864	268.40	5.00	8.56	925	284.50	0.80	1.24
796	251.03	9.67	16.78	865	268.60	5.00	8.26	926	285.75	0.80	1.23
797	251.14	9.67	16.96	866	268.80	5.00	8.15	927	287.00	1.42	2.18
798	251.24	9.67	17.19	867	269.00	5.00	8.01	927	287.00	1.42	2.18
799	251.34	9.67	17.42	868	269.20	5.00	7.97	928	287.71	1.42	2.18
800	251.45	9.67	17.37	869	269.40	5.00	7.94	929	288.41	1.42	2.19
801	251.55	9.67	17.12	870	269.60	5.00	7.92	930	289.12	1.42	2.20
802	251.66	9.67	16.79	871	269.80	5.00	7.84	931	289.82	1.42	2.21
803	251.76	9.67	16.45	872	270.00	5.00	7.77	932	290.53	1.42	2.21
804	251.86	9.67	16.20	873	270.20	5.00	7.71	933	291.24	1.42	2.21
805	251.97	9.67	15.88	874	270.40	5.00	7.71	934	291.94	1.42	2.22
806	252.07	9.67	15.69	875	270.60	5.00	7.70	935	292.65	1.42	2.23
807	252.17	9.67	15.53	876	270.80	5.00	7.68	936	293.35	1.42	2.23
808	252.28	9.67	15.38	877	271.00	5.00	7.65	937	294.06	1.42	2.23
809	252.38	9.67	15.26	878	271.20	5.00	7.62	938	294.76	1.42	2.23
810	252.48	9.67	15.27	879	271.40	5.00	7.59	939	295.47	1.42	2.24
811	252.59	9.67	15.28	880	271.60	5.00	7.59	940	296.18	1.42	2.25
812	252.69	9.67	15.29	881	271.80	5.00	7.57	941	296.88	1.42	2.26
813	252.79	9.67	15.33	882	272.00	14.50	21.94	942	297.59	1.42	2.26
814	252.90	9.67	15.37	883	272.07	14.50	21.95	943	298.29	1.42	2.26
815	253.00	2.50	3.99	884	272.14	14.50	21.97	944	299.00	0.25	0.40
816	253.40	2.50	4.00	885	272.21	14.50	21.98	945	303.00	1.57	2.50
817	253.80	2.50	4.04	886	272.28	14.50	21.96	946	303.64	1.57	2.50

Tab. 11 cont.

Depth (cm)	Age (ka)	LSR (cm/ky)	AR (g/cm²/ky)	Depth (cm)	Age (ka)	LSR (cm/ky)	AR (g/cm²/ky)	Depth (cm)	Age (ka)	LSR (cm/ky)	AR (g/cm²/ky)
947	304.27	1.57	2.50	1008	338.11	2.25	3.69	1070	359.33	3.00	4.93
948	304.91	1.57	2.49	1009	338.56	2.25	3.73	1071	359.67	3.00	4.88
949	305.55	1.57	2.48	1010	339.00	1.67	2.73	1072	360.00	3.00	4.90
950	306.18	1.57	2.49	1011	339.60	1.67	2.70	1073	360.33	3.00	4.92
951	306.82	1.57	2.50	1012	340.20	1.67	2.68	1074	360.67	3.00	4.92
952	307.45	1.57	2.51	1013	340.80	1.67	2.66	1075	361.00	3.00	4.92
953	308.09	1.57	2.52	1014	341.40	1.67	2.61	1076	361.33	3.00	4.91
954	308.73	1.57	2.51	1015	342.00	3.83	5.90	1077	361.67	3.00	4.90
955	309.36	1.57	2.50	1016	342.26	3.83	5.77	1078	362.00	3.00	4.91
956	310.00	2.56	4.07	1017	342.52	3.83	5.65	1079	362.33	3.00	4.92
957	310.39	2.56	4.07	1018	342.78	3.83	5.63	1080	362.67	3.00	4.90
958	310.78	2.56	4.08	1019	343.04	3.83	5.62	1081	363.00	3.00	4.87
959	311.17	2.56	4.08	1020	343.30	3.83	5.64	1082	363.33	3.00	4.86
960	311.57	2.56	4.10	1021	343.57	3.83	5.72	1083	363.67	3.00	4.84
961	311.96	2.56	4.12	1022	343.83	3.83	6.10	1084	364.00	3.00	4.85
962	312.35	2.56	4.13	1023	344.09	3.83	6.43	1085	364.33	3.00	4.86
963	312.74	2.56	4.13	1024	344.35	3.83	6.15	1086	364.67	3.00	4.88
964	313.13	2.56	4.13	1025	344.61	3.83	5.83	1087	365.00	3.00	4.91
965	313.52	2.56	4.13	1026	344.87	3.83	5.84	1088	365.33	3.00	4.89
966	313.91	2.56	4.12	1027	345.13	3.83	5.91	1089	365.67	3.00	4.87
967	314.30	2.56	4.10	1028	345.39	3.83	5.97	1090	366.00	3.00	4.84
968	314.70	2.56	4.07	1029	345.65	3.83	6.02	1091	366.33	3.00	4.82
969	315.09	2.56	4.05	1030	345.91	3.83	6.03	1092	366.67	3.00	4.83
970	315.48	2.56	4.06	1031	346.17	3.83	6.05	1093	367.00	3.00	4.84
971	315.87	2.56	4.08	1032	346.43	3.83	6.16	1094	367.33	3.00	4.81
972	316.26	2.56	4.10	1033	346.70	3.83	6.26	1095	367.67	3.00	4.77
973	316.65	2.56	4.12	1034	346.96	3.83	6.28	1096	368.00	2.25	3.55
974	317.04	2.56	4.09	1035	347.22	3.83	6.28	1097	368.44	2.25	3.52
975	317.43	2.56	4.06	1036	347.48	3.83	6.28	1098	368.89	2.25	3.58
976	317.83	2.56	4.08	1037	347.74	3.83	6.29	1099	369.33	2.25	3.64
977	318.22	2.56	4.11	1038	348.00	3.40	5.56	1100	369.78	2.25	3.65
978	318.61	2.56	4.15	1039	348.29	3.40	5.53	1101	370.22	2.25	3.65
979	319.00	1.08	1.77	1040	348.59	3.40	5.52	1102	370.67	2.25	3.64
980	319.92	1.08	1.75	1041	348.88	3.40	5.51	1103	371.11	2.25	3.62
981	320.85	1.08	1.72	1042	349.18	3.40	5.50	1104	371.56	2.25	3.57
982	321.77	1.08	1.70	1043	349.47	3.40	5.49	1105	372.00	2.25	3.53
983	322.69	1.08	1.68	1044	349.76	3.40	5.51	1106	372.44	2.25	3.53
984	323.62	1.08	1.68	1045	350.06	3.40	5.53	1107	372.89	2.25	3.55
985	324.54	1.08	1.69	1046	350.35	3.40	5.53	1108	373.33	2.25	3.56
986	325.46	1.08	1.69	1047	350.65	3.40	5.54	1109	373.78	2.25	3.56
987	326.38	1.08	1.69	1048	350.94	3.40	5.52	1110	374.22	2.25	3.57
988	327.31	1.08	1.70	1050	351.53	3.40	5.56	1111	374.67	2.25	3.57
989	328.23	1.08	1.70	1051	351.82	3.40	5.61	1112	375.11	2.25	3.57
990	329.15	1.08	1.70	1052	352.12	3.40	5.63	1113	375.56	2.25	3.57
991	330.08	1.08	1.69	1053	352.41	3.40	5.65	1114	376.00	0.62	0.97
992	331.00	2.25	3.49	1054	352.71	3.40	5.73	1115	377.63	0.62	0.97
993	331.44	2.25	3.49	1055	353.00	2.33	3.97	1116	379.25	0.62	0.97
994	331.89	2.25	3.50	1056	353.43	2.33	3.92	1117	380.88	0.62	0.97
995	332.33	2.25	3.51	1057	353.86	2.33	3.84	1118	382.50	0.62	0.97
996	332.78	2.25	3.49	1058	354.29	2.33	3.76	1119	384.13	0.62	0.96
997	333.22	2.25	3.48	1059	354.71	2.33	3.68	1120	385.75	0.62	0.96
998	333.67	2.25	3.50	1060	355.14	2.33	3.67	1121	387.38	0.62	0.96
999	334.11	2.25	3.53	1061	355.57	2.33	3.67	1122	389.00	1.38	2.14
1000	334.56	2.25	3.54	1062	356.00	2.33	3.68	1123	389.73	1.37	2.14
1001	335.00	2.25	3.55	1063	356.43	2.33	3.70	1124	390.45	1.38	2.14
1002	335.44	2.25	3.63	1064	356.86	2.33	3.73	1125	391.18	1.38	2.14
1003	335.89	2.25	3.70	1065	357.29	2.33	3.77	1126	391.91	1.38	2.14
1004	336.33	2.25	3.67	1066	357.71	2.33	3.84	1127	392.64	1.37	2.14
1005	336.78	2.25	3.62	1067	358.14	2.33	3.90	1128	393.36	1.38	2.14
1006	337.22	2.25	3.63	1068	358.57	2.33	3.89	1129	394.09	1.38	2.15
1007	337.67	2.25	3.65	1069	359.00	3.00	4.98	1130	394.82	1.38	2.14

Tab. 11 cont.

Depth (cm)	Age (ka)	LSR (cm/ky)	AR (g/cm²/ky)	Depth (cm)	Age (ka)	LSR (cm/ky)	AR (g/cm²/ky)	Depth (cm)	Age (ka)	LSR (cm/ky)	AR (g/cm²/ky)
1131	395.55	1.37	2.13	1192	422.28	2.78	4.38	1254	454.71	3.78	6.64
1132	396.27	1.38	2.14	1193	422.64	2.78	4.33	1255	454.97	3.78	6.63
1133	397.00	1.38	2.15	1194	423.00	0.83	1.28	1256	455.24	3.78	6.66
1134	397.73	1.37	2.16	1195	424.20	0.83	1.27	1257	455.50	3.78	6.69
1135	398.45	1.38	2.16	1196	425.40	0.83	1.29	1258	455.76	3.78	6.68
1136	399.18	1.38	2.16	1197	426.60	0.83	1.30	1259	456.03	3.78	6.65
1137	399.91	1.38	2.17	1198	427.80	0.83	1.31	1260	456.29	3.78	6.56
1138	400.64	1.37	2.17	1199	429.00	0.83	1.32	1261	456.56	3.78	6.49
1139	401.36	1.38	2.18	1200	430.20	0.83	1.32	1262	456.82	3.78	6.58
1140	402.09	1.38	2.18	1201	431.40	0.83	1.32	1263	457.09	3.78	6.67
1141	402.82	1.38	2.19	1202	432.60	0.83	1.33	1264	457.35	3.78	6.53
1142	403.55	1.37	2.19	1203	433.80	0.83	1.33	1265	457.62	3.78	6.37
1143	404.27	1.38	2.19	1204	435.00	2.25	3.51	1266	457.88	3.78	6.26
1144	405.00	2.78	4.41	1205	435.44	2.25	3.43	1267	458.15	3.78	6.18
1145	405.36	2.78	4.40	1206	435.89	2.25	3.45	1268	458.41	3.78	6.21
1146	405.72	2.78	4.40	1207	436.33	2.25	3.48	1269	458.68	3.78	6.25
1147	406.08	2.78	4.41	1208	436.78	2.25	3.47	1270	458.94	3.78	6.17
1148	406.44	2.78	4.41	1209	437.22	2.25	3.46	1271	459.21	3.78	6.07
1149	406.80	2.78	4.41	1210	437.67	2.25	3.46	1272	459.47	3.78	5.97
1150	407.16	2.78	4.42	1211	438.11	2.25	3.49	1273	459.74	3.78	5.89
1151	407.52	2.78	4.42	1212	438.56	2.25	3.62	1274	460.00	0.80	1.24
1152	407.88	2.78	4.44	1213	439.00	2.25	3.72	1275	461.25	0.80	1.23
1153	408.24	2.78	4.45	1214	439.44	2.25	3.58	1276	462.50	0.80	1.24
1154	408.60	2.78	4.44	1215	439.89	2.25	3.42	1277	463.75	0.80	1.24
1155	408.96	2.78	4.43	1216	440.33	2.25	3.40	1278	465.00	0.80	1.24
1156	409.32	2.78	4.41	1217	440.78	2.25	3.41	1279	466.25	0.80	1.23
1157	409.68	2.78	4.40	1218	441.22	2.25	3.43	1280	467.50	0.80	1.23
1158	410.04	2.78	4.40	1219	441.67	2.25	3.45	1281	468.75	0.80	1.23
1159	410.40	2.78	4.42	1220	442.11	2.25	3.46	1282	470.00	2.25	3.55
1160	410.76	2.78	4.56	1221	442.56	2.25	3.47	1283	470.44	2.25	3.64
1161	411.12	2.78	4.68	1222	443.00	2.25	3.47	1284	470.89	2.25	3.61
1162	411.48	2.78	4.55	1223	443.44	2.25	3.45	1285	471.33	2.25	3.57
1163	411.84	2.78	4.39	1224	443.89	2.25	3.44	1286	471.78	2.25	3.61
1164	412.20	2.78	4.37	1225	444.33	2.25	3.42	1287	472.22	2.25	3.65
1165	412.56	2.78	4.38	1226	444.78	2.25	3.41	1288	472.67	2.25	3.65
1166	412.92	2.78	4.38	1227	445.22	2.25	3.41	1289	473.11	2.25	3.65
1167	413.28	2.78	4.39	1228	445.67	2.25	3.42	1290	473.56	2.25	3.65
1168	413.64	2.78	4.39	1229	446.11	2.25	3.43	1291	474.00	2.25	3.64
1169	414.00	2.78	4.40	1230	446.56	2.25	3.44	1292	474.44	2.25	3.61
1170	414.36	2.78	4.40	1231	447.00	2.25	3.44	1293	474.89	2.25	3.58
1171	414.72	2.78	4.40	1232	447.44	2.25	3.45	1294	475.33	2.25	3.62
1172	415.08	2.78	4.39	1233	447.89	2.25	3.45	1295	475.78	2.25	3.67
1173	415.44	2.78	4.39	1234	448.33	2.25	3.45	1296	476.22	2.25	3.69
1174	415.80	2.78	4.38	1235	448.78	2.25	3.44	1297	476.67	2.25	3.71
1175	416.16	2.78	4.37	1236	449.22	2.25	3.44	1298	477.11	2.25	3.71
1176	416.52	2.78	4.39	1237	449.67	2.25	3.46	1299	477.56	2.25	3.71
1177	416.88	2.78	4.41	1238	450.11	2.25	3.57	1300	478.00	7.25	11.96
1178	417.24	2.78	4.42	1239	450.56	2.25	3.68	1301	478.14	7.25	11.96
1179	417.60	2.78	4.43	1240	451.00	3.78	6.14	1302	478.28	7.25	12.02
1180	417.96	2.78	4.45	1241	451.26	3.78	6.05	1303	478.41	7.25	12.05
1181	418.32	2.78	4.46	1242	451.53	3.78	5.95	1304	478.55	7.25	11.86
1182	418.68	2.78	4.45	1243	451.79	3.78	5.85	1305	478.69	7.25	11.67
1183	419.04	2.78	4.44	1245	452.32	3.78	5.79	1306	478.83	7.25	11.74
1184	419.40	2.78	4.41	1246	452.59	3.78	5.86	1307	478.97	7.25	11.84
1185	419.76	2.78	4.39	1247	452.85	3.78	5.95	1308	479.10	7.25	11.84
1186	420.12	2.78	4.40	1248	453.12	3.78	6.08	1309	479.24	7.25	11.83
1187	420.48	2.78	4.41	1249	453.38	3.78	6.23	1310	479.38	7.25	11.85
1188	420.84	2.78	4.39	1250	453.65	3.78	6.36	1311	479.52	7.25	11.87
1189	421.20	2.78	4.37	1251	453.91	3.78	6.48	1312	479.66	7.25	11.83
1190	421.56	2.78	4.39	1252	454.18	3.78	6.58	1313	479.79	7.25	11.80
1191	421.92	2.78	4.41	1253	454.44	3.78	6.65	1314	479.93	7.25	11.89

Tab. 11 cont.

Depth (cm)	Age (ka)	LSR (cm/ky)	AR (g/cm²/ky)	Depth (cm)	Age (ka)	LSR (cm/ky)	AR (g/cm²/ky)
1315	480.07	7.25	11.99	1377	488.48	7.25	11.54
1316	480.21	7.25	12.02	1378	488.62	7.25	11.56
1317	480.34	7.25	12.03	1379	488.76	2.82	4.51
1318	480.48	7.25	12.02				
1319	480.62	7.25	12.00				
1320	480.76	7.25	11.89				
1321	480.90	7.25	11.79				
1322	481.03	7.25	11.81				
1323	481.17	7.25	11.85				
1324	481.31	7.25	11.80				
1325	481.45	7.25	11.74				
1326	481.59	7.25	11.69				
1327	481.72	7.25	11.66				
1328	481.86	7.25	11.66				
1329	482.00	7.25	11.67				
1330	482.14	7.25	11.67				
1331	482.28	7.25	11.68				
1332	482.41	7.25	11.67				
1333	482.55	7.25	11.67				
1334	482.69	14.50	23.42				
1336	482.83	7.25	11.64				
1337	482.97	7.25	11.54				
1338	483.10	7.25	11.52				
1339	483.24	7.25	11.53				
1340	483.38	7.25	11.60				
1341	483.52	7.25	11.66				
1342	483.66	7.25	11.66				
1343	483.79	7.25	11.66				
1344	483.93	7.25	11.73				
1345	484.07	7.25	11.81				
1346	484.21	7.25	11.80				
1347	484.34	7.25	11.78				
1348	484.48	7.25	11.76				
1349	484.62	7.25	11.75				
1350	484.76	7.25	11.76				
1351	484.90	7.25	11.77				
1352	485.03	7.25	11.79				
1353	485.17	7.25	11.80				
1354	485.31	7.25	11.76				
1355	485.45	7.25	11.72				
1356	485.59	7.25	11.71				
1357	485.72	7.25	11.69				
1358	485.86	7.25	11.64				
1359	486.00	7.25	11.59				
1360	486.14	7.25	11.59				
1361	486.28	7.25	11.59				
1362	486.41	7.25	11.54				
1363	486.55	7.25	11.48				
1364	486.69	7.25	11.47				
1365	486.83	7.25	11.46				
1366	486.97	7.25	11.46				
1367	487.10	7.25	11.46				
1368	487.24	7.25	11.48				
1369	487.38	7.25	11.49				
1370	487.52	7.25	11.47				
1371	487.66	7.25	11.46				
1372	487.79	7.25	11.51				
1373	487.93	7.25	11.56				
1374	488.07	7.25	11.51				
1375	488.21	7.25	11.46				
1376	488.34	7.25	11.49				

M23352
(composite core)

Age vs. Depth

Table 12

Depth (cm)	Age Cal. (ka)	Depth (cm)	Age Cal. (ka)	Depth (cm)	Age Cal. (ka)	Depth (cm)	Age Cal. (ka)	Depth (cm)	Age Cal. (ka)
0	4.06	62	27.78	124	49.72	186	85.15	248	128.93
1	4.15	63	28.05	125	50.17	187	85.71	249	129.41
2	4.24	64	28.32	126	50.62	188	86.26	250	129.91
3	4.34	65	28.59	127	51.08	189	86.82	251	130.44
4	4.45	66	28.87	128	51.53	190	87.38	252	130.97
5	4.56	67	29.14	129	51.98	191	87.94	253	131.51
6	4.68	68	29.41	130	52.43	192	88.49	254	132.05
7	4.81	69	29.69	131	52.89	193	89.05	255	132.58
8	4.95	70	29.96	132	53.34	194	89.61	256	133.12
9	5.09	71	30.23	133	53.79	195	90.16	257	133.66
10	5.28	72	30.51	134	54.24	196	90.72	258	134.19
11	5.47	73	30.78	135	54.70	197	91.62	259	134.73
12	5.67	74	31.05	136	55.15	198	92.85	260	135.25
13	5.86	75	31.33	137	55.60	199	94.08	261	135.75
14	6.05	76	31.60	138	56.05	200	95.31	262	136.25
15	6.24	77	31.87	139	56.51	201	96.54	263	136.75
16	6.43	78	32.14	140	56.96	202	97.77	264	137.25
17	6.62	79	32.42	141	57.41	203	99.00	265	137.75
18	6.81	80	32.69	142	57.86	204	100.23	266	138.25
19	7.09	81	32.96	143	58.32	205	101.47	267	138.75
20	7.38	82	33.31	144	58.77	206	102.70	268	139.25
21	7.67	83	33.74	145	59.22	207	103.93	269	139.75
22	7.96	84	34.17	146	59.75	208	105.16	270	140.25
23	8.30	85	34.60	147	60.35	209	106.39	271	140.75
24	8.70	86	35.03	148	61.04	210	107.62	272	141.25
25	9.15	87	35.46	149	61.79	211	108.85	273	141.75
26	9.65	88	35.89	150	62.55	212	110.08	274	142.32
27	10.15	89	36.31	151	63.31	213	111.00	275	142.96
28	10.72	90	36.74	152	64.06	214	111.60	276	143.61
29	11.36	91	37.17	153	64.82	215	112.20	277	144.25
30	11.99	92	37.60	154	65.58	216	112.80	278	144.89
31	12.60	93	38.03	155	66.33	217	113.40	279	145.53
32	13.17	94	38.46	156	67.09	218	114.00	280	146.18
33	13.77	95	38.89	157	67.85	219	114.60	281	146.82
34	14.40	96	39.27	158	68.60	220	115.20	282	147.46
35	15.03	97	39.61	159	69.36	221	115.76	283	148.10
36	15.67	98	39.95	160	70.12	222	116.27	284	148.75
37	16.32	99	40.30	161	70.87	223	116.77	285	149.39
38	16.88	100	40.64	162	71.63	224	117.26	286	150.03
39	17.36	101	40.98	163	72.39	225	117.74	287	150.67
40	17.87	102	41.32	164	73.14	226	118.23	288	151.32
41	18.37	103	41.66	165	73.84	227	118.72	289	151.96
42	18.88	104	42.00	166	74.41	228	119.20	290	152.83
43	19.39	105	42.34	167	74.93	229	119.69	291	154.14
44	19.89	106	42.69	168	75.44	230	120.18	292	155.69
45	20.40	107	43.03	169	75.96	231	120.66	293	157.23
46	20.91	108	43.37	170	76.47	232	121.15	294	158.78
47	21.41	109	43.71	171	76.99	233	121.63	295	160.32
48	21.92	110	44.05	172	77.50	234	122.12	296	161.87
49	22.43	111	44.39	173	78.01	235	122.61	297	163.41
50	22.93	112	44.73	174	78.53	236	123.09	298	164.96
51	23.46	113	45.08	175	79.04	237	123.58	299	166.50
52	23.99	114	45.42	176	79.58	238	124.07	300	168.05
53	24.53	115	45.76	177	80.14	239	124.55	301	169.59
54	25.13	116	46.15	178	80.69	240	125.04	302	171.14
55	25.78	117	46.58	179	81.25	241	125.52	303	172.68
56	26.19	118	47.01	180	81.81	242	126.01	304	174.23
57	26.41	119	47.46	181	82.36	243	126.50	305	175.23
58	26.68	120	47.91	182	82.92	244	126.98	306	175.68
59	26.96	121	48.36	183	83.48	245	127.47	307	176.14
60	27.23	122	48.81	184	84.04	246	127.96	308	176.60
61	27.50	123	49.27	185	84.59	247	128.44	309	177.05

M23352
(composite core)

Age vs. Depth

Table 12 **contin.**

Depth (cm)	Age Cal. (ka)	Depth (cm)	Age Cal. (ka)	Depth (cm)	Age Cal. (ka)	Depth (cm)	Age Cal. (ka)	Depth (cm)	Age Cal. (ka)
310	177.51	372	218.25	434	259.00	496	317.50	558	337.58
311	177.97	373	219.75	435	260.20	497	318.50	559	337.75
312	178.42	374	221.25	436	261.40	498	319.22	560	337.92
313	178.88	375	222.75	437	262.60	499	319.66	561	338.08
314	179.33	376	224.25	438	263.80	500	320.10	562	338.25
315	179.79	377	225.23	439	265.00	501	320.54	563	338.41
316	180.25	378	225.70	440	266.20	502	320.98	564	338.58
317	180.70	379	226.17	441	267.40	503	321.42	565	338.75
318	181.16	380	226.64	442	268.73	504	321.86	566	338.92
319	181.62	381	227.11	443	270.19	505	322.30	567	339.08
320	182.07	382	227.58	444	271.65	506	322.74	568	339.25
321	182.53	383	228.05	445	273.12	507	323.18	569	339.42
322	182.98	384	228.52	446	274.58	508	323.62	570	339.59
323	183.44	385	228.98	447	276.04	509	324.06	571	339.75
324	183.90	386	229.45	448	277.50	510	324.50	572	339.92
325	184.35	387	229.92	449	278.96	511	326.04	573	340.08
326	184.81	388	230.39	450	280.42	512	328.68	574	340.25
327	185.27	389	230.86	451	281.88	513	330.08	575	340.41
328	185.72	390	231.33	452	283.35	514	330.25	576	340.58
329	186.18	391	231.80	453	284.81	515	330.42	577	340.75
330	186.63	392	232.27	454	286.27	516	330.59	578	340.92
331	187.09	393	232.73	455	287.40	517	330.75	579	341.09
332	187.55	394	233.20	456	288.20	518	330.92	580	341.25
333	188.00	395	233.67	457	289.00	519	331.08	581	341.42
334	188.46	396	234.14	458	289.80	520	331.25	582	341.59
335	188.92	397	234.61	459	290.60	521	331.42	583	341.75
336	189.37	398	235.08	460	291.40	522	331.59	584	341.92
337	189.77	399	235.55	461	292.20	523	331.75	585	343.08
338	190.12	400	236.02	462	293.00	524	331.92	586	345.25
339	190.47	401	236.48	463	293.80	525	332.08	587	347.42
340	190.82	402	236.95	464	294.60	526	332.25	588	349.59
341	191.17	403	237.42	465	295.40	527	332.41	589	351.75
342	191.51	404	237.89	466	296.20	528	332.58	590	353.92
343	191.86	405	238.36	467	297.00	529	332.75	591	356.08
344	192.21	406	238.83	468	297.80	530	332.91	592	358.25
345	192.56	407	239.30	469	298.60	531	333.08	593	360.41
346	192.91	408	239.77	470	299.15	532	333.25	594	362.58
347	193.26	409	240.15	471	299.46	533	333.42	595	364.75
348	193.60	410	240.46	472	299.77	534	333.59	596	366.92
349	194.33	411	240.77	473	300.08	535	333.75	597	368.20
350	195.44	412	241.08	474	300.38	536	333.92	598	368.60
351	196.50	413	241.38	475	300.69	537	334.09	599	369.00
352	197.50	414	241.69	476	301.00	538	334.25	600	369.40
353	198.50	415	242.00	477	301.31	539	334.42	601	369.80
354	199.50	416	242.31	478	301.62	540	334.59	602	370.20
355	200.50	417	242.62	479	301.92	541	334.75	603	370.60
356	201.50	418	242.92	480	302.23	542	334.92	604	371.00
357	202.50	419	243.23	481	302.54	543	335.09	605	371.40
358	203.50	420	243.54	482	302.85	544	335.25	606	371.80
359	204.50	421	243.85	483	303.58	545	335.42	607	372.20
360	205.50	422	244.60	484	304.75	546	335.59	608	372.60
361	206.50	423	245.80	485	305.92	547	335.75	609	373.00
362	207.50	424	247.00	486	307.08	548	335.92	610	373.40
363	208.50	425	248.20	487	308.25	549	336.09	611	373.80
364	209.50	426	249.40	488	309.42	550	336.25	612	374.20
365	210.50	427	250.60	489	310.50	551	336.42	613	374.60
366	211.50	428	251.80	490	311.50	552	336.59	614	375.00
367	212.50	429	253.00	491	312.50	553	336.75	615	375.40
368	213.50	430	254.20	492	313.50	554	336.92	616	375.80
369	214.50	431	255.40	493	314.50	555	337.09	617	376.33
370	215.50	432	256.60	494	315.50	556	337.25	618	376.99
371	216.75	433	257.80	495	316.50	557	337.42	619	377.65

M23352
(composite core)

Age vs. Depth

Table 12 contin.

Depth (cm)	Age Cal. (ka)	Depth (cm)	Age Cal. (ka)	Depth (cm)	Age Cal. (ka)
620	378.31	682	410.08	744	424.72
621	378.97	683	410.32	745	424.96
622	379.62	684	410.55	746	425.20
623	380.28	685	410.79	747	425.43
624	380.94	686	411.02	748	425.67
625	381.60	687	411.26	749	425.91
626	382.26	688	411.49	750	426.14
627	382.92	689	411.73	751	426.38
628	383.58	690	411.97	752	426.62
629	384.24	691	412.21	753	426.85
630	384.90	692	412.44	754	427.09
631	385.56	693	412.68	755	427.33
632	386.22	694	412.92	756	427.56
633	386.88	695	413.15	757	427.80
634	387.54	696	413.39	758	428.04
635	388.19	697	413.62	759	428.27
636	388.85	698	413.86	760	428.51
637	389.51	699	414.10	761	428.74
638	390.17	700	414.33	762	428.97
639	390.83	701	414.57	763	429.21
640	391.49	702	414.80	764	429.45
641	392.15	703	415.04	765	429.68
642	392.81	704	415.28	766	429.92
643	393.47	705	415.51	767	430.16
644	394.12	706	415.75	768	430.39
645	394.78	707	415.98	769	430.63
646	395.44	708	416.22	770	430.86
647	396.10	709	416.45	771	431.10
648	396.76	710	416.69	772	431.34
649	397.42	711	416.93	773	431.58
650	398.08	712	417.16	774	431.81
651	398.74	713	417.41	775	432.05
652	399.40	714	417.67	776	432.29
653	400.06	715	417.93	777	432.52
654	400.72	716	418.18	778	432.76
655	401.38	717	418.44	779	433.00
656	402.04	718	418.70	780	433.23
657	402.69	719	418.89	781	433.47
658	403.35	720	419.08	782	433.70
659	404.01	721	419.29	783	433.94
660	404.67	722	419.53	784	434.17
661	405.12	723	419.76	785	434.41
662	405.36	724	420.00	786	434.65
663	405.59	725	420.24	787	434.88
664	405.83	726	420.47	788	435.12
665	406.07	727	420.71	789	435.36
666	406.30	728	420.95	790	435.59
667	406.54	729	421.18	791	435.83
668	406.77	730	421.42	792	436.07
669	407.01	731	421.66	793	436.30
670	407.24	732	421.89	794	436.54
671	407.48	733	422.13		
672	407.71	734	422.37		
673	407.95	735	422.60		
674	408.19	736	422.84		
675	408.43	737	423.07		
676	408.66	738	423.31		
677	408.90	739	423.54		
678	409.13	740	423.78		
679	409.37	741	424.01		
680	409.60	742	424.25		
681	409.84	743	424.49		

M23352-2/3 and
PS1243-2/1

Weight (mg) and L* of *N. pachyderma* (sin.), 224-250 microns

Table 13

Depth (cm)	Weight (mg) 5000 foraminifers	Weight (mg) 1000 foraminifers	Weight (mg) 500 foraminifers	Weight (mg) 100 foraminifers	L* 500 foraminifers
M23352-2/3					
0	39.63	7.52	3.53	0.84	39.82
57	57.34	11.54	6.10	1.17	36.32
226	49.20	10.06	4.97	1.00	38.59
257	63.83	13.00	6.45	1.28	37.25
657	33.06	6.55	3.36	0.64	44.24

Depth (cm)	Weight (mg) 5000 foraminifers	Weight (mg) 1000 foraminifers	Weight (mg) 500 foraminifers	Weight (mg) 100 foraminifers	L* 500 foraminifers
PS1243-2/1					
4.5	41.97	8.48	4.31	0.84	41.10
50	57.89	11.61	5.82	1.17	35.65
229	50.64	10.06	5.06	1.00	39.01
255	62.17	12.45	6.21	1.28	37.95
623	32.72	6.51	3.36	0.64	41.10

PS1243

Weight and L* of *N. pachyderma* (sin.) tests

Table 14

Depth (cm)	Weight (mg) 500 foraminifers 125-250 microns	L* 500 foraminifers 125-250 microns	Weight (mg) 100 foraminifers 224-250 microns	L* 100 foraminifers 224-250 microns
	PS1243-2			
0.5	2.58	39.91	0.77	30.76
4.5	3.41	41.79	0.94	32.06
8.5	4.14	42.44	0.95	31.52
10.5	4.28	42	0.98	31.08
14.5	4.37	41.94	0.98	30.84
20.5	4.16	41.67	0.99	31.86
24.5	4.27	43.43	0.96	32.05
30.5	3.49	40.08	0.94	31.05
34.5	4.02	41.34	0.91	31.17
40.5	4.51	39.65	1.01	30.67
44.5	3.95	38.18	1.02	29.88
	PS1243-1			
50	4.81	38.17	1.06	29.3
60	4.78	37.97	1.1	29.79
70	4.78	39.19	1.06	29.66
77.5	5.36	38.46	1.17	29.27
83	5.15	38.65	1.16	29.05
87	5.07	37.92	1.16	29.25
93	4.84	36.75	1.15	29.16
97	4.83	37.75	1.17	29.4
103	5.01	36.63	1.19	28.88
107	4.97	36.41	1.15	28.68
113	4.41	35.83	1.11	28.68
117	4.36	35.5	1.15	28.46
123	4.87	37.62	1.14	29.06
127	4.88	35.64	1.18	28.52
133	5.14	36.89	1.18	29.02
137	5.24	37.12	1.19	29.16
143	5.43	38.72	1.21	29.56
147	5.1	39.09	1.19	29.45
153	4.88	39.3	1.12	29.67
157	4.87	38.46	1.12	29.11
163	4.92	38.04	1.12	29.17
167	5	37.38	1.16	28.71
173	5.12	37.72	1.21	29.56
176	5.54	38.25	1.19	29.33
182	4.92	37.7	1.18	29.22
186	4.82	38.09	1.14	29.47
190	5.62	39.08	1.19	29.58
195	4.82	38.1	1.12	29.33
200	4.72	38.39	1.12	29.01
205	4.21	38.46	1.04	30.23
210	4.31	40.55	1.03	30.41
215	4.22	41.03	1.03	30.69
220	4.22	41.16	0.99	31.02
225	4.24	41.4	0.99	30.66
230	4.65	39.72	1.12	30.41
235	3.91	40.01	1.01	31.07
240	4.11	41.51	0.99	31
245	5.36	42.48	1.19	31.23
250	5.58	41.38	1.23	30.91
260	5.35	42.13	1.29	31.4
265	5.65	42.87	1.26	31.29
270	5.37	41.8	1.21	31.4
275	4.91	39.3	1.2	30.9
280	4.46	39.76	1.13	30.96
282	4.78	41.34	1.13	31.03
285	4.19	41.37	1.04	32.01

Weight and L* of *N. pachyderma* (sin.) tests

Table 14 continued

Depth (cm)	Weight (mg) 500 foraminifers 125-250 microns	L* 500 foraminifers 125-250 microns	Weight (mg) 100 foraminifers 224-250 microns	L* 100 foraminifers 224-250 microns
290	4.84	41.82	1.15	31.52
295	4.79	40.48	1.18	30.93
300	4.55	40.78	1.15	31.03
305	5.07	40.59	1.24	30.92
310	5.41	40.4	1.26	30.71
319	5.26	40.51	1.23	30.82
323	5.01	40.98	1.16	30.65
327	4.98	41.53	1.14	31.27
343	5.06	42.01	1.11	31.54
347	4.94	40.65	1.16	30.66
353	4.05	40.34	1.06	30.95
357	4.54	40.31	1.02	30.39
363	4.66	40.2	1.07	30.64
367	4.53	39.89	1.08	30.54
373	4.53	40.43	1.08	30.64
377	4.71	41.76	1.08	31.21
383	4.75	41.99	1.09	31.5
387	4.2	41.48	1.1	31.76
393	4.76	42.1	1.14	31.29
397	4.83	41.67	1.11	31.14
407	5.12	40.22	1.2	29.57
412	4.82	41.62	1.13	31.39
417	4.9	43.36	1.09	31.48
422	3.66	42.24	0.89	31.93
427	4.64	43.86	1.01	31.66
432	4.96	41.06	1.19	31.62
437	5.25	41.74	1.21	31.16
442	5.04	41.61	1.14	30.8
447	4.56	41.13	1.08	31
453	5	42.32	1.11	31.58
457	5.15	41.85	1.13	30.72
463	4.7	39.96	1.13	30.36
467	5.06	39.74	1.16	30.3
473	4.72	39.29	1.12	30.12
477	4.04	38.18	1.07	30.23
482	4.34	39.52	1.02	30.41
487	4.45	38.69	1.06	29.79
492	4.54	38.77	1.1	29.87
497	4.5	40.14	1.06	30.46
502	4.29	38.77	1.11	30.26
507	3.76	40.93	0.95	31.1
510.5	3.14	41.83	0.78	31.49
519	2.9	39.45	0.76	31.15
523.5	2.55	39.64	0.69	31.19
539	3.08	37.28	1.06	30.29
547	2.87	37.3	1	30.18
556.5	3.68	38.58	1.03	30.12
566	2.87	39.57	0.76	30.64
570.5	3.13	43.85	1.01	32.71
580.5	3.92	40.16	0.97	30.76
590.5	3.78	41.76	0.79	30.59
600	3.06	40.7	0.72	32.25
605.5	3.34	45.34	0.75	32.78
610	3.5	47.05	0.75	33.28
615	3.26	45.93	0.74	33.19
620	3	45.57	0.68	32.93
625	2.88	44.87	0.66	33.12
630	2.95	44.32	0.68	32.85
635	2.86	43.91	0.61	32.28
640	2.78	45.96	0.76	32.26
645	1.61	46.65	0.69	32.28

Weight and L*
of *N. pachyderma* (sin.) tests

Table 14 continued

Depth (cm)	Weight (mg) 500 foraminifers 125-250 microns	L* 500 foraminifers 125-250 microns	Weight (mg) 100 foraminifers 224-250 microns	L* 100 foraminifers 224-250 microns
650.5	2.85	47.31	0.86	33.48
658	3.21	40.66	0.82	31.56
662	3.15	40.61	0.84	31.27
669	2.76	38.61	0.79	31.21
674	2.74	39.35	0.8	31.51
678	2.52	37.6	0.98	31.24
683	2.78	39.09	0.62	30.84
699	3.52	38.87	0.82	31.94
708.5	2.26	39.8	0.72	29.41
727.5	2.7	36.68	0.87	30.02
738.5	2.4	36.29	0.76	31.1
747.5	2.9	36.12	0.76	29.41

M23352

Weight and L* of *N. pachyderma* (sin.) tests

Table 15

Depth (cm)	Weight (mg) 500 foraminifers 125-250 microns	L* 500 foraminifers 125-250 microns	Depth (cm)	Weight (mg) 500 foraminifers 125-250 microns	L* 500 foraminifers 125-250 microns
	M23352-2		157	5.21	37.54
1	2.6	40.86	161	5.25	37.84
5	2.71	40.91	164	5.59	39.03
8	3.07	41.11	167	4.96	38.35
11	3.56	42.76	169	5.13	37.89
14	4.18	43.55	172	5.59	39.25
17	4.28	43.42	177	4.76	37.93
			179	4.78	38.41
	M23352-3		182	4.7	37.46
19	4.04	41.63	186	5.13	38.74
22	4.12	41.75	189	4.95	39.54
24	4.12	41.36	191.5	4.86	39.15
27	3.72	42.19	196	5.08	37.39
32	4.19	40.81	199	5.44	38.56
34.5	4.54	38.91	202	5.64	38.28
35	4.45	38.68	204	5.26	38.14
36.5	4.85	38.99	207	5.11	37.86
37	4.88	39.52	209	5.19	38.03
38	4.91	38.86	215	5.14	38.44
39	4.99	39.77	219	5.23	40.05
41	4.56	38.44	221	4.71	40.7
42	4.96	38.16	222	4.48	40.81
43	5.2	39.27	223	4.17	40.38
44	5.19	39.11	224	4.22	40.62
46	5.05	38.46	225	4.21	41.2
47	5.18	38.92	227	3.92	40.57
48	5.05	38.62	228	4.05	40.84
50	4.86	37.87	229	3.89	40.08
53	4.93	37.6	230	4.02	40.9
55	5.14	37.77	236	4.42	42.61
56	4.91	37.53	241	3.57	41.34
59	5.26	38.38	244	4.12	40.18
66	5.16	39.51	245	4.35	40.01
69	5.21	40.52	246	4.45	39.39
72	5.32	38.91	248	5.1	38.56
76.5	5.11	38.8	249	5.31	39.98
79	4.97	39.17	250	5.82	40.89
84	5	39.08	251	5.67	39.91
87	5.13	39.79	252	5.56	40.67
91	4.88	38.92	253	5.71	40.34
94	5.13	40.12	254	5.6	40.71
96	4.96	39.86	255	5.67	40.36
99	4.99	39.02	257	5.1	39.22
102	4.96	39.3	259	5.98	40.29
104	5.33	39.61	260	5.55	38.14
108	5.36	39.14	261	6.15	39.64
111	5.23	38.44	262	5.69	38.54
114	4.99	38.18	265	5.7	39.22
118	4.93	37.73	266	5.77	39.46
121	4.79	37.87	267	5.85	39.24
123	4.78	38.39	268	5.59	39.2
127	4.45	37.42	269	5.42	39.21
129	4.94	38.26	270	5.9	39.55
132	5.04	38.2	271	5.87	40.47
136	4.88	38.34	272	5.1	38.84
139	4.86	37.52	273	5.31	38.57
142	4.81	37.02	275	4.89	38
144	4.57	37.29	276	5.48	39.14
147	4.54	37.54	277	5.22	38.6
151	5.32	38.24	278	5.49	38.69
153	5.49	38.09	279	5.25	38.12

Weight and L* of *N. pachyderma* (sin.) tests

Table 15 continued

Depth (cm)	Weight (mg) 500 foraminifers 125-250 microns	L* 500 foraminifers 125-250 microns	Depth (cm)	Weight (mg) 500 foraminifers 125-250 microns	L* 500 foraminifers 125-250 microns
280	5.23	38.21	344	4.08	41.62
281	5.22	38.88	345	4.17	42
282	5.57	39.11	346	4.43	43.75
284	5.43	39.47	347	4.49	44.32
286	5.14	39.39	348	4.04	42.83
287	5.38	40.15	349	4.16	42.76
288	5.44	40.07	350	4.27	44.12
289	5.56	39.53	351	3.76	42.74
290	5.42	39.62	354	3.31	42.15
291	5.82	40.43	357	2.81	39.51
292	5.84	40.55	359	2.81	39.77
293	5.56	40.27	362	3.4	42.06
294	5.52	40.3	364	3.8	43.79
295	5.72	41.35	367	4.37	43.5
296	5.34	41.42	369	4.48	44.31
297	5.62	41.16	372	4.17	42.42
298	5.46	40.74	374	3.95	41.6
299	5.32	40.53	376	4.34	42.19
300	5.38	40.65	378	4.66	43.79
301	5.51	40.08	382	4.1	42.3
302	5.12	39.23	384	4.44	42.96
303	5.39	39.69	386	4.53	42.5
304	5.31	39.8	388	4.69	43.33
305	5.41	40.24	392	5.15	43.03
306	5.29	39.49	394	4.85	42.15
307	5.7	40.08	396	5.31	42.14
308	5.09	39.37	399	5.2	42.57
309	5.41	40.46	402	5.06	42.2
310	5.26	40.61	406	5.01	42.82
311	5.14	39.88	408	4.87	42.4
312	5.17	40.22	412	4.51	43.86
313	5.1	40.35	414	4.5	44.22
314	5.11	41.73	416	4.45	42.54
315	4.98	40.85	418	4.16	42.73
316	5.07	40.71	422	4.67	42.64
317.5	5.03	40.59	424	4.96	44.27
318.25	5.2	39.78	427	4.65	42.59
319	5.45	39.69	429	5.02	43.06
320	5.32	39.39	432	4.82	42.49
321	5.52	39.64	436	4.91	42.59
322	5.3	38.72	438	4.88	42.5
323	5.49	39.58	442	4.59	43.03
324	5.48	39.43	446	4.71	43.04
326	5.37	39.59	449	4.38	42.31
327	4.89	39.16	452	4.12	44.25
328	5.21	39.94	454	4.03	44.21
329	5.22	40.28	457	4.08	44.01
330	4.87	40.2	461	4.25	42.22
331	4.72	39.94	464	4.51	41.47
332	4.95	40.47	467	4.48	40.59
333	5.15	40.65	469	4.87	41.63
334	4.96	40.61	472	4.74	43
335	5	41.23	476	4.58	43.2
336	4.68	41.25	482	3.49	43.55
337	4.72	40.67	486	2.82	43.24
338	4.93	41.73	488	3.02	41.6
339	4.68	41.07	492	3.6	41.16
340	4.58	41.39	494	3.87	42.44
341	4.67	42.5	497	3.92	42.6
342	4.42	41.46	502	3.59	41.17
343	4.38	42.09	506	3.4	41.75

Weight and L* of *N. pachyderma* (sin.) tests

Table 15 continued

Depth (cm)	Weight (mg) 500 foraminifers 125-250 microns	L* 500 foraminifers 125-250 microns
508	3.34	43.04
512	2.76	41.46
526	3.22	42.01
586	2.56	42.69
588	3.39	41.24
592	4.64	39.6
599	4.68	39.44
602	4.72	38.58
604	4.79	38.75
607	4.56	39.29
609	4.78	40.57
612	4.54	40.42
614	4.28	40.44
616	4.2	41.69
619	3.37	41.82
629	3.79	43.58
636	2.99	42.07
642	2.53	41.89
647	2.59	43.77
654	2.71	43.65
657	2.88	45.29
661	2.46	44.06
666	2.27	44.06